DYNAMIC RESPONSE OF NONLINEAR TORSIONALLY COUPLED STRUCTURES

Pradip Kumar Syamal

A Thesis
in
The Faculty
of
Engineering

Presented in Partial Fulfilment of the Requirements
for the degree of
Doctor of Philosophy
at
Concordia University
Montreal, Quebec, Canada

October 1983

ABSTRACT

DYNAMIC RESPONSE OF NONLINEAR TORSIONALLY COUPLED STRUCTURES

Pradip Kumar Syamal, Ph.D.
Concordia University, 1983

This thesis is concerned with the nonlinear elastic and inelastic dynamic response of both symmetric and unsymmetric structures. The study is performed in two separate but closely related stages.

In the first stage, the work is confined to dynamic instability in the torsional response of both single-story symmetric and eccentric buildings arising from the nonlinear elastic behaviour of resisting elements subjected to harmonic ground excitation. Earlier studies are extended to examine the importance of torsional damping, as well as the distribution and geometric arrangement of lateral load-resisting elements. Equally important, the relationship between the two sets of stability diagrams derived in previous studies with potentially conflicting stability interpretations is clarified. The results for susceptibility to nonlinear torsional coupling are presented in the form of generalized stability diagrams and critical torsional damping which are applicable to quite general structures with different distributions of load-resisting elements. Both torsional stability bounds as well as critical torsional damping are found to be influenced by various systems parameters.

The second stage of this study is concerned with the inelastic response of single-story monosymmetric structures for sinusoidal ground motion where coupling arises from eccentricity; here behaviour of resisting elements is idealized as either fully bilinear or pinched bilinear hysteretic. A steady state harmonic response - frequency sweep analysis is performed using the well-known method of averaging popularly referred to as the Kryloff-Bogoliuboff method. It is found that both the system and resisting element displacements for fully bilinear behaviour are stable even in the absence of viscous damping. The influence of eccentricity on peak ductility demand is found to be more significant than previously reported by other investigators. The pinched-hysteretic structures, on the other hand, experience instability of the so-called "jump phenomenon" type within a certain range of frequencies. Finally, a comparison of performance for a limited number of idealized hysteretic systems representative of common structural systems reveals that pinched elasto-plastic behaviour typical of steel cross-braced frames will experience the highest degree of torsional instability.

ACKNOWLEDGMENTS

The author wishes to express his sincere gratitude to his supervisor Dr. O.A. Pekau, whose engineering judgement, thoroughness and high standard of scholarship were indispensible for the progress of this research. His constructive guidance, discussions and encouragement throughout the course of this study are greatly appreciated.

The financial support for this research was provided by the Natural Sciences and Engineering Research Council of Canada Under grant No. A8258. The use of the facilities of Concordia University's Computer Centre are gratefully acknowledged.

Acknowledgement is also due to Dr. T.D. Bui of the Department of Computer Science for allowing the author access to his subroutine which proved invaluable during the course of the work of Chapter V. Thanks are due to Mr. Pranab Nandimajumdar for his assistance during various phases of the work. Thanks are also extended to Mrs. Marie Berryman for her excellent typing of this thesis.

The moral support of the author's and his father-in-law's entire families has been a source of continuous inspiration for which the author wishes to express his sincere thanks. Another person the author wishes to acknowledge is his eldest brother, Dr. Jajneswar Syamal, for his neverending encouragement, moral and financial support which ensured the author's education.

Finally, the author extends his very special and heartful thanks to his wife, Mitra, for her continued support, encouragement, patience, perseverence and understanding, and to his beautiful little daughter, Mausumi, for her innocent smiles as a continuous source of inspiration to the author.

अज्ञानतिमिरान्धस्य ज्ञानाञ्जनशलाकया ।
चक्षुरुन्मीलितं येन तस्मै श्रीगुरवे नमः ॥

Ajnana Timirandhasya Jnananjana Salakaya
Chaksurunmilitam Yena Tasmai Srigurabve Namah

from Vishwasara Tantra

Salutations to the Guru who with the collyrium stick of knowledge has opened the eyes of one blinded by the disease of ignorance.

TABLE OF CONTENTS

LIST OF FIGURES

LIST OF TABLES

NOMENCLATURE

A_{ij}	element of matrix $\underset{\sim}{A}$ of Mathieu-Hill equation expressed in Equation (3.26) and Appendix C
$\underset{\sim}{A} = [A_{ij}]$	coefficient matrix of Mathieu-Hill equation
$A_1(\tau)$	time-dependent nondimensional translational response amplitude of centre of mass in x-direction
$A_2(\tau)$	time-dependent nondimensional torsional response amplitude of centre of mass in θ-direction
$A_3(t)$	time-dependent nondimensional translational response amplitude of resisting element 1 in x-direction
$A_4(\tau)$	time-dependent nondimensional translational response amplitude of resisting element 2 in y-direction
$\overline{A}_I$	average nondimensional translational response amplitude of centre of mass in x-direction
$\overline{A}_2$	average nondimensional torsional response amplitude of centre of mass in θ-direction

$\bar{A}_3$	average nondimensional translational response amplitude of element 1 (weaker element) in x-direction
$\bar{A}_4$	average nondimensional translational response amplitude of element 2 (stiffer element) in x-direction
a	plan dimension of building
$\underset{\sim}{B}$	coefficient matrix of Mathieu-Hill equation
b	plan dimension of building
C_x, C_y, C_θ	viscous damping coefficients
$\underset{\sim}{C}$	coefficient matrix of Mathieu-Hill equation
$C_1(\bar{A}_1), C_2(r\bar{A}_2)$	integral functions defined in Equation (4.27)
D	nondimensional amplitude of a single degree-of-freedom system
E	stiffness distribution parameter in x-direction
$\underset{\sim}{E}$	identity matrix
E_x, E_y	nondimensional eccentricities defined as e_x/r and e_y/r
e	eccentricity of centre of resistance measured from centre of mass along y-axis

$\bar{e}$	nondimensional eccentricity defined as e/r
e_x, e_y	static eccentricities
F	stiffness-distribution parameter in y-direction
$F(\delta_j, \alpha, t)$, $j=1,4$	hysteretic restoring force
f_i, $i=1,7$	nondimensional constants expressed as various functions of λ, Ω_y, Ω_θ, E, F, ζ_x, ζ_y, ζ_θ, r and D (Appendix A and F)
$f_j(\frac{\delta_j}{\delta_y}, \alpha, \tau)$, $j=1,4$	normalized hysteretic restoring force
G_a	nondimensional ground acceleration amplitude defined as $U/(\delta_y \omega_x^2)$
g_i, $i=1,7$	nondimensional constants expressed as various functions of λ, Ω_y, Ω_θ, E, F, ζ_x, ζ_y, ζ_θ, r and D (Appendix A and F)
h_i, $i=1,12$	nondimensional constants expressed as various functions of λ, Ω_y, Ω_θ, E, F, ζ_x, ζ_y, ζ_θ, r and D (Appendix A and F)
J_m	mass moment of inertia of rigid diaphragm about a vertical axis through centre of mass
K_x, K_y	total translation stiffnesses in x- and y-directions

$K_\theta, K_{\theta m}$	total torsional stiffness of structure at centre of mass
k	initial tangent stiffness of a typical resisting element
k_{ix}, k_{iy}	translational stiffnesses in x- and y-directions of ith resisting element
k_{jx}, j=1,2	linear element stiffness of elements 1 and 2 in x-direction
k_{ij}, j=3,4	linear element stiffness of element 3 and 4 in y-direction
M	total mass of rigid deck
$P(\tau)$	time-dependent nondimensional translational response amplitude of centre of mass in x-direction
$\overline{P}$	average nondimensional translational response amplitude of centre of mass in x-direction
$\overline{P}_{cr}$	critical lateral displacement corresponding static torsional buckling
$Q(\tau)$	time-dependent nondimensional translational response amplitude of centre of mass in y-direction
$\overline{Q}$	average nondimensional translational response

	amplitude of centre of mass in y-direction
$R(\tau)$	time-dependent nondimensional rotational response amplitude in θ-direction
$\bar{R}$	average nondimensional rotational response amplitude in θ-direction
$R(\delta)$	resisting force of a typical resisting element
$R_x(\delta_j)$, $R_y(\delta_j)$	resisting force in element j along x- and y-directions, respectively
R_{yi}, i=1,2	shear strength of resisting elements 1 and 2
r	building plan aspect ratio (a/b)
$S_1(\bar{A}_i)$, $S_2(r\bar{A}_2)$	integral functions defined in Equation (4.27)
s	ratio of length of central core to building dimension
t	time
U	amplitude of sinusoidal ground acceleration in x-direction
$\ddot{U}_g(t)$, $\ddot{u}_g(t)$	time dependent function of ground acceleration in x-direction
$u(t)$, $\dot{u}(t)$, $\ddot{u}(t)$	translational displacement, velocity and acceleration of centre of mass in x-direction

$v(t)$, $\dot{v}(t)$, $\ddot{v}(t)$	translational displacement, velocity and acceleration of centre of mass in y-direction
x,y	principal co-ordinates
x_i,y_i	distances of ith resisting element from principal axes
α	bilinearity parameter in inelastic system, $0 \leq \alpha \leq 1.0$.
α_1,α_2	parametric constants defined in Equation (2.8)
β	geometric parameter of L-shaped building; also stiffness ratio of resisting element (k_{2x}/k_{1x})
β_0	normalized plan dimension of building (a/Γ)
Γ	mass radius of gyration of total mass of diaphragm with respect to a vertical axis through centre of mass
γ	geometric parameter of L-shaped building; also strength ratio of resisting element (R_{y2}/R_{y1})
γ_0	normalized plan dimension of building (b/Γ)
$\bar{\Delta}_2,\bar{\Delta}_3$	phase angle differences $(\bar{\chi}-\bar{\Phi})$ and $(\bar{\chi}-\bar{\Psi})$, respectively

δ	in-plane displacement of a typical resisting element
δ_0	reference displacement for resisting elements
$\delta_{0,d}$, $\delta_{0,s}$	reference displacement for dynamic and static normalizations, respectively
δ_j, j=1,4	in-plane displacements of resisting elements
δ_x	reference translational displacement required for nondimensionalization of translational displacement in x-direction for nonlinear elastic system (Equation (A1))
δ_y	yield translational displacement of resisting element; also reference y-displacement for normalization in nonlinear elastic systems (Equation (F1))
δ_θ	reference torsional displacement required for nondimensionalization of torsional displacement for nonlinear elastic system (Equation (A1))
ε	nonlinearity parameter defined as λ/δ_0^2
$\underset{\sim}{\varepsilon}$	coefficient matrix of Mathieu-Hill equation given in Equation (3.28) and Appendix C
ζ_x, ζ_y, ζ_θ ,ζ_i	uncoupled translational and torsional viscous damping coefficients for x-, y- and

	θ-directions, respectively; and $\zeta=\zeta_x=\zeta_\theta$
$\zeta_{\theta,cr}$	critical torsional damping ratio for non-linear coupling
$\hat{\zeta}_{\theta,cr}$	generalized critical torsional damping ratio for nonlinear coupling
η	unbalanced stiffness factor as a measure of eccentricity
$\theta(t)$, $\dot{\theta}(t)$, $\ddot{\theta}(t)$	rotational displacement, velocity and acceleration response, respectively, of mass centre about vertical axis
θ_i, i=2,3,4	angle of sinusoidal response of resisting elements defined as $\Omega\tau+\bar{\Phi}_i$
θ_i^*, i=3,4	cyclical angle defined in Equations (4.28) and (5.1) for purely bilinear and pinched bilinear systems, respectively
θ_i^{**}, i=3,4	cyclical angle defined in Equation (5.1f) for pinched belinear system
$\theta_{r_2}^*$	cyclical angle defined in Equations (4.29) and (5.2) for fully bilinear and pinched bilinear systems, respectively
$\theta_{r_2}^{**}$	cyclical angle defined in Equation (5.2f) for pinched bilinear system

θ_y	initial yield torsional displacement of structure
κ	fraction of critical torsional damping for nonlinear coupling $(0 \leq \kappa \leq 1.0)$
$\Lambda_x(\tau)$, $\dot{\Lambda}_x$, $\ddot{\Lambda}_x$	nondimensional translational response displacement, velocity and acceleration, respectively, of mass centre in x-direction
$\Lambda_y(\tau)$, $\dot{\Lambda}_y$, $\ddot{\Lambda}_y$	nondimensional translational response displacement, velocity and acceleration, respectively, of mass centre in y-direction
$\Lambda_\theta(\tau)$, $\dot{\Lambda}_\theta(\tau)$, $\ddot{\Lambda}_\theta(\tau)$	nondimensional torsional response displacement, velocity and acceleration, respectively, of mass centre about a vertical axis
λ	nonlinearity coefficient
λ_s, λ_d	nonlinearity coefficients for static and dynamic normalization, respectively
μ	function of apparent torsional frequency defined in Appendix D
ξ_x, ξ_y, ξ_θ	nondimensional displacement perturbations
τ	nondimensional time

$\Phi(\tau)$, $\Phi_1(\tau)$	slowly varying phase angle for translational response of mass centre in x-direction
$\overline{\Phi}$, $\overline{\Phi}_1$	average phase angle for translational response of mass centre in x-direction
$\Phi_2(\tau)$, $\chi(\tau)$	slowly varying phase angle of torsional response of mass centre about vertical axis
$\overline{\Phi}_2$, $\overline{\chi}$	average phase angle of torsional response of mass centre about vertical axis
$\Phi_3(\tau)$, $\Phi_4(\tau)$	slowly varying phase angles of translational response of resisting elements 1 and 2, respectively, in x-direction
$\overline{\Phi}_3$, $\overline{\Phi}_4$	average phase angles of translational response of resisting elements 1 and 2, respectively, in x-direction
Φ_1, χ_1	angle of sinusoidal system response defined as $\Omega\tau+\phi(\tau)$ and $\Omega\tau+\chi(\tau)$, respectively
$\Psi(\tau)$, $\overline{\Psi}$	slowly varying and average phase angles, respectively, of translational response of mass centre in y-direction
Ω	normalized ground excitation frequency (ω/ω_x)

Ω_0	apparent torsional frequency of the system
Ω_1, Ω_2	coupled lateral and torsional normalized frequencies of structure, respectively
Ω_y	normalized uncoupled translational frequency (ω_y/ω_x)
Ω_θ	normalized uncoupled torsional frequency (ω_θ/ω_x)
$\hat{\Omega}$	generalized excitation frequency (Ω/E)
$\hat{\Omega}_\theta$	generalized torsional frequency (Ω_θ/E)
ω_x, ω_y, ω_θ	uncoupled fundamental translational and torsional freqencies of structure, respectively
ω	frequency of sinusoidal ground excitation
ω_1, ω_2	coupled lateral and torsional natural frequencies of structure

CHAPTER I

INTRODUCTION

1.1 BACKGROUND OF THE PROBLEM

Engineering structures are frequently exposed to complex dynamic environments where a variety of nonlinear coupled responses is experienced, such as coupled flexural modes in shell vibration [1-3], buckling of columns due to dynamic axial force [4], and lateral-torsional oscillations of building structures [5-15].

Generally, all buildings are torsionally unbalanced to some extent and any form of translational excitation will therefore cause torsional response associated with lateral vibration. Field observations of earthquake damage show numerous examples of structural failure due to such simultaneous torsional motion.

Earthquake response of linear elastic building structures where the centre of mass is eccentric to the centre of resistance has been the subject of numerous studies [16-24] during the past two decades. Some of these studies [15,23,24] have pointed out the inadequacy of torsional provisions in current codes of practice. An extensive list of publications on this subject can be found in Reference 25.

It has also been discovered that strong modal coupling can occur in a rectangular building with a uniform distribution of columns in plan if the eccentricities and translational-torsional frequency differences are small [16]. Moreover, coupling between lateral and torsional motions induces torsion and generally reduces the base shear [17]. Torsional vibration can even be induced in symmetric structures

by the rotational component of ground motion which accompanies the two horizontal components [26].

1.1.1 Review of Nonlinear Elastic Problems

In recent years numerous studies concerned with the elastic response of symmetric structures have emphasized the effect of nonlinear coupling. Evensen [1,2], while studying the flexural vibration of a geometrically nonlinear thin circular ring, concluded that two coupled bending modes can exist due to elastic nonlinearity of the softening type. With the aid of the method of averaging, a set of coupled nonlinear algebraic equations was established to define the average response amplitude as a function of the exciting frequency. For a stable system this amplitude is of finite magnitude; otherwise, the solution fails thus indicating instability. Later, El-Zaouk and Dym [3] reported similar coupling in the vibration of orthotropic shells. The well-known work of Bolotin [4], on the other hand, deals extensively with the stability criterion of the Mathieu-Hill equation describing the transverse vibration of a rod subjected to longitudinal periodic forces.

By means of numerical time-history analysis, Tso and Asmis [8] showed that torsional motion of a symmetric building structure subjected only to lateral ground motion is possible as a result of nonlinearity in the force-displacement relation of the resisting elements. In a separate paper, Tso [5] successfully cast the torsional equation of motion of the symmetric system into Mathieu-Hill form. The likelihood of induced torsional response was then studied in terms of instability

regions in frequency parameter space. In References 27, 28, 30 this approach was subsequently applied to both nonlinear symmetric and unsymmetric structures. The procedure yielded results similar to those found by Tso [5], but with some corrections. The same corrections were later also reported by Antonelli et al [6].

1.1.2 Review of Coupled Inelastic Problems

Only recently has attention been focused on the coupled torsional-translational response of simple systems [7-15] with inelastic resisting elements subjected to sinusoidal pulse, harmonic or earthquake-type ground excitation and analyzed by means of time-history numerical integration. Shibata et al [7], while studying the nonlinear response of single-story unsymmetric building models with bilinear restoring force and subjected to idealized one to three half-sine pulse ground motion, observed that the rotational displacement in the nonlinear range with strength proportional to stiffness is much greater than for constant strength irrespective of stiffness. Tso and Asmis [8], on the other hand, found that torsional motion can be initiated even in a symmetric structure due to nonlinearity of the Ramberg-Osgood type with hysteretic slip under earthquake excitation, causing significant increase in lateral displacement of elements located at the periphery of the building.

Kan and Chopra [9-11] studied the effect of torsional coupling on the lateral-torsional deformation of a single-story building model subjected to earthquake excitation. They concluded that, due to the influence of force interaction on the yielding behaviour of elastic-perfectly plastic resisting elements, torsional deformation is proportional

to the nondimensional eccentricity, with no dynamic amplification when the uncoupled torsion to translation frequency ratio is greater than 2. They also observed no discernible trend in element deformation due to torsional coupling at small frequency ratio. In a similar study, Irvine and Kountouris [12,13] observed no strong correlation between the peak ductility demand and eccentricity, and therefore concluded that the difference in ductility demand between eccentric and symmetric structures is small. Also, for a wide range of other parameters the peak ductility demand was found to vary roughly linearly with the level of excitation.

Finally, Tso and Sadek [14] found that the influence of eccentricity on the ductility demand is larger than that reported by Irvine and Kountouris [12,13]. They also noted that an eccentric system does not respond primarily in translation when excited well into the inelastic range, as was concluded previously by Kan and Chopra [9-11]. In addition, they proposed approximate bounds to relate the ductility demand to the excitation level.

Awad [15], while studying inelastic responses of a single-story building model to both translational and rotational components of earthquake ground motion, observed that inelasticity can cause a reduction in rotational response of the system. Moreover, the ductility demand in inelastic systems is not the same as the force reduction factor used in determining the strength, and at times may be much higher.

1.1.3 Summary of the Problem

The preceding studies of induced torsional motion in symmetric

structures [5,6,8] due to nonlinear elastic coupling produced stability curves but did not allow for torsional damping. In addition, two sets of stability interpretations were derived, based on different definitions of reference parameter for the force-displacement relationship of the resisting elements [6]. Moreover, only simple cases of peripheral and two-element distributions of structural stiffness in the building plan were considered. Also, earlier studies of linear unsymmetric and nonlinear symmetric structures may not be directly applicable in predicting the behaviour of structures that are both nonlinear elastic and unsymmetric.

In an effort to understand the inelastic behaviour of torsionally coupled single-story buildings under strong earthquake excitation, all earlier studies employed step-by-step time-history integration of the equations of motion. Any consistent relation between the predominant system parameters and the resulting coupled hysteretic response is difficult to establish from these studies. Moreover, a comparison of the structural performance to be expected for systems having different hysteretic behaviour is still lacking. A steady state harmonic response analysis could, however, provide important insight into the dynamic response characteristics of such structures.

1.2 SCOPE AND OBJECTIVE OF THE PRESENT STUDY

The objective of the present study is to investigate the dynamic effect of coupling between the torsional and translational displacements of a simple single-story building model for both nonlinear elastic and inelastic hysteretic behaviour. The scope of the work is

limited to identifying the basic system parameters influencing coupled response and to evaluating the effect of the important parameters on the stability and displacements of the system as a whole, as well as on the deformations of the individual resisting elements.

Thus, this study consists of two closely related but essentially independent parts. The first part of the study is concerned with a system in which torsional coupling arises from the nonlinear elastic behaviour of the resisting elements. The second part deals with the inelastic response of a single-story system, where coupling arises from eccentricity and element behaviour is inelastic hysteretic. The input ground motion, for both phases of the study, is assumed to be sinusoidal and uniform over the base of the structure and contains no rotational components.

1.3 ORGANIZATION OF THE THESIS

The work concerning the nonlinear elastic analysis is presented in Chapters II and III, whereas the inelastic behaviour is described in Chapters IV and V.

Chapter II is confined to the symmetric building model. To extend the earlier studies beyond the aforementioned simple systems, the distribution and geometric arrangement of the lateral load resisting elements are included in the analysis. The importance of torsional damping on induced coupling in symmetric structures is also studied. Equally important, the relationship between the two sets of stability diagrams produced in previous studies is clarified. The results are presented in the form of generalized stability diagrams

which are applicable to quite general structures with different distribution of load resisting elements.

In Chapter III, the study is extended by introducing both single and double eccentricities in the model of Chapter II. Here too, the importance of torsional damping on induced coupling is investigated with the results presented as stability diagrams in frequency parameter space.

In Chapter IV, the coupled inelastic response characteristics for single-story unsymmetric buildings are examined. The resisting elements are considered to be bilinear hysteretic, for which elastic and pure elastic-plastic behaviour are two special cases. The important parameters controlling the response amplitudes are identified and the results are presented in the nondimensional amplitudes (i.e., ductility) versus frequency domain.

Chapter V extends the analysis formulated in Chapter IV to resisting elements with pinched bilinear hysteretic behaviour. As was done in the bilinear hysteretic study, the results are presented in the same nondimensional amplitude versus frequency domain. The possible occurrence of instability is examined and the predominant system parameters causing the instability are identified. Finally, a comparison of performance among several commonly used structural systems, described by the associated hysteretic behaviour, is made.

Finally, in Chapter VI a brief summary of the major conclusions of this study is presented. The implications of the latter on the design of structures, as well as future research needs, are also discussed in this chapter.

CHAPTER II

INSTABILITY IN NONLINEAR ELASTIC SYMMETRIC STRUCTURES

2.1 INTRODUCTION

In all the earlier studies of lateral-torsional coupling of nonlinear elastic systems [5,6,8] a single-story symmetric building model has been used. Even for studies of linear elastic behaviour [16-18, 21,22] similar single-story models were employed. In particular, several previous studies of linear structures [16,22,26] have indicated that the susceptibility of symmetric buildings to induced torsional response is influenced to a significant degree by the distribution of the resisting elements within the plan area of the building.

In this chapter, a single-story building model, similar to that employed in earlier studies but with resisting elements randomly distributed over the plan area, is adopted for study. Since the preceding studies [5,6,8] did not allow for torsional damping, the present study investigates the importance of torsional damping on induced coupling in symmetric structures.

The behaviour of resisting elements, as in previous studies, is taken to remain nonlinear elastic. The influence of the distribution and geometric arrangement of the lateral load resisting elements on the stability curves is investigated in detail. It should be noted that two sets of stability diagrams, with potentially conflicting stability interpretations, were derived in the earlier studies [5,6],

based on two different definitions of the reference parameter for the force-displacement relationship of resisting elements. Thus, in the present study the relationship between these two sets of stability diagrams is clarified. Attention is directed toward identifying the basic system parameters governing the susceptibility to induced torsional response of symmetric structures with nonlinear resisting elements.

Results are presented in the form of stability curves showing the effects of various systems parameters, such as building plan aspect ratio, torsional and translational damping coefficients, arrangement of load resisting elements on the induced torsional coupling in these nonlinear but otherwise symmetric structures. Finally, the susceptibility to nonlinear coupling is summarized in the form of generalized criteria, for both critical damping and the size of the regions of torsional instability, which are applicable to quite general configurations of load-resisting elements encountered in symmetric structural systems.

2.2 DERIVATION OF THE STABILITY EQUATION

2.2.1 Equations for Coupled Motion

The simple structure employed in earlier studies [5,6] is shown in Figure 2.1. It consists of a simple single-story symmetric building with rigid diaphragm and coincident centres of mass and resistance. The driving force is assumed to be sinusoidal support

excitation in only the x-direction. Letting k_{ix} and k_{iy} represent the translational stiffness of the i^{th} resisting element in the x- and y-directions respectively, the total translational stiffness K_x, K_y and the torsional stiffness of the structure K_θ are given by

$$K_x = \Sigma\, k_{ix} \tag{2.1a}$$

$$K_y = \Sigma\, k_{iy} \tag{2.1b}$$

$$K_\theta = \Sigma\, k_{ix}\, y_i^2 + \Sigma\, k_{iy}\, x_i^2 \tag{2.1c}$$

The load-displacement relationship of resisting elements is assumed to be elastic, weakly nonlinear and of the softening type with cubic nonlinearity expressed as

$$R(\delta) = k\delta\,[1 - \lambda(\delta/\delta_0)^2] \tag{2.2}$$

in which δ is the displacement of a typical resisting element, δ_0 is a reference displacement, λ is a measure of the softening and k is the initial tangent stiffness.

The fact that horizontal response may accompany nonlinear resistance was first demonstrated analytically by Tso [5] as follows. The corner displacement, δ_j (see Figure 2.1) may be expressed in terms of mass centre lateral displacements u and v and rotational displacement θ by the following relations

$$\delta_1 = u - b\theta \tag{2.3a}$$

$$\delta_2 = u + b\theta \tag{2.3b}$$

$$\delta_3 = v - a\theta \tag{2.3c}$$

$$\delta_4 = v + a\theta \tag{2.3d}$$

It is now assumed that the restoring forces $R_x(\delta_j)$ and $R_y(\delta_j)$ are antisymmetric (cubic) functions about the origin. Expanding one of the restoring functions, say $R_x(\delta_1)$, in the form of Taylor series about equilibrium position $R_x(0)$ yields

$$R_x(\delta_1) = R_x'(0)(u-b\theta) + \frac{R_x'''(0)}{3!}(u - b\theta)^3 + \ldots \tag{2.4}$$

For a linear load-displacement relationship, $R_x'(0)$ represents the linear stiffness of the resisting element and motions u and θ are uncoupled. However, if the resisting elements are nonlinear, Equation (2.4) shows that torsional motion becomes coupled to the primary lateral response.

To approximate earthquake effects, the structure is subjected to sinusoidal ground acceleration in the x-direction of magnitude

$$\ddot{U}_g = U \cos \omega t \tag{2.5}$$

Initially, the nonlinear system has three degrees-of-freedom (u,v and θ in x-, y- and θ- directions, respectively). Since ground excitation exists only in the x- direction, v is zero and

the system is governed by the following two equations of motion

$$\ddot{u} + 2\zeta_x\omega_x \dot{u} + \omega_x^2 u = -U \cos \omega t + \varepsilon\omega_x^2 u(u^2 + 3b^2\theta^2) \qquad (2.6)$$

$$\ddot{\theta} + 2\zeta_\theta\omega_\theta \dot{\theta} + \omega_\theta^2 \theta = \varepsilon\theta(\alpha_1 u^2 + \alpha_2\theta^2) \qquad (2.7)$$

where

$$r = a/b \qquad (2.8a)$$

$$\varepsilon = \lambda/\delta_0^2 \qquad (2.8b)$$

$$\alpha_1 = (9 \Sigma k_{ix} y_i^2) / \{M(a^2 + b^2)\} \qquad (2.8c)$$

$$\alpha_2 = 3(b^2 \Sigma k_{ix} y_i^2 + a^2 \Sigma k_{iy} x_i^2) / \{M(a^2 + b^2)\} \qquad (2.8d)$$

and ω_x, ω_θ are the uncoupled translational and torsional frequencies of the system as defined in Appendix A, M denotes the total mass and a, b are the building dimensions.

Equations (2.6) and (2.7) are identical to Equation (5) of Antonelli et al. [6] and Equations (15) and (16) of Tso [5], but the expressions for α_1 and α_2 in the present investigation are more general in the sense that they accommodate any type of stiffness distribution over the plan area of the building.

The definition of δ_0 in Equation (2.2) may be taken as the

lateral static displacement induced by the maximum ground acceleration expressed as

$$\delta_{0,s} = U/\omega_x^2 \tag{2.9}$$

However, the following alternative definition for δ_0 (suggested by Antonelli et al. [6]) related to the forcing frequency

$$\delta_{0,d} = UD/\omega_x^2 \tag{2.10}$$

in which D is the dynamic amplification factor for a single degree-of-freedom system given by

$$D = [\{1 - (\omega/\omega_x)^2\}^2 + (2\zeta_x\omega/\omega_x)^2]^{-\frac{1}{2}} \tag{2.11}$$

Thus, in Equations (2.9) and (2.10), subscripts s and d are attached to δ_0 to distinguish between the above static and dynamic reference displacements. In order to work with unique load-displacement characteristic for the system described by Equation (2.2), expressions (2.8b), (2.9) and (2.10) lead to the following important relation

$$\lambda_s = \lambda_d/D^2 \tag{2.12}$$

where nonlinearity parameter λ also carries subscripts s and d to denote static and dynamic normalization, respectively.

It is convenient to express Equations (2.6) and (2.7) in nondimensional form as follows

$$\ddot{\Lambda}_x + f_1 \dot{\Lambda}_x + f_2\Lambda_x - (f_3\Lambda_x^3 + f_5\Lambda_x\Lambda_\theta^2) = -\cos \Omega\tau \qquad (2.13)$$

$$\ddot{\Lambda}_\theta + h_1\dot{\Lambda}_\theta + h_2\Lambda_\theta - \{h_3\Lambda_\theta\Lambda_x^2 + (h_4+h_6)\Lambda_\theta^3\} = 0 \qquad (2.14)$$

where $\tau = \omega_x t$ and displacments Λ_x and Λ_θ, as well as coefficients f_i, h_i are normalized quantities defined in Appendix A. It should also be noted that frequencies are normalized with respect to the structure's translational frequency ω_x, i.e., $\Omega_\theta = \omega_\theta/\omega_x$ and $\Omega = \omega/\omega_x$.

The general form of the foregoing nondimensionalized equations of motion remains unchanged irrespective of whether the static or dynamic reference displacement is used, although coefficients f_i and h_i have magnitudes according to the actual form of normalization (Appendix A).

2.2.2 Approximate Solution for Nonlinear Amplitudes

Equations (2.13) and (2.14) can be solved by applying the method of averaging, i.e., the method of slowly varying amplitude popularly known as the Kryloff-Bogoliuboff method [29]. This method has been successfully applied by Evensen [1] and El-Zaouk and Dym [3] in related problems involving vibration of circular rings and shells.

Following this technique, it is assumed that the solution for

Λ_x and Λ_θ exist in the following form

$$\Lambda_x(\tau) = P(\tau) \cos [\Omega\tau + \Phi(\tau)] \tag{2.15a}$$

$$\Lambda_\theta(\tau) = R(\tau) \cos [\Omega\tau + \chi(\tau)] \tag{2.15b}$$

where P, R, Φ and χ are taken to be slowly varying functions of τ. Substituting the foregoing expressions into Equations (2.13) and (2.14), the averaging method [29] (Appendix B) leads to the following four nonlinear coupled algebraic equations

$$(f_2-\Omega^2)\,\overline{P} - \tfrac{3}{4}f_3\,\overline{P}^3 - \tfrac{1}{4}f_5\,\overline{P}\,R^2(1+2\cos^2\overline{\Delta}_2) = -\cos\overline{\Phi} \tag{2.16a}$$

$$f_1\,\Omega\,\overline{P} - \tfrac{1}{4}f_5\,\overline{P}\,\overline{R}^2 \sin 2\overline{\Delta}_2 = \sin\overline{\Phi} \tag{2.16b}$$

$$(h_2-\Omega^2)\,\overline{R} - \tfrac{1}{4}h_3\,\overline{R}\,\overline{P}^2(1+2\cos^2\overline{\Delta}_2) - \tfrac{3}{4}(h_4+h_6)\,\overline{R}^3 = 0 \tag{2.16c}$$

$$h_1\,\Omega\,\overline{R} + \tfrac{1}{4}h_3\,\overline{R}\,\overline{P}^2 \sin 2\overline{\Delta}_2 = 0 \tag{2.16d}$$

Here $P(\tau)$, $R(\tau)$, $\Phi(\tau)$ and $\chi(\tau)$ have been replaced by values averaged over one cycle, denoted by $\overline{P}$, $\overline{R}$, $\overline{\Phi}$ and $\overline{\chi}$, respectively. The symbol $\overline{\Delta}_2$ is the average phase difference

$$\overline{\Delta}_2 = \overline{\chi} - \overline{\Phi} \tag{2.17}$$

Eliminating phase angles from the Equations (2.16) and (2.17)

results in the following two simultaneous coupled nonlinear algebraic equations in $\bar{P}$ and $\bar{R}$

$$\left\{(f_2-\Omega^2)\,\bar{P}^2 - \tfrac{3}{4}\,\bar{P}^4 - \frac{f_5}{h_3}(h_2-\Omega^2)\,\bar{R}^2 + \tfrac{3}{4}\frac{f_5}{h_3}(h_4+h_6)\,\bar{R}^4\right\}^2$$

$$+\left\{f_1\,\Omega\,\bar{P}^2 + \frac{f_5}{h_3}\,h_1\Omega\,\bar{R}^2\right\}^2 = \bar{P}^2 \qquad (2.18a)$$

$$(4\,\frac{h_1}{h_3}\,\Omega)^2 + \left\{\frac{4(h_2-\Omega^2)}{h_3} - 2\bar{P}^2 - \frac{3(h_4+h_6)}{h_3}\,\bar{R}^2\right\}^2 = \bar{P}^4 \qquad (2.18b)$$

Equation (2.18) can readily be solved by standard numerical techniques [31] and the stability of response $\bar{R}$ can then be examined in the amplitude-frequency (i.e., $\bar{R}$-Ω) parameter space.

2.2.3 Condition for Torsional Coupling

The stability of the coupled response is examined by introducing small perturbations in the solutions expressed by Equations (2.15a,b), say of magnitude $\xi_x(\tau)$ and $\xi_\theta(\tau)$. Hence

$$\Lambda_x(\tau) = \bar{P}\cos(\Omega\tau + \bar{\phi}) + \xi_x(\tau) \qquad (2.19a)$$

$$\Lambda_\theta(\tau) = \bar{R}\cos(\Omega\tau + \bar{\chi}) + \xi_\theta(\tau) \qquad (2.19b)$$

Susbtituting these perturbed solutions into the nondimensionalized differential equations of motion (Equations (2.13) and (2.14)), and retaining only the first order terms in ξ_x and ξ_θ, leads to the following

set of damped coupled Mathieu-Hill variational equations.

$$\underset{\sim}{C}\,\ddot{\underset{\sim}{\xi}} + 2\,\underset{\sim}{\dot{C}}\,\underset{\sim}{\varepsilon}\,\dot{\underset{\sim}{\xi}} + [\underset{\sim}{E} - \tfrac{1}{2}\underset{\sim}{A} - \tfrac{1}{2}\underset{\sim}{B}\cos 2\Omega\tau]\,\underset{\sim}{\xi} = 0 \qquad (2.20)$$

for which details of the derivation and definitions of the coefficient matrices $\underset{\sim}{C}$, $\underset{\sim}{\varepsilon}$, $\underset{\sim}{E}$, $\underset{\sim}{A}$ and $\underset{\sim}{B}$ are available in Appendix C.

The principal region of instability of the above equation is approximated by the criterion established by Bolotin [4] which yields the determinantal equation

$$\begin{vmatrix} \underset{\sim}{E} - \tfrac{1}{2}\underset{\sim}{A} + \tfrac{1}{4}\underset{\sim}{B} - \Omega^2\underset{\sim}{C} & -2\Omega\,\underset{\sim}{C}\,\underset{\sim}{\varepsilon} \\ 2\,\Omega\underset{\sim}{C}\underset{\sim}{\varepsilon} & \underset{\sim}{E} - \tfrac{1}{2}\underset{\sim}{A} - \tfrac{1}{4}\underset{\sim}{B} - \Omega^2\underset{\sim}{C} \end{vmatrix} = 0 \qquad (2.21)$$

for which expansion would result in a fourth order algebraic equation in Ω^2.

Setting the second diagonal term of the above determinant to zero provides a first order approximate value of Ω. Upon substituting this value into all the elements of determinantal Equation (2.21) except the second and fourth elements of the principal diagonal, the expanded form becomes

$$\begin{vmatrix} (1-\frac{1}{4}\frac{A_{11}}{f_2}-\frac{\Omega_\theta^2}{f_2}) & -\frac{1}{4}\frac{A_{12}}{f_2} & -\frac{\Omega_\theta f_1}{f_2} & 0 \\ -\frac{1}{4}\frac{A_{21}}{h_2} & (1-\frac{1}{4}\frac{A_{22}}{h_2}-\frac{\Omega^2}{h_2}) & 0 & -\frac{\Omega_\theta h_1}{h_2} \\ \frac{\Omega_\theta f_1}{f_2} & 0 & (1-\frac{3}{4}\frac{A_{11}}{f_2}-\frac{\Omega_\theta^2}{f_2}) & -\frac{3}{4}\frac{A_{12}}{f_2} \\ 0 & \frac{\Omega_\theta h_1}{h_2} & -\frac{3}{4}\frac{A_{21}}{h_2} & (1-\frac{3}{4}\frac{A_{22}}{h_2}-\frac{\Omega^2}{h_2}) \end{vmatrix} = 0 \qquad (2.22)$$

where the expressions for A_{ij} are given in Appendix C.

The foregoing equation is expanded and, after neglecting terms of higher than the second order in f_1 and h_1, the following quadratic equation results

$$z^2 - (\frac{H_3}{H_2}+\frac{H_4}{H_1})z + (\frac{H_3 H_4}{H_1 H_2}+H_5^2) = 0 \qquad (2.23)$$

in which

$$H_1 = 1-\frac{A_{11}}{4f_2}-\frac{\Omega_\theta^2}{f_2} \qquad (2.24a)$$

$$H_2 = 1 - \frac{3A_{11}}{4f_2} - \frac{\Omega_\theta^2}{f_2} \tag{2.24b}$$

$$H_3 = \left(\frac{A_{22}}{2h_2}\right)H_2 + \frac{9\,A_{12}\,A_{21}}{16\,f_2\,h_2} \tag{2.24c}$$

$$H_4 = \frac{A_{12}\,A_{21}}{16\,f_2\,h_2} \tag{2.24d}$$

$$H_5 = \left(\frac{\Omega_\theta h_1}{h_2}\right) \tag{2.24e}$$

$$z = 1 - \frac{A_{22}}{4h_2} - \frac{\Omega^2}{h_2} \tag{2.24f}$$

The solution of Equation (2.23) can be expressed as

$$\Omega = \left(h_2 - \frac{A_{22}}{4} - h_2\left\{\tfrac{1}{2}\left(\frac{H_3}{H_2} + \frac{H_4}{H_1}\right) \pm \left[\left\{\tfrac{1}{2}\left(\frac{H_3}{H_2} + \frac{H_4}{H_1}\right)\right\}^2 - H_5^2\right]^{\frac{1}{2}}\right\}\right)^{\frac{1}{2}} \tag{2.25}$$

Equation (2.25) is now the stability equation which will be used to determine the influence of torsional damping and to study the potential for torsional coupling of various structural systems.

2.3 CRITICAL TORSIONAL DAMPING

In the preceding, an expression (2.25) has been formulated to determine the condition for torsional coupling in a symmetric system. This expression involves a variety of system parameters such as plan aspect ratio r, torsional frequency Ω_θ, nonlinearity parameter λ, translational and torsional damping coefficients ζ_x, ζ_θ and

system parameters E and F (Appendix A, Equation A4) reflecting the arrangement of resisting elements to be discussed separately.

Equation (2.25) may give rise to complex boundary frequencies if the torsional damping coefficient ζ_θ is taken into consideration, since the quantity within the inner radical becomes negative under certain circumstances. It should be noted that ζ_θ appears as part of only the inner radical term, i.e., in H_5 defined by Equation (2.24e) where $h_1 = 2\,\zeta_\theta \Omega_\theta$ (Equations A5 and A6 of Appendix A). Since the system under consideration is a physical one, the existence of complex frequencies is impossible. Thus, in order to ensure that frequencies remain real, the term within the inner radical must be positive or at least zero. Imposing this condition provides an expression determining the maximum torsional damping $\zeta_{\theta,cr}$ for which induced dynamic torsional coupling is possible. This means

$$\tfrac{1}{2}\left(\frac{H_3}{H_2} - \frac{H_4}{H_1}\right) = H_5 \tag{2.26}$$

This leads to the magnitude of critical torsional damping given by

$$\zeta_{\theta,cr} = \frac{h_3 \bar{P}^2}{8\,\Omega_\theta^2} + \frac{3(h_4 + h_6)\bar{R}^2}{8\,\Omega_\theta^2} + O(\lambda^2) \tag{2.27}$$

where second order form $O(\lambda^2)$ can be neglected.

In the above equation, approximations for the average translational and torsional amplitudes $\bar{P}$ and $\bar{R}$ are necessary to evaluate $\zeta_{\theta,cr}$. Equations (2.18a) and (2.18b), a set of algebraic equations found by the method of averaging, may be used to estimate these

amplitudes.

Since the structure is symmetric, one is interested only in the onset of torsional motion and $\bar{R}$ may therefore by assumed to be small. Consequently, only first order terms in $\bar{R}$ need to be retained in these equations. Similar first order approximation allows the non-linear terms in $\bar{P}$ to be neglected. With these approximations, Equations (2.16a) through (2.16d) become a set of linear algebraic equations yielding the following approximate values of $\bar{P}$ and $\bar{R}$

$$\bar{P} = [(1 - \Omega^2)^2 + (2\,\zeta_x\,\Omega)^2]^{-\frac{1}{2}} \qquad (2.28a)$$

$$\bar{R} = 0 \qquad (2.28b)$$

Tso [5] arrived at similar approximations directly from Equations (2.6) and (2.7) without resorting to the averaging method. However, the general formulation presented here allows the possibility of higher-order analysis in $\bar{P}$ and $\bar{R}$. In addition, when unsymmetric structures with known eccentricity between the centres of stiffness and mass are involved (Chapter III), the magnitude of torsional reponse cannot be neglected as in Equation (2.28b) and estimates of amplitudes, such as provided by Equations (2.18a) and (2.18b), are required. Substituting the approximate values of $\bar{P}$ and $\bar{R}$ from Equations (2.28a,b) into Equation (2.27) leads to the following expression for critical torsional damping

$$\zeta_{\theta,cr} = \frac{h_3 \overline{P}^2}{8 \Omega_\theta^2} \tag{2.29}$$

Equations (2.11) and (2.28a) are identical. Therefore

$$\overline{P} = D \tag{2.30}$$

In static normalization, substituting for h_3 (Appendix A, Equation A5) and $\overline{P}$ (Equation 2.30) yields the specialized expression for critical torsional damping

$$\zeta_{\theta,cr} = \frac{\vartheta \lambda_s E^2 D^2}{8(1 + r^2)\Omega_\theta^2} \tag{2.31}$$

Equation (2.31) involves, along with the usual system variables, the parameter E characterizing the structural geometry.

Figure 2.2a represents the plotting of Equation (2.31) showing the effect of input frequency Ω on critical torsional damping for a typical system. Points falling on the curve indicate the magnitude of torsional damping ratio $\zeta_{\theta,cr}$ required to prevent the initiation of torsional oscillation. For each curve shown, the area below the curve represents the torsionally unstable zone and the area above denotes stable (uncoupled) translational response. It is noted that, in the neighbourhood of $\Omega = 1$, higher torsional damping is necessary to ensure stability against torsional coupling compared to that required for other values of Ω for given system frequency Ω_θ. It is also observed from these curves that, at a particular value of Ω, torsional response may be avoided at lower torsional damping when the torsional

frequency of the structure increases.

Considering dynamic normalization, Equation (2.29) may be cast into the following form after substituting the corresponding expression for h_3 (Appendix A, Equation A6)

$$\zeta_{\theta,cr} = \frac{9\lambda_d E^2}{8(1 + r^2)\Omega_\theta{}^2} \tag{2.32}$$

It is worth noting that Equation (2.31) could have been obtained by simply substituting Equation (2.12) into Equation (2.31).

Dynamic normalization has an advantage over the static normalization procedure in the sense that, while Equation (2.31) will represent the curve for a particular static nonlinearity parameter λ_s, Equation (2.32) represents the curve for any value of λ_s provided dynamic parameter λ_d remains constant. Thus figure (2.2b), representing the plotting of Equation (2.32) shows the behaviour of the system for the whole range of static nonlinearity. In both equations, it is observed that the magnitude of critical torsional damping $\zeta_{\theta,cr}$ increases directly with nonlinearity parameter λ and decreases with aspect ratio r of the system. The latter indicates that nonlinear torsional coupling is more critical for the short direction of a building structure.

Figure (2.2b) also demonstrates the relationship between static and dynamic normalizations. A typical curve of $\zeta_{\theta,cr}$ versus Ω_θ ($r = 1.0$, $\lambda_d = 0.1$) represents an ensemble of structures with an

infinite number of values for translational damping ζ_x, input frequency Ω and static nonlinearity λ_s; i.e., the same curve can be traced for constant $\zeta_x = 0.02$ with Ω and λ_s combinations of 0.2 and .0922, 0.6 and 0.041, 1.0 and 0.00016, 1.4 and 0.0925, and 1.8 and 0.502, and so on. Thus, a single curve for given λ_d represents behaviour for an infinite array of structures with different physical properties defined by ζ_x, λ_s and variable excitation frequency Ω.

Figure 2.3 shows the effect of aspect ratio r on the critical torsional damping for stability, using Equation (2.31). Again, the area under each curve is defined as the unstable zone which is seen to decrease with increase in aspect ratio.

2.4 REGIONS OF INDUCED TORSIONAL COUPLING

In the foregoing, the general criterion for torsional instability of damped systems has been formulated resulting in Equation (2.25). The critical magnitude of torsional damping has also been established (Equations (2.31) and (2.32)) for torsional damping less than this critical value. Equation (2.25) will give rise to two equations describing the upper and lower instability bounds.

2.4.1 Torsionally Undamped Structures

If torsional damping is neglected entirely, Equation (2.25) yields the following respective upper and lower bounds

$$\Omega_\theta^2 = \Omega^2 + \tfrac{3}{4}\{h_3 \bar{P}^2 + 3(h_4+h_6)\bar{R}^2\} + \frac{9 f_5 h_3 \bar{P}^2 \bar{R}^2}{4(1 - \frac{9}{4} f_3 \bar{P}^2 - \frac{3}{4} f_5 \bar{R}^2 - \Omega_\theta^2)} \quad (2.33a)$$

$$\Omega_\theta^2 = \Omega^2 + \tfrac{1}{4}\{h_3\overline{P}^2 + 3(h_4+h_6)\overline{R}^2\} + \frac{f_5 h_3 \overline{P}^2 \overline{R}^2}{4(1-\frac{3}{4}f_3\overline{P}^2-\frac{1}{4}f_5\overline{R}^2-\Omega_\theta^2)} \qquad (2.33b)$$

With the estimation of $\overline{P}$ and $\overline{R}$ given by Equations (2.28) and (2.30), these transform into

$$\Omega_\theta^2 = \Omega^2 + \frac{3h_3 D^2}{4} \qquad (2.34a)$$

$$\Omega_\theta^2 = \Omega^2 + \frac{h_3 D^2}{4} \qquad (2.34b)$$

Following the static normalization procedure described, substituting the expression for h_3 (Appendix A, Equation (A5)) gives*

$$\Omega_\theta^2 = \Omega^2 + \frac{27\lambda_s E^2 D^2}{(1 + r^2)} \qquad (2.35a)$$

$$\Omega_\theta^2 = \Omega^2 + \frac{9\lambda_s E^2 D^2}{4(1 + r^2)} \qquad (2.35b)$$

in which D and E are defined by Equations (2.28a), (2.30) and (A4).

Equations (2.35a,b) are plotted in Figure 2.4 showing the region of induced torsional coupling for stiffness distributed along the boundary. It is noted that the region of instability becomes more pronounced for Ω values between 0.8 and 1.2. It is also interesting to note that the torsional frequency Ω_θ need not be equal to

---

* The corresponding equations and related figures for peripheral systems, where $E = 1.0$, were derived by Tso (Reference [5], Equations (25a,b)) containing inadvertent errors subsequently corrected by [27,6].

input frequency Ω to induce torsional oscillation of the structure.

Torsional stability in a symmetric system implies no torsional response when the input excitation is purely translational. It is observed in Figure 2.4 that the torsional frequency must be greater than the excitation frequency in order for torsional response to occur. At a value of Ω equal to unity, the likelihood of torsional instability is most pronounced. On either side of this point, i.e., $\Omega < 0.8$ and $\Omega > 1.2$, the coupling region narrows and approaches the $\Omega_\theta = \Omega$ line. Hence, away from $\Omega = 1$, the unstable region becomes sufficiently narrow that torsional oscillation is unlikely.

Also plotted in Figure 2.4 is the static torsional buckling region. The static torsional buckling region corresponds to zero magnitude of the apparent torsional frequency Ω_o (see Appendix D, Equation (D3)). This situation can arise for a certain magnitude of translational amplitude $\bar{P}$, described as the critical lateral displacement given by Equation (D5). In terms of static normalization, Equation (D5) may be expressed as

$$\Omega_\theta^2 = \frac{9\lambda_s E^2 D^2}{2(1 + r^2)} \qquad (2.36)$$

which is plotted in Figure 2.4 for stiffness distributed along the boundary. Some overlap between the static torsional buckling region and the zone of torsional coupling is noticed. The boundary of the coupling region is meaningful only when static buckling does not occur. Thus, the portion of the dynamic coupling region overlapping the static buckling region has no physical meaning.

To demonstrate the influence of aspect ratio r and damping ζ_x on the stability, Figures 2.5 and 2.6 show the region of coupling plotted in Ω_θ - Ω parameter space based on Equations (2.35a,b), again for stiffness distributed along the boundary. As shown in Figure 2.5, the unstable region increases with decrease in building plan aspect ratio and shifts away from the $\Omega_\theta = \Omega$ line. Similarly, the unstable region decreases, particularly in the neighbourhood of $\Omega = 1$, and shifts towards the $\Omega_\theta = \Omega$ line with increase in the value of translational damping coefficient ζ_x, as seen in Figure 2.6.

From the above observations, it is evident that uncoupled torsional frequency ratio Ω_θ is an important parameter influencing the torsional stability of a symmetric structure. Tso and Asmis [8] have indicated that the critical value of Ω_θ is restricted to the range 1.11_1 - 1.67. However, it can be observed in Figures 2.5 and 2.6 that the critical range for Ω_θ is strongly influenced by the aspect ratio as well as by the translational damping coefficient.

For dynamic normalization the corresponding equations of the upper and lower bounds of the unstable region are obtained by substituting h_3 (Appendix A, Equation (A6)) into Equations (2.33a,b) giving

$$\Omega_\theta^2 = \Omega^2 + \frac{27\lambda_d E^2}{4(1 + r^2)} \qquad (2.37a)$$

$$\Omega_\theta^2 = \Omega^2 + \frac{9\lambda_d E^2}{4(1 + r^2)} \qquad (2.37b)$$

These equations are independent of translational damping ζ_x and are plotted in Figure 2.7 for a typical system. Similar to Figures 2.4 through 2.6, it may be observed that the stability curves in this figure also lie above the equal frequency line $\Omega_\theta = \Omega$. In this diagram the peaks of Figures 2.4 through 2.5 do not exist and the upper and lower bounds are almost straight lines. Static torsional buckling is also shown, expressed by (from Equations (D5) and (A5))

$$\Omega_\theta^2 = \frac{9\lambda_d E^2}{2(1 + \nu^2)} \tag{2.38}$$

The obvious difference between the coupling regions shown in Figures 2.4 through 2.7 raises the question, which of these curves is the best measure of a system's susceptibility to torsional coupling. This question may also give rise to some misinterpretation when, comparing the work of Tso [5] and Antonelli et al. [6], since the instability regions differ markedly although presented in the same frequency parameter space. Consequently, it needs to be emphasized that the static nonlinearity used by Tso [5] and the dynamic nonlinearity recommended by Antonelli et al. [6] are related by Equation (2.12).

By way of clarification, Figure 2.8 shows that the stability curve for a constant value of λ_d is found to be nothing but the locus of points on the curves for different values of λ_s if the relation of Equation (2.12) is observed. Thus, the stability curves for a constant value of λ_d represent the ensemble of an infinite number of systems with $\lambda_s - \zeta_x$ combinations related by Equation

(2.12). Conversely, the stability bounds for constant λ_s represent systems with an ensemble of $\lambda_d - \zeta_x$ combinations, each also governed by Equation (2.12). For systems with known nonlinearity, the stability curves generated with λ_s will be useful, since λ_s is a unique value, whereas the λ_d curves will apply for systems with unknown nonlinearity because these represent the entire range of λ_s.

2.4.2 Torsionally Damped Structures

The foregoing stability bounds have ignored torsional damping. Equation (2.25) represents the general expression for the stability bounds for any degree of torsional damping. For critical damping the upper and lower bounds merge into a single curve described by the following expression

$$\Omega_\theta^2 = \Omega^2 + \tfrac{1}{2}\{h_3\overline{P}^2 + 3\,(h_4 + h_6)\overline{R}^2\} + \frac{9f_5h_3\,\overline{P}^2\,\overline{R}^2}{8(1 - \frac{9}{4}f_3\overline{P}^2 - \frac{3}{4}f_5\overline{R}^2 - \Omega_\theta^2)} + \frac{f_5h_3\,\overline{P}^2\,\overline{R}^2}{8(1 - \frac{3}{4}f_3\overline{P}^2 - \frac{1}{4}f_5\overline{R}^2 - \Omega_\theta^2)} \tag{2.39}$$

It is observed that Equation (2.39) is the linear average of Equations (2.33a,b); utilizing the approximate values of $\overline{P}$ and $\overline{R}$ from Equations (2.28a,b) and (2.30) reduces the foregoing expression to

$$\Omega_\theta^2 = \Omega^2 + \frac{h_3D^2}{2} \tag{2.40}$$

In terms of static normalization, this may be written as

$$\Omega_\theta^2 = \Omega^2 + \frac{9\lambda_s E^2 D^2}{2(1 + r^2)} \tag{2.41}$$

whereas for dynamic normalization one obtains

$$\Omega_\theta^2 = \Omega^2 + \frac{9\lambda_d E^2}{2(1 + r^2)} \tag{2.42}$$

However, when damping is less than critical, Equation (2.25) gives rise to the following upper and lower bounds

$$\Omega_\theta^2 = \Omega^2 + \left(\frac{2 \pm \sqrt{1 - \kappa^2}}{4}\right)\{h_3\overline{P}^2 + 3(h_4 + h_6)\overline{R}^2\}$$

$$+ \frac{9\,(1 \pm \sqrt{1 - \kappa^2})\, f_5 h_3\, \overline{P}^2\, \overline{R}^2}{8(1 - \frac{9}{4}f_3\overline{P}^2 - \frac{3}{4}f_5\overline{R}^2 - \Omega_\theta^2)} + \frac{(1 \mp \sqrt{1 - \kappa^2})\, f_5 h_3\, \overline{P}^2\, \overline{R}^2}{8(1 - \frac{3}{4}f_3\overline{P}^2 - \frac{1}{4}f_5\overline{R} - \Omega_\theta^2)} \tag{2.43a,b}$$

where parameter κ denotes the degree of critical damping for non-linear torsional coupling given by $\kappa = \zeta_\theta/\zeta_{\theta,cr}$, with the possible range $0.0 \leq \kappa \leq 1.0$. Substituting the approximate expressions of $\overline{P}$ and $\overline{R}$ of Equations (2.28a,b) and (2.30) yields

$$\Omega_\theta^2 = \Omega^2 + \left(\frac{2 + \sqrt{1 - \kappa^2}}{4}\right)h_3 D^2 \tag{2.44a}$$

$$\Omega_\theta^2 = \Omega^2 + \left(\frac{2 - \sqrt{1 - \kappa^2}}{4}\right)h_3 D^2 \tag{2.44b}$$

With static normalization, these become

$$\Omega_\theta^2 = \Omega^2 + \frac{9(2 + \sqrt{1 - \kappa^2})\,\lambda_s\, E^2\, D^2}{4(1 + r^2)} \qquad (2.45a)$$

$$\Omega_\theta^2 = \Omega^2 + \frac{9(2 - \sqrt{1 - \kappa^2})\,\lambda_s\, E^2\, D^2}{4(1 + r^2)} \qquad (2.45b)$$

whereas for dynamic normalization, the corresponding expressions are

$$\Omega_\theta^2 = \Omega^2 + \frac{9(2 + \sqrt{1 - \kappa^2})\,\lambda_d E^2}{4(1 + r^2)} \qquad (2.46a)$$

$$\Omega_\theta^2 = \Omega^2 + \frac{9(2 - \sqrt{1 - \kappa^2})\,\lambda_d E^2}{4(1 + r^2)} \qquad (2.46b)$$

With $\kappa = 1.0$, Equations (2.45) and (2.46) degenerate into Equations (2.41) and (2.42), respectively.

Figures 2.9 and 2.10 show the stability bounds of a system obtained from Equations (2.45) and (2.46) with three different levels of torsional damping, namely: $\zeta_\theta = 0$; $\zeta_\theta = \frac{1}{4}\zeta_{\theta,cr}$; $\zeta_\theta = \zeta_{\theta,cr}$. It is seen that the torsional coupling zone is sensitive to the introduction of torsional damping as would be expected; the region of torsional coupling decreases sharply with increase in torsional damping until, at $\zeta_\theta = \zeta_{\theta,cr}$, coupling is no longer possible.

2.5 INFLUENCE OF STRUCTURAL GEOMETRIES

The preceding formulation for torsional damping and the regions of induced torsional coupling apply for any system with its resisting elements randomly located within the plan area (Figure 2.1). Thus,

Equations (2.31), (2.32), (2.35)-(2.38), (2.41), (2.42), (2.45) and (2.46) contain term E, the coefficient representing the stiffness distribution over the plan area of the building. The expression for E, shown in Equation (A4) of Appendix A, represents the normalized second moment of the translational stiffness k_{ix} about the x-axis. The second stiffness distribution coefficient F represents the corresponding normalized second moment of the translational stiffness k_{iy} about the y-axis. The latter does not appear in the equations because the systems investigated are symmetric and the input excitation is in the x-direction only. However, it can be expected that critical torsional damping, the zones of instability and the magnitude of static torsional buckling will each be influenced by the actual distribution of the resisting elements. Whereas Figures 2.4 through 2.10 were plotted for a system with stiffness distribution parameter set arbitrarily at E = 1.0, i.e. having its resisting elements distributed along the periphery as in References [5,6], in what follows the influence of coefficient E is examined for a variety of commonly used structural strategies.

Figure 2.11 shows typical examples of stiffness distributions encountered in practice namely systems with: (a) periphery resistance; (b) uniformly distributed resistance; (c) central core resistance; (d) nine- and four-column resistances. The plan dimensions are selectively kept constant (2a × 2b) for these systems. Since these structures are symmetric, the magnitudes of coefficients E and F are equal and are related as follows

$$E_p^2 = 3E_d^2 = E_c^2/s = 1.5E_n^2 = E_f^2 \qquad (2.47a)$$

$$F_p^2 = 3F_d^2 = F_c^2/s = 1.5F_n^2 = F_f^2 \qquad (2.47b)$$

where subscripts p, d, c, n and f denote periphery, distributed, core 9- and 4-column systems respectively. The magnitude of E^2 and F^2 for these systems are correspondingly 1.0, 0.33, s^2, 0.67 and 1.0.

Figure 2.12 shows the critical torsional damping curves for these systems obtained from dynamically normalized Equation (2.32). It is observed that, for fixed Ω_θ, the periphery and four-column systems require the largest amount of torsional damping, whereas the core system requires the least. However, to obtain a meaningful comparison, total lateral stiffness K_x and K_y and mass M are assumed equal for all systems. With equal translational stiffness, the torsional frequencies of these systems are related as follows

$$\omega_{p\theta}^2 = 3\omega_{d\theta}^2 = \omega_{c\theta}^2/s^2 = 1.5\omega_{n\theta}^2 = \omega_{f\theta}^2 \qquad (2.48)$$

A relationship between torsional frequency ω_θ and stiffness distribution parameter E exists for the various systems given by

$$\frac{\omega_{p\theta}}{E_p} = \frac{\omega_{d\theta}}{E_d} = \frac{\omega_{c\theta}}{E_c} = \frac{\omega_{n\theta}}{E_n} = \frac{\omega_{f\theta}}{E_f} = \text{constant} \qquad (2.49)$$

The above equation indicates that, for a particular aspect ratio and equal total mass and translational stiffness, the ratio ω_θ/E remains

constant regardless of the actual distribution of resisting elements.

In order to investigate the influence of parameter E on the stability bounds, Equations (2.45a,b) have been plotted in Figure 2.13 for periphery, distributed, core, 9- and 4-column systems. Similarly, Equations (2.46a,d) are plotted in Figure 2.14.* In both, an example set of values for parameters r, λ and ζ_x has been assumed. As these diagrams show, the zone of torsional coupling varies widely with largest area for periphery and 4-column systems and smallest area for the core system. Thus, these diagrams are useful in predicting the torsional stability of different systems. For example, assuming a system with periphery elements to lie within the unstable region, the equivalent distributed system will fall outside the coupling region thereby indicating that the distributed system is less susceptible to nonlinear torsional coupling than the alternative periphery system having equal mass and total lateral stiffnesses. Similarly, the core system encountered in a building relying primarily on a centrally-located elevator shaft for resisting lateral loads will be unlikely to experience nonlinear torsional coupling (see Figures 2.13d and 2.14d).

---

* The special case of a structure simplified to consist of two lateral load resisting elements, with nonzero stiffness in the direction of excitation only, reduces to two straight lines [6].

2.6 GENERALIZED DAMPING AND STABILITY BOUNDS

In order to obtain generalized expressions for critical torsional damping which are independent of the system of resisting elements, Equations (2.31) and (2.32) are normalized with respect to E^2. This yields the following expressions according to static and dynamic normalization, respectively

$$\hat{\zeta}_{\theta,cr} = \frac{9\,\lambda_s D^2}{8(1 + r^2)\hat{\Omega}_\theta^2} \tag{2.50}$$

$$\hat{\zeta}_{\theta,cr} = \frac{9\,\lambda_d}{8(1 + r^2)\hat{\Omega}_\theta^2} \tag{2.51}$$

where generalized torsional frequency $\hat{\Omega}_\theta = \Omega_\theta/E$. Equations (2.50) and (2.51) are plotted in Figure 2.15a,b. It should be recognized that this generalized diagram determines the critical torsional damping for all structural arrangements. Also, Figure 2.15b suffices to represent an ensemble of structures with different combinations of values for ζ_x, λ_s and Ω.

Corresponding generalized upper and lower bound stability curves are obtained from Equation (2.45) for static normalization, given by

$$\hat{\Omega}_\theta^2 = \hat{\Omega}^2 + \frac{9(2 \pm \sqrt{1 - \kappa^2})\,\lambda_s D^2}{4(1 + r^2)} \tag{2.52}$$

and shown in Fgiure 2.16. For dynamically normalized Equation (2.46), the corresponding generalized stability bounds are

$$\hat{\Omega}_\theta^2 = \hat{\Omega}^2 + \frac{9(2 \pm \sqrt{1 - \kappa^2})\ \lambda_d}{4(1 + r^2)} \tag{2.53}$$

which are shown in Figure 2.17. In the above equations, generalized input and system frequencies are defined as

$$\hat{\Omega} = \Omega/E \tag{2.54a}$$

$$\hat{\Omega}_\theta = \Omega_\theta/E \tag{2.54b}$$

Such expressions for the upper and lower bound curves can be formulated for any value of torsional damping ζ_θ less than critical, i.e., $\kappa < 1.0$. It is interesting to note that the generalized upper and lower bounds are identical to those of the periphery and 4-column systems (see Figures 2.13a, 2.14a); this results from $E^2 = 1.0$ for those systems. The diagrams indicate that the torsional coupling region always falls above the equal frequency line $\hat{\Omega}_\theta = \hat{\Omega}$, thus indicating that the structure's torsional frequency must be greater than the exciting frequency for torsional response to occur.

Also plotted in Figures 2.16 and 2.17 is the static torsional buckling region. Some overlap between the static torsional buckling region and the zone of torsional coupling is noticed. The boundary of the torsional coupling region is meaningful only when static buckling does not occur. Thus, that portion of the dynamic coupling region which overlaps the static buckling region has no particular physical meaning.

2.7 CONCLUSIONS

Earlier studies of torsional instability in symmetric structures have been extended. In particular, the originality of the work in the present chapter consists of the introduction of torsional damping and the subsequent study of the susceptibility to nonlinear coupling of a variety of structural systems common in the planning and design of buildings. Within the scope of this investigation, the following conclusions are noted.

1. Both critical torsional damping and the torsional stability bounds are influenced by: nonlinearity parameter λ; building plan aspect ratio r; translational damping coefficient ζ_x; normalized system frequency Ω_θ; normalized input frequency Ω; and the stiffness distribution coefficient E.

2. Critical torsional damping and the associated stability diagrams, obtained from alternative static and dynamic definitions of nonlinearity (λ_s and λ_d), are found to be related by Equation (2.12). While curves for a particular λ_s value represent behaviour for one specific nonlinear force-displacement relation, corresponding diagrams for a fixed value of λ_d, on the other hand, represent an array structures with all possible values of λ_s.

3. The magnitude of critical torsional damping $\zeta_{\theta,cr}$, beyond which induced torsional oscillation due to translational ground excitation only is no longer possible, is directly proportional to nonlinearity parameter λ (i.e., λ_s for

static normalization and λ_d for dynamic normalization), and inversely proportional to $(1 + r^2)$, where r is the plan aspect ratio of the system.

4'. The highest magnitude of critical torsional damping to prevent coupling is required when input normalized frequency $\Omega = 1$; thus, in order to avoid torsional motion it is a conservative measure to incorporate damping equal to $\zeta_{\theta,cr}$ at $\Omega = 1$.

5. The zone of induced torsional coupling is critically influenced by the magnitude of torsional damping; for zero torsional damping the region of torsional coupling is large, it decreases with increase in torsional damping and finally degenerates into a single line at critical torsional damping, thereby indicating complete stability against nonlinear torsional coupling.

6. Translational damping helps to decrease the instability zone of torsional response, i.e., the smaller the translational damping, the greater the likelihood of significant torsional response.

7. The region of induced torsional oscillation is more pronounced for Ω values between 0.8 and 1.2 for a particular value of static nonlinearity parameter λ_s, whereas such motion is more pronounced for decreasing Ω considering dynamic nonlinearity parameter λ_d.

8. It has been shown that, irrespective of which normalization of nonlinearity is used (λ_s or λ_d), torsional oscillation will be induced only when Ω_θ is greater than Ω. While it is known that coincident lateral input and translational frequencies result in translational resonance, coincident torsional and input lateral frequencies (i.e., $\Omega_\theta = \Omega$) do not induce torsional coupling. Parametric excitation is thus possible only when the magnitude of torsional frequency of the system is slightly higher than the translational exciting frequency. Both upper and lower bound stability curves are asymptotic to the $\Omega_\theta = \Omega$ line at higher values of Ω. Also, at larger Ω values the unstable region becomes sufficiently narrow that induced torsional oscillation is unlikely.

9. Building plan aspect ratio r influences the initiation of torsional oscillations in a symmetric structure. Torsional response is more likely if the ground motion is in the direction parallel to the short dimension of a symmetric or nominally symmetric building.

10. The distribution of the resisting elements influences stability against induced torsion; thus, selectively rearranging the resisting elements can eliminate torsional coupling. The zone of torsional coupling shrinks dramatically in magnitude when going from periphery and 4-column systems to a core system.

11. Stability diagrams have been presented in generalized form to identify the susceptibility of structures with different stiffness distributions and equal mass and total lateral stiffness to torsional coupling. If the generalized frequencies $\hat{\Omega}_\theta$ and $\hat{\Omega}$ are such that they fall within the unstable region, torsional motion is to be expected if lateral resisting elements are nonlinear; otherwise the structure is not susceptible to torsional coupling.

Since interest in this chapter has focussed on the initiation of torsional coupling in symmetric structures, the assumption of elastic nonlinearity can easily be justified. Actual magnitudes of response with coupling could, if desired, be estimated by the averaging procedure described. It is, however, recognized that in real situations, such as buildings subjected to earthquake ground excitation, structrual elements are forced into the inelastic range and response amplitudes estimated on the basis of elastic behaviour do not apply. Thus, the minimal contribution to response based on elastic behaviour reported in [6] for torsional coupling fails to represent the real situation. The more realistic time-history analysis reported by Tso [5], on the other hand, assumed nonlinear elastic-plastic and also Ramberg-Osgood behaviour and this showed a 70% increase in response at the periphery of the structure, compared to uncoupled translational response. It must therefore be concluded that, for those structural arrangements which demonstrate a high susceptibility to torsional coupling, incorporating the expected magnitude of response and introducing plastic action for the resisting elements appear to be a useful extension of this work.

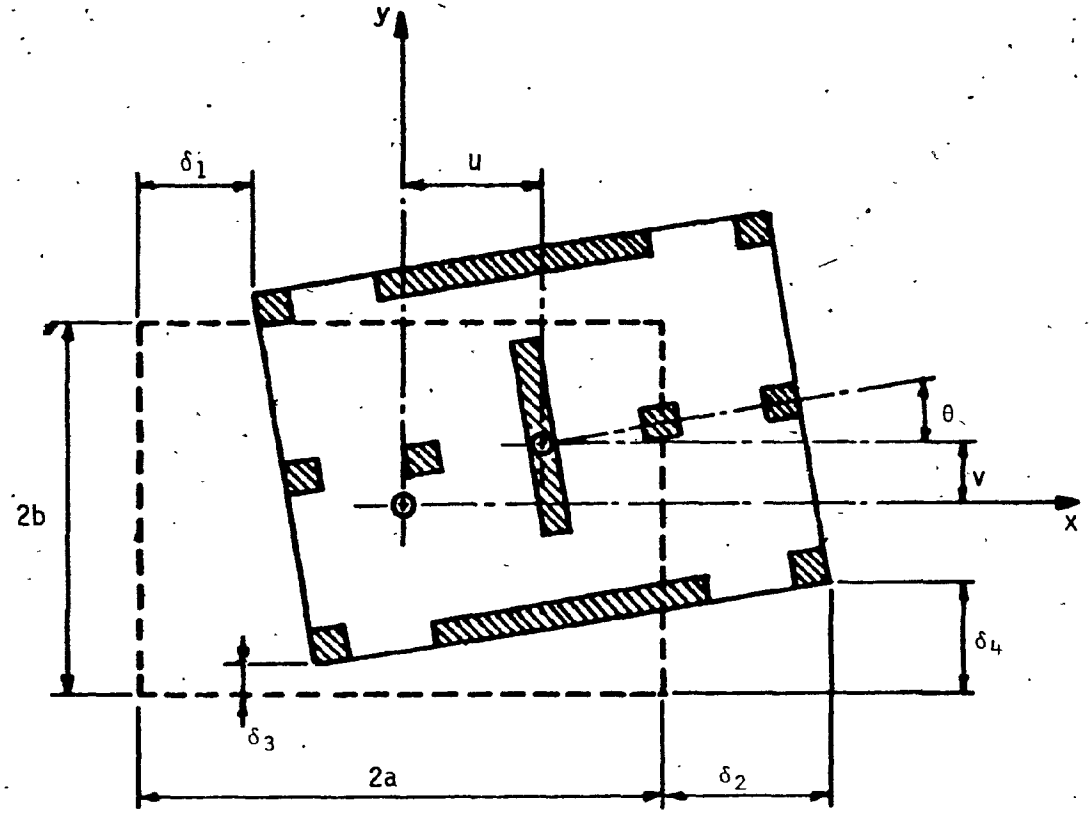

Figure 2.1 Lateral-torsional displacement of symmetric structure with randomly located resisting elements.

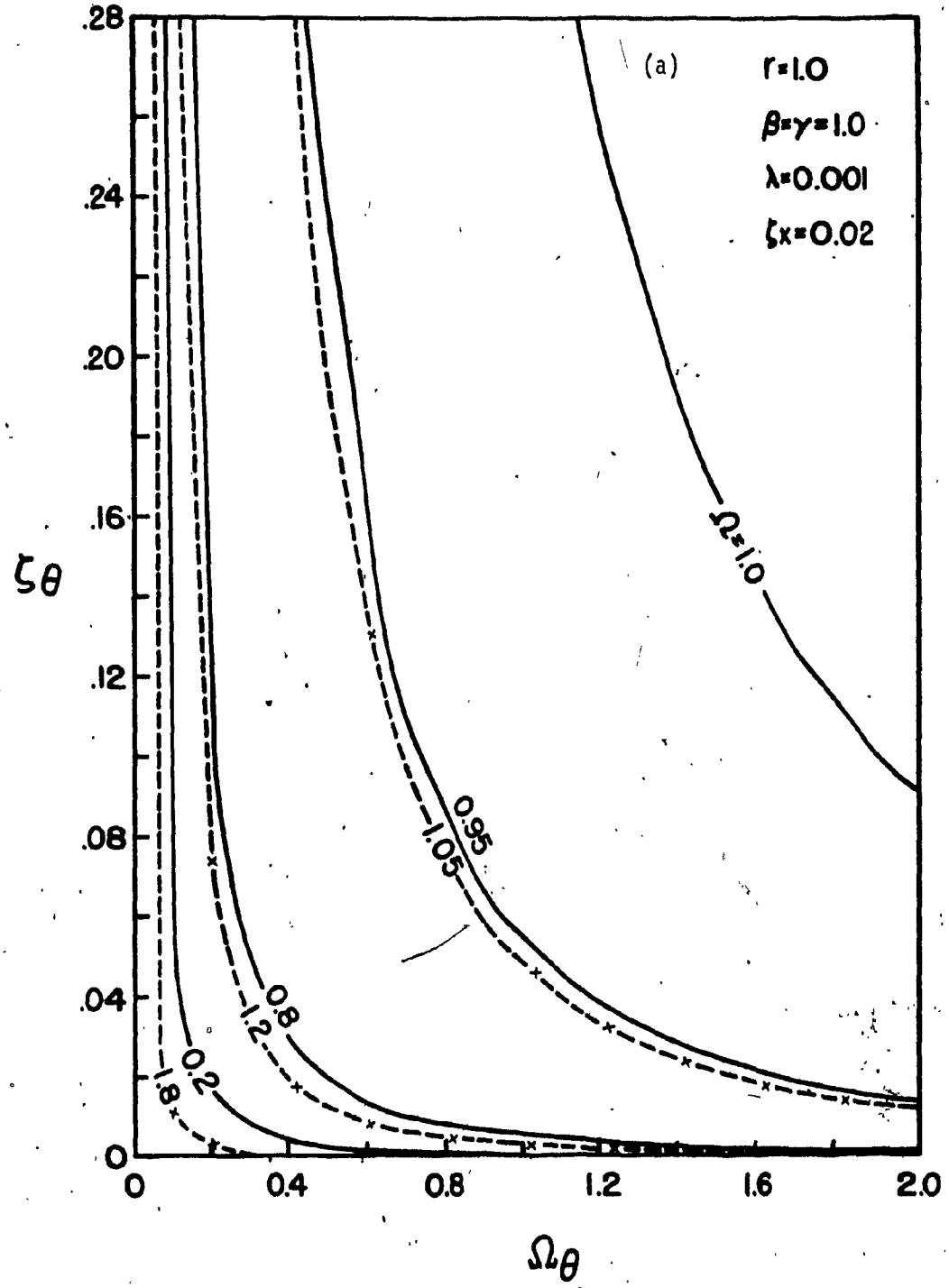

Figure 2.2 Critical torsional damping to prevent coupling (E^2=1.0): (a) static nonlinearity and the effect of input frequency Ω; (b) dynamic nonlinearity.

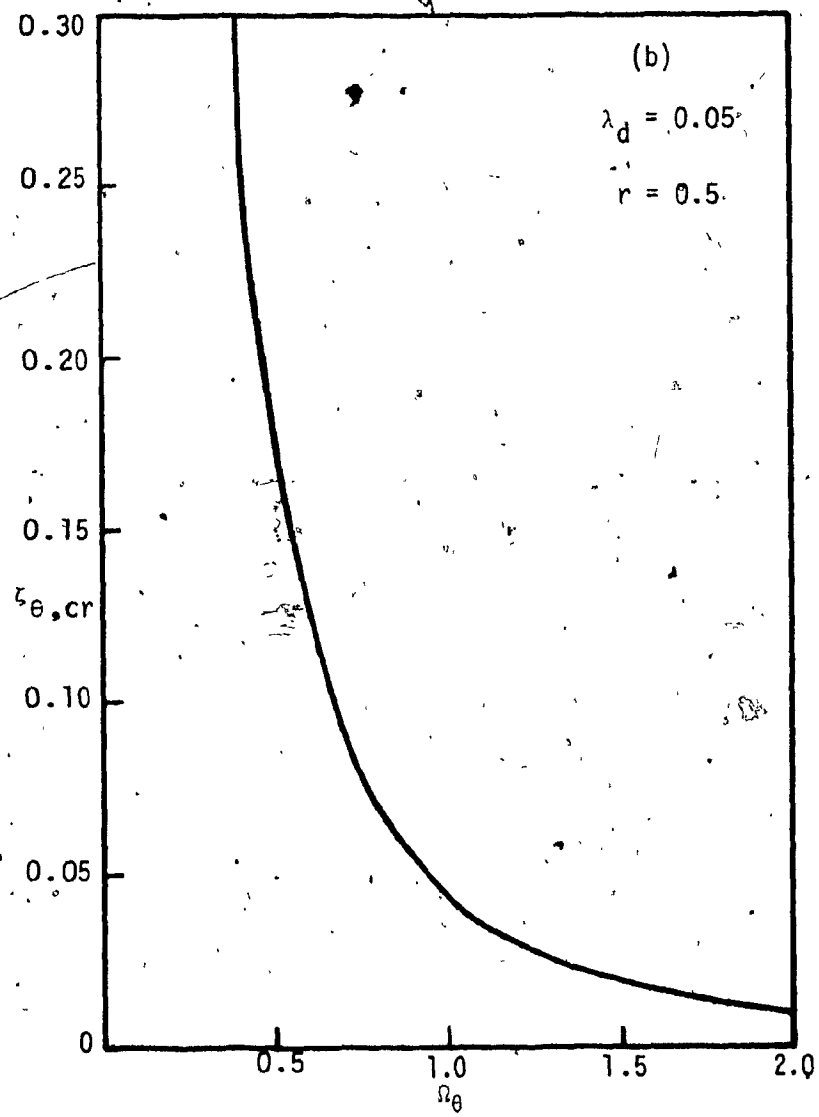

Figure 2.2 Critical torsional damping to prevent coupling (E^2=1.0): (a) static nonlinearity and the effect of input frequency Ω; (b) dynamic nonlinearity.

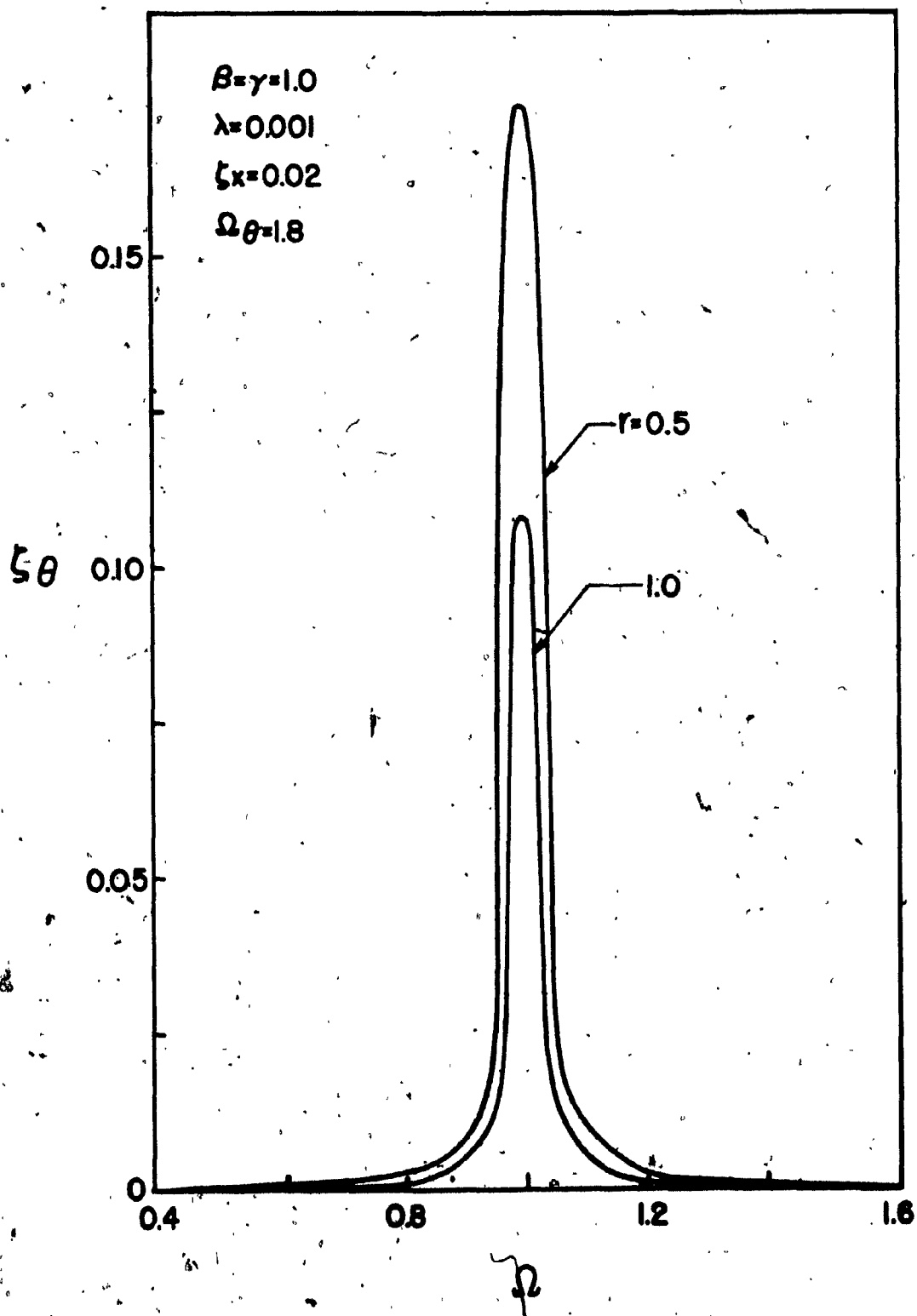

Figure 2.3 Effect of building aspect ratio r on minimum torsional damping (E^2=1.0).

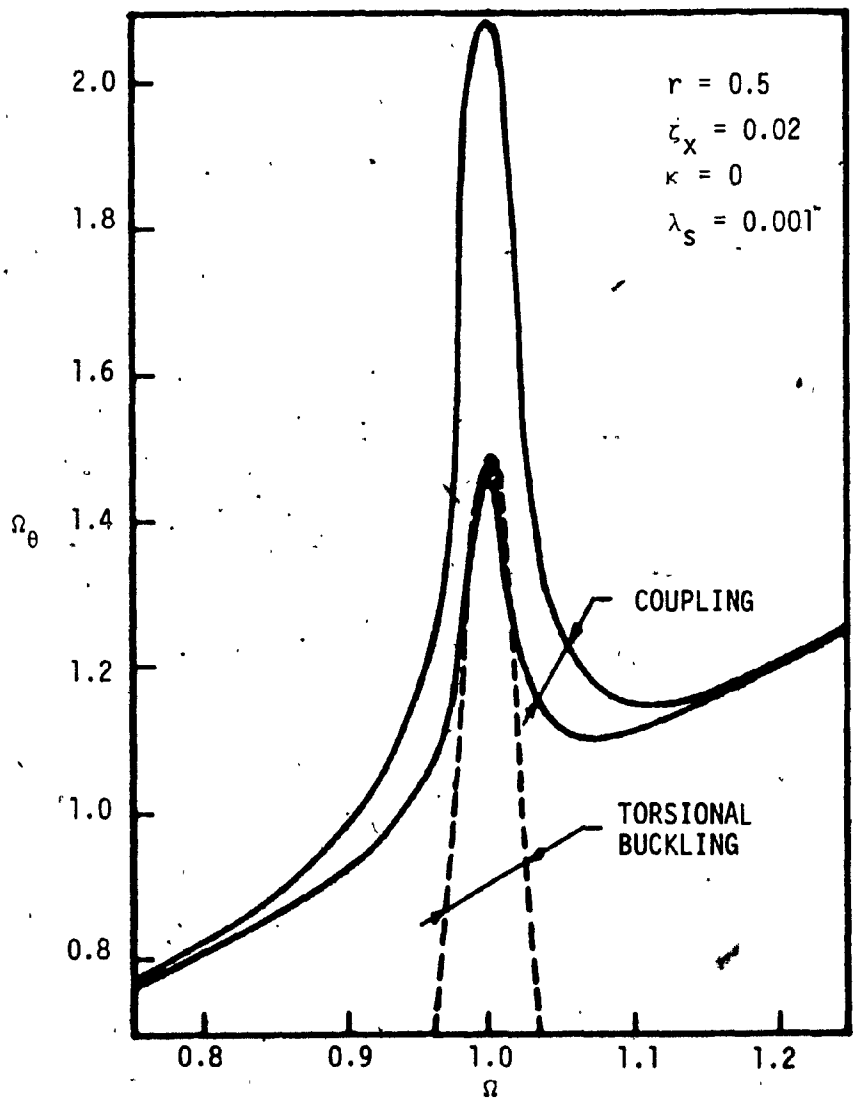

Figure 2.4 Region of torsional coupling for static nonlinearity $\lambda_s = 0.001$.

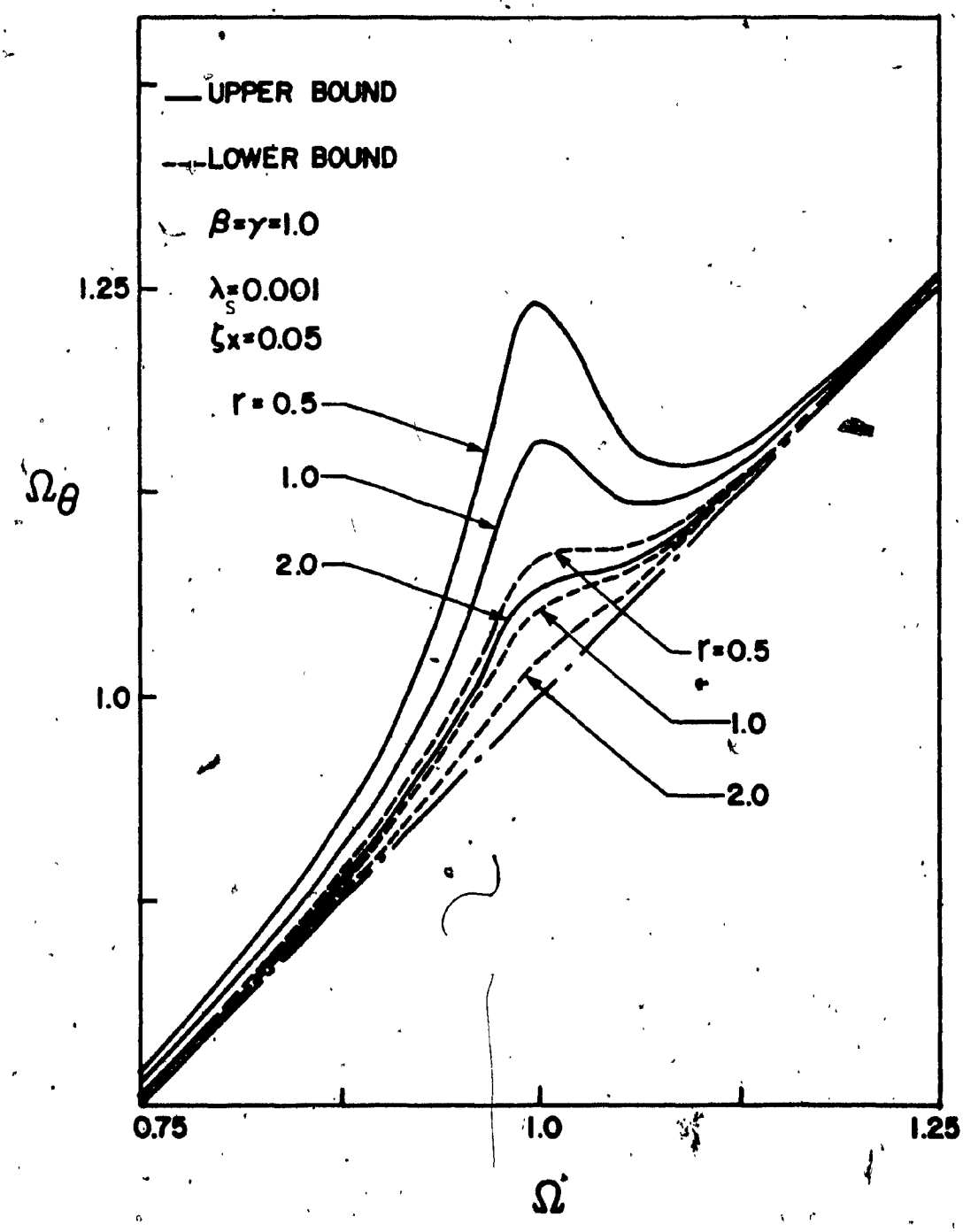

Figure 2.5 Effect of building aspect ratio r on the region of induced torsional response ($E^2 = 1.0$).

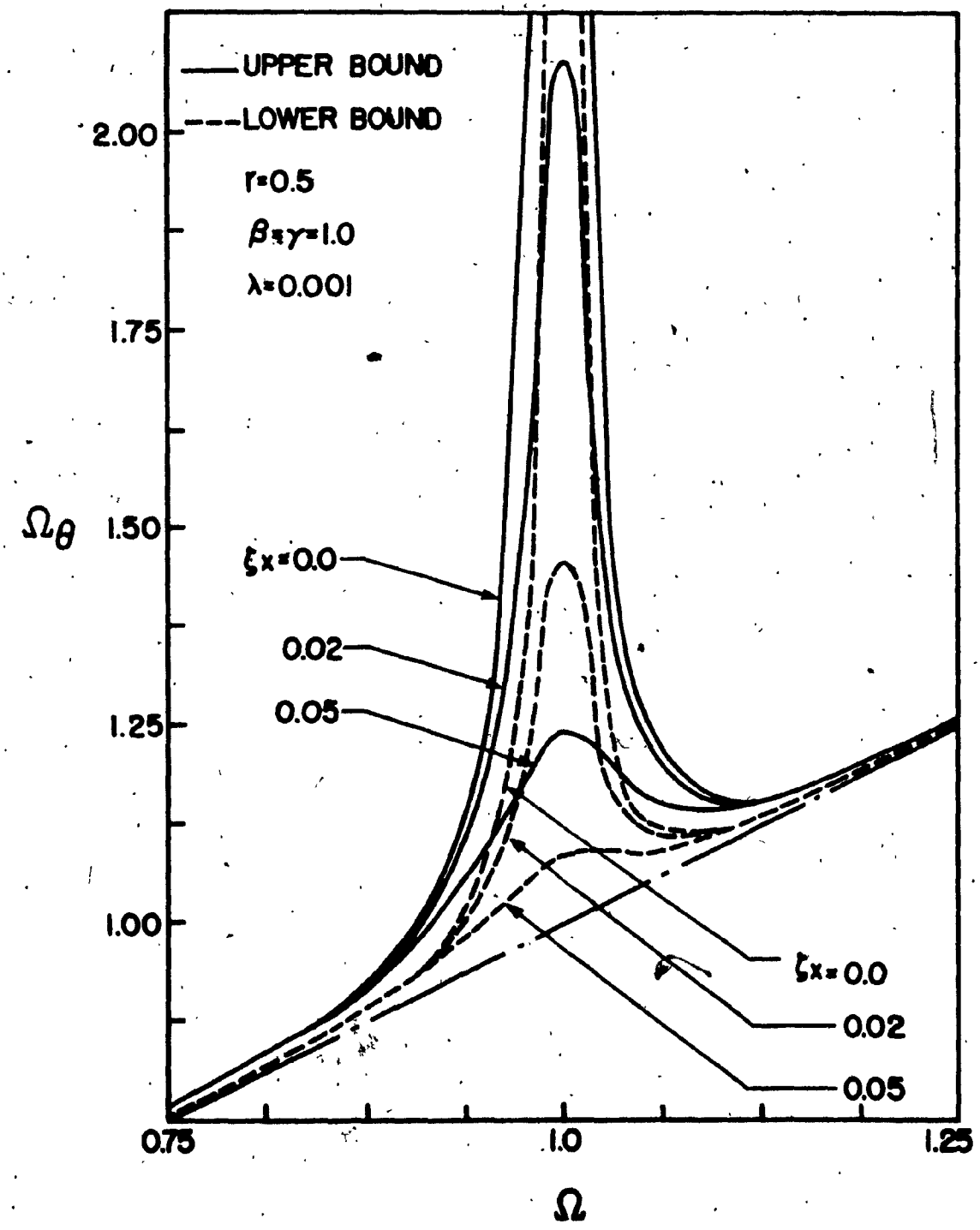

Figure 2.6 Effect of translational damping coefficient ζ_x on the region of induced torsional response ($E^2=1.0$).

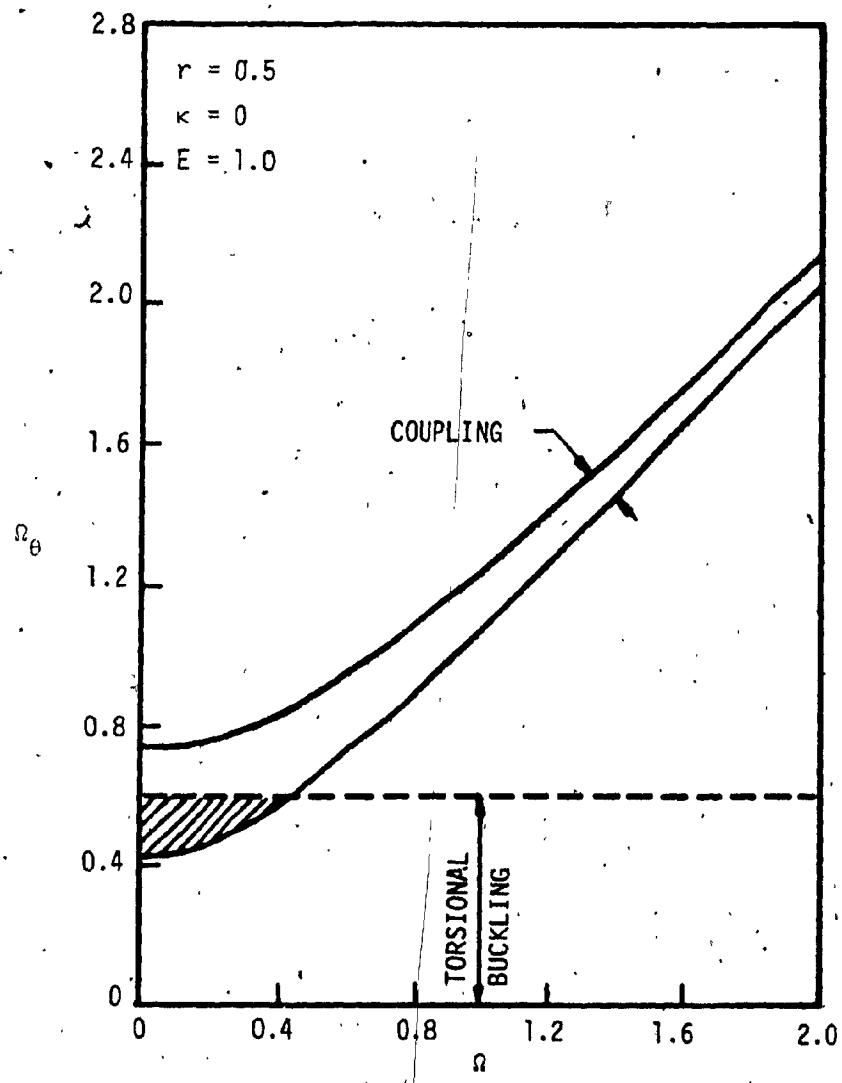

Figure 2.7 Region of torsional coupling for dynamic nonlinearity $\lambda_d = 0.1$.

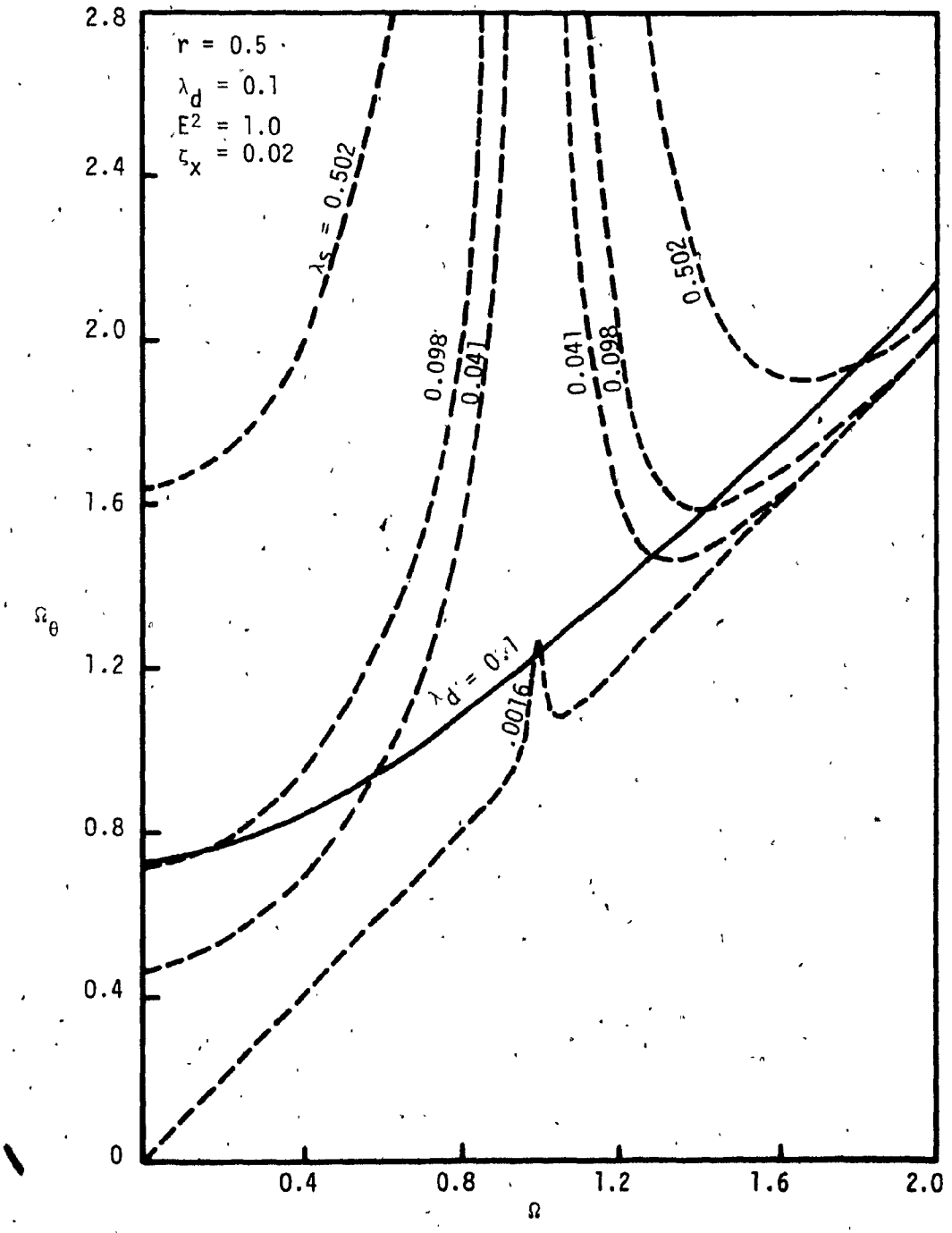

Figure 2.8 Upper bound torsional coupling curve for dynamic nonlinearity λ_d=0.1 clarifying relation with ensemble of curves for λ_s-ζ_x combinations.

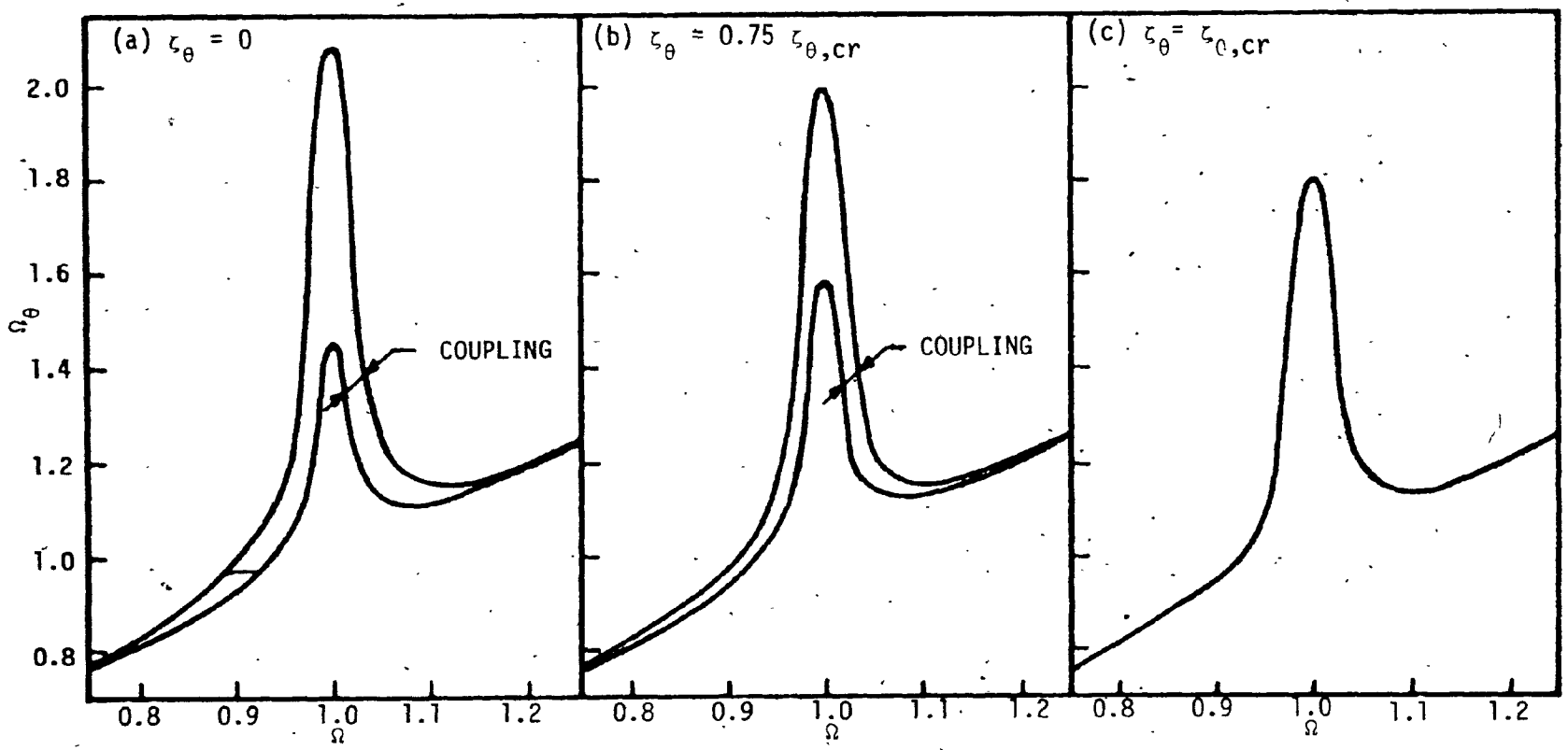

Figure 2.9 Effect of torsional damping on susceptibility to coupled response for static nonlinearity $\lambda_s = 0.001$ ($E^2 = 1.0$, $r = 0.5$, $\zeta_x = 0.02$).

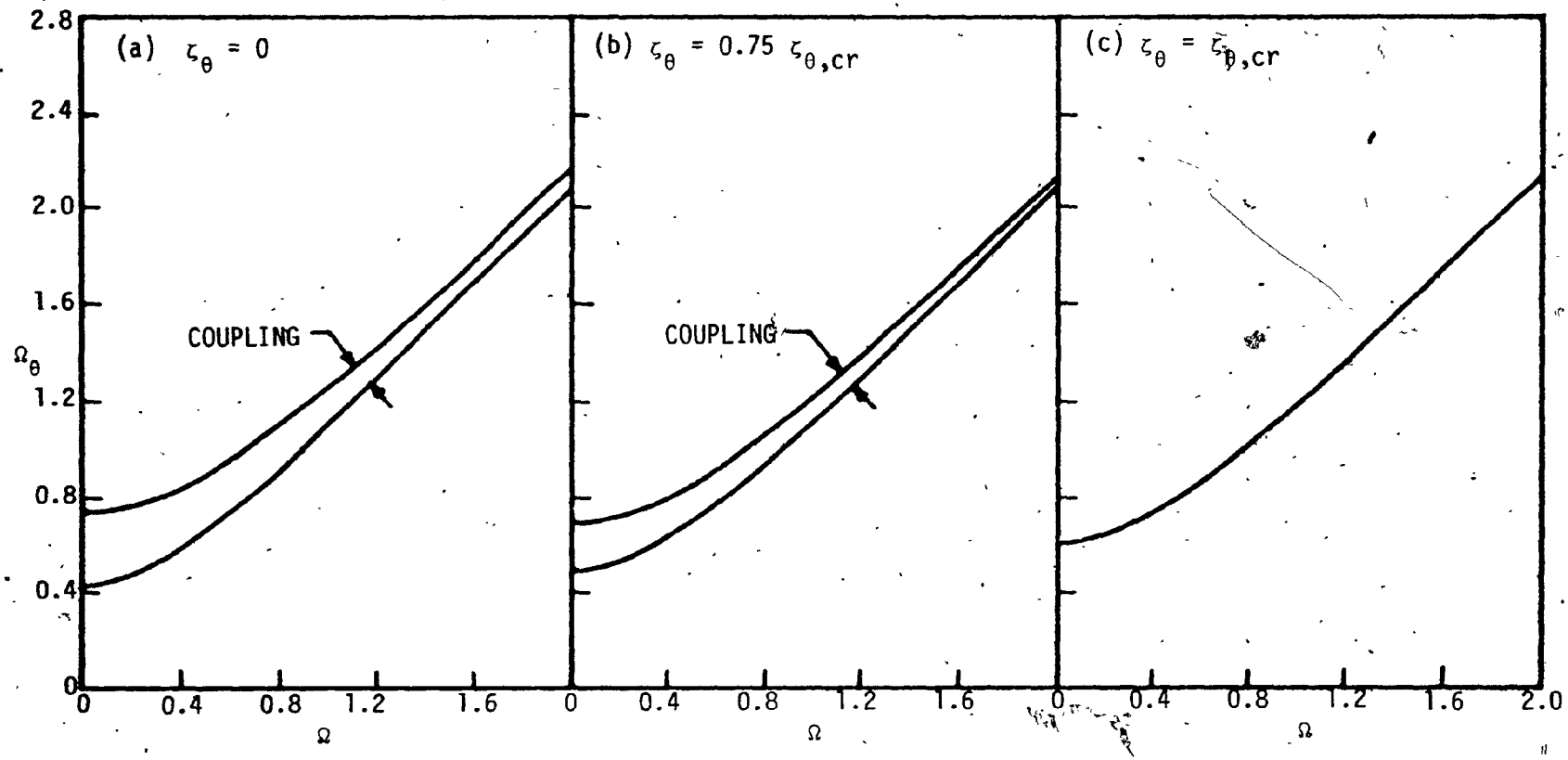

Figure 2.10 Effect of torsional damping on susceptibility to coupled response for dynamic nonlinearity $\lambda_d = 0.1$ ($E^2 = 1.0$, $r = 0.5$).

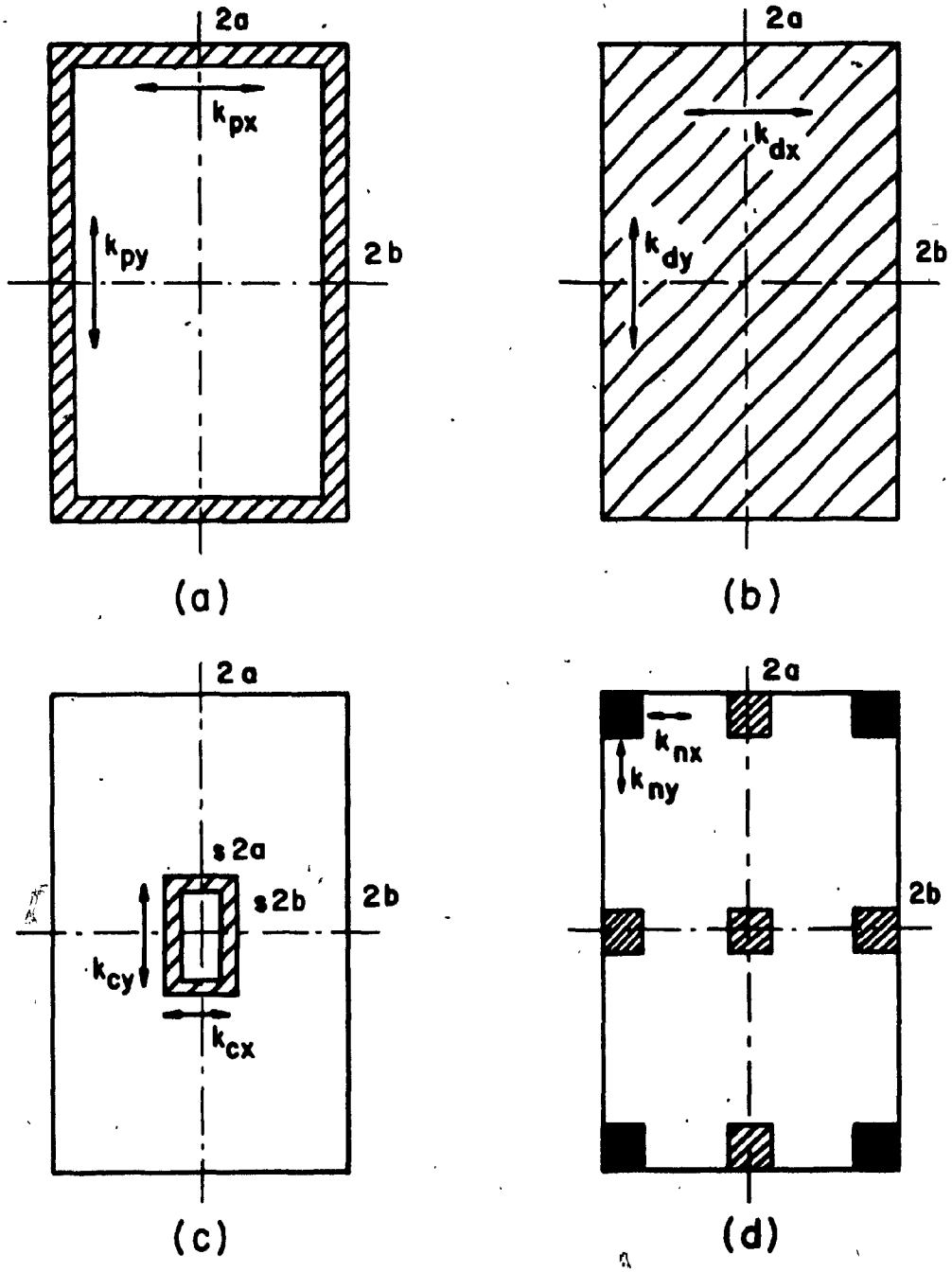

Figure 2.11 Typical structural geometries: (a) periphery resistance (b) uniformly distributed resistance; (c) central core; (d) nine- and four-column systems.

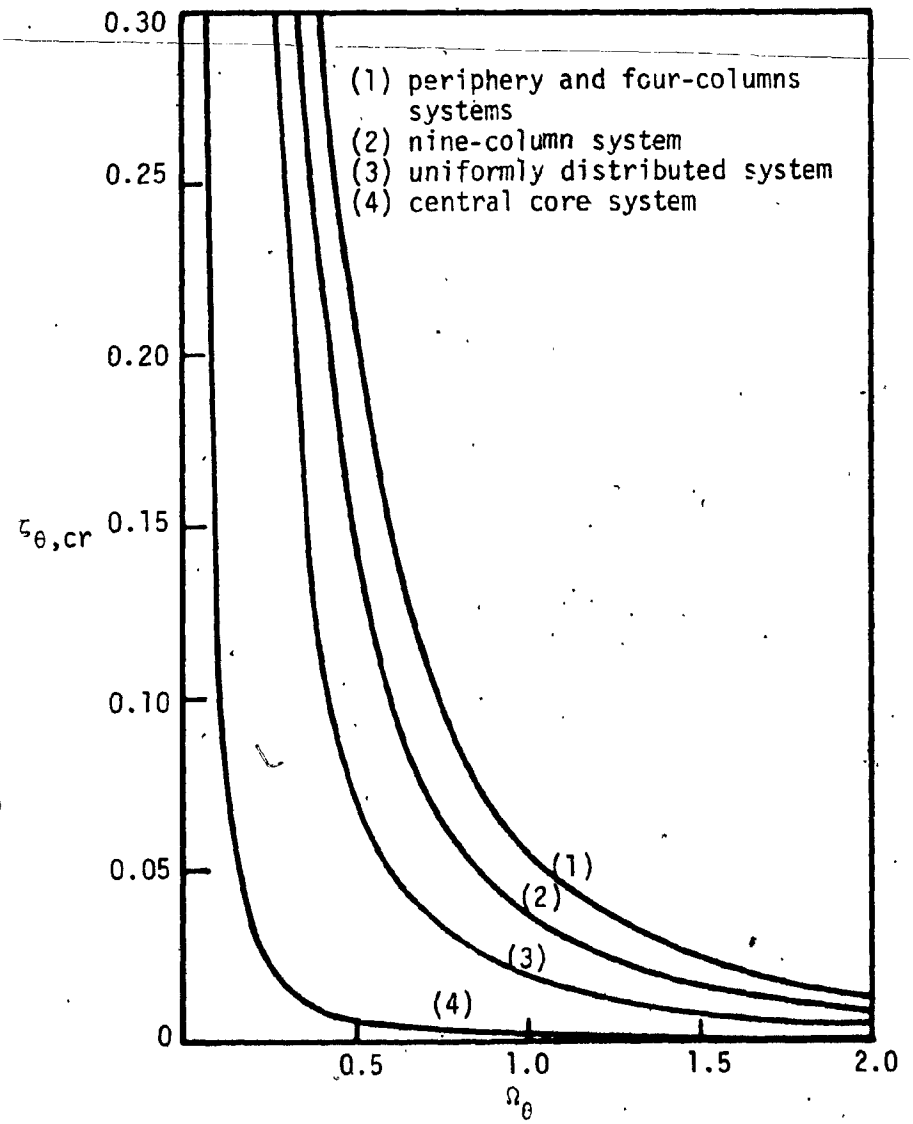

Figure 2.12 Effect of structural geometry on critical torsional damping to prevent coupling (λ_d=0.1, r=1.0).

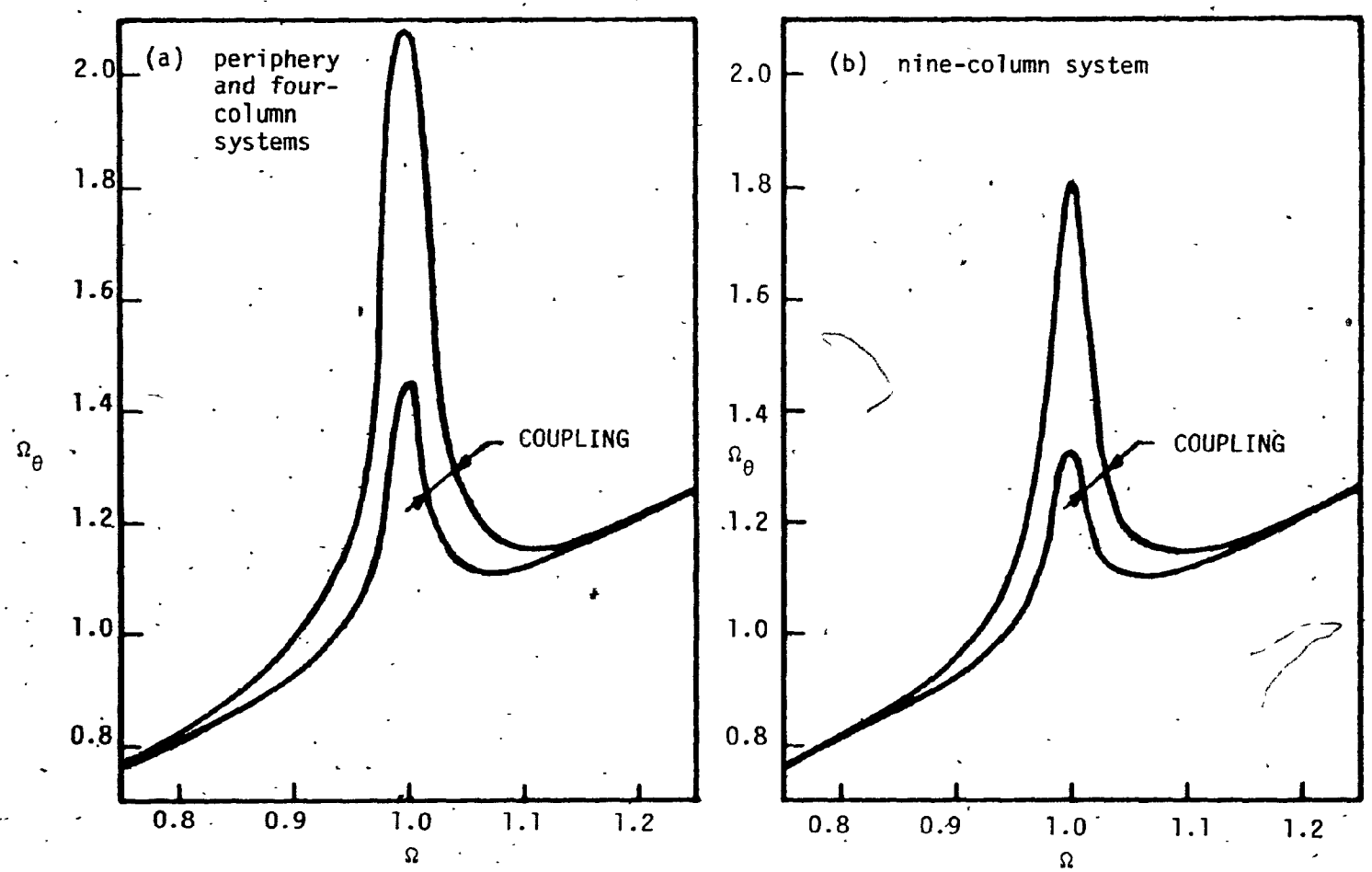

Figure 2.13(a) and 2.13(b)

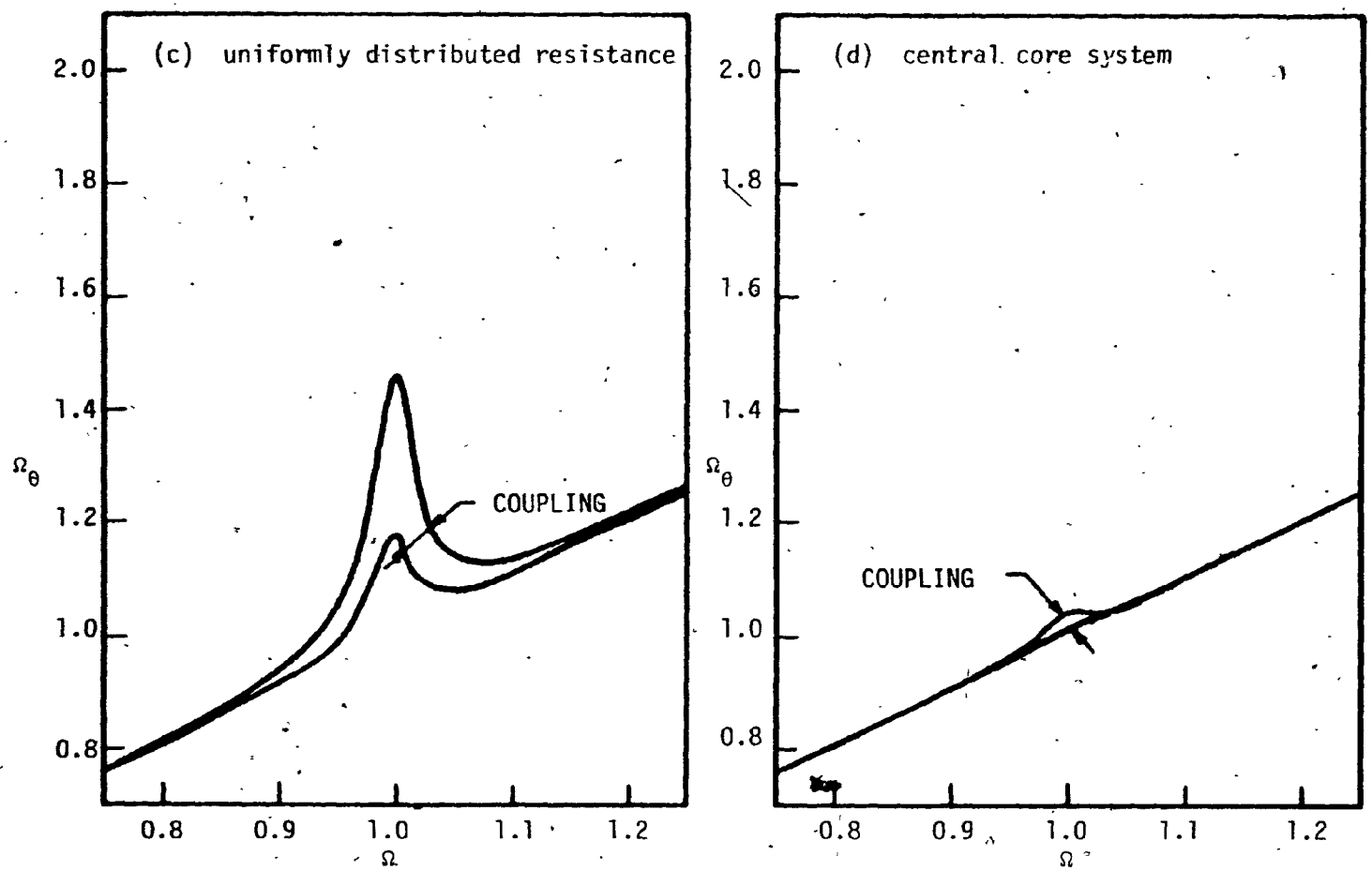

Figure 2.13 Effect of structural geometry on regions of torsional coupling for static nonlinearity $\lambda_s = 0.001$ ($r = 0.5$, $\zeta_x = 0.02$, $\kappa = 0$).

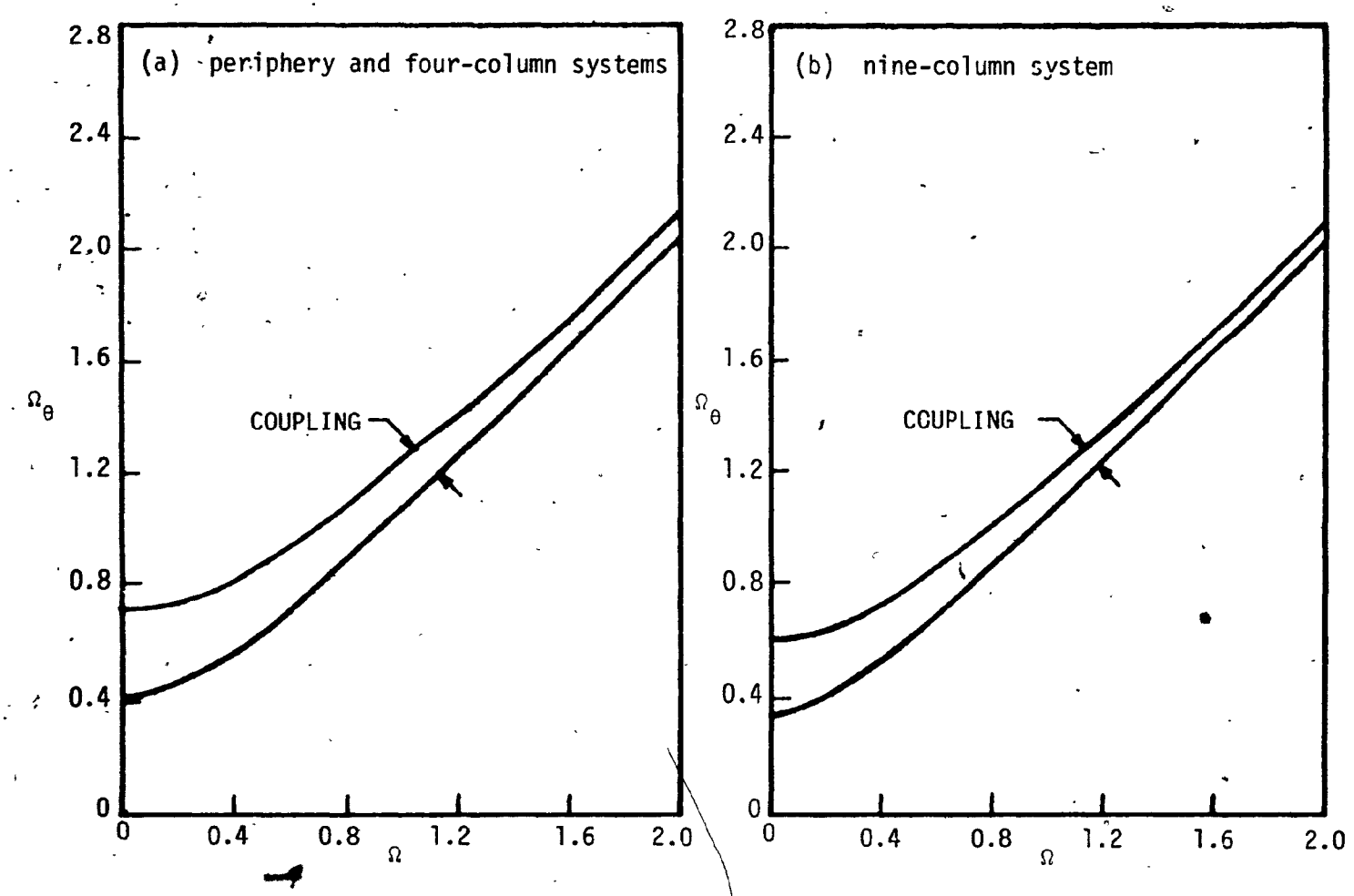

Figure 2.14(a) and 2.14(b)

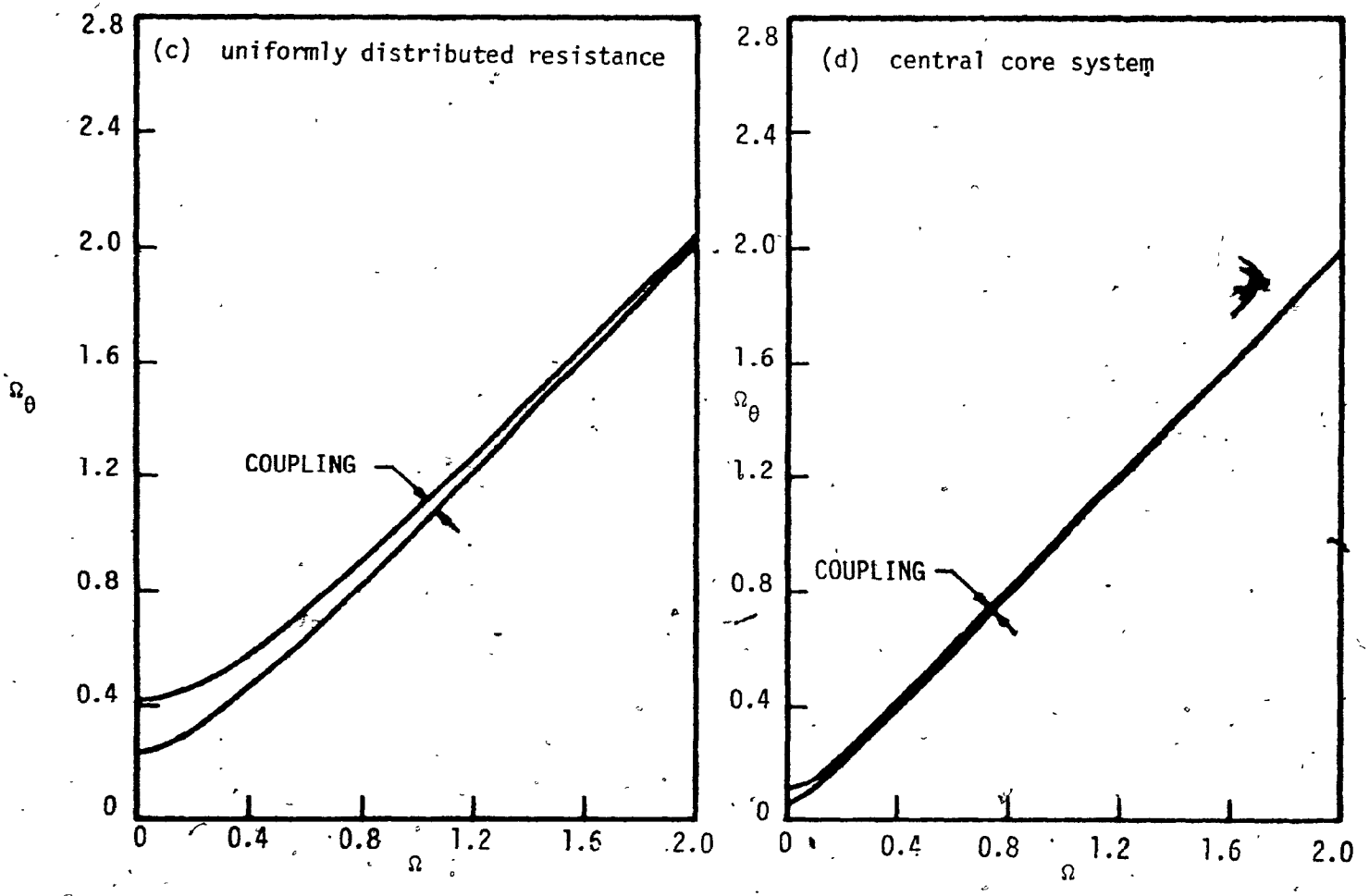

Figure 2.14 Effect of structural geometry on regions of torsional coupling for dynamic nonlinearity $\lambda_d = 0.1$ ($r = 0.5$, $\kappa = 0$).

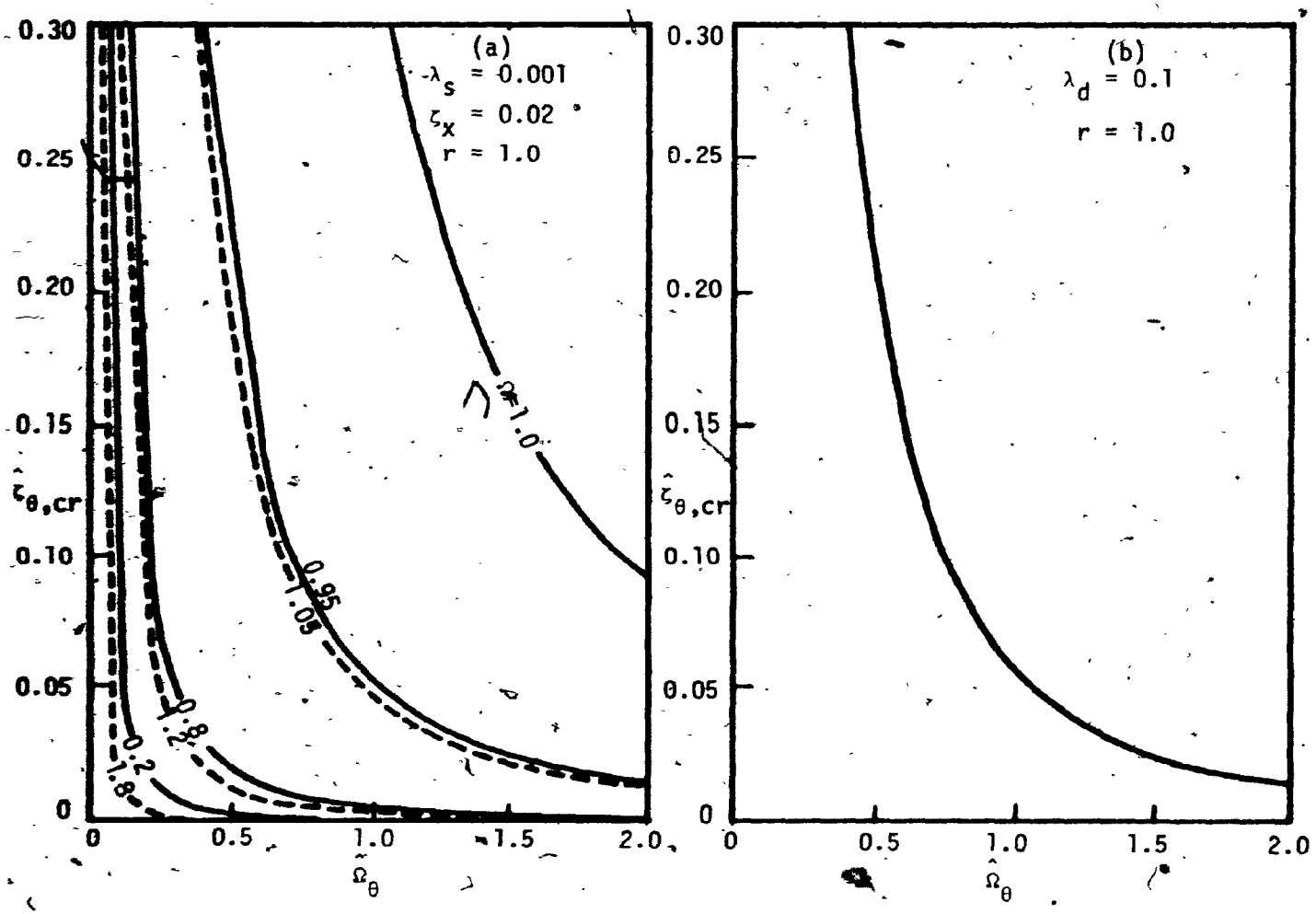

Figure 2.15 Generalized critical torsional damping: (a) static nonlinearity; (b) dynamic nonlinearity.

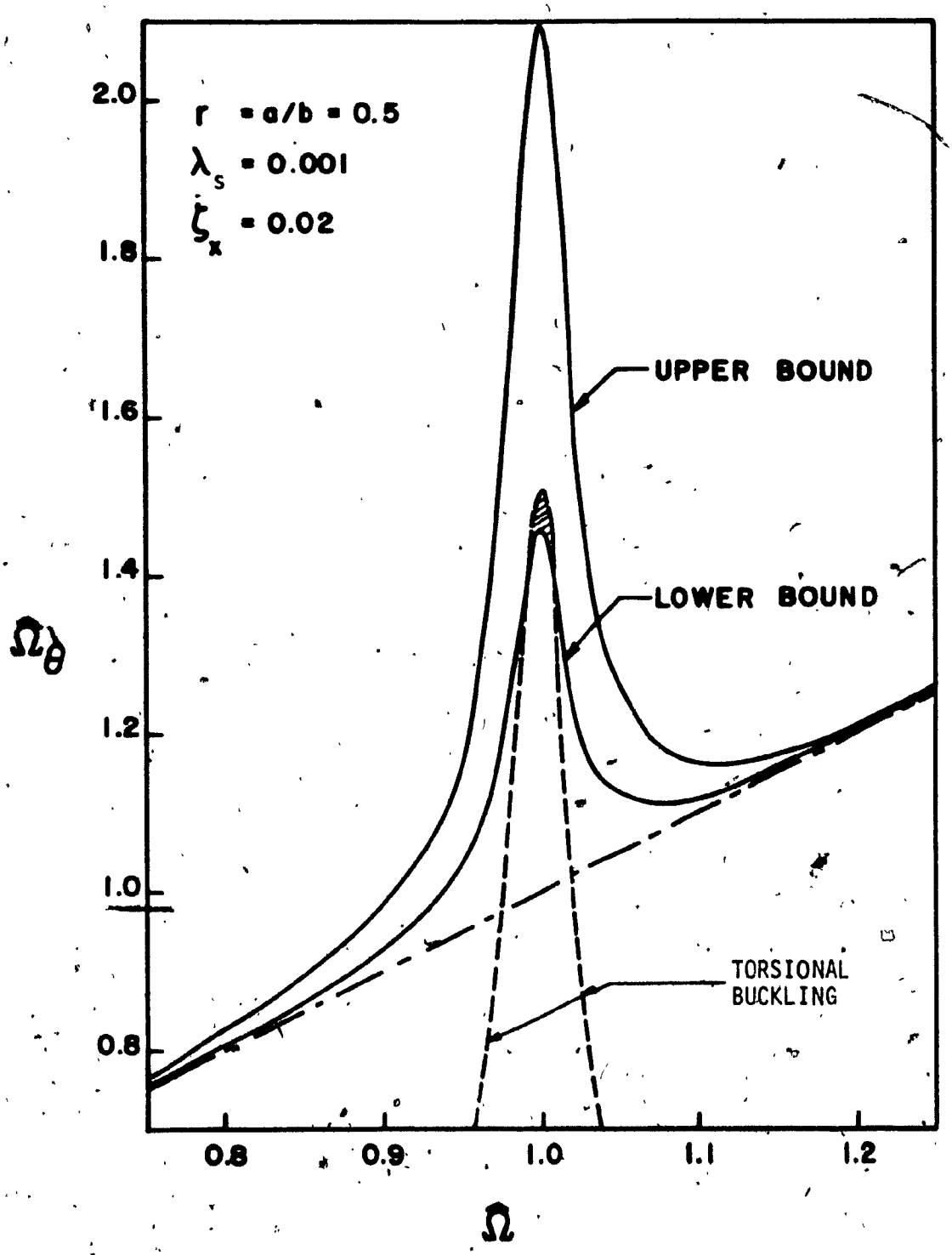

Figure 2.16 Generalized region of torsional coupling for static nonlinearity $\lambda_s = 0.001$, $\kappa = 0$.

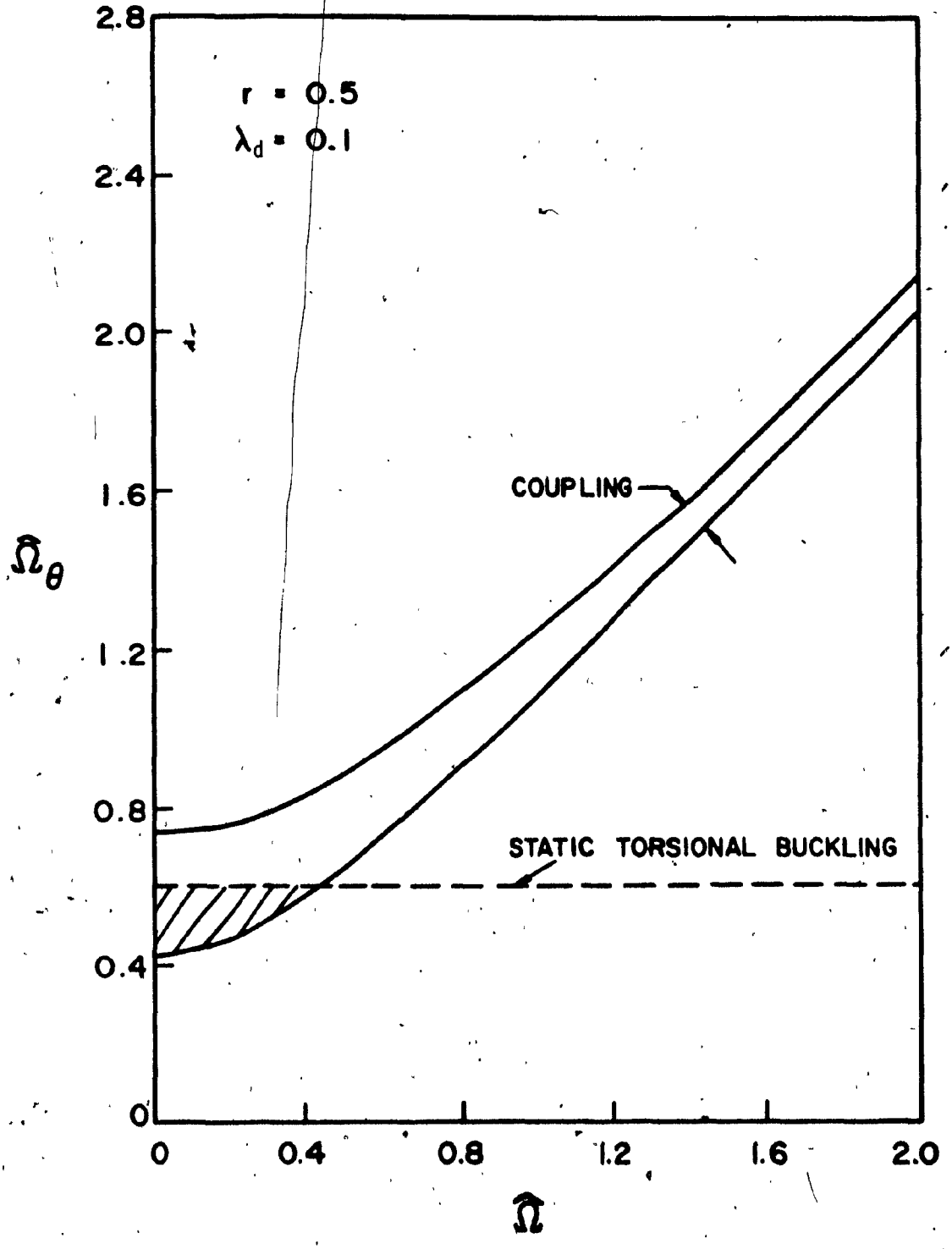

Figure 2.17 Generalized region of torsional coupling for dynamic nonlinearity $\lambda_d = 0.1$; $\kappa = 0$.

CHAPTER III

INSTABILITY IN ELASTIC ASYMMETRIC STRUCTURES

3.1 INTRODUCTION

In the preceding chapter, the instability of symmetric systems with nonlinear elastic resisting elements has been studied in some detail. It will now be worthwhile to investigate how asymmetric systems behave when the resisting elements exhibit similar nonlinear elastic characteristics, particularly since the existing studies of linear unsymmetric structures [16-22], as well as of nonlinear symmetric structures [5-6], are not directly applicable in predicting the behaviour of structures that are both nonlinear elastic and unsymmetric.

Thus, the method presented in Chapter II is extended to systems having either single or double eccentricity (see Figure 3.1). As was the case for symmetric systems, the resisting elements are considered randomly distributed over the plan area when single eccentricity is introduced, whereas for double eccentricity resisting elements are along the periphery. In both the singly and doubly eccentric systems, translational and torsional viscous damping has been included.

It is shown that the nonlinear equations of motion are governed by a set of two or three damped coupled Mathieu-Hill type equations which also exhibit regions of instability. For illustration, torsional stability curves for an example L-shaped building plan are presented and the effect of torsional damping on the instability is

investigated. Convergence problems, encountered in the form of 'gaps' in the resulting closed form solution, are also examined.

3.2 SYSTEMS WITH SINGLE ECCENTRICITY

3.2.1 Governing Equations of Motion

Similar to the symmetric system investigated in Chapter II, the simple structure idealized here also consists of a rigid deck supported on massless, axially inextensible resisting elements randomly located over the plan area but with the centre of resistance eccentric only in the y-direction (Figure 3.1 with $e_x = 0.$). The load displacement relationship of resisting elements is taken to be weakly nonlinear, elastic and of the softening type with cubic nonlinearity expressed by Equation (2.2). The structure is subjected to sinusoidal ground excitation in the x-direction given by Equation (2.5).

Since ground excitation exists only in the x-direction and the structure is monosymmetric (i.e., $e_x = 0$ in this section) translational displacement u in the x-direction and rotational displacement θ about a vertical axis represent the degrees-of-freedom. Thus, the system is governed by the following two equations of motion

$$\ddot{u} + 2\zeta_x\omega_x \dot{u} + \omega_x^2 u \{1 - \varepsilon(u^2 + 3\bar{b}^2\theta^2)\}$$

$$- \omega_x^2 e_y\theta \{1 - \varepsilon(3u^2 + b^2\theta^2)\} = -U \cos \omega t \qquad (3.1)$$

$$\ddot{\theta} + 2\,\zeta_\theta\omega_\theta\,\dot{\theta} + \omega_\theta^2\theta - \frac{\omega_x^2 e_y}{\Gamma^2}\,u\{1 - \varepsilon(u^2 + 3\,b^2\theta^2)\}$$

$$- \varepsilon\theta(\alpha_1 u^2 + \alpha_2\theta^2) = 0 \qquad (3.2)$$

in which the expressions for ε, α_1 and α_2 are the same as those in the symmetric system of chapter II, given by Equation (2.8); Γ is the mass radius of gyration defined by $\Gamma^2 = (a^2+b^2)/3$; ζ_x and ζ_θ are the viscous damping ratios; ω_x and ω_θ may be interpreted as the uncoupled lateral and torsional frequencies about the centre of mass (Equation (A2)); and e_y denotes the eccentricity of the centre of resistance with respect to the centre of mass.

Throughout the derivation in the present chapter, the static reference displacement $\delta_{0,s}$ is used; thus, all subsequent equations and discussions refer to the static normalization procedure.

For the sake of convenience, Equations (3.1) and (3.2) are expressed in the following nondimensional form following the procedure of Appendix A

$$\ddot{\Lambda}_x + f_1\dot{\Lambda}_x + f_2\Lambda_x - (f_3\Lambda_x^3 + f_4\Lambda_x^2\Lambda_\theta + f_5\Lambda_x\Lambda_\theta^2$$

$$+ f_6\Lambda_\theta + f_7\Lambda_\theta^3) = -\cos\Omega\tau \qquad (3.3)$$

$$\ddot{\Lambda}_\theta + h_1\dot{\Lambda}_\theta + h_2\Lambda_\theta - \{(h_4+h_6)\,\Lambda_\theta^3 + h_9\Lambda_\theta^2\Lambda_x + h_3\Lambda_\theta\Lambda_x^2$$

$$+ h_7\Lambda_x + h_8\Lambda_x^3\} = 0 \qquad (3.4)$$

Coefficients f_i and h_i, except f_4, f_6, f_7, h_7, h_8 and h_9, are identical to those found for the symmetric system and are given in Appendix A, Equation (A5). Also, nondimensional frequencies Ω_θ and Ω, both normalized with respect to the translational frequency ω_x, are given in Appendix A, Equation (A2). Expressions for additional coefficients f_4, f_6, f_7, h_7, h_8, and h_9 are given in the following

$$f_4 = -3\lambda E_y/\Omega_\theta^2 \qquad h_7 = E_y \Omega_\theta^2 \tag{3.5a}$$

$$f_6 = E_y/\Omega_\theta^2 \qquad h_8 = -\lambda E_y \Omega_\theta^2 \tag{3.5b}$$

$$f_7 = -\lambda E_y \gamma_0^2 \Omega_\theta^6 \qquad h_9 = -3\lambda E_y \gamma_0^2/\Omega_\theta^2 \tag{3.5c}$$

It should be noted that Equations (3.3) and (3.4) involve the added terms of Equation (3.5), as compared to Equation (2.13) and (2.14), because of the eccentricity of the centre of resistance with respect to the mass centre. Thus, the expressions for the coefficients of Equation (3.5) involve the nondimensional eccentricity E_y, expressed as

$$E_y = e_y/r \tag{3.6}$$

3.2.2 Approximate Solution for Response Amplitudes

This section presents an approximate solution for the translational and torsional response amplitudes applying the method of averaging

[29] for Equations (3.3) and (3.4). Here also, the solution is assumed in the form of slowly-varying sinusoidal expressions since the non-linearity is assumed to be small. Thus, the solutions for Λ_x and Λ_θ are expressed as shown in Equation (2.15). Following the averaging method described in Appendix B, a set of four algebraic equations, similar to Equation (2.16) for the symmetric system but this time for a singly eccentric system, is obtained; namely,

$$(f_2-\Omega^2)\,\bar{P} - \tfrac{3}{4} f_3 \bar{P}^3 - \tfrac{1}{4} f_5 \bar{P}\,\bar{R}^2\,(1+2\cos^2\bar{\Delta}_2) - \tfrac{3}{4}\bar{R}\,(f_4\,\bar{P}^2 + f_7\,\bar{R}^2)\cos\bar{\Delta}_2 - f_6\,\bar{R}\cos\bar{\Delta}_2 = -\cos\bar{\Phi} \tag{3.7a}$$

$$f_1\Omega\,\bar{P} - (\tfrac{1}{4} f_4\,\bar{P}^2\,\bar{R} + f_6\,\bar{R} + \tfrac{3}{4} f_7\,\bar{R}^3)\sin\bar{\Delta}_2 - \tfrac{1}{4} f_5\,\bar{P}\,\bar{R}^2 \sin 2\bar{\Delta}_2 = \sin\Phi \tag{3.7b}$$

$$(h_2-\Omega^2)\,\bar{R} - \tfrac{3}{4}(h_4+h_6)\,\bar{R}^3 - \tfrac{1}{4} h_3\,\bar{P}^2\,\bar{R}\,(1+2\cos^2\bar{\Delta}_2) - \tfrac{3}{4}\bar{P}\,(h_8\,\bar{P}^2 + h_9\,\bar{R}^2)\cos\bar{\Delta}_2 - h_7\,\bar{P}\cos\bar{\Delta}_2 = 0 \tag{3.7c}$$

$$h_1\Omega\,\bar{R} + (\tfrac{1}{4} h_9\,\bar{P}\,\bar{R}^2 + h_7\,\bar{P} + \tfrac{3}{4} h_8\,\bar{P}^3)\sin\bar{\Delta}_2 + \tfrac{1}{4} h_3\,\bar{P}^2\,\bar{R}\sin 2\bar{\Delta}_2 = 0 \tag{3.7d}$$

where $\bar{P}$, $\bar{R}$, $\bar{\Phi}$ and $\bar{x}$ are the average amplitudes and phase angles

over one cycle and $\bar{\Delta}_2$ represents the average phase difference shown in Equation (2.17).

Equation (3.7) can be solved using a standard numerical technique and the stability of the response can be examined in amplitude-frequency parameter space. However, in the following an attempt is made to obtain an approximate closed-form solution for $\bar{P}$ and $\bar{R}$ with the following two additional assumptions.

(a) Since the nonlinearity is assumed to be small, the response amplitudes will not be far from those for linear solutions; thus, as a first-order approximate solution only the linear terms in $\bar{P}$ and $\bar{R}$ are retained in Equation (3.7).

(b) It is also assumed that both the translational and torsional responses will maintain a negligibly small phase lag (or probably zero), i.e., the magnitude of $\bar{\Delta}_2$ will be negligibly small as evident from the time history response in symmetric structures by Tso and Asmis [8]; thus one may assume $\sin \bar{\Delta}_2 \simeq \bar{\Delta}_2$ and $\cos \bar{\Delta}_2 \simeq 1.0$.

The reason of finding such closed-form expressions will become obvious later in this chapter when the torsional stability bounds are examined.

With the foregoing first-order assumptions, one may note that all terms in Equation (3.7) containing the nonlinearity parameter λ will be absent. After imposing the second assumption (i.e., regarding phase angle $\bar{\Delta}_2$), Equation (3.7) transforms into a set of linear algebraic equations as follows

$$(f_2 - \Omega^2)\,\bar{P} - f_6\,\bar{R} = -\cos\bar{\Phi} \tag{3.8a}$$

$$f_1\,\Omega\,\bar{P} - f_6\,\bar{R}\,\bar{\Delta}_2 = \sin\bar{\Phi} \tag{3.8b}$$

$$(h_2 - \Omega^2)\,\bar{R} - h_7\,\bar{P} = 0 \tag{3.8c}$$

$$h_1\,\Omega\,\bar{R} + h_7\,\bar{P}\,\bar{\Delta}_2 = 0 \tag{3.8d}$$

Equation (3.8) is readily solved and, after substituting the values of coefficients f_1, f_2, f_6, h_1, h_2 and h_7 from Equations (3.5) and (A6), the following expressions for $\bar{P}$ and $\bar{R}$ are obtained

$$\bar{P}^2 = \frac{1}{\left[\left\{(1-\Omega^2) - \frac{E_y^2}{\Omega_\theta^2-\Omega^2}\right\}^2 + 4\Omega^2\left\{\zeta_x + \frac{\zeta_\theta\Omega_\theta E_y^2}{(\Omega_\theta^2-\Omega^2)^2}\right\}^2\right]} \tag{3.9a}$$

$$\bar{R} = \left(\frac{E_y\Omega_\theta^2}{\Omega_\theta^2-\Omega^2}\right)\bar{P} \tag{3.9b}$$

It should be remembered that it is erroneous to use Equation (3.9) to examine the stability of response amplitude because this equation does not involve nonlinearity parameter λ. The sole purpose of obtaining Equation (3.9) is to obtain a first-order approximation of amplitudes to be used later in this chapter for the investigation of torsional coupling due to nonlinearity.

However, these first-order approximations in $\bar{P}$ and $\bar{R}$ involve nondimesional eccentricity, translational and torsional damping coefficients, and torsional and input frequency ratios. For a symmetric

structure, where eccentricity is zero, it can be seen that Equation (3.9) transforms readily into Equation (2.28). As is obvious from Equation (3.9), torsional response amplitudes cannot be neglected in investigating the torsional stability of an eccentric system, at least not for systems with medium to large eccentricities.

3.2.3 Condition for Torsional Instability

In order to investigate the stability of coupled response by the same procedure as adopted in Chapter II for symmetric systems, solutions for response are made to undergo small perturbations $\xi_x(\tau)$ and $\xi_\theta(\tau)$. Following the procedure described in Appendix C, equations of motion (3.3) and (3.4) are transformed into a set of damped coupled Mathieu-Hill variational equations which are identical in form to Equation (2.20), but with minor differences in the coefficient matrices $\underset{\sim}{A}$ and $\underset{\sim}{B}$ to accommodate the effect of eccentricity (Appendix E).

Since the form of the equations for an eccentric system remains the same as that for the symmetric system, the determinantal form given in Equation (2.21) representing the principal region of instability will also remain valid for the eccentric system, except that some of the coefficients of the determinantal equation are modified for the eccentric system. The expanded form of this determinantal equation is also shown in Appendix E, Equation (E3).

Equation (E3) is expanded and, after neglecting terms higher than the second order in f_1 and h_1, the following quadratic equation results

$$z^2 - \left(\frac{H_3}{H_2} + \frac{H_4}{H_1}\right) z + \left(\frac{H_3 H_4}{H_1 H_2} + H_5^2\right) = 0 \qquad (3.10a)$$

$$H_1 = 1 - \frac{A_{11}}{4f_2} - \frac{\Omega_\theta^2}{f_2} \qquad (3.10b)$$

$$H_2 = 1 - \frac{3A_{11}}{4f_2} - \frac{\Omega_\theta^2}{f_2} \qquad (3.10c)$$

$$H_3 = \frac{A_{22}}{2h_2} H_2 + \left(\frac{3}{4}\frac{A_{12}}{f_2} + \frac{2f_6}{f_2}\right)\left(\frac{3}{4}\frac{A_{21}}{h_2} + \frac{2h_7}{h_2}\right) \qquad (3.10d)$$

$$H_4 = \left(\frac{1}{4}\frac{A_{12}}{f_2} + \frac{2f_6}{f_2}\right)\left(\frac{1}{4}\frac{A_{21}}{h_2} + \frac{2h_7}{h_2}\right) \qquad (3.10e)$$

$$H_5 = \frac{\Omega_\theta h_1}{h_2} \qquad (3.10f)$$

$$z = 1 - \frac{A_{11}}{4h_2} - \frac{\Omega^2}{h_2} \qquad (3.10g)$$

The solution of Equation (3.10a) can be expressed in the same form as Equation (2.25), because Equations (2.24) and (3.10a) are identical. Thus, Equation (2.25) forms the stability equation also for a single-eccentricity system but with H_1 to H_5 given in Equations (3.10b-g). The latter can be used to determine the influence of torsional damping on the zone of torsional coupling in a monosymmetric system.

3.2.4 Critical Torsional Damping

In order to avoid complex frequencies, the inner radical term of Equation (2.25) is set to a positive value or at least zero. This

condition provides an expression for the maximum torsional damping $\zeta_{\theta,cr}$ for which induced dynamic torsional coupling is still possible. This leads to the magnitude of critical torsional damping, which after substituting the expressions for f_i and h_i, takes the form

$$\zeta_{\theta,cr} = \frac{3\lambda}{8\Omega_\theta^2}\left\{\left(\frac{\gamma_0^2E^2(\gamma_0^2-\beta_0^2)+\beta_0^2\Omega_\theta^2}{\Omega_\theta^4}\right)\bar{R}^2 - \frac{2E_y\gamma_0^2}{\Omega_\theta^2}\bar{P}\bar{R} + \gamma_0^2E^2\bar{P}^2\right\}$$
$$+\frac{E_y^2\left\{1-\frac{9\lambda}{4}\left(\bar{P}^2-\frac{\gamma_0^2(1+E^2)}{E_y\Omega_\theta^2}\bar{P}\bar{R}+\frac{\gamma_0^2}{\Omega_\theta^4}\bar{R}^2\right)\right\}}{\Omega_\theta^2\left\{1-\frac{9\lambda}{4}\left(\bar{P}^2-\frac{2E_y}{\Omega_\theta^2}\bar{P}\bar{R}+\frac{\gamma_0^2}{\Omega_\theta^4}\bar{R}^2\right)-\Omega_\theta^2\right\}}$$
$$-\frac{E_y^2\left\{1-\frac{3\lambda}{4}\left(\bar{P}^2-\frac{\gamma_0^2(1+E^2)}{E_y\Omega_\theta^2}\bar{P}\bar{R}+\frac{\gamma_0^2}{\Omega_\theta^4}\bar{R}^2\right\}\right.}{\Omega_\theta^2\left\{1-\frac{3\lambda}{4}\left(\bar{P}^2-\frac{2E_y}{\Omega_\theta^2}\bar{P}\bar{R}+\frac{\gamma_0^2}{\Omega_\theta^4}\bar{R}^2\right)-\Omega_\theta^2\right\}} \qquad (3.11)$$

The foregoing equation requires average translational and torsional amplitudes $\bar{P}$ and $\bar{R}$ which can be estimated from Equation (3.9). Since Equation (3.9) is a function of ζ_θ, an iterative approach is necessary in order to satisfy both Equations (3.9) and (3.11). It should be noted that Equation (3.11) transforms into Equation (2.31), specialized for a symmetric structure after substituting $E_y = 0$.

Figure 3.2 displays the critical torsional damping curve for a typical unsymmetric system in which a "gap" or discontinuity in the solution is encountered in the neighbourhood of Ω_θ=1.0. Similar critical damping curves for a doubly eccentric system will be presented in Section 3.3.4.

3.2.5 Stability Bounds

In the absence of torsional damping, Equation (2.25) yields the

following upper and lower bound expressions for the stability boundaries

$$\Omega_\theta^2 = \Omega^2 + \frac{9\lambda}{4}\{(\frac{\gamma_0^2\, E^2\, (\gamma_0^2-\beta_0^2)+\beta_0^2\Omega_\theta^2}{\Omega_\theta^4})\,\bar{R}^2 - \frac{2E_y\gamma_0^2}{\Omega_\theta^2}\,\bar{P}\,\bar{R} + \gamma_0^2\, E^2\,\bar{P}^2\}$$

$$+ \frac{4E_y^2\{1 - \frac{9\lambda}{4}(\bar{P}^2 - \frac{\gamma_0^2(1+E^2)}{E_y\,\Omega_\theta^2}\,\bar{P}\,\bar{R} + \frac{\gamma_0^2}{\Omega_\theta^4}\,\bar{R}^2)\}}{\{1 - \frac{9\lambda}{4}(\bar{P}^2 - \frac{2E_y}{\Omega_\theta^2}\,\bar{P}\,\bar{R} + \frac{\gamma_0^2}{\Omega_\theta^4}\,\bar{R}^2) - \Omega_\theta^2\}} \qquad (3.12a)$$

$$\Omega_\theta^2 = \Omega^2 + \frac{3\lambda}{4}\,(\frac{\gamma_0^2\, E^2(\gamma_0^2-\beta_0^2)+\beta_0^2\Omega_\theta^2}{\Omega_\theta^4})\,\bar{R}^2 - \frac{2E_y\gamma_0^2}{\Omega_\theta^2}\,\bar{P}\,\bar{R} + \gamma_0^2\, E^2\,\bar{P}^2\}$$

$$+ \frac{4E_y^2\{1 - \frac{3\lambda}{4}(\bar{P}^2 - \frac{\gamma_0^2\,(1+E^2)}{E_y\,\Omega_\theta^2}\,\bar{P}\,\bar{R} + \frac{\gamma_0^2}{\Omega_\theta^4}\,\bar{R}^2)\}}{\{1 - \frac{3\lambda}{4}(\bar{P}^2 - \frac{2E_y}{\Omega_\theta^2}\,\bar{P}\,\bar{R} + \frac{\gamma_0^2}{\Omega_\theta^4}\,\bar{R}^2) - \Omega_\theta^2\}} \qquad (3.12b)$$

In the above equations, the average magnitude of $\bar{P}$ and $\bar{R}$ can be found from Equation (3.9) after setting the term containing ζ_θ to zero, since Equation (3.12) has been derived neglecting torsional damping.

Corresponding expressions for upper and lower stability bounds, similar to Equation (2.43) for symmetric structures, could be derived for non-zero torsional damping. However, for the sake of simplicity the present investigation of eccentric structures is limited to the stability of torsionally undamped system.

In figure 3.3, Equations (3.12a) and (3.12b) are plotted for a typical single-eccentric building. The shape of these curves resembles

that for a symmetric system, except with some minor difference to the left of $\Omega = 1.0$, where a 'gap' or discontinuity in the solution is encountered. 'Similar 'gaps' were also found by Evensen [1] while investigating ring vibrations. The reason for the occurrence of such gaps is investigated in more detail in Section 3.3.4. where the results for a doubly eccentric system are presented.

3.3 SYSTEMS WITH DOUBLE ECCENTRICITY

3.3.1 Equation of Coupled Motion

An idealized one-story structure similar to Figure 2.1 but having eccentric centre of mass with respect to the centre of resistance in both the x- and y-directions is now considered (see Figure 3.1). This system has three degrees-of-freedom, namely the two horizontal displacements u and v of the mass centre relative to the ground along the x- and y-axes and the rotation θ about the vertical axis. The centre of resistance is located at distances e_x and e_y, the eccentricities measured from the centre of mass along the x- and y-axes and defined by

$$e_x = \frac{1}{K_y} \Sigma\, x_i k_{iy}, \quad e_y = \frac{1}{K_x} \Sigma\, y_i k_{ix} \qquad \cdots \quad (3.13)$$

The force-displacement relationship of the lateral resisting elements is assumed to be elastic and weakly nonlinear with cubic softening-type nonlinearity as expressed by Equation (2.2). For simplicity, the ground motion is assumed to be sinusoidal and directed along the

x-axis, of magnitude given by the expressions of Equation (2.5). The resisting elements are located only at the periphery of the building. As in the case for symmetric and single-eccentric systems, the governing equations of motion are conveniently expressed in nondimensional form following the procedure described in Appendix A. Some additional changes of variables needed for nondimensionalization are given in Appendix F (Equation F1).

The process of nondimensionalization yields the following three coupled, nondimensional equations of motion for sinusoidal ground accerlation directed along the x-axis

$$\ddot{\Lambda}_x + f_1\dot{\Lambda}_x + \{f_2\Lambda_x - (f_3\Lambda_x^3 + f_4\Lambda_x^2\Lambda_\theta + f_5\Lambda_x\Lambda_\theta^2 + f_6\Lambda_\theta + f_7\Lambda_\theta^3)\} = -\cos\Omega\tau \tag{3.14}$$

$$\ddot{\Lambda}_\theta + h_1\dot{\Lambda}_\theta + \{h_2\Lambda_\theta - (h_4\Lambda_\theta^3 + h_9\Lambda_\theta^2\Lambda_x + h_3\dot{\Lambda}_\theta\Lambda_x^2 + h_8\Lambda_x^3) - (h_6\Lambda_\theta^3 + h_{12}\Lambda_\theta^2\Lambda_y + h_5\Lambda_\theta\Lambda_y^2 + h_{11}\Lambda_y^3) - (h_7\Lambda_x + h_{10}\Lambda_y)\} = 0 \tag{3.15}$$

$$\ddot{\Lambda}_y + g_1\dot{\Lambda}_y + \{g_2\Lambda_y^3 - (g_3\Lambda_y + g_4\Lambda_y^2\Lambda_\theta + g_5\Lambda_y\Lambda_\theta^2 + g_6\Lambda_\theta + g_7\Lambda_\theta^2)\} = 0 \tag{3.16}$$

where f_i, g_i and h_i are nondimensional constants that may be

expressed as functions of ζ_x, ζ_y, ζ_θ, Ω_y, Ω_θ and the geometric arrangement of the stiffnesses. Typical forms of f_i, g_i and h_i, derived for an example structure, are given in Appendix F. In the foregoing equation Λ_x, Λ_y and Λ_θ represent nondimensional response at the centre of mass as a function of nondimensional time τ; ζ_x, ζ_y, and ζ_θ represent the ratios of critical damping in x-, y- and θ-directions respectively; and Ω_y, Ω_θ are the uncoupled frequency ratios in the y- and θ- directions normalized with respect to the natural frequency of the system in the x-direction, given by Equation (A2) of Appendix A.

3.3.2 Approximate Response Amplitudes

Equations (3.14) to (3.16) can be solved by applying the method of averaging, the same approach as adopted for the approximate solutions for the response amplitudes of the symmetric and singly eccentric systems (see Section 2.2.2. and 3.3.2.).

It is assumed that the solution exists in the form

$$\begin{aligned} \Lambda_x(\tau) &= P(\tau) \cos [\Omega\tau + \Phi(\tau)] \\ \Lambda_y(\tau) &= Q(\tau) \cos [\Omega\tau + \Psi(\tau)] \\ \Lambda_\theta(\tau) &= R(\tau) \cos [\Omega\tau + \chi(\tau)] \end{aligned} \qquad (3.17)$$

where variables P, Q, R, Φ, ψ, and χ are approximated by their averaging values $\bar{P}$, $\bar{Q}$, $\bar{R}$, $\bar{\Phi}$, $\bar{\Psi}$, and $\bar{\chi}$ respectively. The averaging procedure thus leads to a set of six nonlinear simultaneous algebraic equations, which yield the approximate solution

$$\Lambda_x(\tau) = \bar{P} \cos(\Omega\tau + \bar{\Phi})$$
$$\Lambda_y(\tau) = \bar{Q} \cos(\Omega\tau + \bar{\Psi}) \qquad (3.18)$$
$$\Lambda_\theta(\tau) = \bar{R} \cos(\Omega\tau + \bar{\chi})$$

The following set of six simultaneous, coupled, nonlinear algebric equations result from the averaging procedure described in Appendix B

$$(f_2-\Omega^2)\,\bar{P} - \tfrac{3}{4} f_3 \bar{P}^3 - \tfrac{3}{4} \bar{R}(f_4\bar{P}^2 + f_7\bar{R}^2)\cos\bar{\Delta}_2$$
$$- \tfrac{1}{4} f_5 \bar{P}\bar{R}^2(1 + 2\cos^2\bar{\Delta}_2) - f_6 \bar{R}\cos\bar{\Delta}_2 = -\cos\bar{\Phi} \qquad (3.19a)$$

$$f_1 \Omega \bar{P} - (\tfrac{1}{4} f_4 \bar{P}^2 \bar{R} + f_6 \bar{R} + \tfrac{3}{4} f_7 \bar{R}^3)\sin\bar{\Delta}_2$$
$$- \tfrac{1}{4} f_5 \bar{P}\bar{R}^2 \sin 2\bar{\Delta}_2 = \sin\bar{\Phi} \qquad (3.19b)$$

$$(g_2-\Omega^2)\,\bar{Q} - \tfrac{3}{4} g_3 \bar{Q}^3 - \tfrac{3}{4} \bar{R}(g_4\bar{Q}^2 + g_7 \bar{R}^2)\cos\bar{\Delta}_2$$
$$- \tfrac{1}{4} g_5 \bar{Q}\bar{R}^2(1 + 2\cos^2\bar{\Delta}_3) - g_6 \bar{R}\cos\bar{\Delta}_3 = 0 \qquad (3.19c)$$

$$g_1\Omega\bar{Q} - (\tfrac{1}{4} g_4\bar{Q}^2 \bar{R} + g_6 \bar{R} + \tfrac{3}{4} g_7 \bar{R}^3)\sin\bar{\Delta}_3$$
$$- \tfrac{1}{4} g_5 \bar{Q}\bar{R}^2 \sin 2\bar{\Delta}_3 = 0 \qquad (3.19d)$$

$$(h_2-\Omega^2)\,\bar{R} - \tfrac{3}{4}\,h_4\,\bar{R}^3 - \tfrac{3}{4}\,\bar{P}\,(h_8\,\bar{P}^2 + h_9\,\bar{R}^2)\cos\bar{\Delta}_2$$

$$- \tfrac{1}{4}\,h_3\,\bar{P}^2\,\bar{R}\,(1 + 2\cos^2\bar{\Delta}_2) - \tfrac{3}{4}\,h_6\,\bar{R}^3 - \tfrac{3}{4}\,\bar{Q}\,(h_{11}\bar{Q}^2 + h_{12}\bar{R}^2)\cos\bar{\Delta}_3$$

$$- \tfrac{1}{4}\,h_5\,\bar{Q}^2\,\bar{R}\,(1 + 2\cos^2\bar{\Delta}_3) - h_7\,\bar{P}\cos\bar{\Delta}_2 - h_{10}\,\bar{Q}\cos\bar{\Delta}_3 = 0 \qquad (3.19e)$$

$$h_1\Omega\,\bar{R} + (\tfrac{1}{4}\,h_9\,\bar{R}^2 + \tfrac{3}{4}\,h_8\,\bar{P}^2 + h_7)\,\bar{P}\sin\bar{\Delta}_2 + \tfrac{1}{4}\,h_3\,\bar{P}^2\,\bar{R}\sin 2\bar{\Delta}_2$$

$$+ (\tfrac{1}{4}\,h_{12}\,\bar{R}^2 + \tfrac{3}{4}\,h_{11}\,\bar{Q}^2 + h_{10})\,\bar{Q}\sin\bar{\Delta}_3 + \tfrac{1}{4}\,h_5\,\bar{Q}^2\,\bar{R}\sin 2\bar{\Delta}_3 = 0 \qquad (3.19f)$$

in which $\bar{\Delta}_2$ and $\bar{\Delta}_3$ represent average phase differences given by

$$\bar{\Delta}_2 = \bar{\chi} - \bar{\Phi} \qquad (3.20a)$$

$$\bar{\Delta}_3 = \bar{\chi} - \bar{\Psi} \qquad (3.20b)$$

Equations (3.19) and (3.20) can be solved using a standard numerical method yielding the magnitudes of amplitudes and phase angles of the system, thus providing an approximate solution expressed by Equation (3.18). However, as was the case for the single-eccentric system, approximate closed-form solutions for $\bar{P}$, $\bar{Q}$ and $\bar{R}$ are sought with assumptions similar to those described in Section 3.2.2. These are: (a) phase lags $\bar{\Delta}_2$ and $\bar{\Delta}_3$ are negligibly small so that $\sin\bar{\Delta}_2 \simeq \bar{\Delta}_2$ and $\cos\bar{\Delta}_2 \simeq 1.0$; and (b) only linear terms in $\bar{P}$, $\bar{Q}$ and $\bar{R}$ are retained as amplitudes will be close to linear solutions

since nonlinearity is assumed to be small. With the foregoing assumptions, Equation (3.19) transforms into

$$(f_2-\Omega^2)\,\bar{P} - f_6\bar{R} = -\cos\bar{\Phi} \tag{3.21a}$$

$$f_1\Omega\,\bar{P} + f_6\,\bar{R}\,\bar{\Delta}_2 = \sin\bar{\Phi} \tag{3.21b}$$

$$(g_2-\Omega^2)\,\bar{Q} - g_6\,\bar{R} = 0 \tag{3.21c}$$

$$g_1\Omega\bar{Q} - g_6\,\bar{R}\,\bar{\Delta}_3 = 0 \tag{3.21d}$$

$$(h_2-\Omega^2)\,\bar{R} - h_7\,\bar{P} - h_{10}\bar{Q} = 0 \tag{3.21e}$$

$$h_1\Omega\,\bar{R} + h_7\,\bar{P}\,\bar{\Delta}_2 + h_{10}\,\bar{Q}\,\bar{\Delta}_3 = 0 \tag{3.21f}$$

Equation (3.21) yields the following closed-form expressions for $\bar{P}$, $\bar{Q}$ and $\bar{R}$, after substituting for coefficients f_1, f_2, f_6, g_1, g_2, g_6, h_1, h_2, h_7 and h_{10} (see Equation (3.41) for a doubly eccentric building

$$\bar{P}^2 = \frac{1}{\left(\left[(1-\Omega^2) - \frac{E_y^2\,(\Omega_y^2-\Omega^2)}{\{(\Omega_y^2-\Omega^2)(\Omega_\theta^2-\Omega^2) - E_x^2\Omega_y^4\}}\right]^2 + 4\,\Omega^2\left[\zeta_x + \frac{E_y^2\,\{\zeta_\theta\Omega_\theta(\Omega_y^2-\Omega^2)^2 + \zeta_y\Omega_y^5\,E_x^2\}}{\{(\Omega_y^2-\Omega^2)(\Omega_\theta^2-\Omega^2) - E_x^2\,\Omega_y^4\}^2}\right]^2\right)} \tag{3.22a}$$

$$\bar{Q} = -\frac{E_x E_y \Omega_y^4}{\{(\Omega_y^2-\Omega^2)(\Omega_\theta^2-\Omega^2) - E_x^2 \Omega_y^4\}} \bar{P} \qquad (3.22b)$$

$$\bar{R} = \frac{E_y \Omega_\theta^2 (\Omega_y^2-\Omega^2)}{\{(\Omega_y^2-\Omega^2)(\Omega_\theta^2-\Omega^2) - E_x^2 \Omega_y^4\}} \bar{P} \qquad (3.22c)$$

It should be noted that the foregoing equation is a general expression for the approximate amplitude of an almost linear but doubly eccentric system. For a single-eccentric system, after substituting $E_x = 0$, Equation (3.22) transforms into Equation (3.9). The above expressions for $\bar{P}$, $\bar{Q}$ and $\bar{R}$ are required, as will be seem latter, to determine the zone of torsional coupling of the eccentric system. It can be observed that Equation (3.22) does not involve the nonlinearity parameter λ, although the response amplitudes are certainly not independent of λ. However, for the purpose of establishing stability zones, the first-order approximation of amplitudes calculated from Equation (3.22) seems sufficient.

Since interest herein is limited to the torsional stability for small eccentric (i.e., a nominally symmetric) system, simpler expressions for amplitudes, similar to those in Equation (2.28) but incorporating the effect of eccentricity, are desired. Consequently, an alternative approach, based on the interaction equation for base shear and torque derived by Kan and Chopra [17], is applied yielding the following simple expressions for response amplitudes as described in Appendix G

$$\bar{P}^2 = \frac{D^2}{(1+E_y^2)} \qquad (3.23a)$$

$$\bar{Q} = \bar{R} = 0 \tag{3.23b}$$

Where D is given by Equation (2.11).

3.3.3 Stability of Coupled Response

The stability of the solution can be examined by the perturbation technique [1,3]. The form of the solution expressed by Equation (3.18) is perturbed by letting

$$\begin{aligned} \Lambda_x(\tau) &= \bar{P} \cos(\Omega\tau + \bar{\Phi}) + \xi_x(\tau) \\ \Lambda_y(\tau) &= \bar{Q} \cos(\Omega\tau + \bar{\Psi}) + \xi_y(\tau) \\ \Lambda_\theta(\tau) &= \bar{R} \cos(\Omega\tau + \bar{\chi}) + \xi_\theta(\tau) \end{aligned} \tag{3.24}$$

where $\xi_x(\tau)$, $\xi_y(\tau)$ and $\xi_\theta(\tau)$ represent small perturbations.

Substituting the expressions of Equation (3.24) into differential Equations (3.14) through (3.16) and retaining only the first order terms in perturbations ξ_x, ξ_y and ξ_θ lead to the following set of variational equations (damped coupled Mathieu-Hill equations)

$$\begin{bmatrix} \frac{1}{f_2} & 0 & 0 \\ 0 & \frac{1}{h_2} & 0 \\ 0 & 0 & \frac{1}{g_2} \end{bmatrix} \begin{Bmatrix} \ddot{\xi}_x \\ \ddot{\xi}_\theta \\ \ddot{\xi}_y \end{Bmatrix} + \begin{bmatrix} \frac{f_1}{f_2} & 0 & 0 \\ 0 & \frac{h_1}{h_2} & 0 \\ 0 & 0 & \frac{g_1}{g_2} \end{bmatrix} \begin{Bmatrix} \dot{\xi}_x \\ \dot{\xi}_\theta \\ \dot{\xi}_y \end{Bmatrix}$$

$$+\left(\begin{bmatrix}1&0&0\\0&1&0\\0&0&1\end{bmatrix}-\tfrac{1}{2}\begin{bmatrix}\frac{A_{11}}{f_2} & (\frac{A_{12}}{f_2}+\frac{2f_6}{f_2}) & 0\\ (\frac{A_{21}}{h_2}+\frac{2h_7}{h_2}) & \frac{A_{22}}{h_2} & (\frac{A_{23}}{h_2}+\frac{2h_{10}}{h_2})\\ 0 & (\frac{A_{32}}{g_2}+\frac{2g_6}{g_2}) & \frac{A_{33}}{g_2}\end{bmatrix}-\tfrac{1}{2}\cos 2\Omega\tau\begin{bmatrix}\frac{A_{11}}{f_2} & \frac{A_{12}}{f_2} & 0\\ \frac{A_{21}}{h_2} & \frac{A_{22}}{h_2} & \frac{A_{23}}{h_2}\\ 0 & \frac{A_{32}}{g_2} & \frac{A_{33}}{g_2}\end{bmatrix}\right)\begin{Bmatrix}\xi_x\\ \xi_\theta\\ \xi_y\end{Bmatrix}=0 \qquad (3.25)$$

in which

$$\left.\begin{aligned}
A_{11} &= 3f_3\,\bar{P}^2 + 2f_4\,\bar{P}\,\bar{R} + f_5\,\bar{R}^2\\
A_{12} &= f_4\,\bar{P}^2 + 2f_5\,\bar{P}\,\bar{R} + 3f_7\,\bar{R}^2\\
A_{21} &= h_9\,\bar{R}^2 + 2h_3\,\bar{P}\,\bar{R} + 3h_8\,\bar{P}^2\\
A_{22} &= 3h_4\,\bar{R}^2 + 2h_9\,\bar{P}\,\bar{R} + h_3\,\bar{P}^2\\
&\quad + 3h_6\,\bar{R}^2 + 2h_{12}\bar{Q}\,\bar{R} + h_5\,\bar{Q}^2\\
A_{23} &= h_{12}\bar{R}^2 + 2h_5\,\bar{Q}\,\bar{R} + 3h_{11}\,\bar{Q}^2\\
A_{32} &= g_4\,\bar{Q}^2 + 2g_5\,\bar{Q}\,\bar{R} + 3g_7\,\bar{R}^2
\end{aligned}\right\} \qquad (3.26)$$

$$A_{33} = 3g_3 \overline{Q}^2 + 2g_4 \overline{Q}\,\overline{R} + g_5 \overline{R}^2 \qquad (3.26)$$

Equation (3.25) may be written in condensed form as

$$\underset{\sim}{C}\,\ddot{\underset{\sim}{\xi}} + 2\,\underset{\sim}{C}\,\underset{\sim}{\varepsilon}\,\dot{\underset{\sim}{\xi}} + [\underset{\sim}{E} - \tfrac{1}{2}\underset{\sim}{A} - \tfrac{1}{2}\underset{\sim}{B}\cos 2\Omega\tau]\,\underset{\sim}{\xi} = 0 \qquad (3.27)$$

where

$$\underset{\sim}{\varepsilon} = \tfrac{1}{2}\begin{bmatrix} f_1 & 0 & 0 \\ 0 & h_1 & 0 \\ 0 & 0 & g_1 \end{bmatrix} \qquad (3.28)$$

and $\underset{\sim}{C}$, $\underset{\sim}{E}$, $\underset{\sim}{A}$ and $\underset{\sim}{B}$ are defined by Equation (3.25).

The principal region of instability of the above equation can be approximated by [4]

$$\begin{vmatrix} \underset{\sim}{E} - \tfrac{1}{2}\underset{\sim}{A} + \tfrac{1}{4}\underset{\sim}{B} - \Omega^2\underset{\sim}{C} & -2\,\Omega\,\underset{\sim}{C}\,\underset{\sim}{\varepsilon} \\ 2\,\Omega\,\underset{\sim}{C}\,\underset{\sim}{\varepsilon} & \underset{\sim}{E} - \tfrac{1}{2}\underset{\sim}{A} - \tfrac{1}{4}\underset{\sim}{B} - \Omega^2\underset{\sim}{C} \end{vmatrix} = 0 \qquad (3.29)$$

which, upon expansion, becomes a sixth-order algebraic equation in Ω^2. For the first approximation, let

$$\Omega \approx \Omega_\theta \qquad (3.30)$$

Upon substituting this into all the elements of determinantal Equation (3.29), except the second and fifth elements of the principal diagonal, the following 6x6 determinantal equation is obtained.

$$
\begin{vmatrix}
\left(1 - \frac{A_{11}}{4f_2} - \frac{\Omega_\theta^2}{f_2}\right) & -\left(\frac{A_{12}}{4f_2} + \frac{f_6}{f_2}\right) & 0 \\
-\left(\frac{A_{21}}{4h_2} + \frac{h_7}{h_2}\right) & \left(1 - \frac{A_{22}}{4h_2} - \frac{\Omega^2}{h_2}\right) & -\left(\frac{A_{23}}{4h_2} + \frac{h_{10}}{h_2}\right) \\
0 & -\left(\frac{A_{32}}{4g_2} + \frac{g_6}{g_2}\right) & \left(1 - \frac{A_{33}}{4g_2} - \frac{\Omega_\theta^2}{g_2}\right) \\
\frac{\Omega_\theta f_1}{f_2} & 0 & 0 \\
0 & \frac{\Omega_\theta h_1}{h_2} & 0 \\
0 & 0 & \frac{\Omega_\theta g_1}{g_2}
\end{vmatrix}
\begin{vmatrix}
-\frac{\Omega_\theta f_1}{f_2} & 0 & 0 \\
0 & -\frac{\Omega_\theta h_1}{h_2} & 0 \\
0 & 0 & -\frac{\Omega_\theta g_1}{g_2} \\
\left(1 - \frac{3A_{11}}{4f_2} - \frac{\Omega_\theta^2}{f_2}\right) & -\left(\frac{3A_{12}}{4f_2} + \frac{f_6}{f_2}\right) & 0 \\
-\left(\frac{3A_{21}}{4h_2} + \frac{h_7}{h_2}\right) & \left(1 - \frac{3A_{11}}{4h_2} - \frac{\Omega^2}{h_2}\right) & -\left(\frac{3A_{23}}{4h_2} + \frac{h_{10}}{h_2}\right)
\end{vmatrix} = 0 \qquad (3.31)
$$

$$\begin{vmatrix} 0 & -\left(\frac{3A_{32}}{4g_2} + \frac{g_6}{g_2}\right) & \left(1 - \frac{3A_{33}}{4g_2} - \frac{\Omega_\theta^2}{g_2}\right) \end{vmatrix}$$

(3.31)

The foregoing equation is expanded, neglecting terms of higher than the second order in f_1, g_1, and h_1. To express the solution for Ω in concise form the following substitutions are made

$$\left.\begin{aligned}
H_1 &= \left(1 - \frac{A_{11}}{4f_2} - \frac{\Omega_\theta^2}{f_2}\right)\left(1 - \frac{A_{33}}{4g_2} - \frac{\Omega_\theta^2}{g_2}\right) \\
H_2 &= \left(1 - \frac{3A_{11}}{4f_2} - \frac{\Omega_\theta^2}{f_2}\right)\left(1 - \frac{3A_{33}}{4g_2} - \frac{\Omega_\theta^2}{g_2}\right) \\
H_3 &= \left(\frac{A_{22}}{2h_2}\right)H_2 + \left(1 - \frac{3A_{11}}{4f_2} - \frac{\Omega_\theta^2}{f_2}\right)\left(\frac{3A_{23}}{4h_2} + \frac{h_{10}}{h_2}\right)\left(\frac{3A_{32}}{4g_2} + \frac{g_6}{g_2}\right) \\
&\quad + \left(1 - \frac{3A_{33}}{4g_2} - \frac{\Omega_\theta^2}{g_2}\right)\left(\frac{3A_{12}}{4f_2} + \frac{f_6}{f_2}\right)\left(\frac{3A_{21}}{4h_2} + \frac{h_7}{h_2}\right) \\
H_4 &= \left(1 - \frac{A_{11}}{4f_2} - \frac{\Omega_\theta^2}{f_2}\right)\left(\frac{A_{23}}{4h_2} + \frac{h_{10}}{h_2}\right)\left(\frac{A_{32}}{4g_2} + \frac{g_6}{g_2}\right) \\
&\quad + \left(1 - \frac{A_{33}}{4g_2} - \frac{\Omega_\theta^2}{g_2}\right)\left(\frac{A_{12}}{4f_2} + \frac{f_6}{f_2}\right)\left(\frac{A_{21}}{4h_2} + \frac{h_7}{h_2}\right)
\end{aligned}\right\} \quad (3.32)$$

$$H_5 = \left(\frac{\Omega_\theta h_1}{h_2}\right)$$

This allows the solution of Equation (3.31) to be expressed as

$$\Omega = \left(h_2 - \frac{A_{22}}{4} - h_2\left\{\frac{1}{2}\left(\frac{H_3}{H_2} + \frac{H_4}{H_1}\right) \pm \left[\left\{\frac{1}{2}\left(\frac{H_3}{H_2} - \frac{H_4}{H_1}\right)\right\}^2 - H_5^2\right]^{\frac{1}{2}}\right\}\right)^{\frac{1}{2}}$$

(3.33)

It should be noted that the above equation contains the torsional

damping term, h_1, within the inner radical term in H_5. If $[\{\frac{1}{2}(\frac{H_3}{H_2} - \frac{H_4}{H_1})\}^2 - H_5^2] < 0$, Ω yields complex values for the boundary frequencies. Thus, the largest value of torsional damping for which dynamic instability is still possible is defined by

$$\frac{1}{2}\left(\frac{H_3}{H_2} - \frac{H_4}{H_1}\right) \geq H_5 \tag{3.34}$$

This results in the following expressions defining the minimum value of torsional damping necessary to ensure stability

$$2\Omega_\theta h_1 = \frac{A_{22}}{2} + \frac{(\frac{3A_{23}}{4} + h_{10})(\frac{3A_{32}}{4} + g_6)}{(g_2 - \frac{3A_{33}}{4}\Omega_\theta^2)} + \frac{(\frac{3A_{12}}{4} + f_6)(\frac{3A_{21}}{4} + h_7)}{(f_2 - \frac{3A_{11}}{4} - \Omega_\theta^2)}$$

$$- \frac{(\frac{A_{23}}{4} + h_{10})(\frac{A_{32}}{4} + g_6)}{(g_2 - \frac{A_{33}}{4} - \Omega_\theta^2)} - \frac{(\frac{A_{12}}{4} + f_6)(\frac{A_{21}}{4} + h_7)}{(f_2 - \frac{A_{11}}{4} - \Omega_\theta^2)} \tag{3.35}$$

However, if torsional damping is neglected Equation (3.33) gives rise to two equations, one representing an upper bound and the other expressing a lower bound for the zone of instability. The upper bound curve is given by

$$\Omega^2 = h_2 - \frac{3A_{22}}{4} - \frac{(\frac{3A_{23}}{4} + h_{10})(\frac{3A_{32}}{4} + g_6)}{(g_2 - \frac{3A_{33}}{4} - \Omega_\theta^2)} - \frac{(\frac{3A_{12}}{4} + f_6)(\frac{3A_{21}}{4} + h_7)}{(f_2 - \frac{3A_{11}}{4} - \Omega_\theta^2)} \tag{3.36}$$

whereas the lower bound curve is

$$\Omega^2 = h_2 - \frac{A_{22}}{4} - \frac{(\frac{A_{23}}{4} + h_{10})(\frac{A_{32}}{4} + g_6)}{A\,(g_2 - \frac{A_{33}}{4} - \Omega_\theta^2)} - \frac{(\frac{A_{12}}{4} + f_6)(\frac{A_{21}}{4} + h_7)}{A\,(f_2 - \frac{A_{11}}{4} - \Omega_\theta^2)} \tag{3.37}$$

Typical results obtained from the foregoing analysis are presented in the following discussion of an illustrative unsymmetric building structure.

3.3.4 Typical Results and Discussion

It is clear that Equations (3.35) through (3.37) involve the geometric parameters, damping coefficients, fundamental frequencies, input frequency and the nonlinearity parameter, λ. Although these equations have been formulated for an unsymmetric system, they are equally applicable for symmetric structures as well. These equations are useful in studying the torsional instability of the system as well as in identifying values of the system parameters for which such instability may take place.

To demonstrate the application of the method described above, a typical unsymmetric building, L-shaped in plan as shown in Figure 3.4, is selected for study.

Application of Analysis to Example Structure

The elements of lateral resistance are assumed to be distributed along the perimeter of the structure as shown in Figure 3.4. The building is assumed to be nominally symmetric, i.e., eccentricities e_x

and e_y are small. (For the L-shaped building; values of the geometric parameters β and $\gamma \geq 0.3$ correspond to eccentricities $\leq 10\%$). For this condition, one may neglect response amplitudes $\bar{Q}$ and $\bar{R}$ in Equations (3.26) and (3.35) through (3.37). The upper and lower bounds of Equations (3.36) and (3.37) are then transformed, respectively as follows

$$\Omega_\theta^2 = \Omega^2 + \frac{3h_3\,\bar{P}^2}{4} + \frac{h_{10}g_6}{(\Omega_y^2 - \Omega_\theta^2)} + \frac{(\frac{3f_4\,\bar{P}^2}{4} + f_6)\,(\frac{9h_8\,\bar{P}^2}{4} + h_7)}{(1 - \frac{9f_3\,\bar{P}^2}{4} - \Omega_\theta^2)} \tag{3.38}$$

and

$$\Omega_\theta^2 = \Omega^2 + \frac{h_3\,\bar{P}^2}{4} + \frac{h_{10}g_6}{(\Omega_y^2 - \Omega_\theta^2)} + \frac{(\frac{f_4\,\bar{P}^2}{4} + f_6)(\frac{3h_8\,\bar{P}^2}{4} + h_7)}{(1 - \frac{3f_3\,\bar{P}^2}{4} - \Omega_\theta^2)} \tag{3.39}$$

It is instructive to transform Equations (3.38) and (3.39) in terms of the nondimensional eccentricities of the system. The nondimensional eccentricities, E_x and E_y, are given by

$$E_x = \frac{e_x}{r}, \qquad E_y = \frac{e_y}{r} \tag{3.40}$$

All coefficients, except h_3, of Equations (3.38) and (3.39) can now be expressed in terms of E_x, E_y, λ, Ω_y and Ω_θ; namely

$$f_3 = \lambda, \qquad h_7 = E_y\,\Omega_\theta^2$$

$$
\left.
\begin{aligned}
f_4 &= -\frac{3\lambda E_y}{\Omega_\theta^2} & h_8 &= -\lambda E_y \Omega_\theta^2 \\
f_6 &= \frac{E_y}{\Omega_\theta^2} & h_{10} &= -E_x \Omega_\theta^2 \\
g_6 &= \frac{E_x \Omega_y^4}{\Omega_\theta^2}
\end{aligned}
\right\} \qquad (3.41)
$$

It is somewhat complicated to express h_3 in terms of E_x and E_y; therefore, the expression for h_3 is written in terms of the geometric parameters as

$$h_3 = 3 \lambda \gamma_0^2 \left(\frac{c_3}{c_1}\right)^2 \qquad (3.42)$$

in which

$$
\left.
\begin{aligned}
\gamma_o &= \frac{\sqrt{3}\, c_1}{\sqrt{c_6 r^2 + c_1}} \\
c_1 &= 1 - (1-\beta)(1-\gamma) \\
c_2 &= 1 - (1-\beta^2)(1-\gamma) \\
c_3 &= 1 - (1-\beta)(1-\gamma^2) \\
c_4 &= \gamma\,(1-\gamma)(1-\beta)^2 \\
c_5 &= \beta\,(1-\beta)(1-\gamma)^2 \\
c_6 &= c_2^2 + 4\beta\, c_4 \\
c_7 &= c_3^2 + 4\gamma\, c_5
\end{aligned}
\right\} \qquad (3.43)
$$

and where r is the aspect ratio a/b of the building and parameters.

β and γ, defined in Fig. 3.4, represent the two geometric parameters of a particular L-shaped building plan. The approximation for translational amplitude $\bar{P}$ in the direction of ground motion for the nominally symmetric building is obtained from Equation (3.23). Substituting Equations (3.41), (3.42) and (3.23) into Equations (3.38) and (3.39) yields the following upper and lower bound instability equations

$$\Omega_\theta^2 = \Omega^2 + \left(\frac{9\lambda D^2}{4(1+E_y^2)}\right)\left(\frac{c_3}{c_1}\gamma_0\right)^2 + \left(\frac{E_x^2\Omega_y^4}{\Omega_y^2-\Omega_\theta^2}\right) + \left(\frac{\left[1 - \frac{9\lambda D^2}{4(1+E_y^2)}\right]^2 E_y}{\left[1 - \frac{9\lambda D^2}{4(1+E_y^2)}\right] - \Omega_\theta^2}\right) \tag{3.44}$$

$$\Omega_\theta^2 = \Omega^2 + \left(\frac{3\lambda D^2}{4(1+E_y^2)}\right)\left(\frac{c_3}{c_1}\gamma_0\right)^2 + \left(\frac{E_x^2\Omega_y^4}{\Omega_y^2-\Omega_\theta^2}\right) + \left(\frac{\left[1 - \frac{3\lambda D^2}{4(1+E_y^2)}\right]^2 E_y}{\left[1 - \frac{3\lambda D^2}{4(1+E_y^2)}\right] - \Omega_\theta^2}\right) \tag{3.45}$$

The foregoing allows Equation (3.35) to be expressed in terms of the nondimensional eccentricities. The largest value of torsional damping in a nominally symmetric building for which dynamic instability is still possible is thus given by

$$\zeta_\theta = \left(\frac{3\lambda D^2}{8\Omega_\theta^2(1+E_y^2)}\right)\left(\frac{c_3}{c_1}\gamma_0\right)^2 + \frac{E_y^2}{4\Omega_\theta^2}\left[\frac{\{1 - \frac{9\lambda D^2}{4(1+E_y^2)}\}^2}{\{1 - \frac{9\lambda D^2}{4(1+E_y^2)}\} - \Omega_\theta^2} - \frac{\{1 - \frac{9\lambda D^2}{4(1+E_y^2)}\}^2}{\{1 - \frac{9\lambda D^2}{4(1+E_y^2)}\} - \Omega_\theta^2}\right] \tag{3.46}$$

Stability Curves for Example Structure.

Figures 3.5 and 3.6 present the stability curves in Ω_θ-Ω parameter space computed from Equations (3.44) and (3.45). An interesting feature in the computation of Ω_θ is the appearance of a discontinuity or 'gap' in the solution to the left of Ω=1, where the approximate solution for Ω_θ from both the upper and the lower bound equations breaks down. To investigate the possible reason for this behaviour, examination of Equations (3.44) and (3.45) shows that when the denominator of the fourth term in these equations approaches zero, the term becomes large.

Curves plotted in Figure 3.5 trace the behaviour of the fourth term; the curves for the partial denominators, $\sqrt{1 - \frac{9\lambda D^2}{4(1+E_y^2)}}$ and $\sqrt{1 - \frac{3\lambda D^2}{4(1+E_y^2)}}$ from Equations (3.44) and (3.45), are seen to cross the upper and lower bound instability curves at the location of the gap. A similar breakdown in the solution is also noticed for some of the lower bound curves, this time to the right of Ω=1. However, here the partial denominator curves do not cross the expected solutions of the lower bound equation. It is found that the gaps diminish with decrease in eccentricity. This is evident also from the fact that the numerator of the fourth term contains the eccentricity as a compensating factor. It is interesting to note that a similar 'gap' phenomenon was observed by Evensen [1] in the study of nonlinear vibrations of thin circular rings. Figure 3.6 is the plotting of some instability curves similar to those described in Figure 3.5 for various values of aspect ratio r, to demonstrate the influence of this parameter on the zone of instability of the system. It is seen that the instability zone

decreases and shifts towards the $\Omega_\theta=\Omega$ line as r increases in magnitude. Also the length of gap decreases with the increased r values for both upper and lower bound curves.

The effect of torsional damping ζ_θ (Equation (3.46)) is demonstrated in Figures 3.7 and 3.8. A value of ζ_θ less than the magnitude plotted for a particular system implies that the structure is unstable. This equation also exhibits computational difficulties, producing a 'gap' at or somewhat to the left of $\Omega_\theta=1$ (Figure 3.7), similar to that for the upper and lower bound curves of Figures 3.5 and 3.6. The denominator of the second term of Equation (3.46), when approaching small values, is responsible for this gap. In Figure 3.8 the same equation is replotted in the ζ_θ-Ω plane for several ζ_x and Ω_θ values to demonstrate the influence of the aspect ratio r. The results show that, the smaller the value of the aspect ratio, the larger the value of ζ_θ required to stabilize the system.

In the present study, the resisting elements have been assumed to be distributed along the perimeter of the structure. However, in actual buildings the resisting elements are frequently distributed over the plan area. To handle such systems, appropriate expressions for E_x, E_y, K_x and K_y should be employed in the general formulation expressed by Equations (3.35) through (3.37).

The system considered here is subjected to sinusoidal ground motion in only one direction, although earthquake ground motion is multi-directional and more complex in nature. However, this would not significantly alter the parametric conditions for torsional instability.

3.4 CONCLUSIONS

The purpose of this chapter is to present the mathematical relationships for the parameters of an unsymmetric structure subjected to ground motion, in order to identify situations where the system will be torsionally unstable.

Two mathematical relationships have been formulated, one for the upper bound and the other for the lower bound instability curve. The torsional motion is found to be unstable due to nonlinearity of the resisting elements as well as the eccentricities between centres of resistance and mass, provided that parameters of the system are such that they fall within the zone between the upper and lower bound instability curves. Also, an expression has been presented for torsional damping, in terms of the system parameters. This expression may be used to determine the minimum torsional damping necessary to stabilize torsional response accompanying purely translational excitation.

Some numerical problems in the computation of instability and torsional damping curves have been encountered in the form of 'gaps'. Otherwise, the numerical computation is simple enough to be used for both truly symmetric and the nominally symmetric structures of the present study.

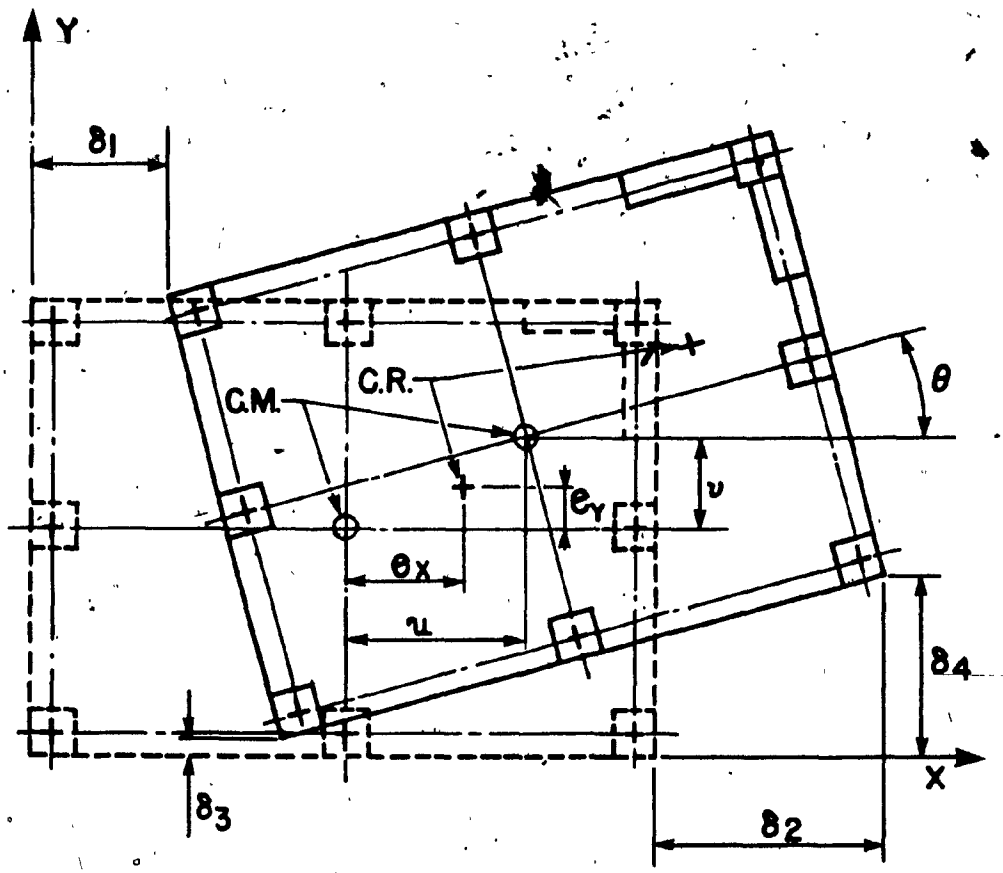

Figure 3.1 Lateral-torsional displacement of asymmetric structure.

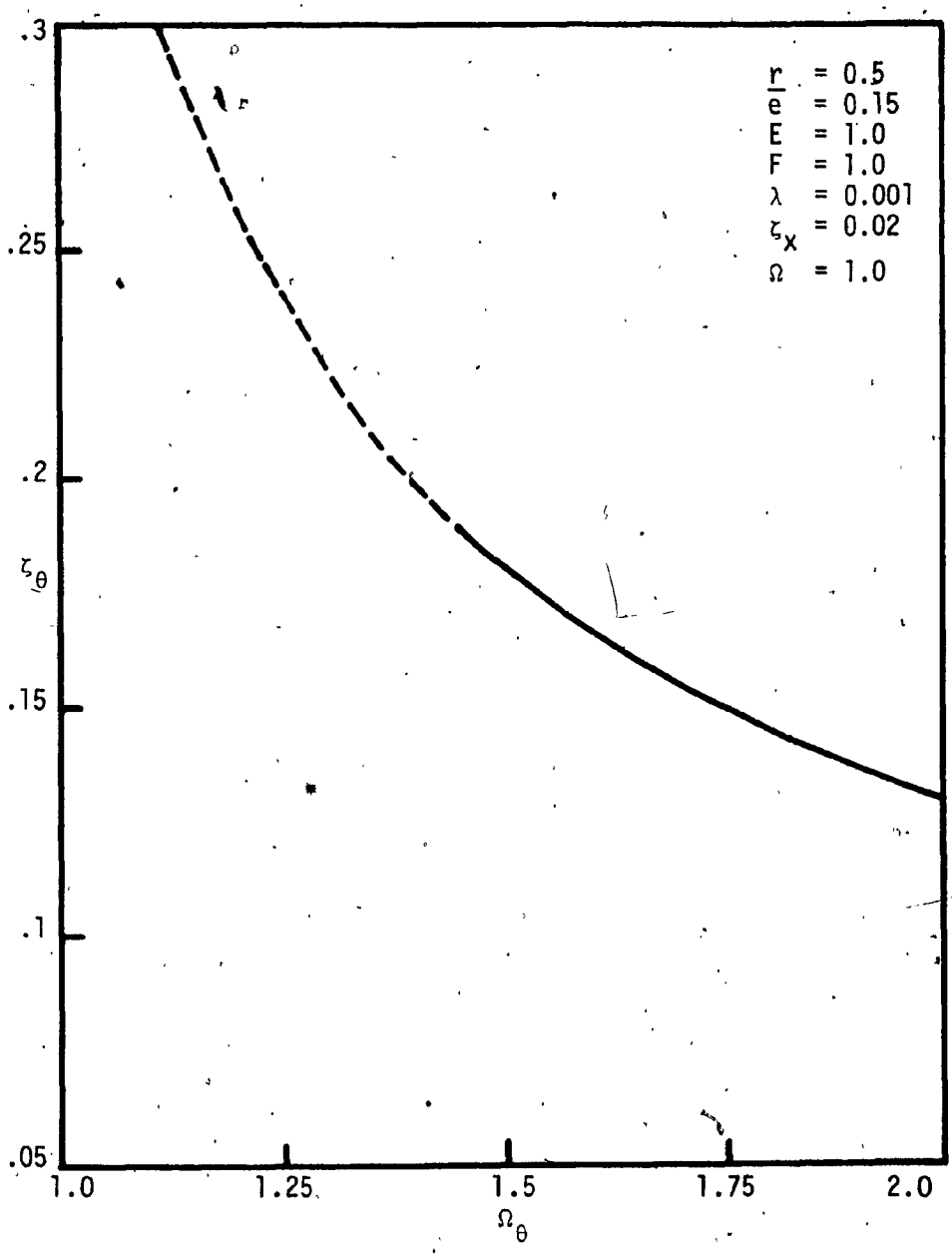

Figure 3.2 Critical torsional damping for an unsymmetric system.

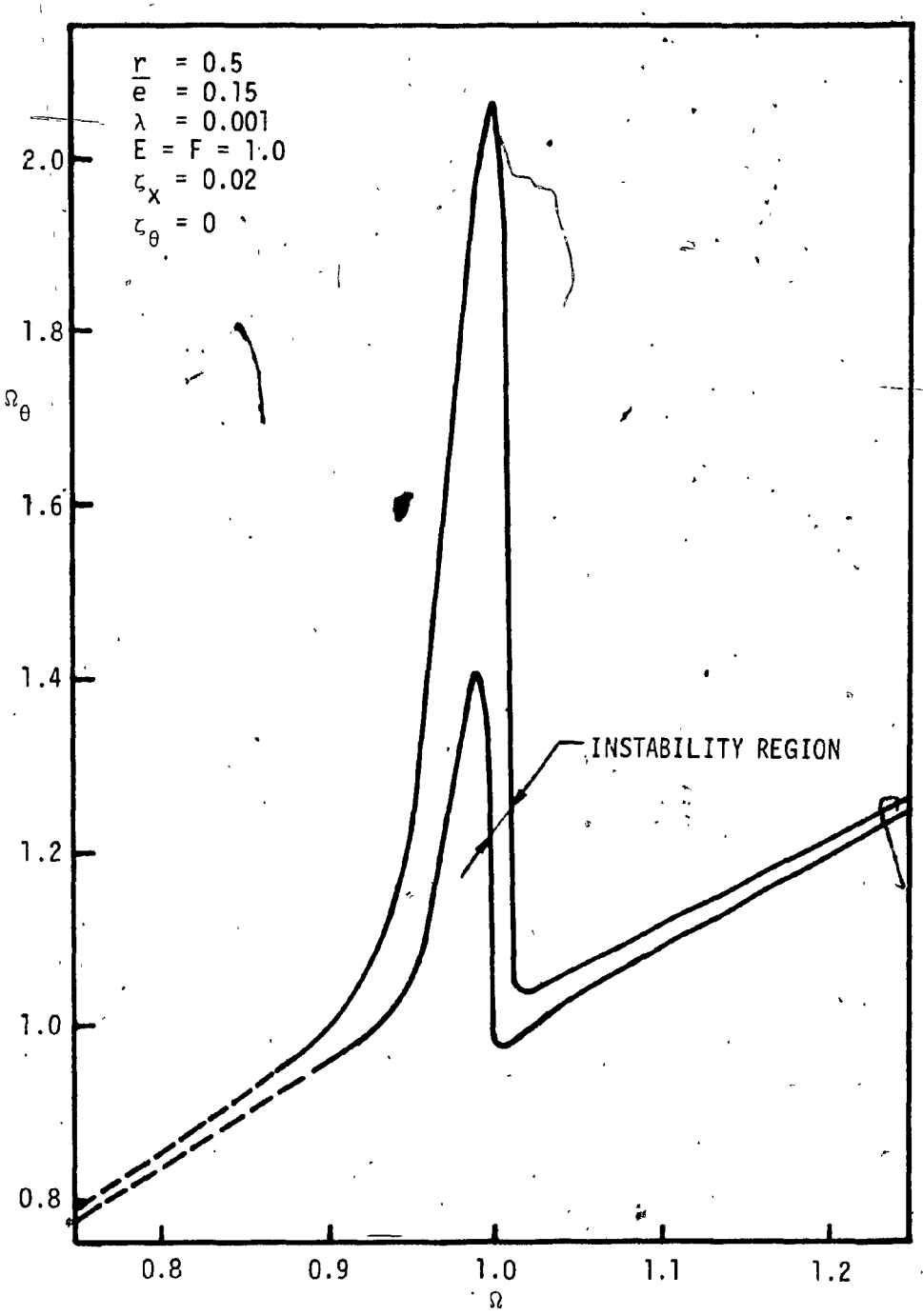

Figure 3.3 Region of torsional instability for single eccentric system

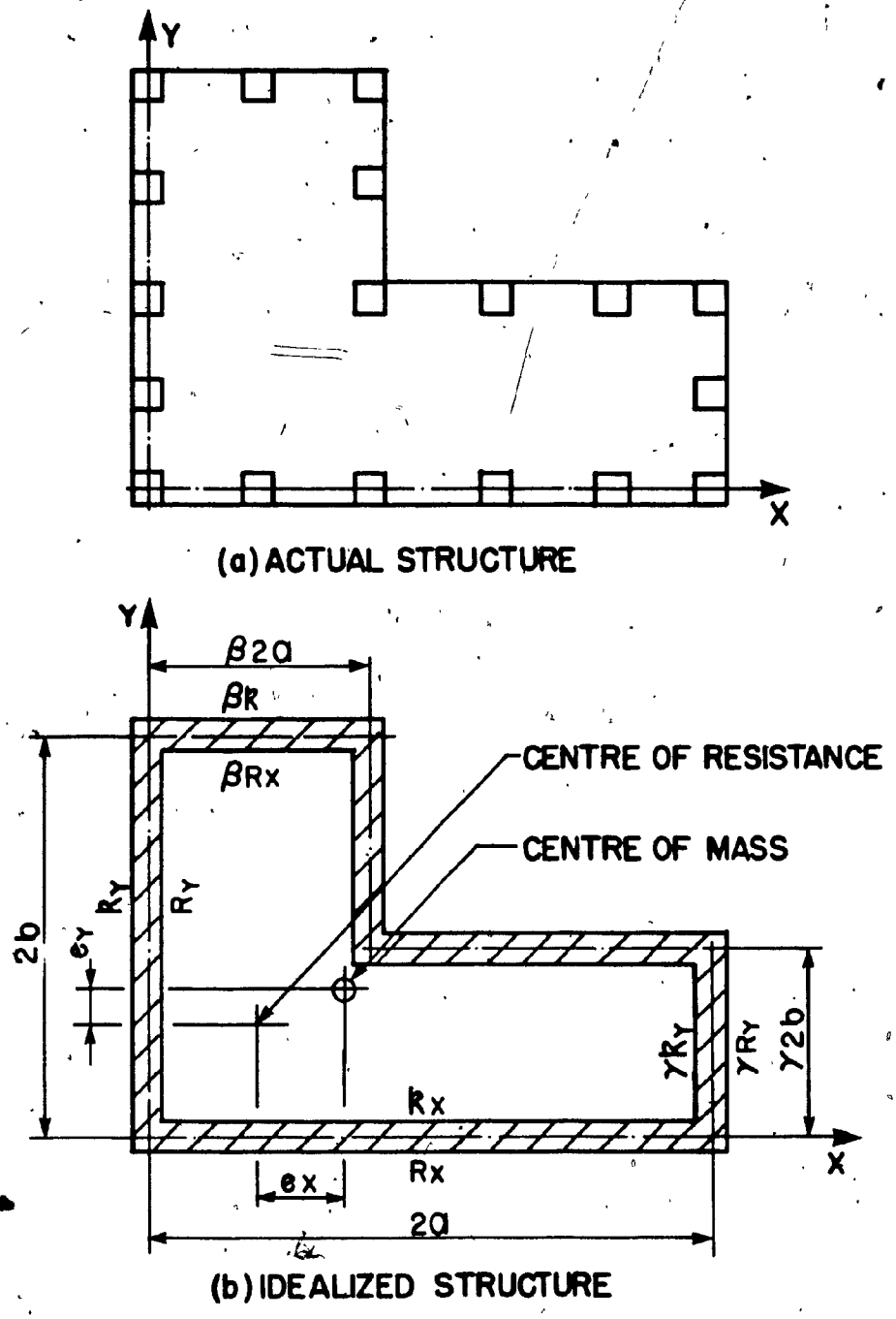

Figure 3.4 Plan of example L-shaped building.

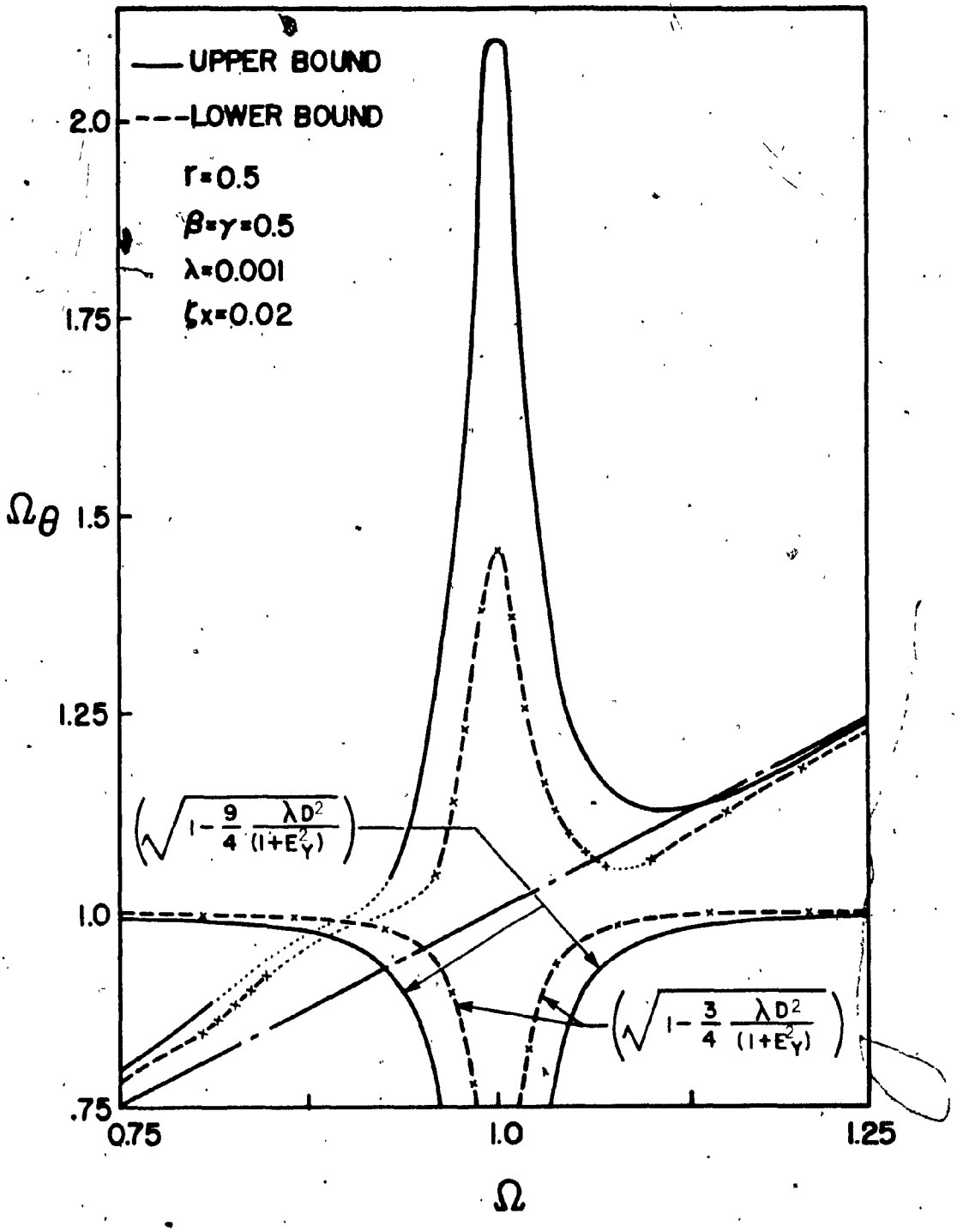

Figure 3.5 Instability curves for example L-shaped building.

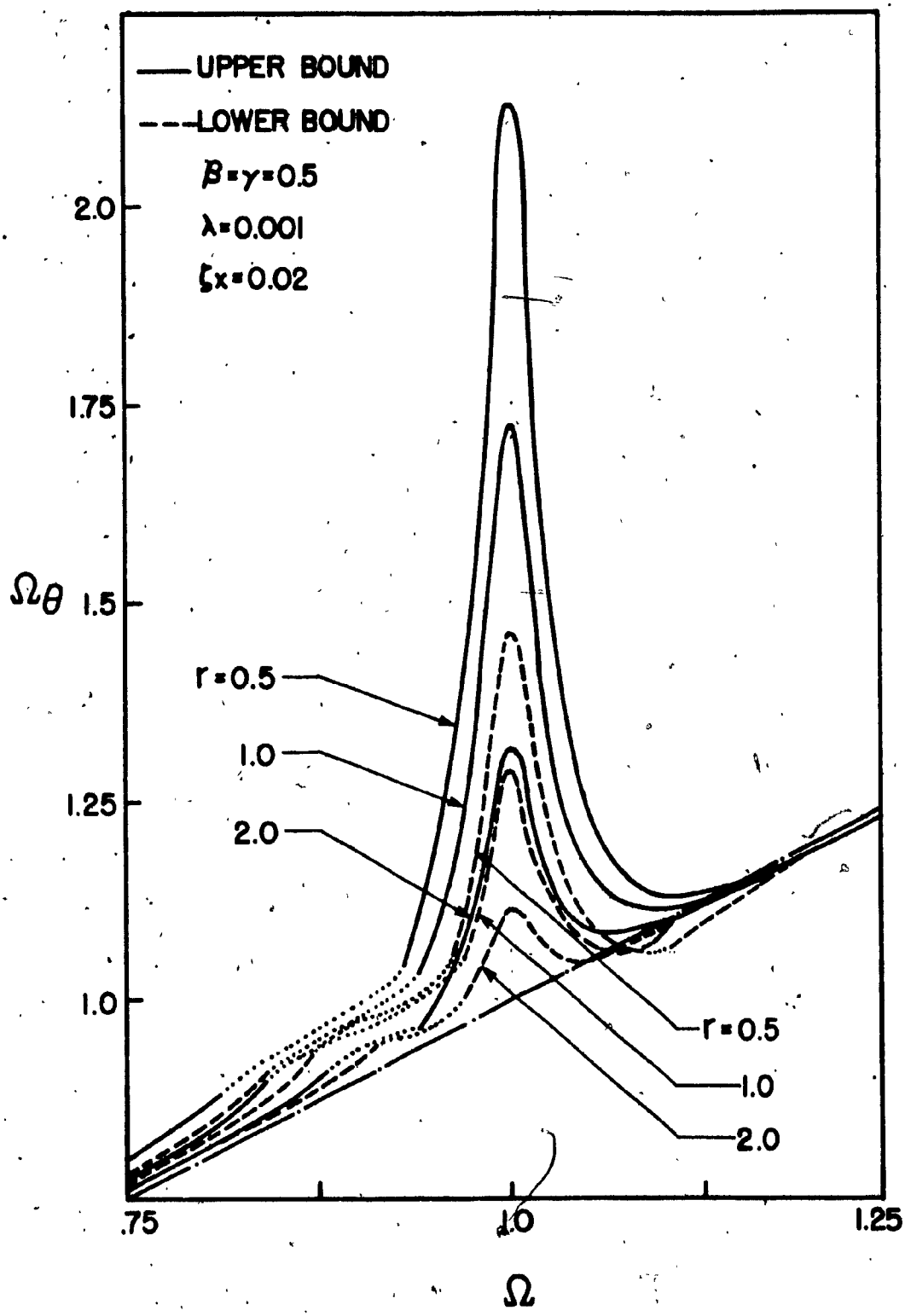

Figure 3.6 Effect of aspect ratio r on instability.

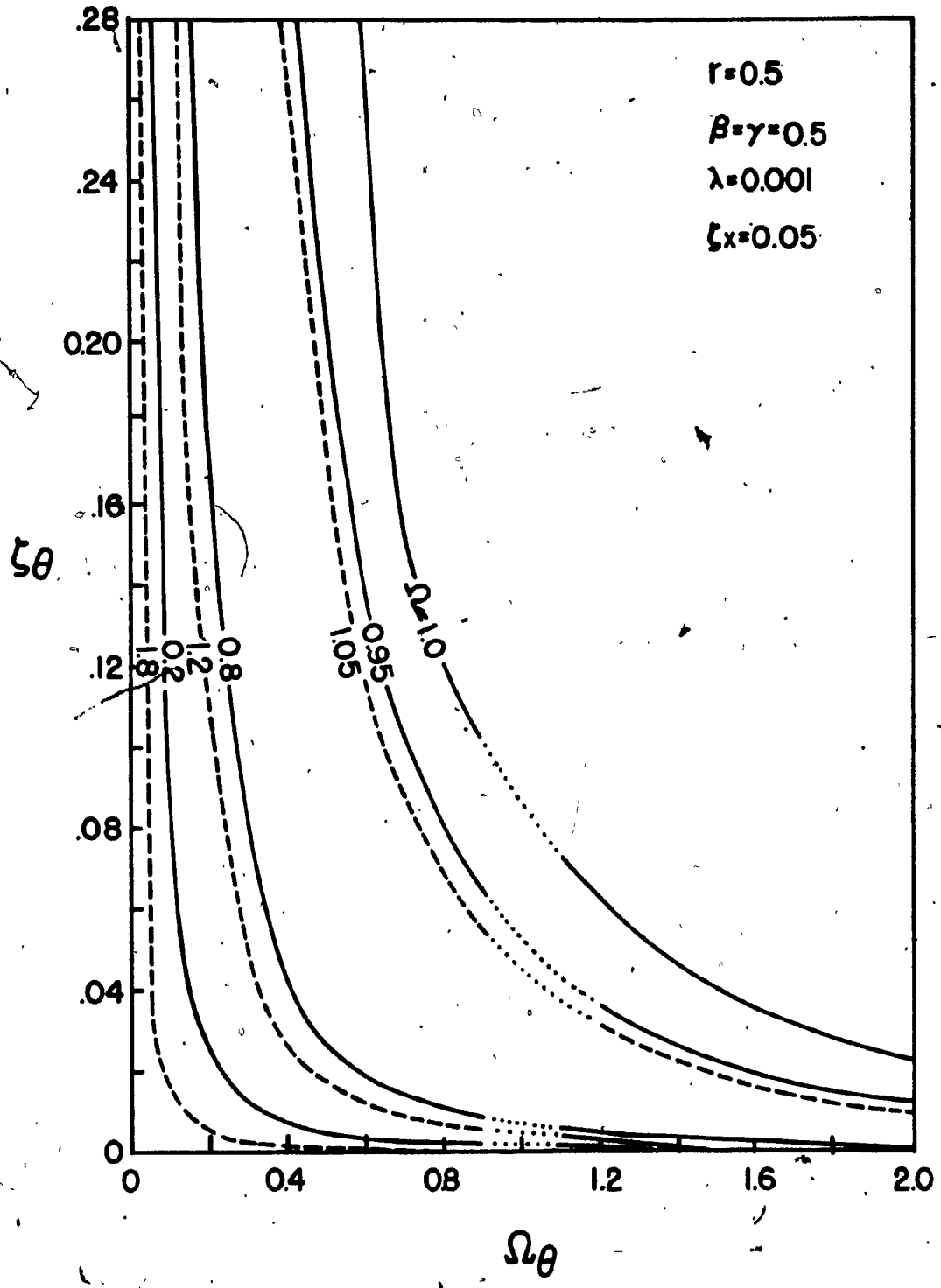

Figure 3.7 Maximum torsional damping for stability.

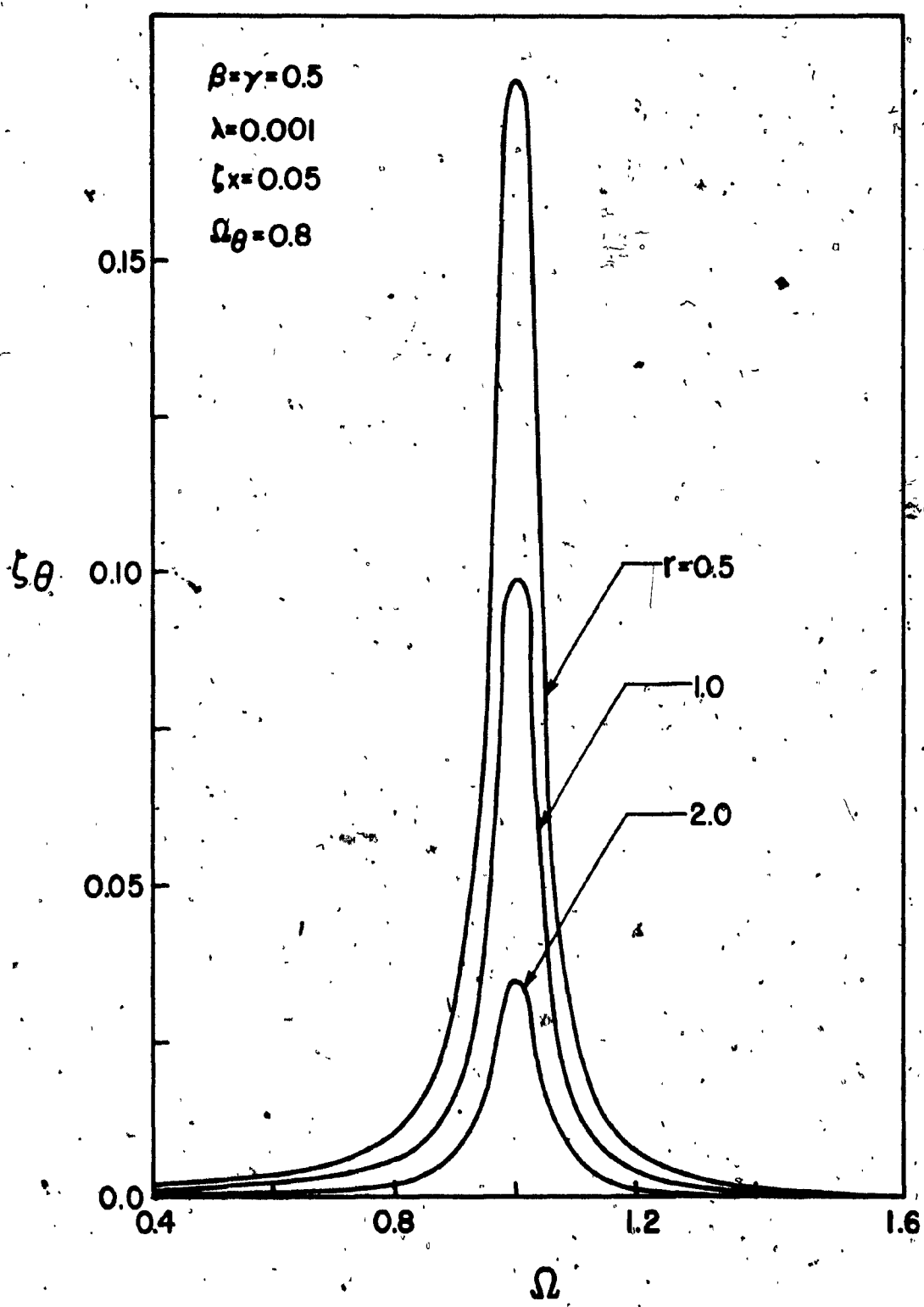

Figure 3.8 Effect of aspect ratio r on minimum torsional damping.

CHAPTER IV

INELASTIC RESPONSE OF BILINEAR UNSYMMETRIC STRUCTURES

4.1 INTRODUCTION

During the last two decades considerable research has involved the dynamic response of inelastic systems. The majority of investigations concentrated either on simple single [33-36] or purely translational mutli degree-of-freedom systems [37-39] in which the resisting elements exhibited Ramberg-Osgood, bilinear or elasto-plastic hysteretic behaviour. However, only lately has interest focussed on the coupled lateral-torsional response of simple single-story systems [7-14]. Recent forced vibration tests of a multi-story eccentric building [40] confirmed that buildings behave in a nonlinear fashion when excited to different force levels during frequency sweep tests.

The primary cause of nonlinearity in large amplitude oscillation of structures is due to inelastic hysteretic behaviour resulting from the yielding of structural components or from interface slip between adjacent elements.

By far the most important among many characteristics of a single degree-of-freedom bilinear hysteretic system, as studied by Caughey and Iwan [33,34], is the softening behaviour for large amplitude response. Even for a general nonlinear hysteretic model of the Ramberg-Osgood type, Jennings [35,36] observed the same softening response characteristics.

Similarly, for a two degree-of-freedom translational system Iwan

[37] found the low frequency response peaks of both amplitudes to be typical of soft system response. Nigam [38] and Nigam and Housner [39], while investigating the translational response characteristics of a single-story symmetric frame, observed that the amplitude of response in one direction increased with simultaneous reduction in amplitude in the perpendicular direction due to coupling introduced through interaction among force-displacement relations, as well as due to energy dissipation by hysteresis. Nevertheless, the system exhibited softening frequency-response behaviour under harmonic excitation. In Reference 41, many interesting characteristics of both single and multi degree-of-freedom translational systems with a variety of hysteretic models are illustrated.

In Chapter I of this thesis, a review of the current literature describing the coupled lateral-torsional response of simple systems [7-14] has been presented.

This chapter is devoted to a study of the inelastic lateral-torsional response of a single-story monoeccentric building subjected to sinusoidal ground excitation. A frequency sweep analysis is employed because it can expose fundamental characteristies of an eccentric system similar to the results obtained experimentally from vibration tests [40]. The resisting elements are considered to be bilinear hysteretic for which elastic and pure elastic-plastic behaviour are the two limiting cases.

Results are presented in amplitude-frequency parameter space. The important system parameters controlling the response amplitudes are identified and their influence on the peak ductility demand is examined.

4.2 METHOD OF ANALYSIS

4.2.1 Equations of Motion

In order to study the inelastic behaviour of eccentric buildings, the single-story model shown in Figure 4.1 is considered. This idealized structure consists of a rigid deck supported by planar frame or wall assemblages situated at the periphery. In order to simplify the problem, the structure is assumed to be eccentric for excitation in the x-direction only. To follow the general trend in building design, this eccentricity is the result of unbalanced stiffnesses of the structural elements rather than due to eccentric mass. This system has two coupled degrees-of-freedom, namely horizontal displacement u of the mass centre relative to the ground in the x-direction and rotation θ about the vertical axis. For simplicity, the ground motion is assumed to be sinusoidal and directed along the x-axis. Thus

$$\ddot{u}_g = U \cos \omega t \qquad (4.1)$$

Letting k_{ix} and k_{iy} represent the translational stiffnesses of the i-th resisting element in the x- and y-directions respectively, total translational stiffness K_x and K_y and torsional stiffness of the structure with respect to centre of mass, $K_{\theta m}$, are given by

$$K_x = \Sigma\, k_{ix} \qquad (4.2a)$$

$$K_y = \Sigma\, k_{iy} \qquad (4.2b)$$

$$K_{\theta m} = \Sigma\, k_{ix}\, y_i^2 + \Sigma\, k_{iy}\, x_i^2 \qquad (4.2c)$$

The centre of resistance is located at distance e, the eccentricity measured from the centre of mass along the y-axis. Hence

$$e = \Sigma\, k_{ix}\, y_i / K_x \qquad (4.3)$$

The equation of motion of the system can then be written as

$$\begin{bmatrix} M & 0 \\ 0 & J_m \end{bmatrix} \begin{Bmatrix} \ddot{u} \\ \ddot{\theta} \end{Bmatrix} + \begin{bmatrix} C_x & 0 \\ 0 & C_\theta \end{bmatrix} \begin{Bmatrix} \dot{u} \\ \dot{\theta} \end{Bmatrix} + \begin{bmatrix} K_x & -K_x e \\ -K_x e & K_{\theta m} \end{bmatrix} \begin{Bmatrix} u \\ \theta \end{Bmatrix}$$

$$= - \begin{Bmatrix} U \cos \omega t \\ 0. \end{Bmatrix} \qquad (4.4)$$

where M is the mass of the deck, J_m is the mass moment of inertia of the deck about the vertical axis through the centre of mass, and C_x and C_θ are the translational and torsional viscous damping coefficients, respectively; the dots denote differentiation with respect to time t. It is assumed that linear element stiffnesses in the x-direction are such that $k_{2x} = (1+\eta)\, k_{1x}$, whereas for the y-direction $k_{3y} = k_{4y}$. The general hysteretic restoring forces of the resisting

elements can then be defined as

$$R_x(\delta_j) = k_{jx}\, F(\delta_j, \alpha, t) \ , \quad j = 1,2 \tag{4.5a}$$

$$R_y(\delta_j) = k_{jy}\, F(\delta_j, \alpha, t) \ , \quad j = 3,4 \tag{4.5b}$$

in which $F(\delta_j, \alpha, t)$ is any general function for the geometric description of the hysteretic skeleton curve, and δ_j $(j = 1, \ldots, 4)$ are the corresponding element displacements. The latter can be expressed as linear functions of system displacements u, θ and building plan dimensions a,b as follows

$$\delta_{1,2} = u \pm b\theta \tag{4.6a}$$

$$\delta_{3,4} = \mp\, a\theta \tag{4.6b}$$

after substituting Equations (4.5) and (4.6) into Equation (4.4) and letting

$$J_m = M\, r^2 \tag{4.7a}$$

$$\omega_x^2 = K_x/M \tag{4.7b}$$

$$\omega_y^2 = K_y/M \tag{4.7c}$$

$$\omega_\theta^2 = K_{\theta m}/J_m \tag{4.7d}$$

$$2\,\zeta_x\,\omega_x = C_x/M \tag{4.7e}$$

$$2\,\zeta_\theta\omega_\theta = C_\theta/J_m \tag{4.7f}$$

the equations of motion transform into

$$\ddot{u} + 2\zeta_x\omega_x\dot{u} + \frac{\omega_x^2}{(2+\eta)}\{(1+\eta)\,F(\delta_2,\,\alpha,\,t) + F(\delta_1,\,\alpha,\,t)\} = -U\cos\omega t \tag{4.8}$$

$$\ddot{\theta} + 2\zeta_\theta\omega_\theta\dot{\theta} - \frac{b\,\omega_x^2}{(2+\eta)\,r^2}\{(1+\eta)\,F(\delta_2,\,\alpha,\,t) - F(\delta_1,\,\alpha,\,t)\} + \frac{a\,\omega_y^2}{2\,r^2}\{F(\delta_4,\,\alpha,\,t) - F(\delta_3,\,\alpha,\,t)\} = 0 \tag{4.9}$$

in which r is the mass radius of gyration of the rigid diaphragm about the vertical axis through the centre of mass; ω_x, ω_y and ω_θ are the frequency parameters that may be interpreted as the uncoupled frequencies of the system, i.e., the fundamental natural frequencies of the structure if torsionally uncoupled but otherwise retaining translational and torsional stiffnesses identical to the coupled system; and ζ_x, ζ_θ denote the uncoupled ratios of critical viscous damping in x- and θ-directions, respectively.

In order to represent the model in a more meaningful manner, two important characteristics of the system must be accounted for. These are the stiffness and strength ratios given by

$$\beta = k_{2x}/k_{1x} \tag{4.10a}$$

$$\gamma = R_{y2}/R_{y1} \tag{4.10b}$$

in which β represent the ratio of the element stiffness in the unsymmetric direction and γ defines the corresponding ratio for yield shear strengths. These two parameters determine the degree of asymmetry in stiffness and strength of the system which have also been employed in earlier studies [7,9]. For the present study these ratios are assumed to be equal. The physical interpretation of this assumption is demonstrated in Figure 4.2, which shows that yield displacements δ_y of the elements are equal and that the yield shears are proportional to the elastic stiffness. The foregoing leads to the following relations

$$k_{1x} = R_{y1}/\delta_y \tag{4.11a}$$

$$k_{2x} = R_{y2}/\delta_y \tag{4.11b}$$

$$\beta = \gamma = 1+\eta \tag{4.11c}$$

It is convenient to express Equations (4.8) and (4.9) in nondimensional form with the following change of variables

$$\tau = \omega_x t \tag{4.12a}$$

$$\Lambda_x(t) = u(t)/\delta_y; \quad \Lambda_\theta(t) = \theta(t)/\theta_y \tag{4.12b}$$

in which τ represents nondimensional time, and Λ_x, Λ_θ represent nondimensional response of the system as functions of τ. The definition of θ_y could be taken as either of the following relations

$$\theta_y = \delta_y/b \qquad (4.13a)$$

$$\theta_y = \delta_y/a \qquad (4.13b)$$

depending upon aspect ratio $r = a/b$ and whether stiffnesses k_{iy} are situated at the periphery as in Figure 4.1 or directly on the y-axis as in Figure 4.3. Hence, four cases are possible, namely

(i) $b \geq a$ (i.e., $r \leq 1.0$) and $F(\delta_3)$ and $F(\delta_4)$ are situated at the periphery,

(ii) $a \geq b$ (i.e., $r \geq 1.0$) and $F(\delta_3)$ and $F(\delta_4)$ are situated at the periphery,

(iii) $b \geq a$ (i.e., $r \leq 1.0$) and $F(\delta_3)$ and $F(\delta_4)$ are situated directly on the y-axis,

(iv) $a \geq b$ (i.e., $r \geq 1.0$) and $F(\delta_3)$ and $F(\delta_4)$ are situated directly on the y-axis.

In cases (i), (iii) and (iv) the expression of Equation (4.13a) for θ_y is valid; otherwise Equation (4.13b) holds. It may be observed that, when the stiffness k_{iy} are located at the periphery, the resisting element situated farthest from the centre of mass will yield first due purely to rotational displacement. However, in cases where stiffnesses in the y-direction are situated on the y-axis, only the elements in the x-direction yield regardless of the magnitude of aspect ratio r, thus resulting in Equation (4.13a). Consequently, whatever the governing situation, θ_y always represents the initial

rotational yield displacement.

In order to confine the problem and yet allow differing structural strategies, only cases (iii) and (iv) are considered for the present study (Figure 4.3), although case (i) is included in the derivation of the general equation of motion.

Substituting Equations (4.11), (4.12) and (4.13a) and noting that $\delta_3 = -\delta_4$, one obtains the following two nondimensional equations of motion

$$\ddot{\Lambda}_x + 2\zeta_x\dot{\Lambda}_x + \frac{1}{2+\eta}\{f(\frac{\delta_1}{\delta_y}, \alpha, \tau) + f(\frac{\delta_2}{\delta_y}, \alpha, \tau)\}$$

$$+ \frac{\eta}{2+\eta} f(\frac{\delta_2}{\delta_y}, \alpha, \tau) = -\frac{U}{\delta_y \omega_x^2}\cos \Omega\tau \qquad (4.14)$$

$$\ddot{\Lambda}_\theta + 2\zeta_\theta\Omega_\theta\dot{\Lambda}_\theta + \frac{\gamma_0^2}{2+\eta}\{f(\frac{\delta_1}{\delta_y}, \alpha, \tau) - f(\frac{\delta_2}{\delta_y}, \alpha, \tau)\}$$

$$- \frac{\eta\gamma_0^2}{2+\eta} f(\frac{\delta_2}{\delta_y}, \alpha, \tau) + \frac{\beta_0^2\Omega_y^2}{r} f(\frac{\delta_4}{\delta_y}, \alpha, \tau) = 0 \qquad (4.15)$$

in which β_0, γ_0, Ω_y, Ω_θ and Ω are defined as follows

$$\beta_0 = a/\Gamma \quad ; \quad \gamma_0 = b/\Gamma \qquad (4.16a)$$

$$\Omega_y = \omega_y/\omega_x \quad ; \quad \Omega_\theta = \omega_\theta/\omega_x \quad ; \quad \Omega = \omega/\omega_x \qquad (4.16b)$$

For the case where stiffnesses k_{iy} fall on the y-axis, the last term of Equation (4.15) disappears since δ_4 is zero.

It is convenient to express $f(\frac{\delta_i}{\delta_y}, \alpha, \tau)$ explicitly in terms of Λ_x and Λ_θ, for which it is easy to establish the following relations

$$\frac{\delta_1}{\delta_y} = \Lambda_x + \Lambda_\theta \tag{4.17a}$$

$$\frac{\delta_2}{\delta_y} = \Lambda_x - \Lambda_\theta \tag{4.17b}$$

$$\frac{\delta_4}{\delta_y} = r\,\Lambda_\theta \tag{4.17c}$$

Substituting Equation (4.17) into Equations (4.14) and (4.15) reduces the equations of motion to the following form

$$\ddot{\Lambda}_x + 2\zeta_x\dot{\Lambda}_x + \frac{1}{2+\eta}\{f(\Lambda_x + \Lambda_\theta, \alpha, \tau) + f(\Lambda_x - \Lambda_\theta, \alpha, \tau)\}$$

$$+ \frac{\eta}{2+\eta} f(\Lambda_x - \Lambda_\theta, \alpha, \tau) = -\frac{U}{\delta_y \omega_x^2}\cos\Omega\tau \tag{4.18}$$

$$\ddot{\Lambda}_\theta + 2\zeta_\theta\Omega_\theta\dot{\Lambda}_\theta + \frac{\gamma_0^2}{2+\eta}\{f(\Lambda_x + \Lambda_\theta, \alpha, \tau) - f(\Lambda_x - \Lambda_\theta, \alpha, \tau)\}$$

$$- \frac{\eta\gamma_0^2}{2+\eta} f(\Lambda_x - \Lambda_\theta, \alpha, \tau) + \frac{\beta_0^2\,\Omega_y^2}{r} f(r\,\Lambda_\theta, \alpha, \tau) = 0 \tag{4.19}$$

4.2.2 Method of Solution

Equations (4.18) and (4.19) can be solved by applying the method of averaging, i.e., the method of slowly varying amplitude based on

the work of Kryloff and Bogoliuboff [29]. This method has been successfully used in the last three decades for a wide variety of problems such as nonlinear elastic ring and shell vibration [1-3], elastic torsional vibrations of buildings [27], and inelastic harmonic excitation of single and multi degree-of-freedom systems [33-38, 41, 42].

The use of the Kryloff-Bogoliuboff method in solving nonlinear inelastic problems has been demonstrated to be highly accurate provided the nonlinearity is small [33,34]. Caughey's amplitude-frequency response curve, based on this method, was normalized to predict response regardless of the degree of nonlinearity. In later work, both Jennings [35] and Nigam [38] used this curve to determine the response amplitude of elastic-perfectly plastic systems. Iwan [34] found the accuracy of this method to be within approximately 10% for hysteretic behaviour close to elasto-plastic, with the averaging method always predicting larger response. Motivated by this demonstration of its accuracy, the Kryloff-Bogoliuboff method was considered to provide approximate solutions that are accepted for the purposes of this study.

In this method it is assumed that the solution exists in the form

$$\Lambda_x(\tau) = A_1(\tau) \cos \{\Omega\tau + \Phi_1(\tau)\} \tag{4.20a}$$

$$\Lambda_\theta(\tau) = A_2(\tau) \cos \{\Omega\tau + \Phi_2(\tau)\} \tag{4.20b}$$

where A_1, A_2 are the slowly varying system amplitudes, and Φ_1 and Φ_2 are the corresponding slowly varying phase angles for the translational and torsional responses of the system. It can easily

be shown that the magnitudes of the resisting element displacements are certain functions of system amplitudes A_1 and A_2 and phase angles Φ_1 and Φ_2 as follows

$$\frac{\delta_1}{\delta_y} = \Lambda_x + \Lambda_\theta = A_3(\tau) \cos \{\Omega\tau + \Phi_3(\tau)\} \quad (4.21a)$$

$$\frac{\delta_2}{\delta_y} = \Lambda_x - \Lambda_\theta = A_4(\tau) \cos \{\Omega\tau + \Phi_4(\tau)\} \quad (4.21b)$$

$$\frac{\delta_4}{\delta_y} = r\,\Lambda_\theta = r\,A_2(\tau) \cos \{\Omega\tau + \Phi_2(\tau)\} \quad (4.21c)$$

in which A_3 and A_4 are the slowly varying amplitudes and Φ_3 and Φ_4 are the corresponding slowly varying phase angles for the translational displacements of the resisting elements. These are related to A_1, A_2, Φ_1 and Φ_2 by the following relations

$$A_3^2 = A_1^2 + A_2^2 + 2\,A_1A_2 \cos (\Phi_1 - \Phi_2) \quad (4.22a)$$

$$A_4^2 = A_1^2 + A_2^2 - 2\,A_1A_2 \cos (\Phi_1 - \Phi_2) \quad (4.22b)$$

$$\Phi_3 = \tan^{-1} \left\{\frac{(A_1 \sin \Phi_1 + A_2 \sin \Phi_2)}{(A_1 \cos \Phi_1 + A_2 \cos \Phi_2)}\right\} \quad (4.22c)$$

$$\Phi_4 = \tan^{-1} \left\{\frac{(A_1 \sin \Phi_1 - A_2 \sin \Phi_2)}{(A_1 \cos \Phi_1 - A_2 \cos \Phi_2)}\right\} \quad (4.22d)$$

Substituting Equations (4.20) - (4.22) into Equations (4.18) and (4.19), neglecting first-order variational terms as these will remain essentially constant while averaging over one cycle, and replacing A_i

and Φ_i by average values $\bar{A}_i$ and $\bar{\phi}_i$, one obtains the following four nonlinear coupled algebraic equations

$$\Omega^2\bar{A}_1 - \frac{1+\eta}{2+\eta}\{c_4(\bar{A}_4)\cos(\bar{\Phi}_4 - \bar{\Phi}_1) + S_4(\bar{A}_4)\sin(\bar{\Phi}_4 - \bar{\Phi}_1)\}$$

$$- \frac{1}{2+\eta}\{c_3(\bar{A}_3)\cos(\bar{\Phi}_3 - \bar{\Phi}_4) + S_3(\bar{A}_3)\sin(\bar{\Phi}_3 - \bar{\Phi}_1)\}$$

$$= \frac{U}{\delta_y \omega_x^2}\cos\bar{\Phi}_1 \qquad (4.23)$$

$$2\zeta_x\Omega\bar{A}_1 - \frac{1+\eta}{2+\eta}\{S_4(\bar{A}_4)\cos(\bar{\Phi}_4 - \bar{\Phi}_1) - c_4(\bar{A}_4)\sin(\bar{\Phi}_4 - \bar{\Phi}_1)\}$$

$$- \frac{1}{2+\eta}\, S_3(\bar{A}_3)\cos(\bar{\Phi}_3 - \bar{\Phi}_1) - c_3(\bar{A}_3)\sin(\bar{\Phi}_3 - \bar{\Phi}_1)$$

$$= \frac{U}{\delta_y \omega_x^2}\sin\bar{\Phi}_1 \qquad (4.24)$$

$$\Omega^2\bar{A}_2 + \frac{(1+\eta)\gamma_0^2}{2+\eta}\{c_4(\bar{A}_4)\cos(\bar{\Phi}_4 - \bar{\Phi}_2) + S_4(\bar{A}_4)\sin(\bar{\Phi}_4 - \bar{\Phi}_2)\}$$

$$- \frac{\gamma_0^2}{2+\eta}\{c_3(\bar{A}_3)\cos(\bar{\Phi}_3 - \bar{\Phi}_2) + S_3(\bar{A}_3)\sin(\bar{\Phi}_3 - \bar{\Phi}_2)\}$$

$$- \frac{\beta_0^2\,\Omega_y^2}{r}\, c_2(r\,\bar{A}_2) = 0 \qquad (4.25)$$

$$2\,\zeta_\theta\Omega_\theta\Omega\,\bar{A}_2 + \frac{(1+\eta)\,\gamma_0^2}{2+\eta}\, S_4(\bar{A}_4)\cos(\bar{\Phi}_4 - \Phi_2) - c_4(\bar{A}_4)\sin(\bar{\Phi}_4 - \bar{\Phi}_2)\}$$

$$- \frac{\gamma_0^2}{2+\eta}\{S_3(\bar{A}_3)\cos(\bar{\Phi}_3 - \bar{\Phi}_2) - c_3(\bar{A}_3)\sin(\bar{\Phi}_3 - \bar{\Phi}_2)\}$$

$$- \frac{\beta_0^2\,\Omega^2}{r}\, S_2(r\,\bar{A}_2) = 0 \qquad (4.26)$$

In the above, the general expressions for $C_i(\bar{A}_i)$, $S_i(\bar{A}_i)$ $i = 3,4$ and $C_2(r\,\bar{A}_2)$, $S_2(r\,\bar{A}_2)$ have the following forms

$$C_i(\bar{A}_i) = \frac{1}{\pi} \int_0^{2\pi} f(\bar{A}_i, \theta_i) \cos\theta_i \, d\theta_i \quad ; \quad i = 3,4 \qquad (4.27a)$$

$$S_i(\bar{A}_i) = \frac{1}{\pi} \int_0^{2\pi} f(\bar{A}_i, \theta_i) \sin\theta_i \, d\theta_i \quad ; \quad i = 3,4 \qquad (4.27b)$$

$$C_2(r\,\bar{A}_2) = \frac{1}{\pi} \int_0^{2\pi} f(r\,\bar{A}_2, \theta_2) \cos\theta_2 \, d\theta_2 \qquad (4.27c)$$

$$S_2(r\,\bar{A}_2) = \frac{1}{\pi} \int_0^{2\pi} f(r\,\bar{A}_2, \theta_2) \sin\theta_2 \, d\theta_2 \qquad (4.27d)$$

$$\theta_i = \Omega\tau + \bar{\Phi}_i \quad ; \quad i = 2,3,4 \qquad (4.27e)$$

Algebraic Equations (4.23) through (4.26) may now be regarded as a complete statement of the problem in terms of the four variables $\bar{A}_1$, $\bar{A}_2$, $\bar{\Phi}_1$ and $\bar{\Phi}_2$ which, when solved, yield the steady state approximate solutions for the system displacements and corresponding phase angles.

The functions $C_i(\bar{A}_i)$ and $S_i(\bar{A}_i)$ of Equation (4.27) are integrals over one complete cycle of oscillation. However, due to symmetry of the steady state normalized hysteresis loop shown in Figure 4.4, these integrals may be replaced by twice the integral over one half-cycle.

4.2.3 Functions $C_i(\bar{A}_i)$ and $S_i(\bar{A}_i)$

The general expressions for $C_i(\bar{A}_i)$ and $S_i(\bar{A}_i)$ of Equation (4.27) are similar to those derived by Iwan [37], since the same normalized shape of the bilinear hysteretic model was employed. Without going through the detailed derivation of these expressions, as this is done in References 33 and 37, the final forms of $C_i(\bar{A}_i)$ and $S_i(\bar{A}_i)$ reduce to

$$C_i(\bar{A}_i) = \frac{\bar{A}_i}{\pi}\left[\alpha\pi + (1-\alpha)\,\theta_i^* - \frac{(1-\alpha)}{2}\sin 2\theta_i^*\right];\ \bar{A}_i \geq 1.0;\quad i = 3,4 \tag{4.28a}$$

$$= \bar{A}_i \quad ;\ \bar{A}_i \leq 1.0\ ;\ i = 3,4 \tag{4.28b}$$

$$S_i(\bar{A}_i) = -\frac{\bar{A}_i}{\pi}(1-\alpha)\sin^2\theta_i^* \quad ;\ \bar{A}_i \geq 1.0\ ;\ i = 3,4 \tag{4.28c}$$

$$= 0 \qquad\qquad ;\ \bar{A}_i \leq 1.0\ ;\quad i = 3,4 \tag{4.28d}$$

where

$$\theta_i^* = \cos^{-1}\left(\frac{\bar{A}_i - 2}{\bar{A}_i}\right) \quad ;\ i = 3,4 \tag{4.28e}$$

The expressions for $C_2(r\,\bar{A}_2)$ and $S_2(r\,\bar{A}_2)$ do not differ much from the expressions for $C_i(\bar{A}_i)$ and $S_i(\bar{A}_i)$, except that amplitude $\bar{A}_2$ is associated with factor r. Thus, the expressions for $C_2(r\,\bar{A}_2)$ and $S_2(r\,\bar{A}_2)$ become

$$C_2(r\,\bar{A}_2) = \frac{r\,\bar{A}_2}{\pi}\left[\alpha\pi + (1-\alpha)\,\theta^*_{r_2} - \frac{(1-\alpha)}{2}\sin 2\theta^*_{r_2}\right] \quad ; \; r\,\bar{A}_2 \geq 1.0 \tag{4.29a}$$

$$= r\,\bar{A}_2 \quad ; \; r\,\bar{A}_2 \leq 1.0 \tag{4.29b}$$

$$S_2(r\,\bar{A}_2) = -\frac{r\,\bar{A}_2}{\pi}(1-\alpha)\sin^2\theta^*_{r_2} \quad ; \; r\,\bar{A}_2 \geq 1.0 \tag{4.29c}$$

$$= 0 \quad ; \; r\,\bar{A}_2 \leq 1.0 \tag{4.29d}$$

where

$$\theta^*_{r_2} = \cos^{-1}\left(\frac{r\,\bar{A}_2 - 2}{r\,\bar{A}_2}\right) \tag{4.29e}$$

4.2.4 Numerical Evaluation of Steady State Response

Equations (4.23) to (4.26), together with Equation (4.22) and Equations (4.28) and (4.29), form a complete set of nonlinear algebraic equations which yield the steady state average response of the system. It should be noted that Caughey [33], Iwan [34] and Jennings [35, 36], while dealing with single degree-of-freedom systems, successfully eliminated the phase angle from the two governing algebraic equations, thereby obtaining a single quadratic equation for the response amplitude. Even for a two degree-of-freedom translational system, Iwan [37] succeeded in eliminating the phase angles from the set of four equations and obtained two higher-order coupled nonlinear polynomial equations in terms of the average amplitudes. This reduction was possible because the system displacements were also the physical resisting

element displacements. Furthermore, in none of these systems was damping considered. For a similar situation, El-Zaouk and Dym [3] ignored the phase angles and damping from the start, thereby reducing two coupled algebraic equations to a single tenth-order equation. On the other hand, Evensen [1,2] failed in eliminating the phase angles from the set of four coupled algebraic equations derived for a two degree-of-freedom system even though the system displacements were also the resisting element displacements, in his case the modal displacements. However, modal damping was included in this formulation.

In the present investigation system displacements Λ_x and Λ_θ do not represent directly the element displacements, although one can be derived from the other by the relations of Equations (4.21) and (4.22). Furthermore, viscous damping has been included in the formulation presented here, making the consideration of phase angles necessary for the derivation of the approximate solutions. Because of the aforementioned considerations (i.e., damping and element vs. system displacements) algebraic Equations (4.23) through (4.26), together with Equations (4.21), (4.22), (4.28) and (4.29), are too cumbersome to allow elimination of the phase angles. Thus, amplitudes A_1-A_4 and phase angles Φ_1-Φ_4 were obtained directly from Equations (4.21) through (4.26), (4.28) and (4.29) without further modification using the IMSL* library subroutine. This subroutine, developed to solve a system of simultaneous nonlinear equations, is based on Brown's method

---

* International Mathematical and Statistical Libraries, Inc.; Houston, Texas, U.S.A.

[31] which is a quadratically convergent Newton-like method employing Gaussian elimination.

Equations (4.23) through (4.26), together with Equations (4.22), (4.28) and (4.29), contain the system parameters α, η, r, Ω_y, ζ_x, ζ_θ and $G_a = U/(\delta_y \omega_x^2)$. The nonlinearity parameter α ranges from zero for elasto-plastic to 1.0 for elastic behaviour, whereas intermediate values account for strain hardening. The parameters η, r and Ω_y represent, respectively, unbalanced stiffness as a measure of eccentricity, building plan aspect ratio and normalized lateral frequency. However, in order to conform with the parameters considered in earlier studies, it is worthwhile to replace η, r and Ω_y by nondimensional eccentricity ratio $\bar{e}$ and torsional to translational frequency ratio Ω_θ.

Parameters Ω_θ and $\bar{e}$ are related to η, r and Ω_y by the following expressions

$$\bar{e} = \frac{e}{r} = \frac{\sqrt{3}\ \eta}{(\eta+2)\ \sqrt{1+r^2}} \tag{4.30a}$$

$$\Omega_\theta^2 = \frac{3\ (1+r^2\Omega_y^2)}{(1+r^2)} \tag{4.30b}$$

For cases where stiffness k_{iy} lie directly on the y-axis, these lateral stiffness do not contribute to the torsional stiffness expressed in Equation (4.2c), thereby reducing the above expressions to

$$\bar{e} = \frac{\eta\ \Omega_\theta}{\eta+2} \tag{4.31a}$$

$$\Omega_\theta^2 = \frac{3}{1+r^2} \tag{4.31b}$$

which yield

$$\eta = \frac{2\bar{e}}{\Omega_\theta - \bar{e}} \tag{4.32a}$$

$$r = \sqrt{\frac{3-\Omega_\theta^2}{\Omega_\theta^2}} \tag{4.32b}$$

Thus, Equations (4.32a) and (4.32b) are employed in conjunction with Equations (4.23) through (4.29) in the following parametric study where the influence of system parameters Ω_θ, $\bar{e}$, α, ζ_x, ζ_θ and G_a is presented.

4.3 PARAMETRIC STUDY

4.3.1 System Properties and Ground Motion

In order to arrive at meaningful conclusions, system properties r, Ω_θ, $\bar{e}$, ζ_x and ζ_θ, bilinearity parameter α of the resisting elements, and the amplitude of input ground acceleration G_a are selected to possess commonly encountered values. In practice aspect ratio r varies over the range $0.5 \leq r \leq 2.0$; eccentricity $\bar{e}$ generally lies between $0 \leq \bar{e} \leq 0.4$; and for the torsional frequency ratio, $0.8 \leq \Omega_\theta \leq 2.0$ [9, 10, 12, 14].

It should also be noted that various investigators have interpreted the torsional frequency ratio Ω_θ differently; for example Irvine and Kountouris [12] considered torsional stiffness K_θ at the

centre of resistance and mass moment of inertia J at the centre of mass, whereas Kan and Chopra [9, 10, 11] considered both K_θ and J at the centre of mass to determine the uncoupled torsional frequency ω_θ. On the other hand, Tso and Dempsey [23] considered both K_θ and J at centre of resistance. The present study interprets the parameter Ω_θ in the same manner as Kan and Chopra [9-11].

Both the translational and torsional damping ratios, ζ_x and ζ_θ respectively, have magnitudes from 0 - 0.20 although in actual structures this depends upon the level of inelastic deformation experienced by the resisting elements. The latter is a function primarily of the amplitude of input ground acceleration G_a. For the present parametric study maximum normalized element deformation, or peak ductility demand (PDD), of 5 to 10 is considered sufficient and is achieved for a standard level of excitation corresponding to G_a=1.0. Irvine and Kountouris [12,13] studied behaviour with G_a as high as 12 by adjusting mass, yield strength and spectral acceleration of reference earthquakes and obtained peak ductility demands in the resisting elements up to a magnitude of 42.

Unless subjected to parametric variation or stated otherwise, the aforementioned system variables remain fixed at the standard values listed in Table 4.1.

4.3.2 Response Amplitudes

Effect of coefficient α

In order to determine the effect of bilinearity parameter α, the system was analyzed for α = 0, 0.05 and 1,0, for which the results

are presented in Figures 4.5 and 4.6. With $\alpha = 0$, the system is considered to have elasto-plastic resisting elements; with $\alpha = 1.0$ the system behaves elastically, whereas for $\alpha = 0.05$ the resisting elements exhibit some strain hardening.

The peak ductility demands of the translational and torsional displacements Λ_x and Λ_θ of the system are shown in Figures 4.5a and 4.5b, respectively. It is noted that two amplitude peaks appear for most systems, identifying some sort of resonance with the two coupled natural frequencies of the system. For the linear system (i.e., $\alpha = 1.0$), the coupled frequencies ω_1 and ω_2 can be expressed in terms of uncoupled frequency ratio Ω_θ and eccentricity $\bar{e}$ as follows

$$\Omega_{1,2}^2 = \left(\frac{\omega_{1,2}}{\omega_x}\right)^2 = \tfrac{1}{2}\,(\Omega_\theta^2+1) \mp \sqrt{\tfrac{1}{4}(\Omega_\theta^2-1)^2 + \bar{e}^2} \qquad (4.33)$$

With the standard magnitudes $\Omega_\theta = 1.0$ and $\bar{e} = 0.2$ the values of Ω_1 and Ω_2 are 0.894 and 1.095, which correspond to the resonant input frequencies Ω at which the peaks are observed for $\alpha = 1.0$ in Figure 4.5.

In the case of elasto-plastic and bilinear hysteretic systems, these two peaks occur for translational amplitude (Figure 4.5a) but not for the torsional amplitude (Figure 4.5b). It is difficult to express the system frequency equations in terms of Ω_θ, $\bar{e}$ and α since the system is nonlinear. Nevertheless, the peaks in the nonlinear systems appear at frequencies considerably lower than for the corresponding linear system. It is also noted that, for $\alpha = 0$ and 0.05, the torsional response curves of Figure 4.5b appear to lean

toward the lower frequency direction, which characterizes the behaviour typical of soft systems. Since a unique set of amplitude values are found over the entire frequency range, the so-called "jump-phenomenon" or instability does not occur. Both the torsional and translational amplitudes remain virtually unaffected by the change in the magnitude of α at high frequencies, i.e., beyond $\Omega \approx 1.5$. For the elasto-plastic system (i.e., $\alpha = 0$), infinite values of lateral and rotational displacements are observed at $\Omega=0$ indicating an unstable or continuously yielding structure when loading is static. However, with the introduction of slight strain hardening (i.e., $\alpha=0.05$), the structure remains stable with finite values of lateral and rotational amplitudes even when $\Omega=0$.

The corresponding response amplitudes of the resisting elements are shown in Figures 4.6a and 4.6b for elements 1 and 2, the far and near elements with respect to the centre of resistance, respectively. It is observed that the frequencies corresponding to the peak ductility demands in these elements are in conformity with the lower and higher frequencies related to the translational amplitude peaks of Figure 4.5a. Both elements remain elastic and exhibit the same amplitude for input frequencies beyond 1.5 for any magnitude of α. However, the situation is quite different at low values of Ω, where the far element (element 1) exhibits increasing inelastic response with decreased magnitude of α but the near element (element 2) shows elastic and equal magnitude of response for all α at frequencies between 0-0.5, approximately.

For the particular set of standard values for the system parameters considered here (see Table 4.1), both peak system and element

displacements are lower for inelastic behaviour compared to peak elastic response; however, the situation may be reversed with increasing G_a. For example, with G_a=2.0 the PDD for element 1 with α=0.05 is found to be 53, whereas the corresponding response ratio is 22 for elastic behaviour (see Figure 4.5c).

4.3.3 Effect of Damping

Figures 4.7a and 4.7b present the effect of translational damping ζ_x on the far and near element response amplitudes for α=0.05. As for all dynamic systems, the amplitude of response decreases with increased translational damping. Similar behaviour is observed for varying torsional damping ζ_θ, as shown in Figure 4.8. It may be noted that damping has virtually no effect on the element response when Ω>1.3, approximately. Also, comparing Figure 4.7 with Figure 4.8 one observes that torsional and translational damping appear to be equally effective in reducing the response.

4.3.4 Effect of Ω_θ

Figures 4.9 and 4.10 illustrate the effect of torsional to translational frequency ratio Ω_θ on the response amplitudes and peak ductility demand of the resisting elements.

From the response amplitude curves for element 1, shown in Figure 4.9, it is observed that when the structure is harmonically excited at a fixed value of input frequency Ω, the system's torsional frequency Ω_θ hardly influences the element response. However, the peak ductility demand, obtained as the maximum response amplitude over Ω, shows

substantially different behaviour as indicated by Figure 4.10. It is seen that, although Ω_θ does not influence element 2 in a major way, element 1 is critically affected, particularly for torsionally flexible systems possessing large eccentricities.

It may also be observed in Figure 4.10 that a structure with low eccentricity does not experience pronounced torsional coupling when the torsional and translational frequencies are close (i.e., $\Omega_\theta \simeq 1.0$), as has frequently been demonstrated in the case of linear elastic structures. This absence of amplitifed response in inelastic systems is a relatively important observation, since much emphasis has been given to the problem of sympathetic resonance caused by coincident frequencies, in both earlier studies [16,17] as well as by building codes [23,24]. Nevertheless, Tso and Sadek [14] reported a similar absence of magnification in response for yielding systems even though torsional and translational frequencies are close.

4.3.5 Effect of Eccentricity $\bar{e}$

Figures 4.11 through 4.13 show the effect of nondimensional eccentricity $\bar{e}$ on the element response amplitudes for structures of differing torsional stiffness for which Ω_θ=0.5, 1.0 and 1.5. The response amplitude of element 1 (Figures 4.11a, 4.12a and 4.13a) increases with increase in eccentricity at low input frequency Ω and decreases somewhat with increased eccentricity at higher values of Ω . At a particular magnitude of Ω , the response amplitude is stationary irrespective of eccentricity $\bar{e}$. However, a reverse trend is observed for the response amplitude of element 2 (Figures

4.11b, 4.12b, and 4.13b), again with stationary amplitude at a frequency ratio which is close to that observed for element 1.

The magnitude of excitation frequency Ω, for which amplitude is stationary with respect to eccentricity $\bar{e}$, shifts toward higher frequency Ω for torsionally stiffer structures. This phenomenon appears to result from a high degree of torsional coupling with increasing eccentricity when excitation frequency $\Omega<1.0$, this produces an increase in deformation for element 1 and a corresponding decrease for element 2 at low frequency ratio Ω. The reverse effect, although less pronounced, occurs at higher values of Ω. However, Kan and Chopra [9] observed a similar trend only in systems where $\Omega_\theta>2.0$ but for earthquake response.

Figure 4.14 shows the effect of eccentricity on the amplitude of phase angle Φ_3 and Φ_4 for elements 1 and 2, respectively. At any particular input frequency Ω, the near element phase angle Φ_4 is larger than the far element phase angle Φ_3; the former is consistently larger and the latter consistently smaller than the phase angle of the corresponding symmetric system where $\bar{e}=0$. This indicates that, for any excitation frequency Ω, the response of the near and far elements of an eccentric system are always out of phase, clearly indicating the absence of absolute resonance in deformation amplitude.

The effect of eccentricity on the peak ductility demand (PDD) for the two nonlinear resisting elements, as well as for the translational and torsional system displacements, is presented in Figure 4.15a through 4.15c for $\Omega_\theta=0.5$, 1.0 and 1.5 respectively. It is observed that the peak ductility demand in element 1 increases rapidly with increase in eccentricity, whereas for element 2 it decreases relatively slowly with increase in $\bar{e}$. In the case of peak displacements of the

system, the translational displacement initially decreases somewhat with increase in eccentricity followed by a consistent increase at large eccentricity. On the other hand, torsional displacement increases with increase in eccentricity from the start. Generally, at large eccentricity ($\bar{e}$>0.15, say) the PDD of both the torsional and translational system displacements are nearly equal. However, the magnitude of the peak ductility demand, both for the system as well as the resisting elements, appears to be most pronounced for torsionally flexible structures (i.e., Ω_θ=0.5) and decreases as the system becomes torsionally stiffer, i.e., at higher values of Ω_θ.

Thus, it appears that in torsionally flexible structures, eccentricity $\bar{e}$ does not affect the PDD of the near resisting element. However, for torsionally stiff structures, increase in eccentricity rapidly brings this element toward the elastic range. This agrees with the observation of Irvine and Kountouris [12], but only in a restricted sense. They observed a similar trend for an element near the centre of mass and were also able to demonstrate this analytically for elastic behaviour, concluding that "there does not appear to be strong correlation between PDD and eccentricity, provided that the eccentricity ratio is limiated to about 0.25". However, PDD curves vs eccentricity for the far element were unfortunately not studied.

4.3.6 Effect of Excitation Level G_a

The effect of increasing ground acceleration amplitude G_a is shown in Figure 4.16 for elements 1 and 2. The structure remains elastic beyond input frequency Ω≈1.5, even when G_a=2.0. With increased

magnitude of G_a the peak response amplitude of the resisting element shifts gradually toward the low frequency range. This is probably due to decreasing natural frequency of the coupled system caused by increased deterioration accompanying yielding of the resisting elements at higher levels of excitation.

In Figure 4.17, the peak amplitudes of response of the resisting elements as well as the system displacements are plotted against amplitude of ground acceleration G_a. It is observed that, for both the resisting elements and the translational displacement of the system, the peak amplitudes are almost linearly related to G_a beyond G_a=1.25 - 1.5, approximately. However, the torsional system displacement, although increasing, does not increase proportionately with increase in G_a probably due to comparatively slow deterioration in torsional stiffness of the system. Similar trends for resisting elements were also observed by Irvine and Kountouris [12] for real earthquakes with a maximum PDD of 42.

4.4 CONCLUSIONS

This chapter is concerned with the coupled inelastic lateral-torsional response of a single-story monosymmetric building with bilinear hysteretic elements. The results of the frequency sweep analysis employed lead to the following conclusions.

1. The response of a bilinear hysteretic structure is found to be free from the "jump-phenomenon", indicating stable behaviour within the entire frequency domain.

2. The bilinearity parameter α appears to have no influence

on response amplitudes of the resisting elements for input frequency ratio Ω larger than 1.5. However, at $\Omega<0.5$ the system as well as some element response amplitudes are strongly influenced by α. At $\Omega=0$ the system becomes unstable when α is set at zero.

3. Torsional and translational damping appear to be equally effective in their usual role of reducing response. However, damping has virtually no effect on element response when $\Omega>1.3$, approximately.

4. The uncoupled torsional to translational frequency ratio Ω_θ of the system hardly influences element response when the structure is harmonically excited at a fixed magnitude of input frequency ratio Ω. However, Ω_θ does have major effect on the peak ductility demand of element 1 although it does not influence element 2 for torsionally flexible systems possessing large eccentricity.

5. A structure with low eccentricity does not experience pronounced torsional coupling when the torsional and translational frequencies are close, in contrast to the observation for linear elastic structures.

6. The response of the near and far elements of a damped eccentric system are always out of phase when the system is excited at a particular frequency Ω, clearly indicating the absence of absolute resonance in deformation amplitude.

7. The peak ductility demand of element 1 increases rapidly with increase in eccentricity, whereas for element 2 it decreases relatively slowly with increase in $\bar{e}$. Thus, it appears that in torsionally flexible structures, eccentricity $\bar{e}$ does not affect the PDD of the near resisting element; however, for a torsionally stiff structure

an increase in eccentricity rapidly brings this element toward the elastic range.

8. The peak ductility demand of the resisting elements is related almost bilinearly to ground acceleration amplitude G_a, having different slopes with a transition in the neighbourhood of $G_a \simeq 1.0$ to 1.5. Between $0 < G_a < 1.0$, the resisting elements, although undergoing inelastic deformation, lose stiffness only moderately compared to the respective elastic stiffness. The drastic change in element response beyond $G_a \simeq 1.5$ occurs because the resisting elements retain only the reduced stiffness αk when undergoing pronounced yielding at high levels of excitation.

TABLE 4.1

STANDARD VALUES OF SYSTEM PARAMETERS

PARAMETER	Ω_θ	$\bar{e}$	ζ_x	ζ_θ	α	G_a
Value	1.0	0.2	0.05	0.05	0.05	1.0

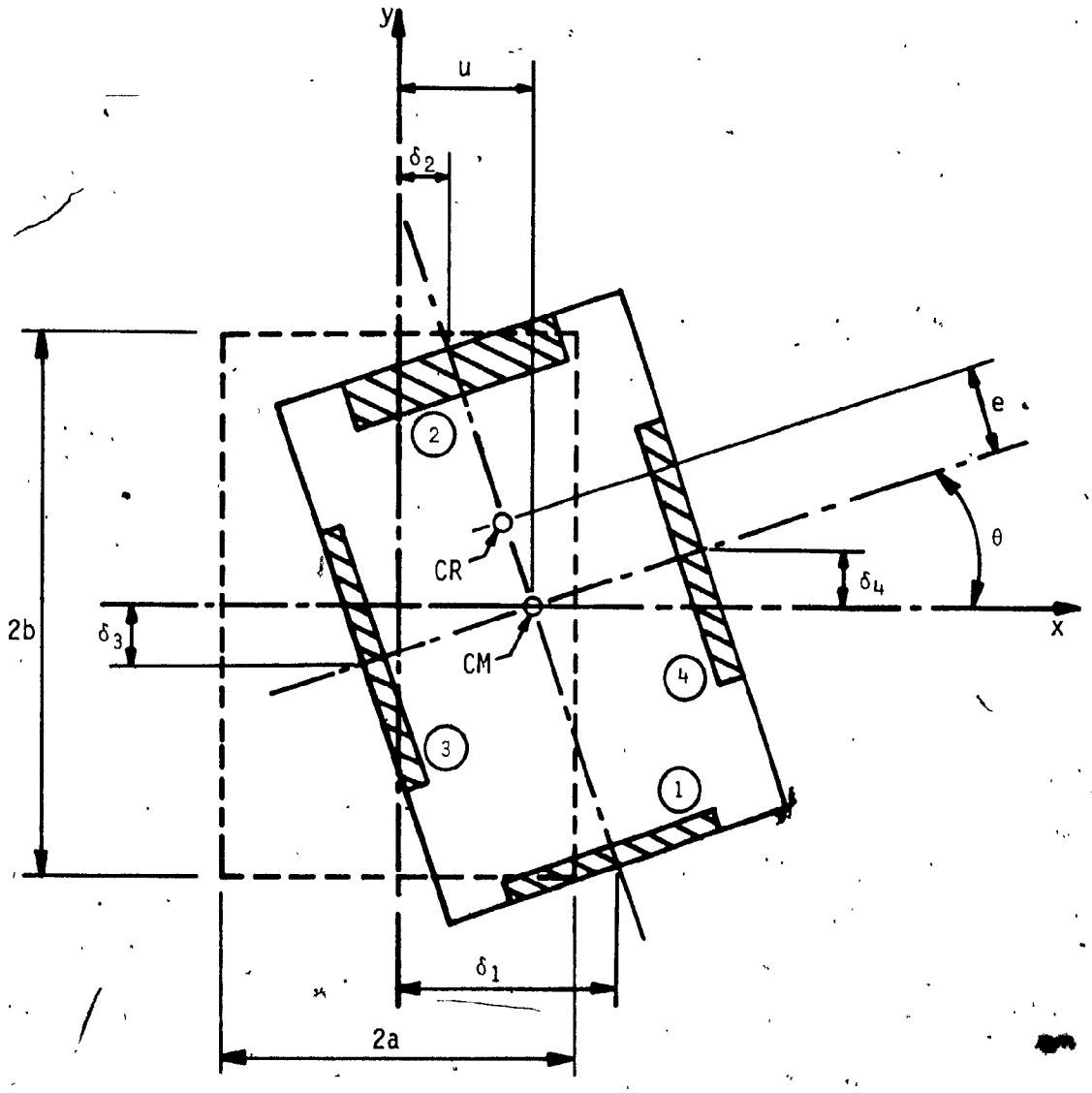

Figure 4.1. Lateral-torsional displacement of unsymmetric structure.

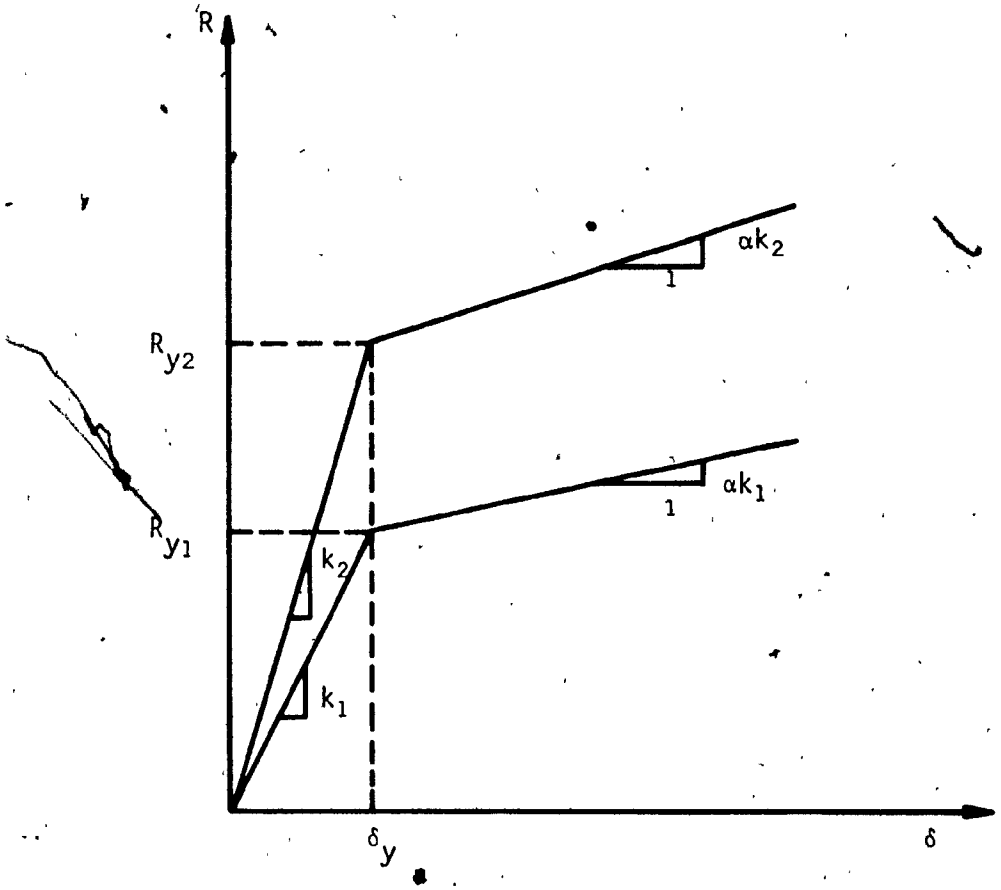

Figure 4.2 Restoring force vs. displacement relations.

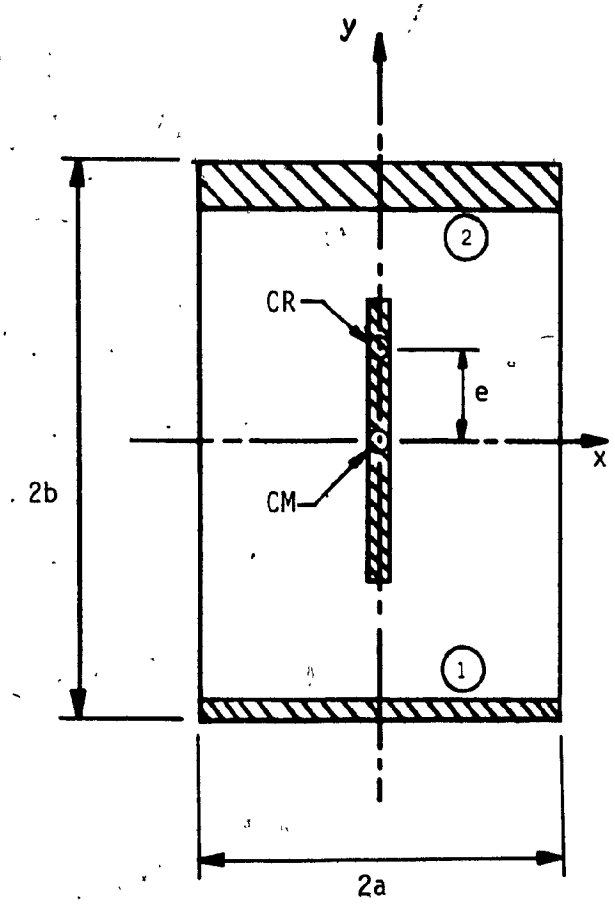

Figure 4.3 Structural arrangement of load resisting elements.

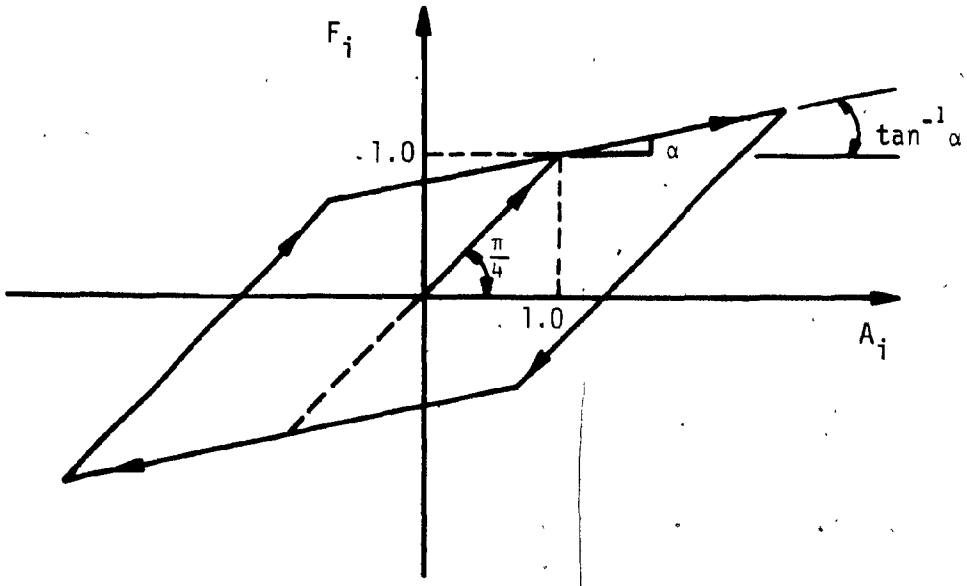

Figure 4.4 Normalized bilinear hysteretic force-displacement relation.

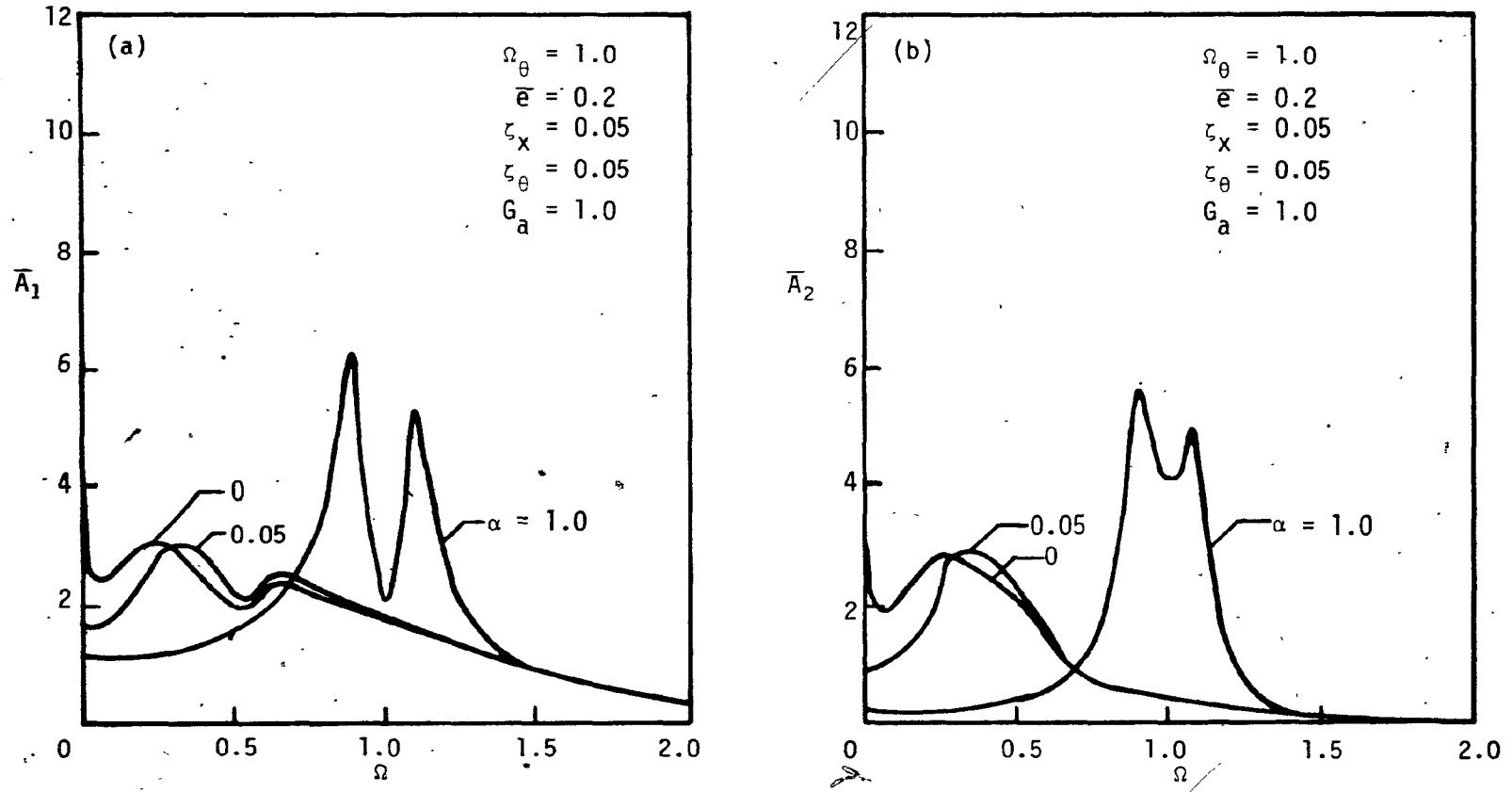

Figure 4.5 Effect of bilinearity parameter α on response amplitudes for G_a=1.0: (a) translational amplitudes; (b) torsional amplitudes; (c) amplitudes of resisting element 1 for G_a=2.0.

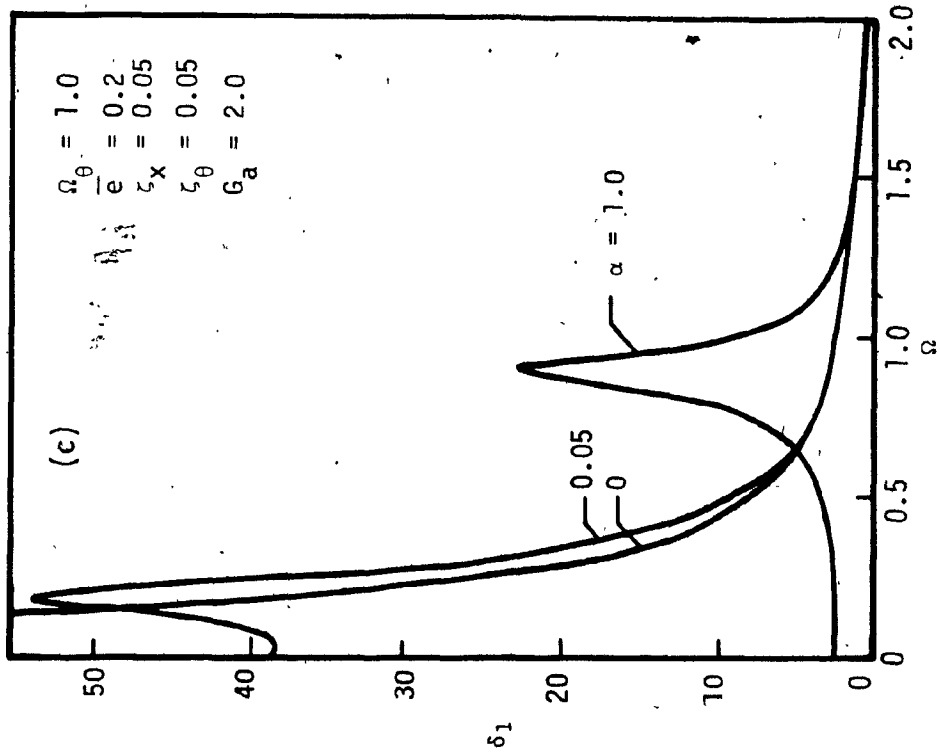
(c)
Ω_θ = 1.0
e = 0.2
ζ_x = 0.05
ζ_θ = 0.05
G_a = 2.0
α = 1.0
0.05
0
δ_1
Ω
0
10
20
30
40
50
0
0.5
1.0
1.5
2.0

Figure 4.5(c)

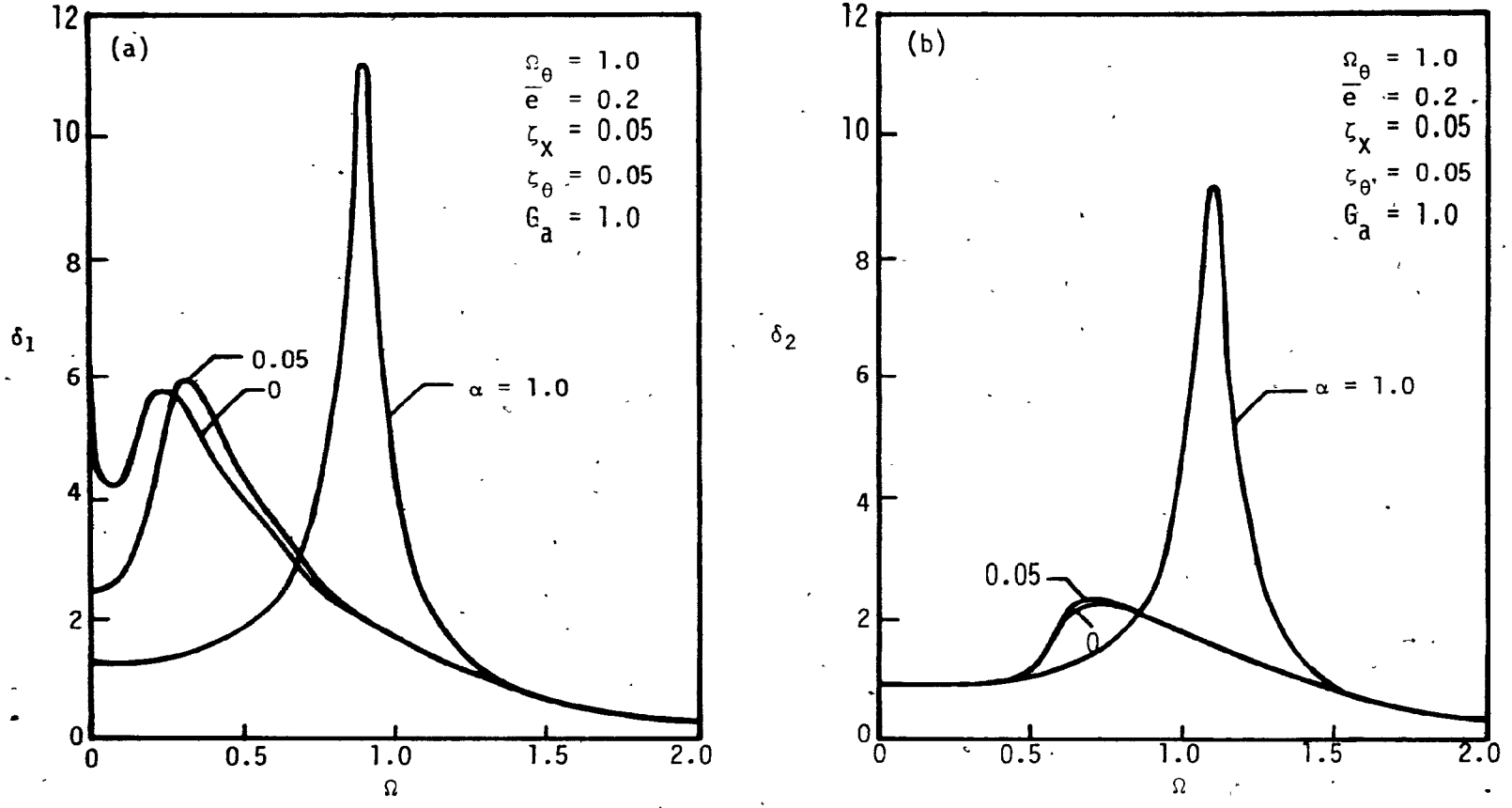

Figure 4.6 Effect of bilinearity parameter α on response amplitudes of resisting elements.

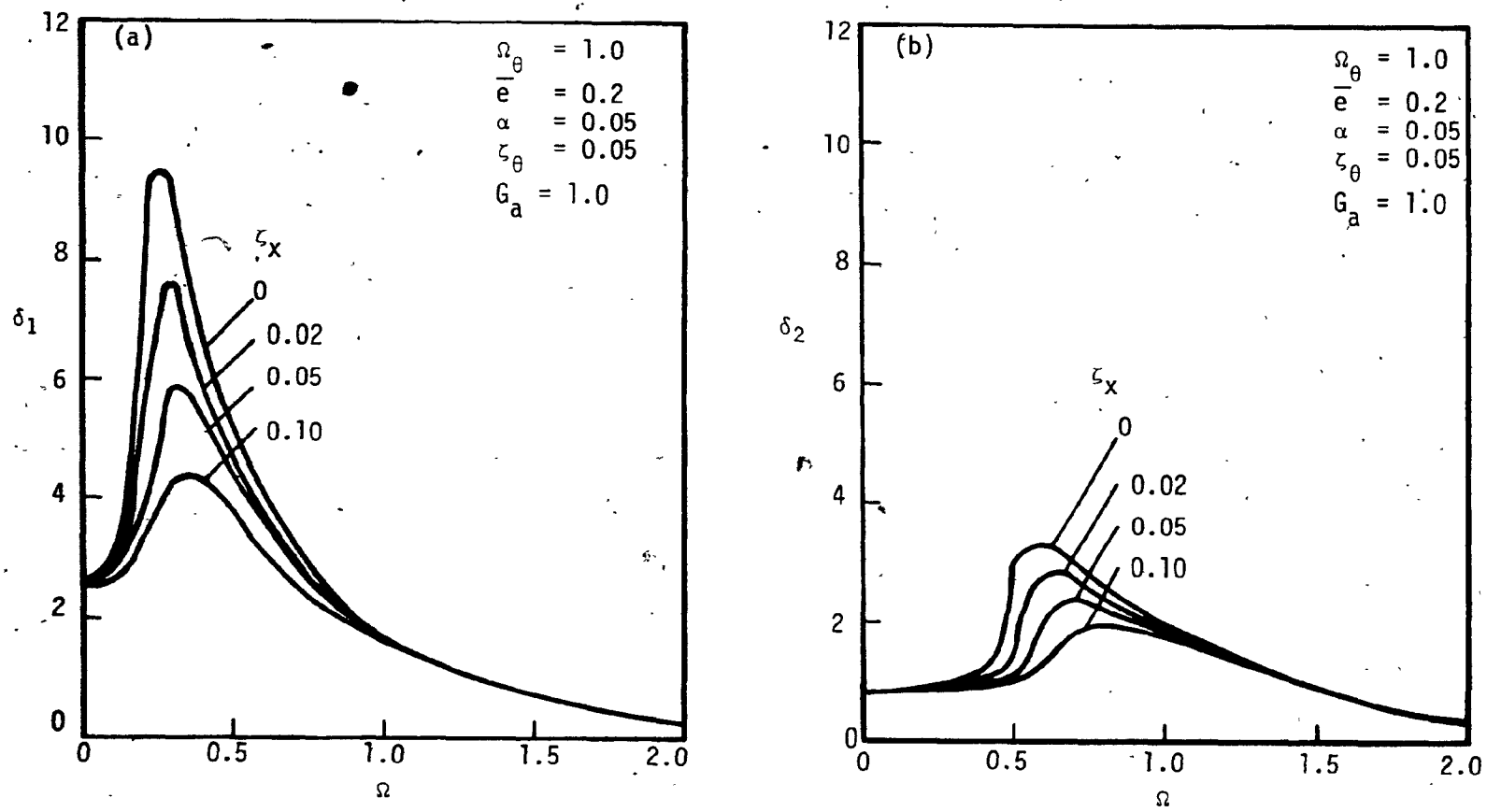

Figure 4.7 Effect of translational damping ζ_x on response amplitudes of resisting elements.

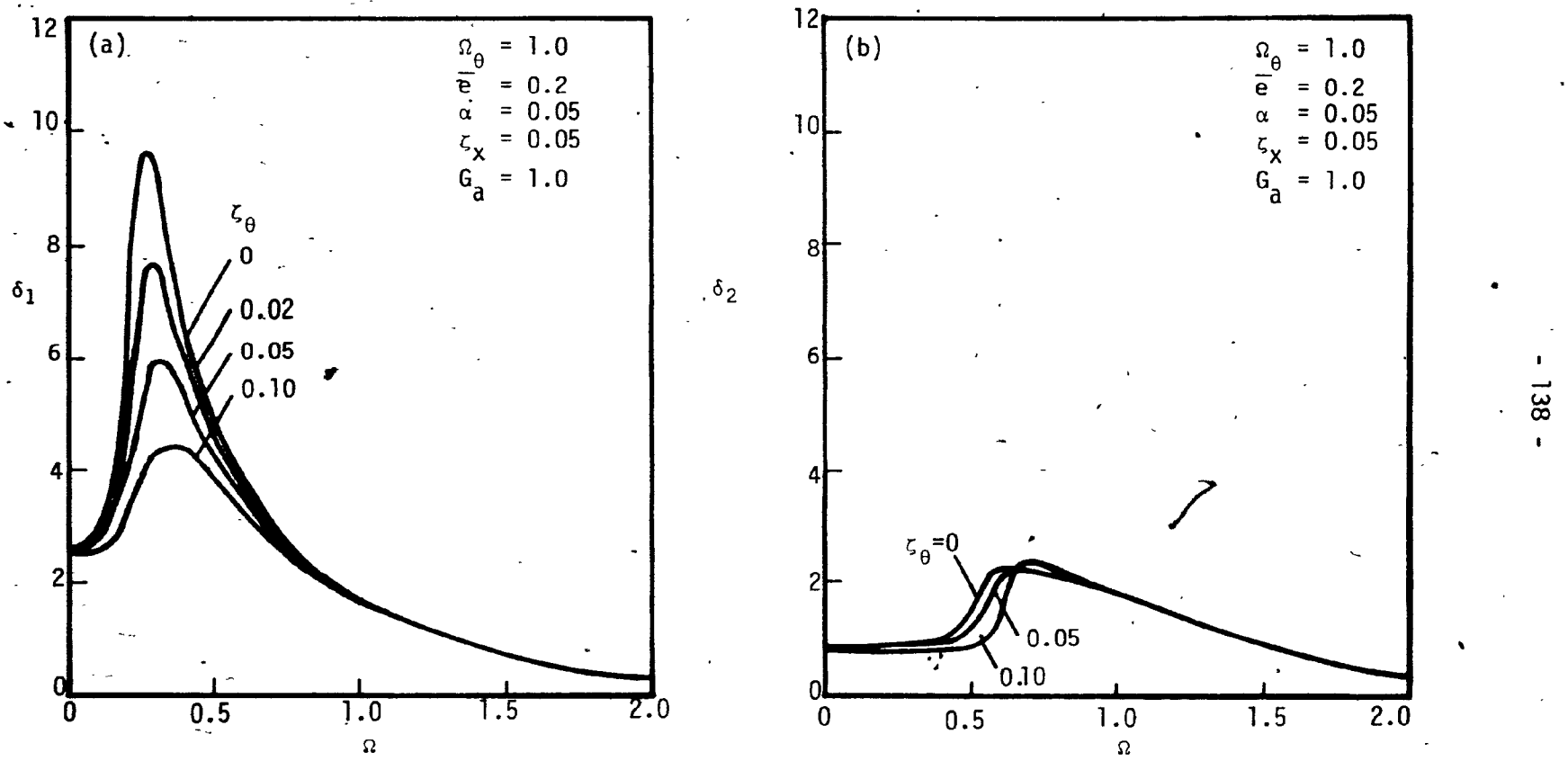

Figure 4.8 Effect of torsional damping ζ_θ on response amplitudes of resisting elements.

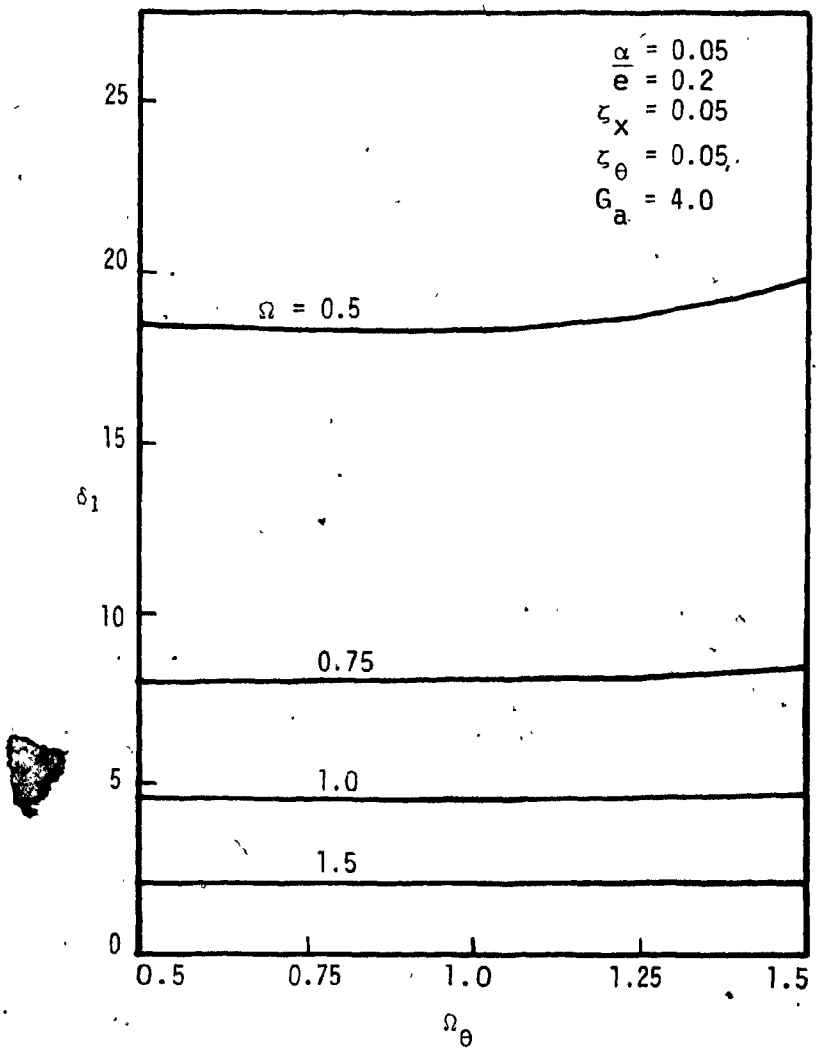

Figure 4.9 Effect of torsional to translational frequency ratio Ω_θ on element response amplitudes

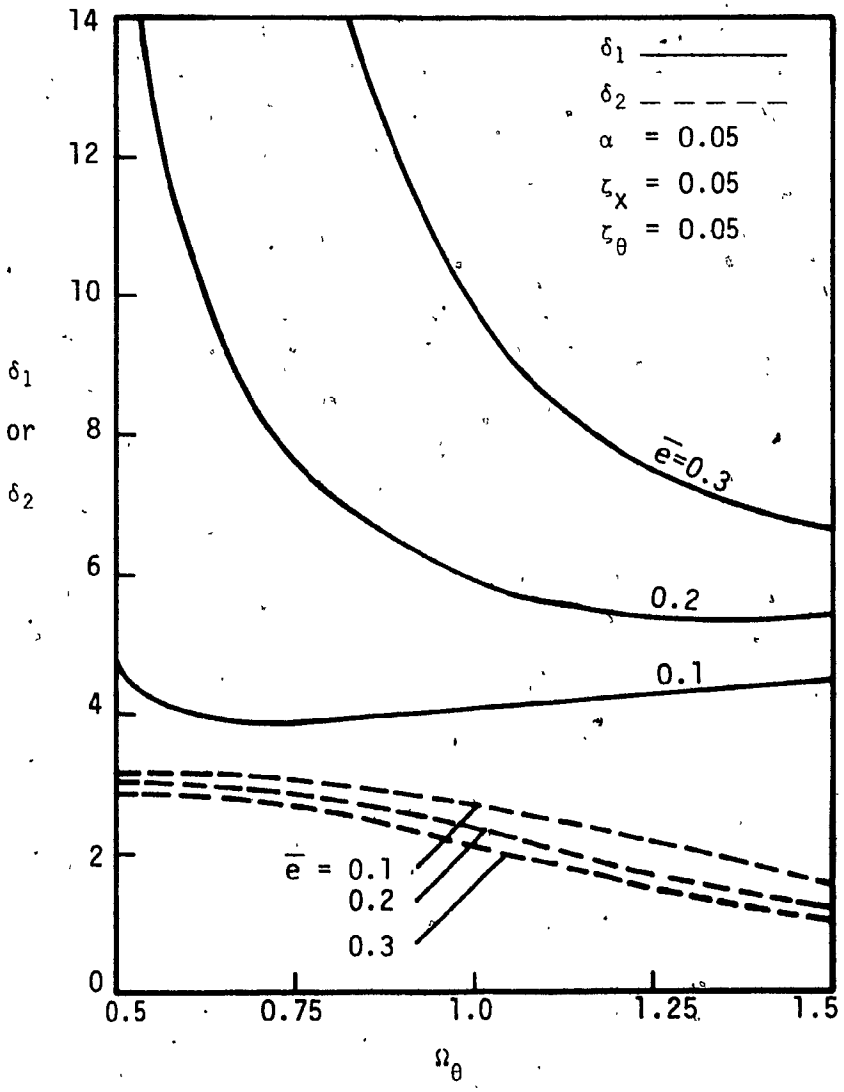

Figure 4.10 Effect of torsional to translational frequency ratio Ω_θ and nondimensional eccentricity $\bar{e}$ on peak ductility demand of resisting elements.

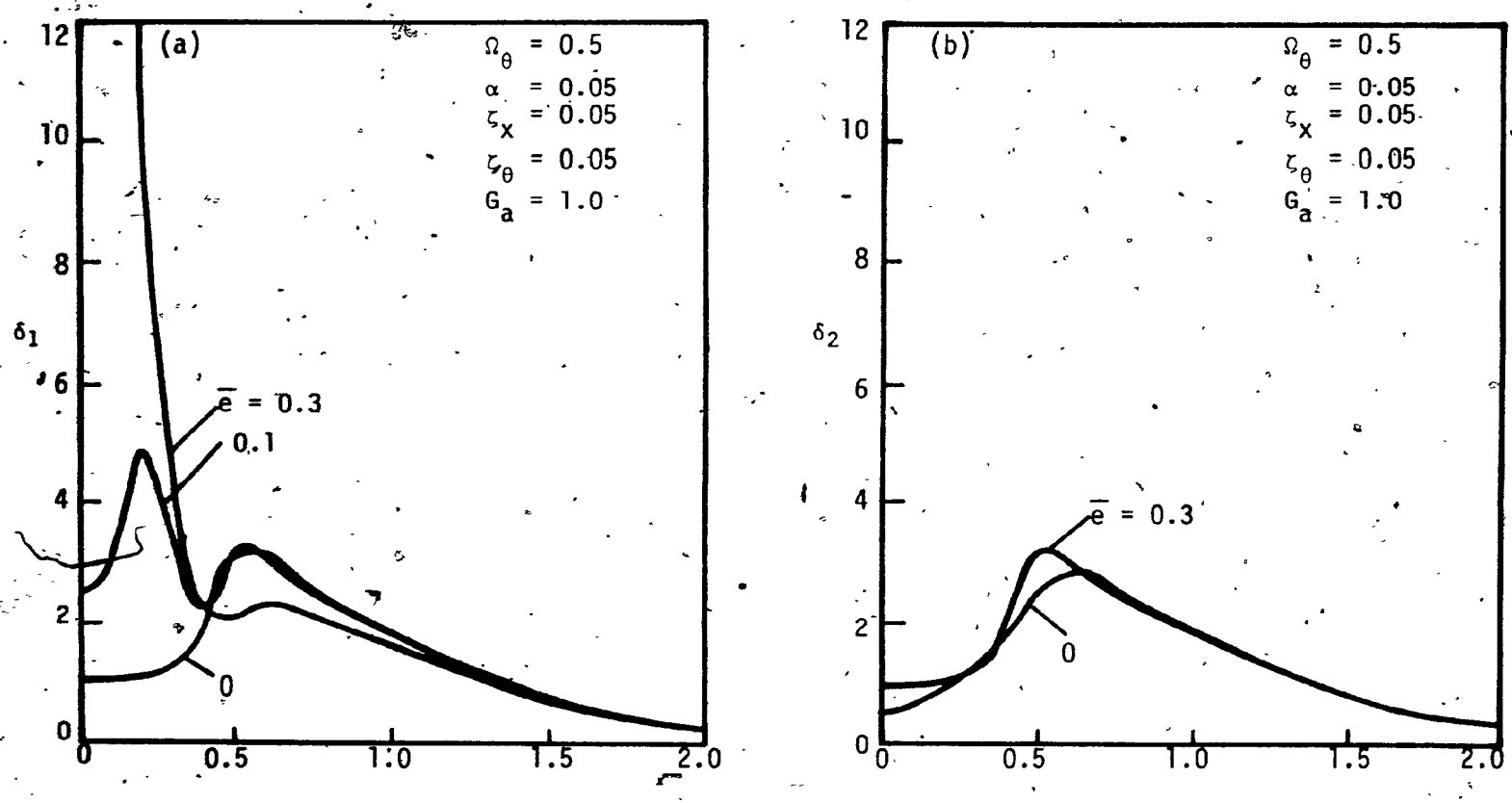

Figure 4.11 Effect of eccentricity $\bar{e}$ on element response amplitudes for $\Omega_\theta = 0.5$.

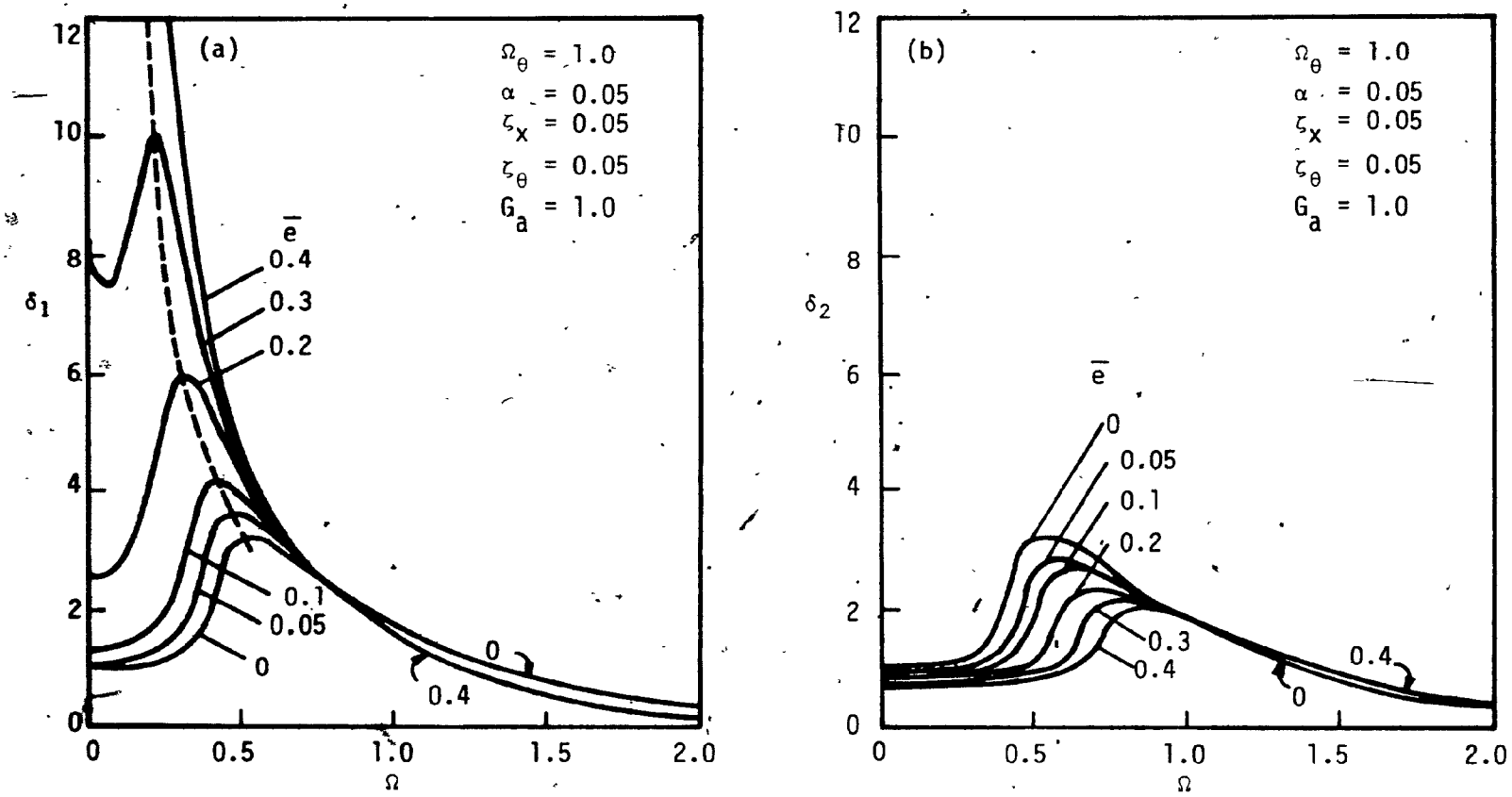

Figure 4.12 Effect of eccentricity $\bar{e}$ on element response amplitudes for $\Omega_\theta = 1.0$.

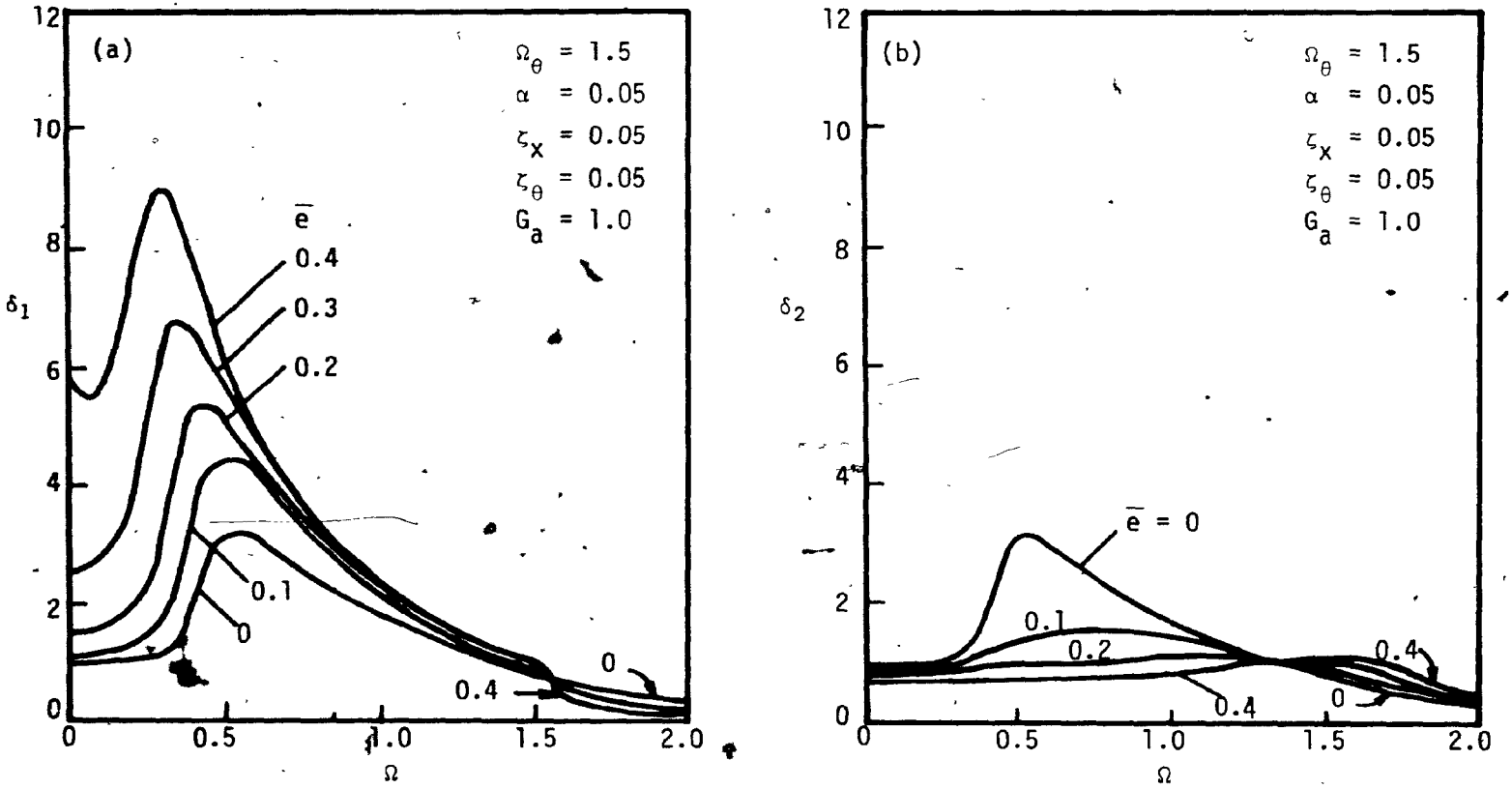

Figure 4.13 Effect of eccentricity $\bar{e}$ on element response amplitudes for Ω_θ = 1.5.

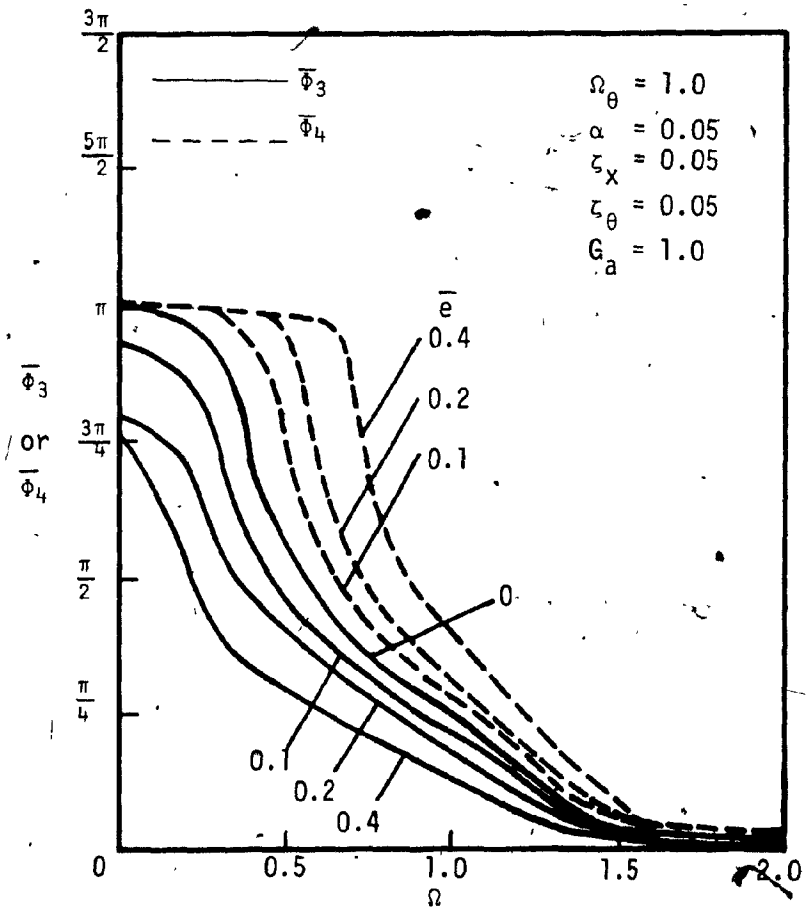

Figure 4.14 Effect of eccentricity $\bar{e}$ on amplitude of phase angles $\bar{\Phi}_3$ and $\bar{\Phi}_4$ for resisting elements.

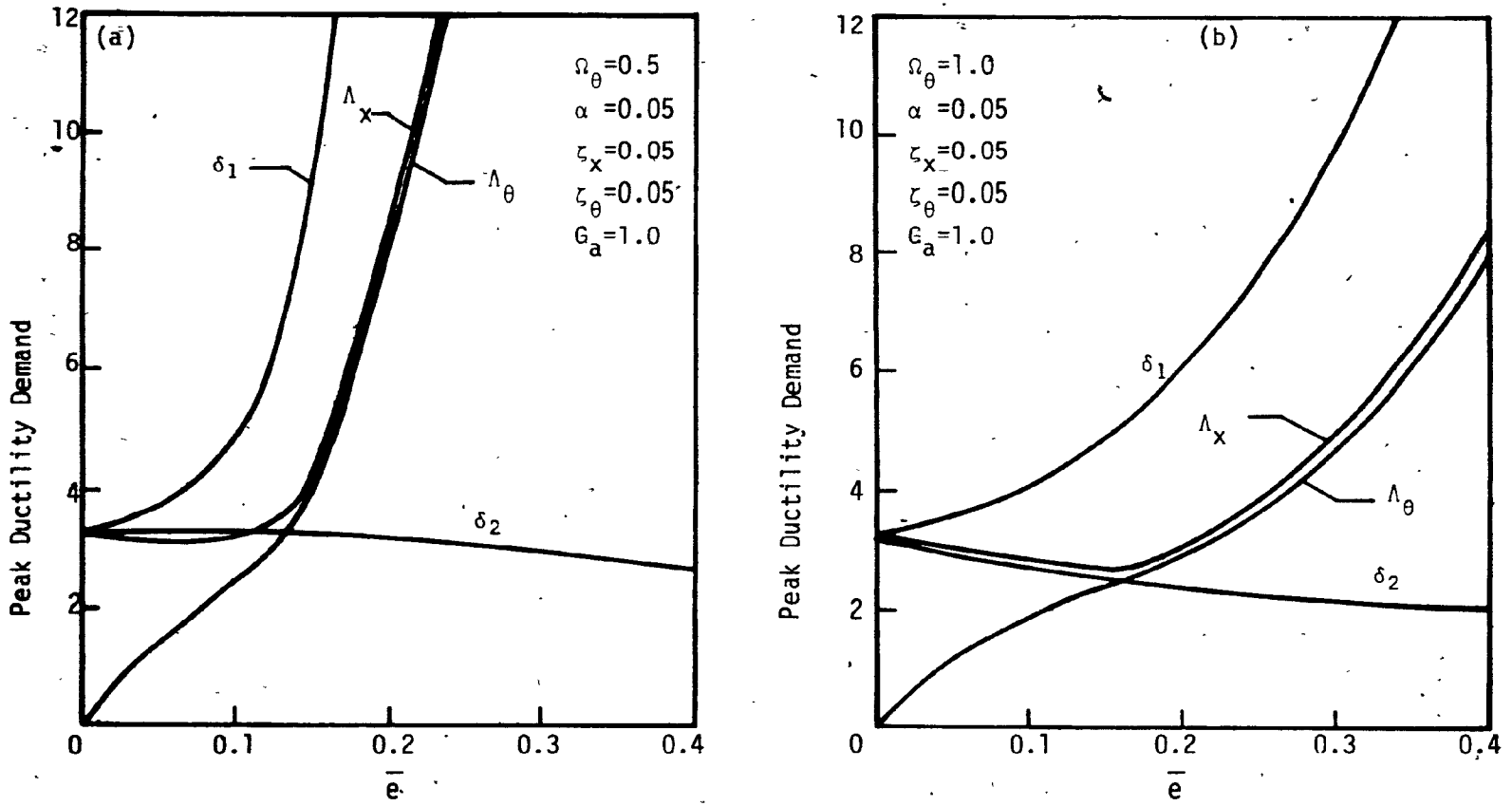

Figure 4.15 Effect of eccentricity $\bar{e}$ on peak ductility demand for resisting elements and translational and torsional system displacements.

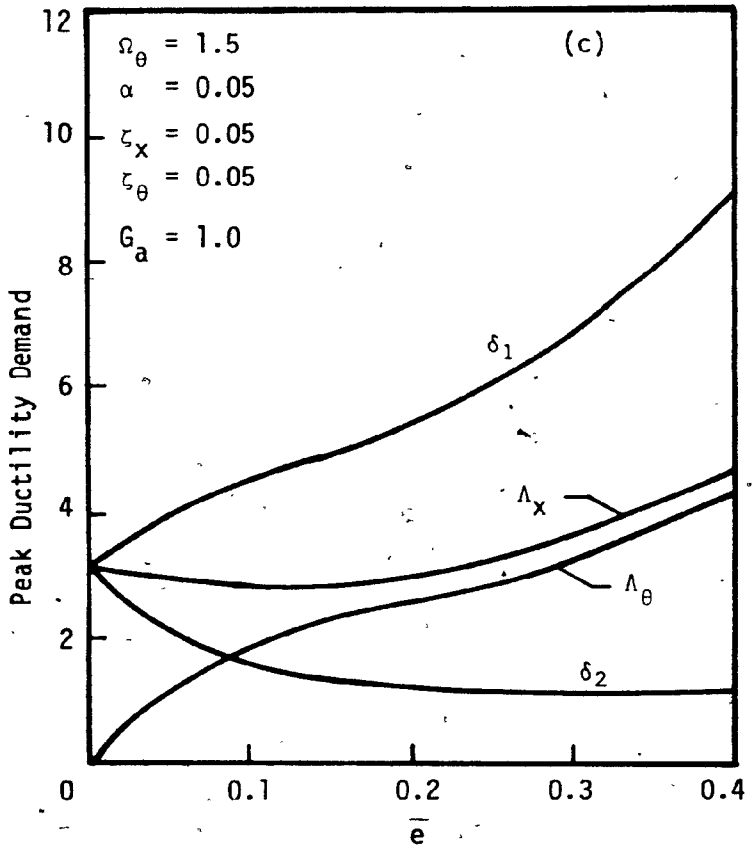
12
10
8
6
4
2
0
Ω_θ = 1.5
(c)
α = 0.05
ζ_x = 0.05
ζ_θ = 0.05
G_a = 1.0
δ_1
Λ_x
Λ_θ
δ_2
Peak Ductility Demand
0.1
0.2
0.3
0.4
$\bar{e}$

Figure 4.15(c)

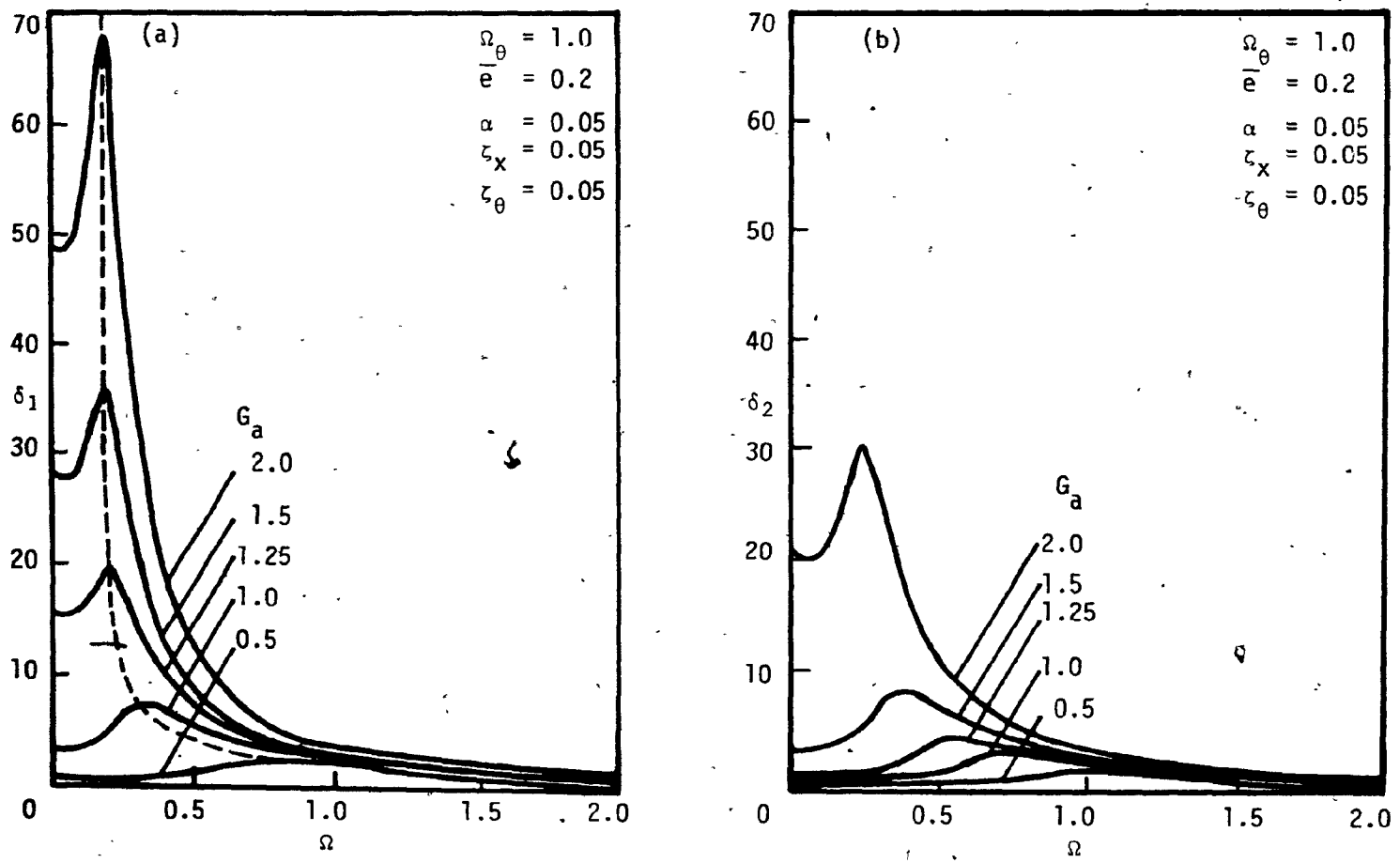

Figure 4.16 Effect of ground excitation level G_a on response amplitude of resisting elements

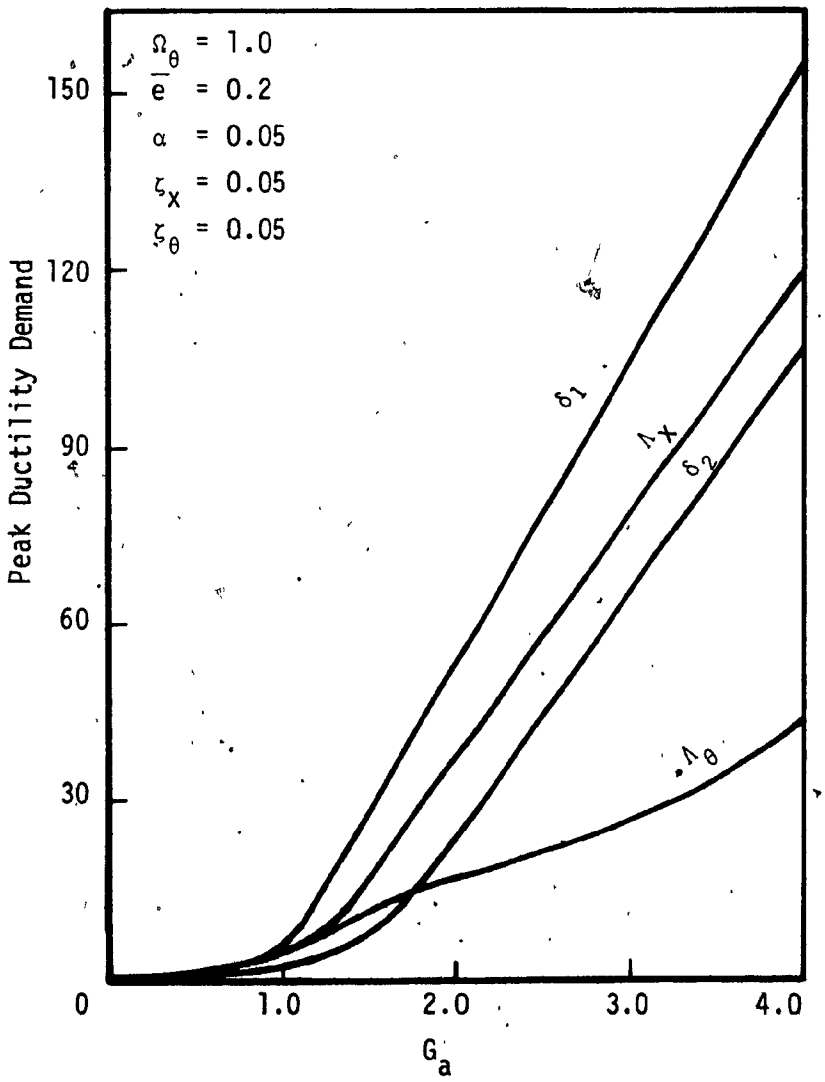

Figure 4.17 Effect of ground excitation level G_a on peak ductility demand for resisting elements and translational and torsional system displacements.

CHAPTER V

INSTABILITY IN BILINEAR HYSTERETIC STRUCTURES

5.1 INTRODUCTION

During the past several decades, much research effort has been concentrated on determining the dynamic behaviour of simple mechanical systems having nonlinear elastic restoring force. Among the known response properties of such systems, by far the most important and interesting characteristic is the existence of the "jump phenomenon", or instability in response, within a certain frequency range which is well described in numerous papers and texts [42-45]. Later, similar instability was demonstrated to exist in various nonlinear elastic Civil Engineering structures, as for example coupled flexural vibrations of thin circular rings [1,2] and the vibration of orthotropic shallow shells [3]. However, the only known work on the "jump phenomenon" in an inelastic system is due to Iwan [46], in which he showed that the steady state response of a one degree-of-freedom doubly-bilinear hysteretic model also gives rise to the "jump phenomenon", apart from exhibiting "softening".

In this chapter, work is first devoted to idealization of several experimentally available hysteresis loops typifying a wide class of structures. The steady state response of an eccentric system with these idealized loops is found following the analytical procedure described in Chapter IV. The response is presented in the form of ductility demand versus nondimensional excitation frequency. The possibility of experiencing instability in response

for the different classes of hysteretic behaviour is examined and the predominant system parameters responsible for this instability are identified. Finally, a parametric study is performed for pinched elasto-plastic structures since this type of hysteretic behaviour is found to experience the highest degree of torsional instability.

5.2 IDEALIZATION OF HYSTERETIC BEHAVIOUR FOR VARIOUS INELASTIC SYSTEMS

This section is devoted to the idealization of hysteresis loops for a variety of structures such as reinforced concrete frames, shear walls, steel braced frames, etc. These behavioural models are based on the load-displacement characteristics obtained from various experimental investigations of actual structures, wherein yielding of elements within the structure or interface slip between adjacent elements determines its hysteretic nature.

The cyclic inelastic load-deformation characteristics of moment connections and beam-column joints in moment resisting steel frames were recently studied experimentally by Krawinkler and Popov [47]. Similar experimental observations for reinforced concrete ductile frame structures have been reported by Fenwick [48], whereas repaired reinforced concrete members under cyclic loading were investigated by Popov and Bertero [49]. Typical load-deformation diagram for these steel and reinforced concrete framed structures is shown in Figure 5.1. The shapes of these diagrams are similar and can easily be idealized by the mathematically manageable bilinear hysteretic model, with the second slope α calculated to be within 0.02 - 0.10.

A different class of cyclic load-deformation behaviour has been observed for coupled wall systems [51], where the hysteretic loops are pinched as shown in Figure 5.2. This pinching occurs due to degradation in flexure-shear resistance combined with a gradual loss of bond attributable to bar pull-out. This type of inelastic behaviour may be idealized by the pinched-bilinear hysteretic model for which the second slope α is measured to lie within 0.05 - 0.17 (see Figure 5.2).

By setting α to zero, both fully bilinear and pinched-bilinear hysteretic models transform into elasto-plastic and pinched elastic-plastic behaviour respectively. The pinched elasto-plastic model, sometimes also referred to as the hysteretic slip model, represents the behaviour of a plane cross-braced frame and has been the subject of several studies [8,41,62].

Recently, attention has been paid to the study of more complex forms of yielding behaviour, in which the hysteresis loops associated with successive loading cycles show progressive decrease in both stiffness and energy dissipation [53,54]. However, for the present investigation, the analysis is restricted to the two simple hysteretic models described above.

Both the fully bilinear and the pinched-bilinear models are the two simplest idealizations of hysteretic behaviour, compared to other models such as Ramberg-Osgood or stiffness degradation, able to preserve approximate cyclic energy dissipation but neglecting strength deterioration and creep. In fact, it has occasionally been found that the hysteresis loss specified by the bilinear model is slightly higher and that of the pinched-bilinear model slightly

lower than the corresponding experimental load-deformation diagrams. The hysteresis loss in a pinched-bilinear model is exactly half that of a fully bilinear model for the same amplitude of response. It is believed that other forms of hysteretic behaviour, namely Ramberg-Osgood or stiffness degradation, will be covered by the two limiting cases of hysteretic behaviour considered in the present study regarding cyclic energy dissipation.

5.3 ANALYTICAL PROCEDURE

The coupled lateral-torsional behaviour of an inelastic asymmetric single-story building is examined for the two types of hysteretic models described in the foregoing section. The single-story model of Chapter IV (see Figure 4.1 and 4.3), also with harmonic ground shaking, is considered here. The study of steady state harmonic response for inelastic structures is useful because, quite often, structural testing employs forced harmonic excitation to determine structural characteristics such as natural frequencies and damping [40]. Moreover, the response of a structure to strong-motion earthquakes is close to harmonic in character [38].

The equations of motion given by Equations (4.18) and (4.19), and the corresponding four nonlinear coupled algebraic Equations (4.23) through (4.26) obtained by employing the method of averaging, are valid for any shape of hysteresis loop. In these equations, the expressions for $C_i(\bar{A}_i)$ and $S_i(\bar{A}_i)$ (see Equation 4.27) do not require the explicit form of $f(\bar{A}_i,\bar{\theta}_i)$. However, Equations (4.23) through (4.27) can be specialized for a particular inelastic system provided corresponding closed form expressions for $f(\bar{A}_i,\bar{\theta}_i)$, $C_i(\bar{A}_i)$

and $S_i(\bar{A}_i)$ can be established. In the following, the exact expressions of these terms for the two idealized hysteresis models studied herein are described.

5.3.1 Fully Bilinear System

The explicit forms for $C_i(\bar{A}_i)$, $S_i(\bar{A}_i)$, $c_2(r\bar{A}_2)$ and $S_2(r\bar{A}_2)$ for the fully bilinear hysteretic model have been presented in Chapter IV (see Section 4.2.3, Equations (4.28) and (4.29). Similar expressions can be found for an elasto-plastic system by setting α to zero. Thus, Equations (4.23) through (4.26), (4.28) and (4.29) can be solved to estimate the steady state average response of idealized bilinear and elasto-plastic hysteretic systems.

5.3.2 Pinched-Bilinear System

Figure 5.3 illustrates the normalized shape for idealized pinched-bilinear hysteretic behaviour. The general expressions for $C_i(\bar{A}_i)$ and $S_i(\bar{A}_i)$ for this type of hysteretic model have been derived for a single degree-of-freedom translational system by Iwan [46]. Without showing the detailed derivation, the final form of these expressions are

$$C_i(\bar{A}_i) = \frac{\bar{A}_i}{\pi}\left[(1-\alpha)\left(\theta_i^{*} + \theta_i^{**} - \frac{\sin 2\theta_i^{*}}{2} - \frac{\sin 2\theta_i^{**}}{2} - \frac{\pi}{2}\right) + \alpha\pi\right]$$

$$; \bar{A}_i \geq 1.0 \; ; \; i=3,4 \qquad (5.1a)$$

$$= \bar{A}_i \qquad ; \bar{A}_i \leq 1.0 \; ; \; i=3,4 \qquad (5.1b)$$

$$S_i(\bar{A}_i) = -\frac{2}{\pi}(1-\alpha)\left(\frac{\bar{A}_i - 1}{\bar{A}_i}\right) \; ; \; \bar{A}_i \geq 1.0 \; ; \; i=3,4 \qquad (5.1c)$$

$$= 0 \qquad ; \; \bar{A}_i \leq 1.0 \; ; \; i=3,4 \qquad (5.1d)$$

where

$$\theta_i^* = \cos^{-1}\left(\frac{\bar{A}_i - 1}{\bar{A}_i}\right) \qquad (5.1e)$$

$$\theta_i^{**} = \cos^{-1}\left(-\frac{1}{\bar{A}_i}\right) \qquad (5.1f)$$

Similarly, expressions for $C_2(r\bar{A}_2)$ and $S_2(r\bar{A}_2)$ are given by

$$C_2(r\bar{A}_2) = \frac{r\bar{A}_2}{\pi}\left[(1-\alpha)\left(\theta_{r2}^* + \theta_{r2}^{**} - \frac{\sin 2\theta_{r2}^*}{2} - \frac{\sin 2\theta_{r2}^{**}}{2} - \frac{\pi}{2}\right) + \alpha\pi\right]$$

$$; \; r\bar{A}_2 \geq 1.0 \qquad (5.2a)$$

$$= r\bar{A}_2 \qquad ; \; r\bar{A}_2 \leq 1.0 \qquad (5.2b)$$

$$S_2(r\bar{A}_2) = -\frac{2}{\pi}(1-\alpha)\left(\frac{r\bar{A}_2 - 1}{r\bar{A}_2}\right) \; ; \; r\bar{A}_2 \geq 1.0 \qquad (5.2c)$$

$$= 0 \qquad ; r\bar{A}_2 \leq 1.0 \qquad (5.2d)$$

in which

$$\theta_{r2}^* = \cos^{-1}\left(\frac{r\bar{A}_2 - 1}{r\bar{A}_2}\right) \qquad (5.2e)$$

$$\theta_r^{**} = \cos^{-1}\left(-\frac{1}{r\bar{A}_2}\right) \qquad (5.2f)$$

Substituting $\alpha=0$ in the foregoing equations specializes in the expressions for pinched elasto-plastic behaviour. Hence, Equations (4.23) through (4.26), together with Equations (5.1) and (5.2),

yield the steady state average response of a pinched-bilinear hysteretic system for nonzero α as well as for pinched elasto-plastic systems when $\alpha=0$.

5.4 NUMERICAL EVALUATION OF STEADY STATE RESPONSE

In Section 4.2.4, it was mentioned that nonlinear algebraic Equations (4.23) through (4.26), (4.22) and Equations (4.28), (4.29), when specialized for fully bilinear hysteretic behaviour, were solved with the IMSL library subroutine without encountering difficulties, because the solution is found to be single-valued within the observed frequency range.

Although this subroutine also solved the same set of algebraic equations specialized for pinched-bilinear behaviour (Equations (5.1) and (5.2)) for a large portion of the input frequency range Ω, it failed to converge at certain values when $\Omega<1.0$. The solution for this portion was obtained with a recent but unpublished program developed by Bui [55], however only after a great deal of effort. Several trial and error runs had to be performed with both the IMSL and Bui's subroutines to obtain complete solutions for the desired frequency range.

The IMSL subroutine can solve for amplitudes and phase angles at a specified magnitude of Ω, whereas Bui's program solves along the entire route or path of a curve at constant interval points starting from a known solution at any point on the path. One severe restriction of the present version of this routine is that, just after the starting point, it always converges to the next point on the path provided Ω at the new point is greater than the starting

point Ω. Difficulties were encountered because, for most cases, the exact roots at or near $\Omega=0$ could not be predicted a priori. Thus, all curves for the bilinear hysteretic systems were obtained with the IMSL routine starting at $\Omega=2.0$ and sweeping toward $\Omega=0$; this was possible because the system parameters do not significantly affect the response amplitudes beyond $\Omega=1.5$ (see Figures 4.5-4.8, 4.11-4.13 and 4.16). Similarly, the IMSL routine was also used to solve for pinched-hysteretic behaviour with the starting point always at $\Omega=2.0$ but, because in most cases the solution failed at Ω somewhere near or less than 0.5, no solution was obtained between $0.2\leq\Omega\leq0.5$. Fortunately, in some cases the IMSL routine gave solutions at $\Omega<0.2$; these known solutions were then used in Bui's routine to complete the range $0\leq\Omega\leq0.5$. For cases where no known solution was available from the IMSL routine, several trial runs had to be performed with Bui's routine by intutive judgement based on previously obtained curves.

After each successful run with Bui's program, it was found that triple set of solutions exist for that frequency range in a pinched-bilinear hysteretic system where the IMSL routine failed (Figures 5.5-5.14). In most cases of triple solutions, the IMSL subroutine either failed or gave only one solution. It should be noted that triple solutions of a single nonlinear equation were also found by Iwan [46]; even five values were successfully obtained by El-Zaouk and Dym [3]. Thusfar, no example of a complete solution of triple values for two degree-of-freedom systems is reported in the literature. Evensen [1,2] attempted to solve uniquely for system amplitudes by a numerical method but was unsuccessful for a comparatively

less complicated system than the one studied here. Similar evidence of unsuccessful attempts in finding triple values resulting in incomplete amplitude-frequency curves can be found in the recent work of Reference 56.

In order to verify the correctness of the solution obtained from both the IMSL and Bui's routines, the linear elastic case was solved. A closed-form solution for amplitudes and phase angles can be obtained by first substituting $\alpha=1.0$ in Equations (4.28), (4.29), (5.1), (5.2) to estimate $C_i(\bar{A}_i)$, $S_i(\bar{A}_i)$, $C_2(r\bar{A}_2)$, $S_2(r\bar{A}_2)$ and then substituting into Equations (4.23) through (4.26) and (4.22)(see also Appendix H). The solutions obtained for $\alpha=1.0$ from both routines were found to match the closed form solution within reasonable accuracy. Moreover, both programs were also tested for $\alpha=0.95$ producing solutions which were different from but close to the solution of the linear system. Additional verification of Bui's program was also made by comparing several spot-check runs for typical nonlinear systems with solutions from the IMSL subroutine for both bilinear hysteretic and pinched-bilinear hysteretic systems.

5.5 COMPARISON OF RESPONSE FOR DIFFERENT HYSTERETIC SYSTEMS

In Section 5.2, simple idealizations of hysteresis loops for various structural systems are presented. As illustrated in Figure 5.1, a bilinear hysteretic model may be conceived for the load-displacement characteristics of a moment resisting steel frame or a reinforced concrete ductile frame. Similarly, a pinched-bilinear loop can be substituted for hysteretic behaviour of a coupled wall

system (see Figure 5.2). The pinched elasto-plastic model has been considered earlier [52] to represent the cyclic behaviour of a cross-braced frame. The elasto-plastic model has also been the subject of a number of recent studies [7,9,15].

In this section a comparison of performance, in terms of frequency response characteristics, among these idealized loops is presented. Figure 5.4 presents schematic diagrams of these idealized hysteresis loops. The set of standard values of system parameters Ω_θ, $\bar{e}$, ζ_x, ζ_θ and α, listed in Table 4.1, is also used here for all hysteretic models, with the exception $\alpha=0$ for elasto-plastic models.

Furthermore, in order to achieve meaningful comparisons, it is desirable to examine equal cyclic energy dissipation, equal maximum restoring force, or equal yield strength for all hysteretic systems. But, because of the typical nature of the set of algebraic equations relating system parameters (Equations (4.23) through (4.26)), it is difficult to achieve the condition for equal energy. Moreover, from the designer's point of view, the concept of equal energy dissipation is difficult to implement. The equal maximum restoring force concept is also difficult to exercise because, although it is easy to employ in an elasto-plastic or pinched elasto-plastic system where maximum restoring force is well-defined as yield strength, for a bilinear hysteretic or pinched-bilinear model maximum restoring force is difficult to determine a priori because the corresponding maximum displacement is an unknown quantity required to be solved from the set of algebraic Equations (4.23) through (4.26). On the other hand, the equal yield strength concept meaning equal δ_y for

all systems (see Figure 4.2) is the most desirable condition from a practical point of view; however, this is also difficult to implement because nondimensionalization of the equations of motion has eliminated δ_y in favour of ductility demand δ_i/δ_y.

It is believed that meaningful comparisons of the various hysteretic responses will still be possible by employing equal acceleration G_a. For the present study the magnitude of G_a is 1.0.

5.5.1 Response Amplitudes

Figures 5.5 and 5.6 illustrate the lateral and torsional responses of all four hysteretic structures, and Figures 5.7 and 5.8 show the corresponding response amplitudes for resisting elements. It is observed that the peak ductility demand (PDD) appears to lean in the lower frequency direction thus indicating that these systems belong to the family of softing systems.

An interesting phenomenon observed in Figures 5.5 through 5.8 is that, while a unique set of amplitude values are found over the entire frequency range for both bilinear and elasto-plastic hysteretic systems, a triple set of amplitude values are obtained over a certain frequency range for both pinched bilinear and pinched elasto-plastic structures, identifying the existence of the "jump phenomenon" or instability in pinched-loop systems. The zone of instability is found to lie in the range $0.23 \leq \Omega \leq 0.48$ for a pinched elasto-plastic system, whereas for the pinched-bilinear system $0.36 \leq \Omega \leq 0.46$. Thus, the frequency zone of instability of a pinched elasto-plastic system expands somewhat compared to that of a pinched-bilinear system. This probably occurs because the former is a continuously yielding

system at a fixed magnitude of yield strength which, together with pinching behaviour, produces the observed instability.

For both elasto-plastic and pinched elasto-plastic structures (see Figure 5.5), infinite values of lateral and rotational displacements are observed at $\Omega=0$ indicating that the structure is continuously yielding at static load. But the structure is stable at $\Omega=0$, for both bilinear and pinched-bilinear behaviour (see Figure 5.6). In terms of displacements of resisting elements, Figure 5.7 illustrates that element 1 (far element) is yielding continuously, whereas element 2 (near element) is stable showing finite magnitude at $\Omega=0$.

A particularly important feature for element displacements is shown in Figures 5.7 and 5.8, where, within the unstable frequency zone of pinched hysteretic systems, the far element experiences a unique magnitude of response and is therefore perfectly stable; on the other hand, near element response is triple valued due to the existence of "jump" instability. Each element, however, remains elastic and exhibits the same amplitude irrespective of the type of hysteresis for $\Omega>1.5$. However, the situation is quite different at $\Omega<0.4$ (outside the unstable zone), where the near element (element 2) response remains elastic and of equal magnitude for all hysteretic models, whereas the far element (element 1) exhibits varying inelastic response which differs drastically in magnitude for different hysteretic models.

Generally two amplitude peaks appear for bilinear hysteretic systems, irrespective of whether the system is fully bilinear or pinched-bilinear (see Figure 5.6(a)). But only one peak is observed

in fully elasto-plastic or pinched elasto-plastic structures, in which the second peak may be imagined at $\Omega=0$. These peaks for all systems indicate some kind of resonance with the two coupled natural frequencies of the system. The frequencies at which the peaks appear in the system response curves correspond to those of the element response peaks. The lower frequency is associated with element 1 and the higher frequency is associated with element 2; this becomes evident when comparing Figure 5.5 with Figure 5.7 and Figure 5.6 with Figure 5.8.

5.5.2 Effect of α in Pinched-Bilinear Model

In the foregoing section, it has been observed that the frequency zone of instability is larger in a pinched elasto-plastic system compared to a pinched-bilinear system. Therefore, it is worthwhile to investigate the size of the instability zone for varying magnitude of bilinearity coefficient α.

Figure 5.9 presents response amplitudes of both resisting elements for different magnitudes of α. Element 1 is found to be perfectly stable, whereas element 2 exhibits instability at low α values. With increasing α the unstable frequency zone shrinks, becoming marginally stable at $\alpha=0.20$. For $\alpha=0.20$, the structure appears to become stable. At $\alpha=1.0$ (i.e., for an elastic system), the structure is perfectly stable as expected. Thus, the lower the magnitude of α, the larger is the unstable zone; consequently, the largest frequency zone of instability is associated with $\alpha=0$, i.e., for a pinched elasto-plastic system.

Since the experimentally obtained pinched loops of real

structures (Figure 5.2) indicate that the bilinearity parameter α does not exceed 0.20, it may be concluded that a structure consisting of coupled shear walls or cross-braced frames will exhibit some degree of instability whereas a structure consisting of moment resistant steel or ductile reinforced concrete frames will not.

5.5.3 Effect of Damping

In Chapter IV, the effect of damping in a fully bilinear hysteretic structure has been presented. It was found that damping does not play a significant role apart from decreasing response.

Since it has been observed that a pinched-bilinear hysteretic structure can become unstable within a certain frequency range, it is worthwhile to investigate the influence of damping on instability.

Figures 5.10 and 5.11 display response amplitude curves for elements 1 and 2 with bilinearity parameter α=0.05, 0.20 respectively, and varying magnitude of uncoupled damping.

In Figure 5.10 element 2 is unstable at $\zeta \leq 0.10$. However, it becomes stable at ζ=0.20 thus stabilizing the whole structure. Hence, there exists viscous damping somewhere between 0.1 - 0.2 at which the pinched-bilinear hysteretic structure ceases to be unstable.

Similarly, Figure 5.11 shows that the marginally unstable structure (with α=0.20) exhibits stability at relatively lower damping, in this case at ζ<0.1 , compared to a structure with α=0.05. The importance of damping therefore increases with

decreasing magnitude of α . It follows that the role of damping is most critical in pinched elasto-plastic structures, where the instability zone is largest.

From the foregoing discussion, it is clear that damping plays an important role in stabilizing response in a pinched hysteretic structure, in addition to its usual role of decreasing response. It is therefore, important to have adequate viscous damping in coupled-wall systems and cross-braced frame structures, compared to steel and reinforced concrete moment resistant frames, if torsional instability is to be prevented.

5.6 PARAMETRIC STUDY OF PINCHED ELASTO-PLASTIC STRUCTURES

In Section 5.5 it has been shown that a pinched elasto-plastic structure has the broadest frequency range of instability. Therefore, it appears important to conduct a parametric investigation on this system. The results will generally be applicable to other pinched hysteretic systems, i.e., systems having bilinearity parameter α within $0<\alpha<0.2$ for which the unstable frequency band-width is smaller but where, nevertheless, torsional instability is to be expected.

5.6.1 Effect of Damping

Figure 5.12 presents the effect of damping on the response amplitudes of both the far and near elements. The torsional and translational damping values are taken to be equal because it has been found in Section 4.3.3 that, for a fully bilinear hysteretic

structure, both torsional and translational damping possess equal ability to reduce response. Moreover, for simple dynamic analysis of structures the practice is generally to assume a single value for damping in both torsion and translation if the structure is nominally symmetric.

Figure 5.12(a) shows that far element is stable for all input frequency and damping, except that response becomes unbounded at $\Omega=0$. Figure 5.12(b), by contrast, indicates that near element 2 experiences instability even at damping as high as 0.1. The width of the unstable frequency range diminishes with increasing damping and eventually, at some magnitude of damping higher than 0.1, instability is eliminated altogether. The element becomes perfectly stable and exhibits unique response amplitudes for all Ω at $\zeta \geq 0.2$. Damping has virtually no effect on response of both elements beyond Ω of 1.5, approximately.

Whereas element 1 becomes unstable with unbounded response as Ω approaches zero, element 2 remains both stable and elastic. Comparing Figures 5.10(a) and 5.12(a) shows stable and finite magnitude of response in element 1 for pinched-bilinear behaviour at or near $\Omega=0$. This occurs because a pinched-bilinear structure can sustain load beyond its initial yield strength, whereas a pinched elasto-plastic structure is incapable of sustaining load beyond its yield strength since thereafter the structure yields continuously. This is perhaps the major difference in behaviour between pinched-bilinear and pinched elasto-plastic structures.

When a pinched hysteretic structure becomes unstable within some frequency range at $\Omega<0.5$, only one resisting element becomes

unstable. This is because the system investigated herein has only two translational resisting elements in the x-direction contributing towards both lateral and torsional resistance. An instability mechanism can therefore be formed with only one element becoming unstable. Thus, at $\Omega=0$, i.e., at static loading only, weaker element 1 forms a plastic hinge; for $0<\Omega<0.5$, where "jump" phenomenon or instability occurs, only the stronger element 2 becomes unstable. The latter form of instability does not however, mean that the structure or the unstable element will exhibit unbounded response; rather, it simply means that some beating-type of response occurs with finite but large magnitude for the unstable resisting element.

5.6.2 Effect of Ω_θ

The effect of torsional to translational frequency ratio Ω_θ on response amplitudes is illustrated in Figure 5.13. It is seen that, although Ω_θ does not influence element 1 significantly, element 2 is strongly affected. It may be recalled from Section 4.3.4 that, in a purely bilinear hysteretic system, the peak ductility demand of element 2 is not influenced greatly by Ω_θ whereas element 1 is critically affected (see Figure 4.10). However, comparing Figure 5.13(b) with Figure 4.10, it is easy to conclude that the peak ductility demand of element 2 in a pinched elastoplastic system decreases rapidly with increase in Ω_θ , from 22.3 for $\Omega_\theta=0.5$ to 1.4 for $\Omega_\theta=1.5$, but is only marginally affected in a bilinear hysteretic structure.

Another interesting observation regarding the behaviour of element 2 (see Figure 5.13(b)) is that a torsionally flexible structure, with Ω_θ=0.5, is found to be marginally stable whereas a torsionally stiff structure, with Ω_θ=1.5, is perfectly stable; a structure with intermediate stiffness, Ω_θ=1.0 , is unstable within a certain frequency range.

5.6.3 Effect of $\bar{e}$

Figure 5.14 illustrates the effect of nondimensional eccentricity $\bar{e}$ on response amplitudes for both elements 1 and 2 in structures with Ω_θ=1.0. The response amplitude of element 1 (see Figure 5.14(a)) is virtually unaffected by change in eccentricity. The situation is somewhat different for the same resisting element in a bilinear hysteretic structure at Ω<0.5 (see Figure 4.12(a)). However, beyond a certain value of Ω , the response amplitude of element 2 is independent of $\bar{e}$, as evident in Figure 5.14(b).

Figure 5.14(b) also shows that element 2 is significantly affected by eccentricity for input frequency Ω<0.7 , approximately. Structures with small eccentricity exhibit large magnitude of peak ductility demand which decreases with increasing eccentricity, in constrast to a minimal effect on the same element when behaviour is fully bilinear (see Figure 4.15(b)).

Moreover, the eccentricity is not capable of eliminating the occurrence of instability in element 2, although for small eccentricity the frequency range is slightly reduced compared to a large-eccentricity system. The unstable frequency rage is observed to

shift towards $\Omega=0$ with decrease in $\bar{e}$, which is a characteristic of a softing system.

5.7 CONCLUSIONS

This chapter has been devoted to comparison of the frequency-domain response of a wide class of structures with idealized hysteretic load-displacement characteristics. In addition, a parametric study is performed for pinched elasto-plastic structures where torsional instability is most pronounced.

The following conclusions are drawn on the basis of the foregoing discussions.

1. The responses of both fully bilinear and fully elasto-plastic hysteretic systems are found to be always stable, whereas the corresponding pinched-bilinear and pinched elasto-plastic structures exhibit the so-called "jump phenomenon" within certain frequency ranges.

2. The frequency zone of instability of a pinched elasto-plastic structure is widest compared to that of a pinched-bilinear system. Thus, a cross-braced frame idealized as pinched elasto-plastic has greater possibility of becoming unstable compared to coupled-wall buildings which may be represented by pinched-bilinear behaviour.

3. Within the unstable frequency domain of both the pinched-bilinear and pinched elasto-plastic structures, the response of weaker element 1 always remains stable, whereas that of stiffer element 2 exhibits torsional instability of the "jump phenomenon"

type.

4. Both fully and pinched elasto-plastic structures exhibit unbounded amplitudes of lateral and torsional response at $\Omega=0$. Although at that frequency the response of element 1 is unbounded, that of element 2 remains perfectly stable. In contrast, both system and element responses of fully and pinched-bilinear hysteretic structures remain perfectly stable at $\Omega=0$.

5. For a pinched-bilinear structure, the frequency zone of instability decreases with increase in bilinearity parameter α. At $\alpha\simeq0.20$ the structure is marginally stable, while beyond this magnitude of strain hardening instability disappears altogether. However, in real structures α is found not to exceed 0.20, structures consisting of coupled-walls or cross-braced frames represented by pinched hysteretic models will exhibit some degree of instability.

6. In both pinched-bilinear and pinched elasto-plastic structures, viscous damping plays an important role by eliminating the "jump phenomenon" and stabilizing response beyond some magnitude of damping, in addition to its usual role of decreasing amplitude of response.

7. The torsional to translational frequency ratio Ω_θ performs a comparatively important role for pinched hysteretic systems in stabilizing response. A torsionally flexible structure ($\Omega_\theta=0.5$) is marginally stable and a torsionally stiff structure ($\Omega_\theta=1.5$) is perfectly stable, whereas structures with Ω_θ in the neighbourhood of 1.0 exhibits torsional instability due to the "jump phenomenon".

8. Eccentricity in pinched hysteretic systems cannot eliminate torsional instability. In such systems, the peak ductility demand of the unstable resisting element (element 2) increases with decreasing eccentricity, in contrast to the minimal effect on the same element when element behaviour is fully bilinear.

9. The frequency zone of instability is not much affected by eccentricity, especially for medium and large eccentric structures; however, it may be slightly reduced for nominally eccentric pinched hysteretic structures.

From the foregoing conclusions it is evident that a pinched elasto-plastic structure representing steel cross-braced frame structures will experience the highest degree of torsional instability. Moreover, the situation will be more severe for this system when torsional and lateral frequencies are close. Therefore, one should try to avoid designing structures with nearly equal lateral and torsional frequencies for pinched-hysteretic structures in general and braced frame structures in particular. Unless other considerations such as cost, ease of fabrication etc., govern, it will be preferable to adopt ductile moment resistant frames compared to either coupled-shear walls or cross-braced frames; the former exhibit full hysteretic loops and dynamic stability in contrast to the latter which exhibit pinched hysteretic behaviour resulting in the "jump" type instability.

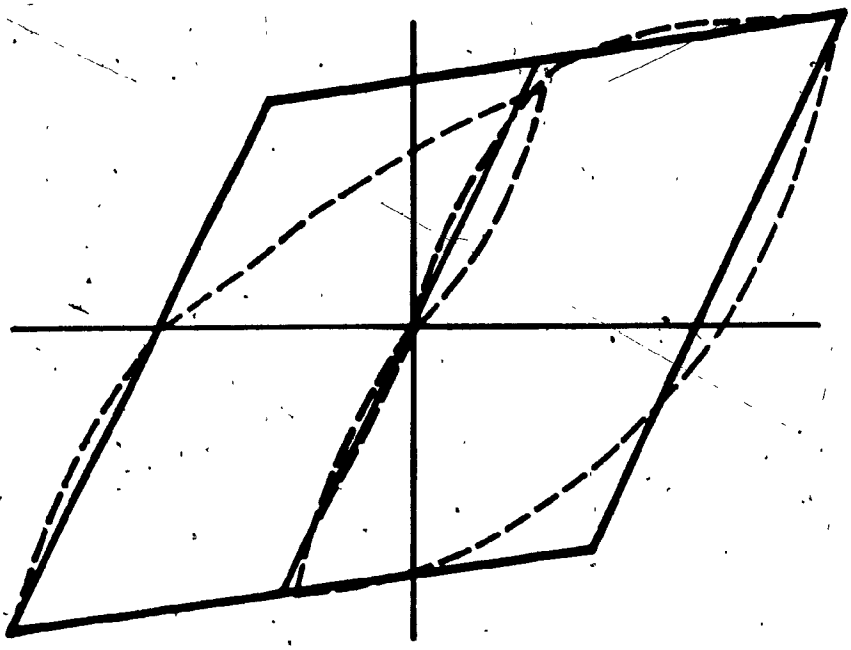

Figure 5.1 Fully bilinear idealization of load-displacement characteristic of a ductile moment resistant frame

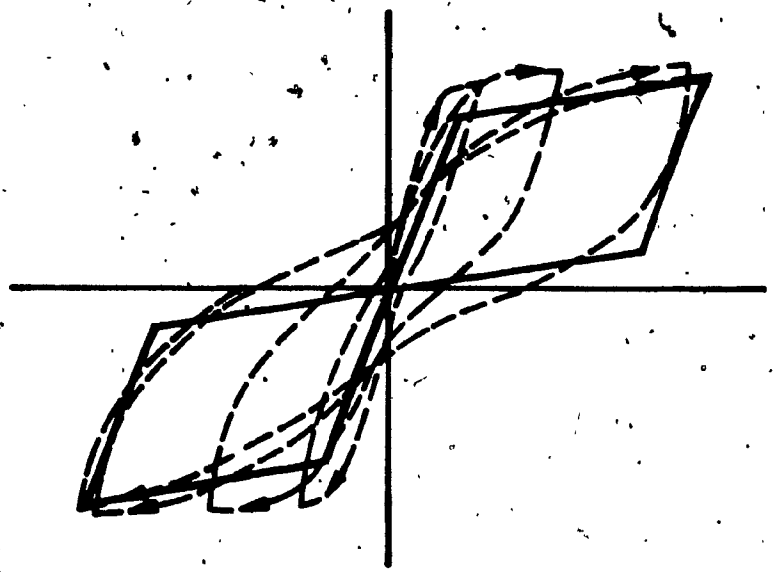

Figure 5.2 Pinched bilinear idealization of load-displacement characteristic of a coupled shear wall or cross-braced frame.

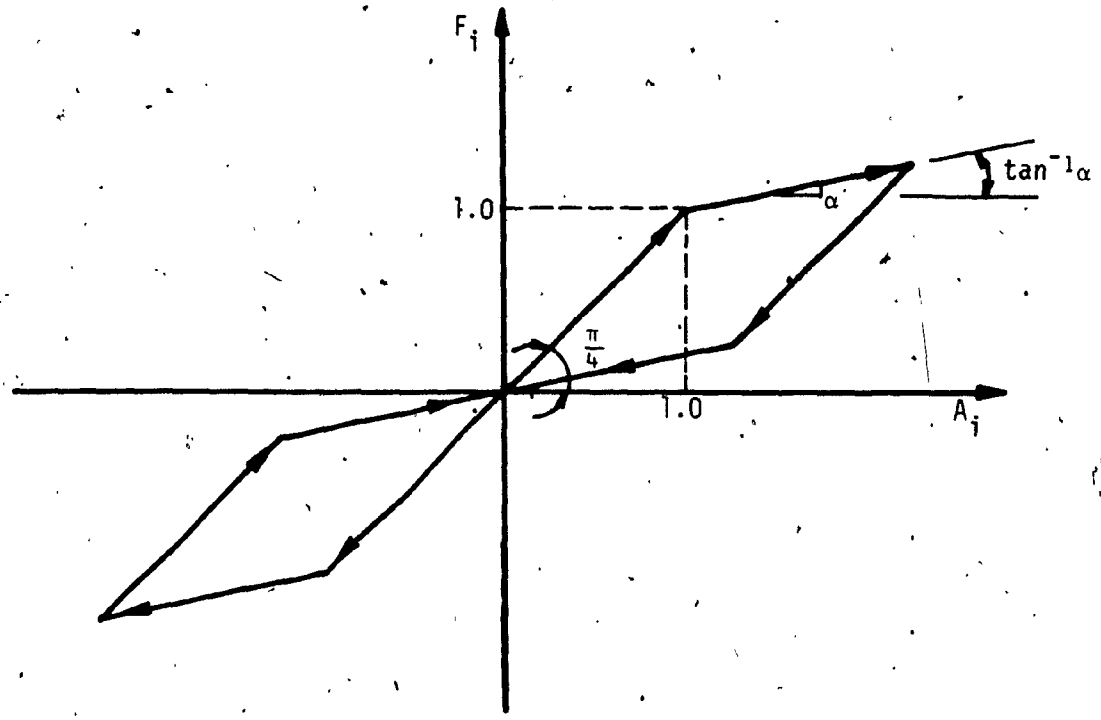

Figure 5.3 Normalized pinched bilinear hysteretic force-displacement relation.

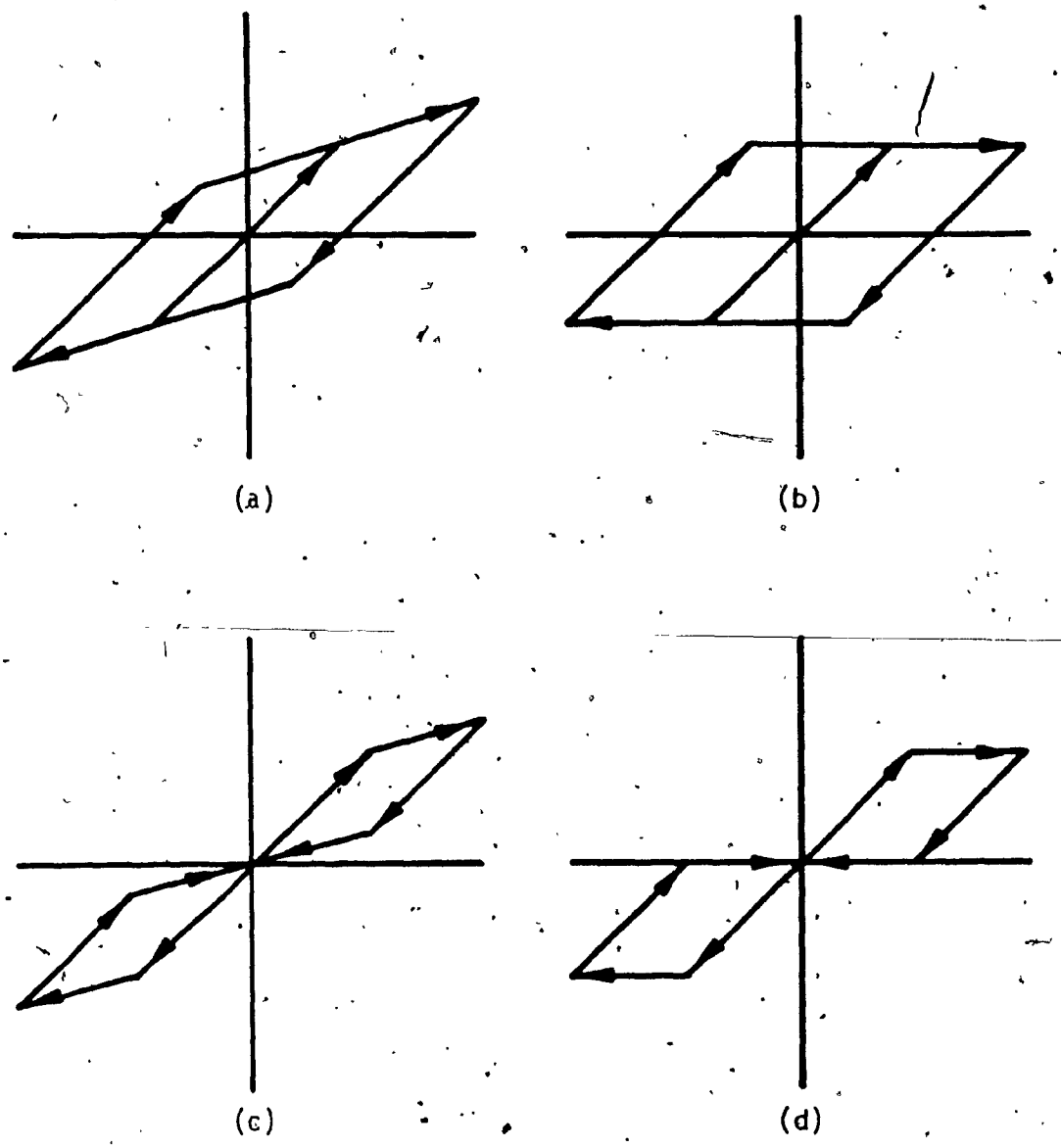

Figure 5.4 Normalized force-displacement hysteretic loops:
(a) fully bilinear; (b) fully elasto-plastic;
(c) pinched bilinear; (d) pinched elasto-plastic.

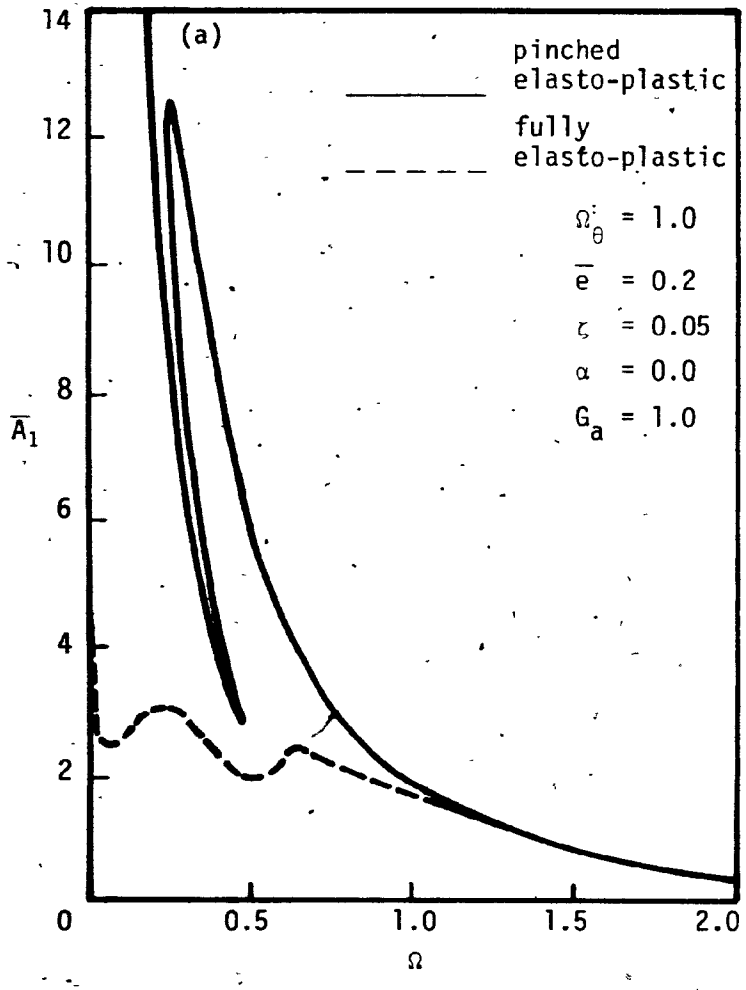

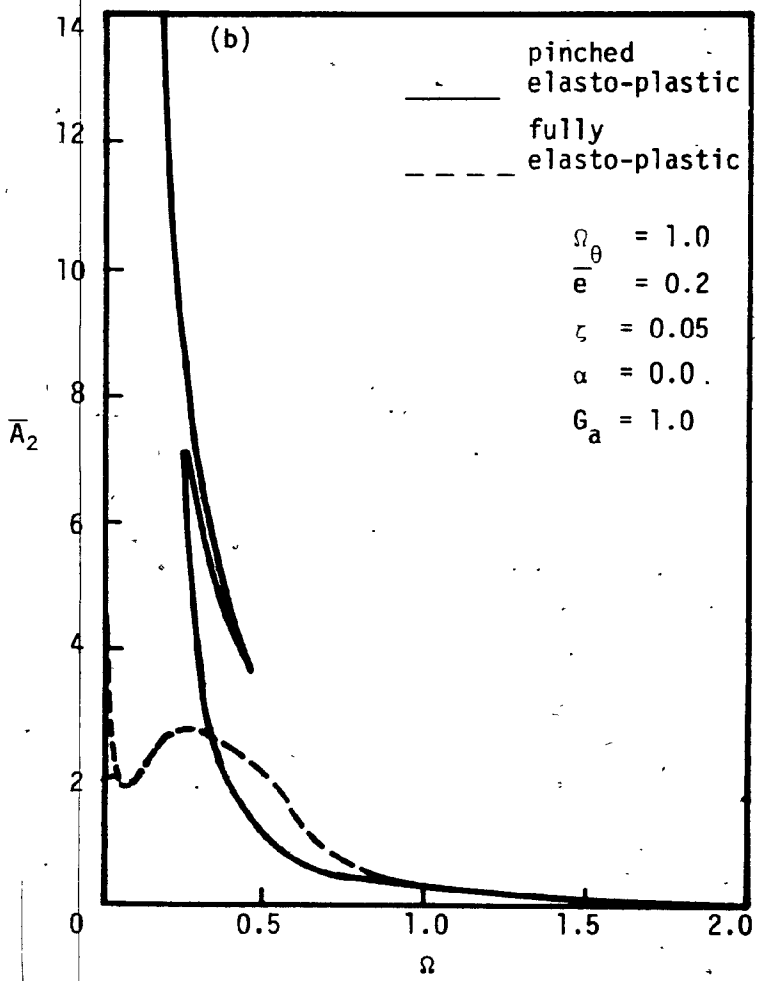

Figure 5.5 System response amplitudes for fully elasto-plastic and pinched elasto-plastic structures.

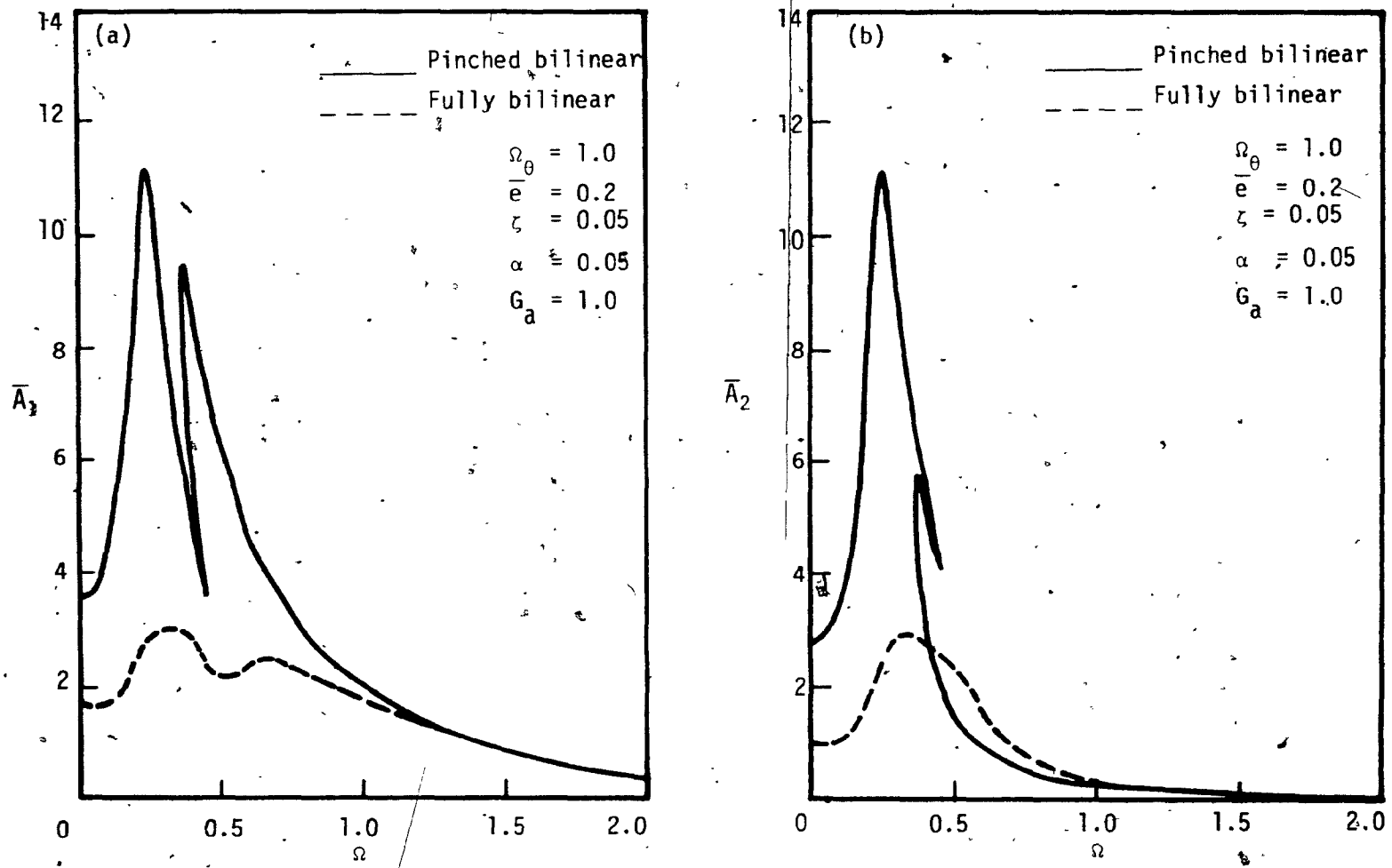

Figure 5.6 System response amplitudes for fully bilinear and pinched bilinear hysteretic structures.

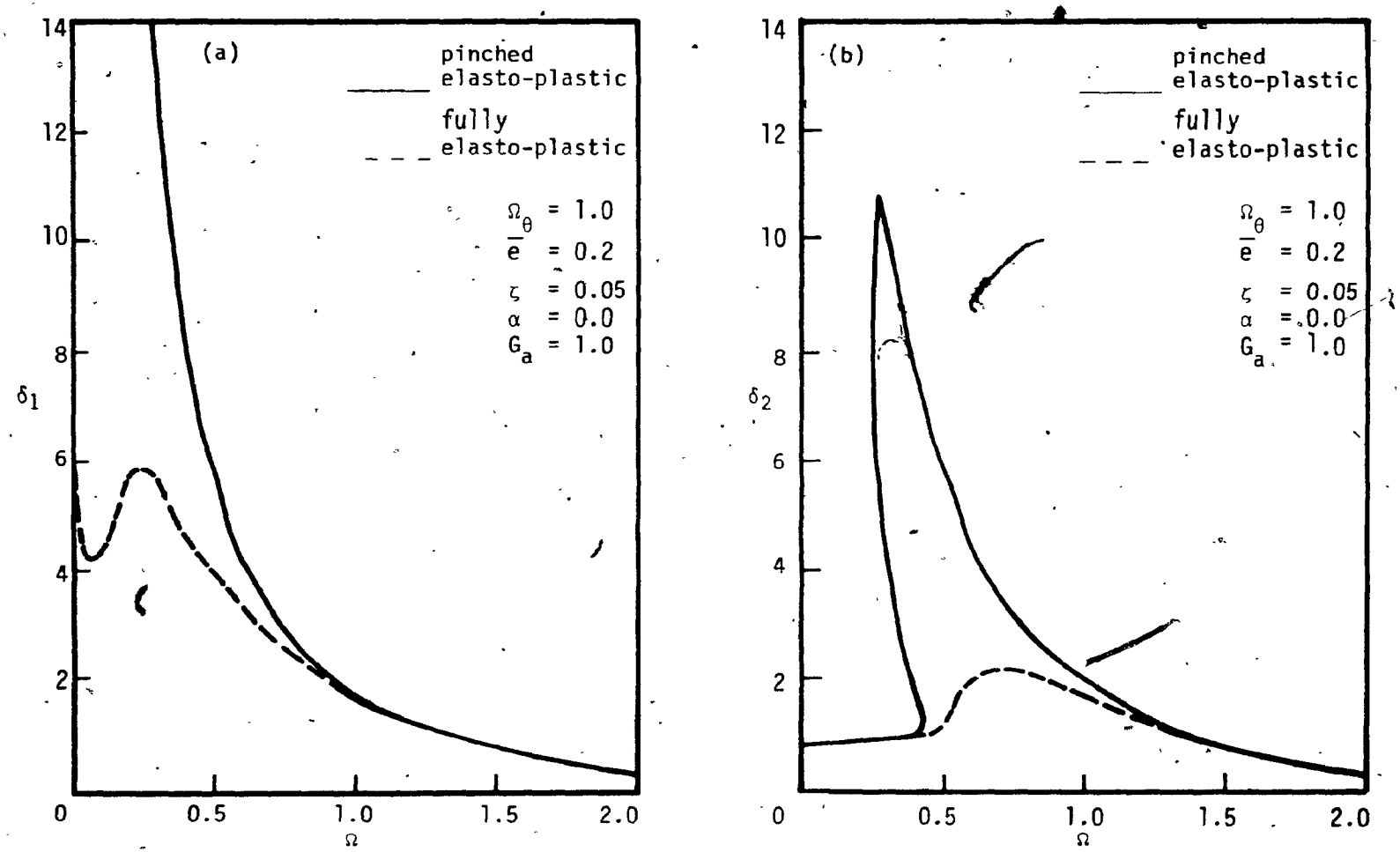

Figure 5.7 Response amplitudes of resisting elements for fully elasto-plastic and pinched elasto-plastic structures.

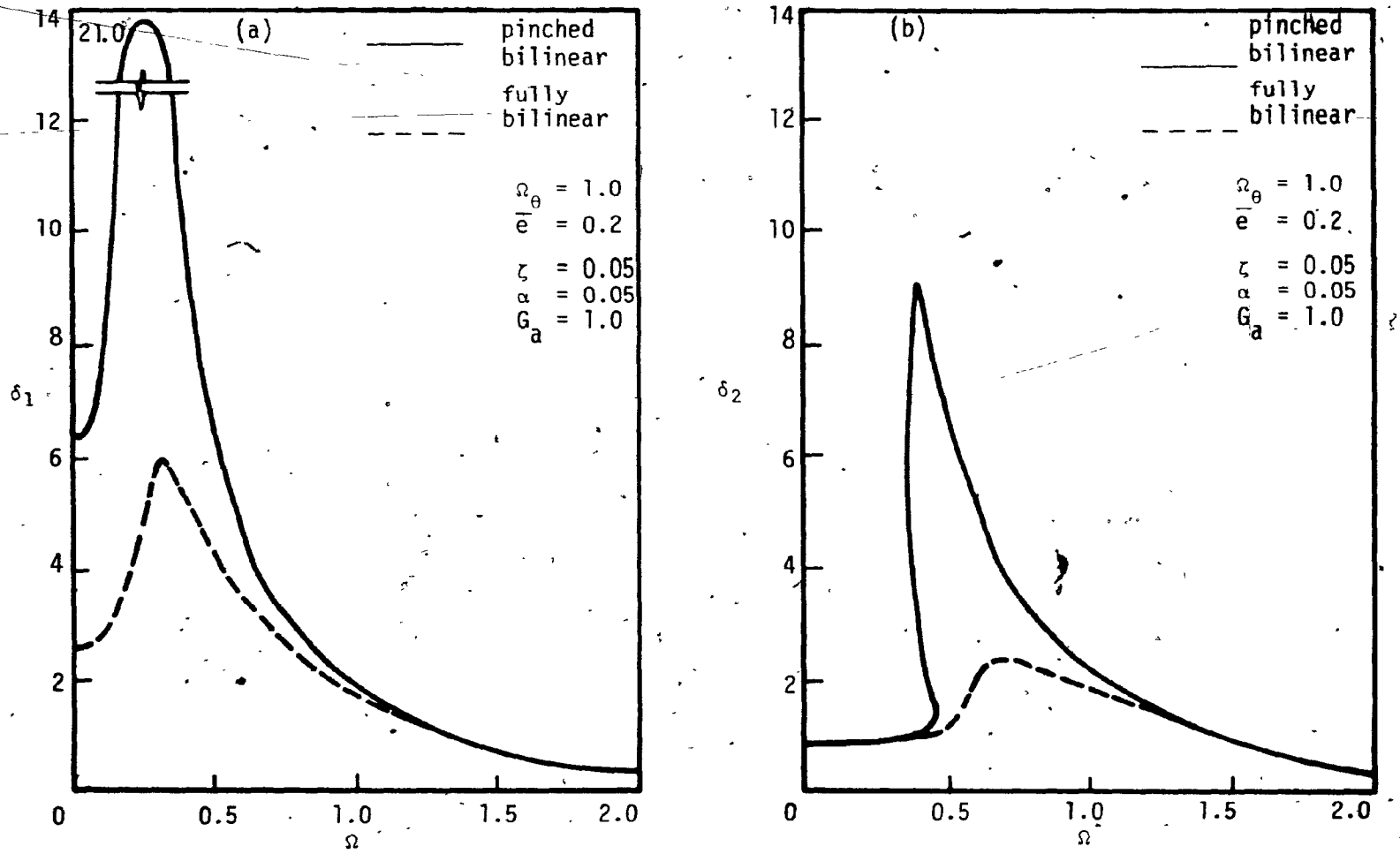

Figure 5.8 Response amplitudes of resisting elements for fully bilinear and pinched bilinear hysteretic structures.

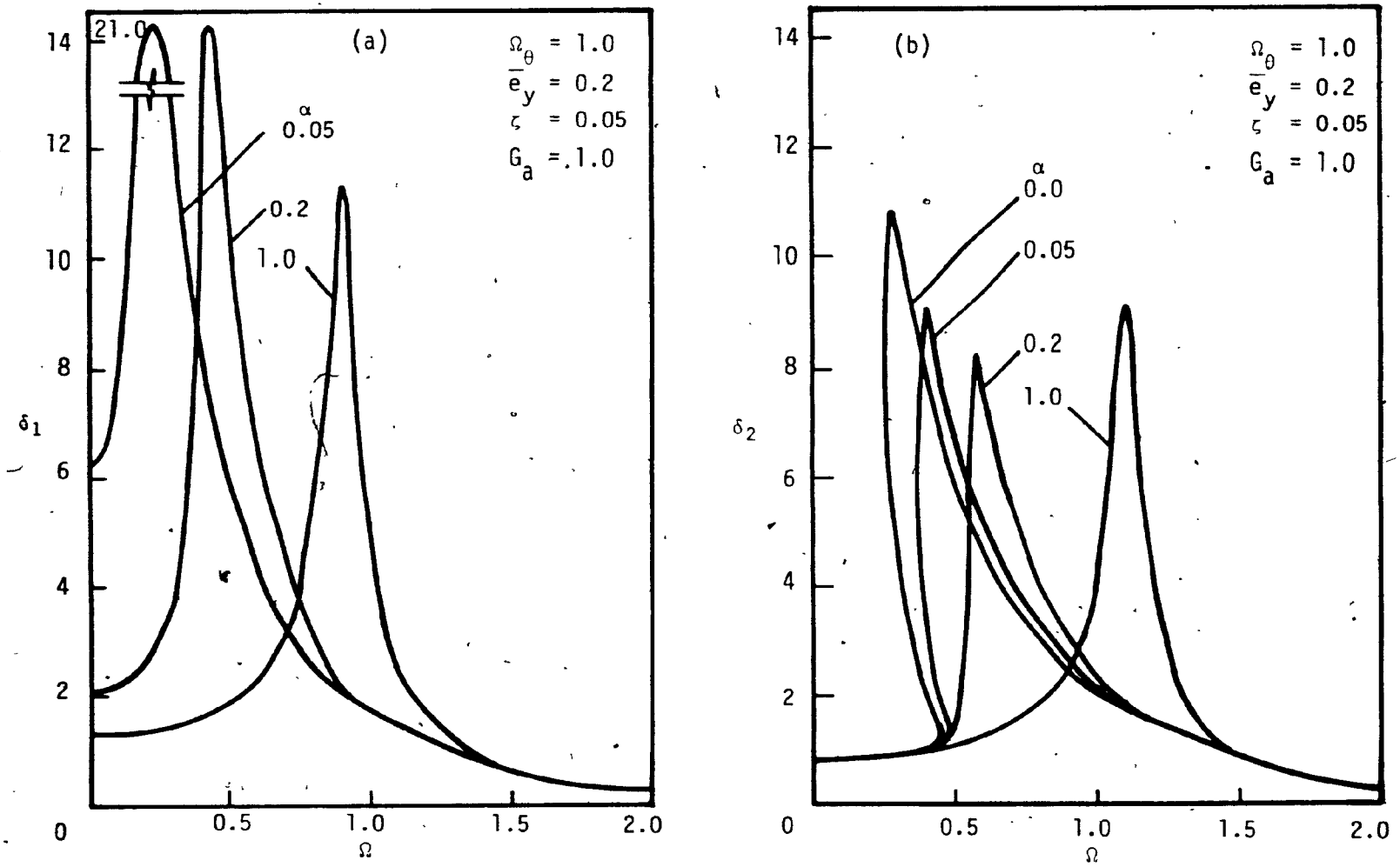

Figure 5.9 Effect of bilinearity parameter α on response amplitudes of resisting elements for pinched bilinear hysteretic structures.

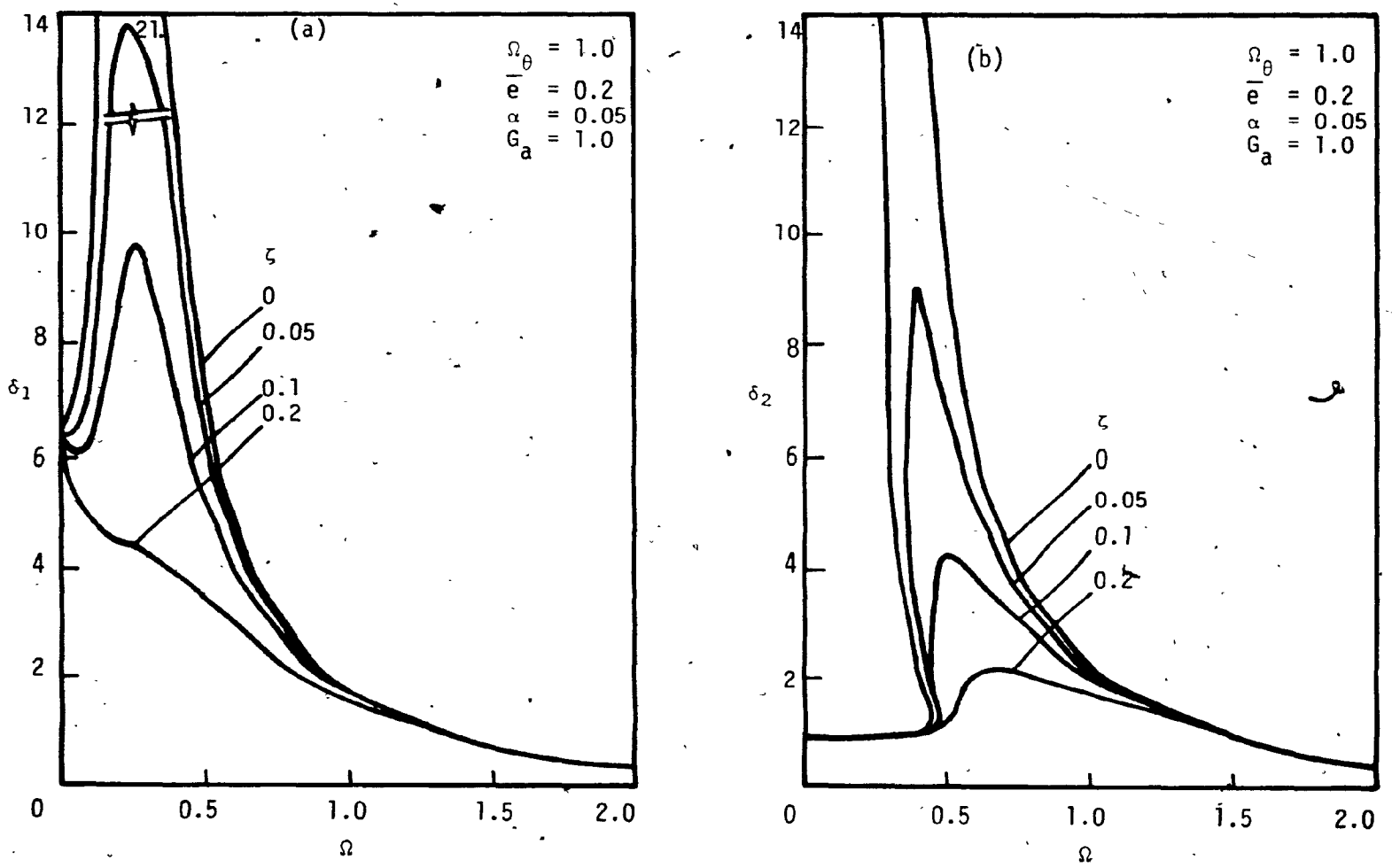

Figure 5.10 Effect of viscous damping ζ on response amplitudes of resisting elements for pinched bilinear hysteretic structures with $\alpha = 0.05$.

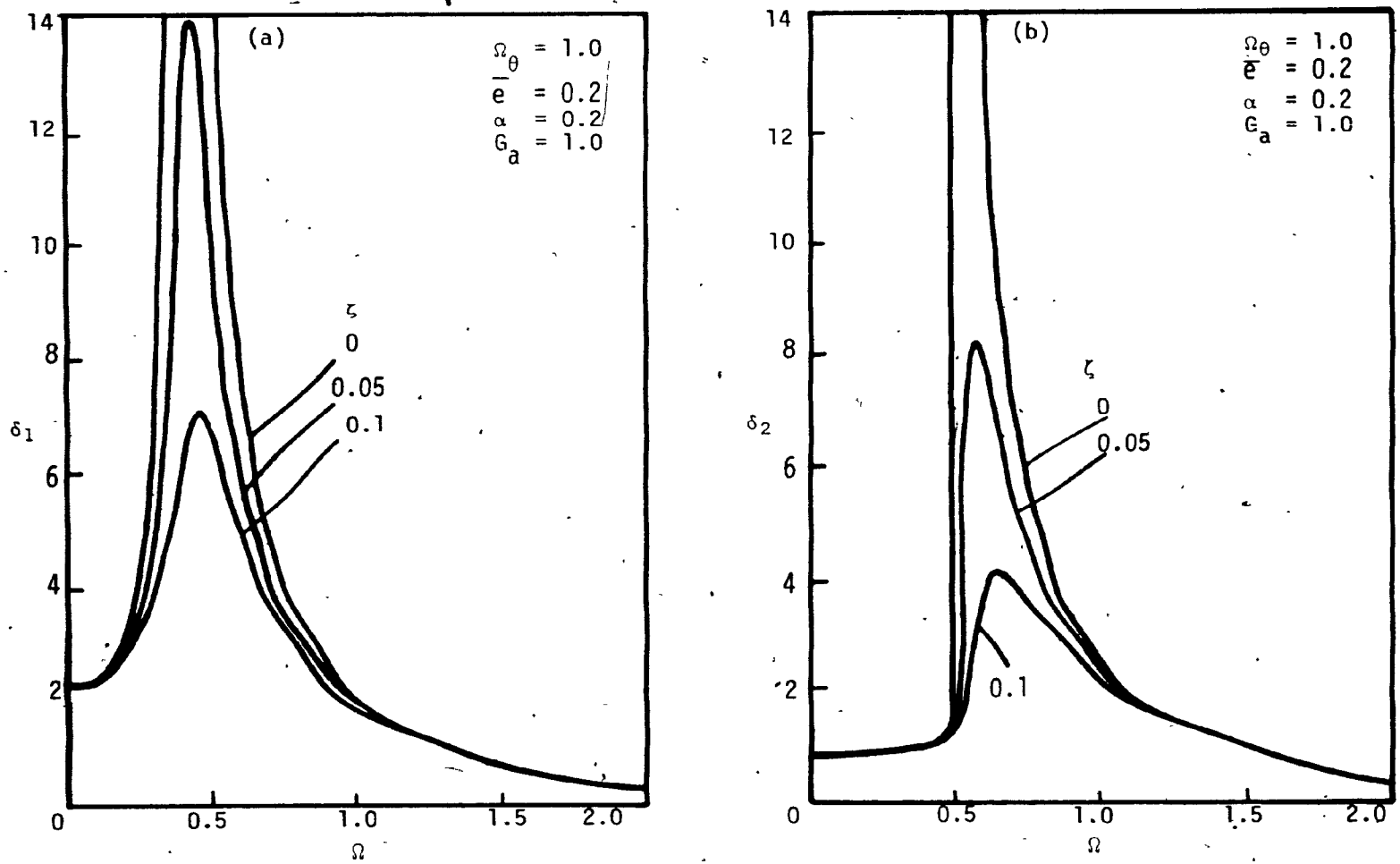

Figure 5.11 Effect of viscous damping ζ on response amplitudes of resisting for pinched bilinear hysteretic structures with α = 0.2.

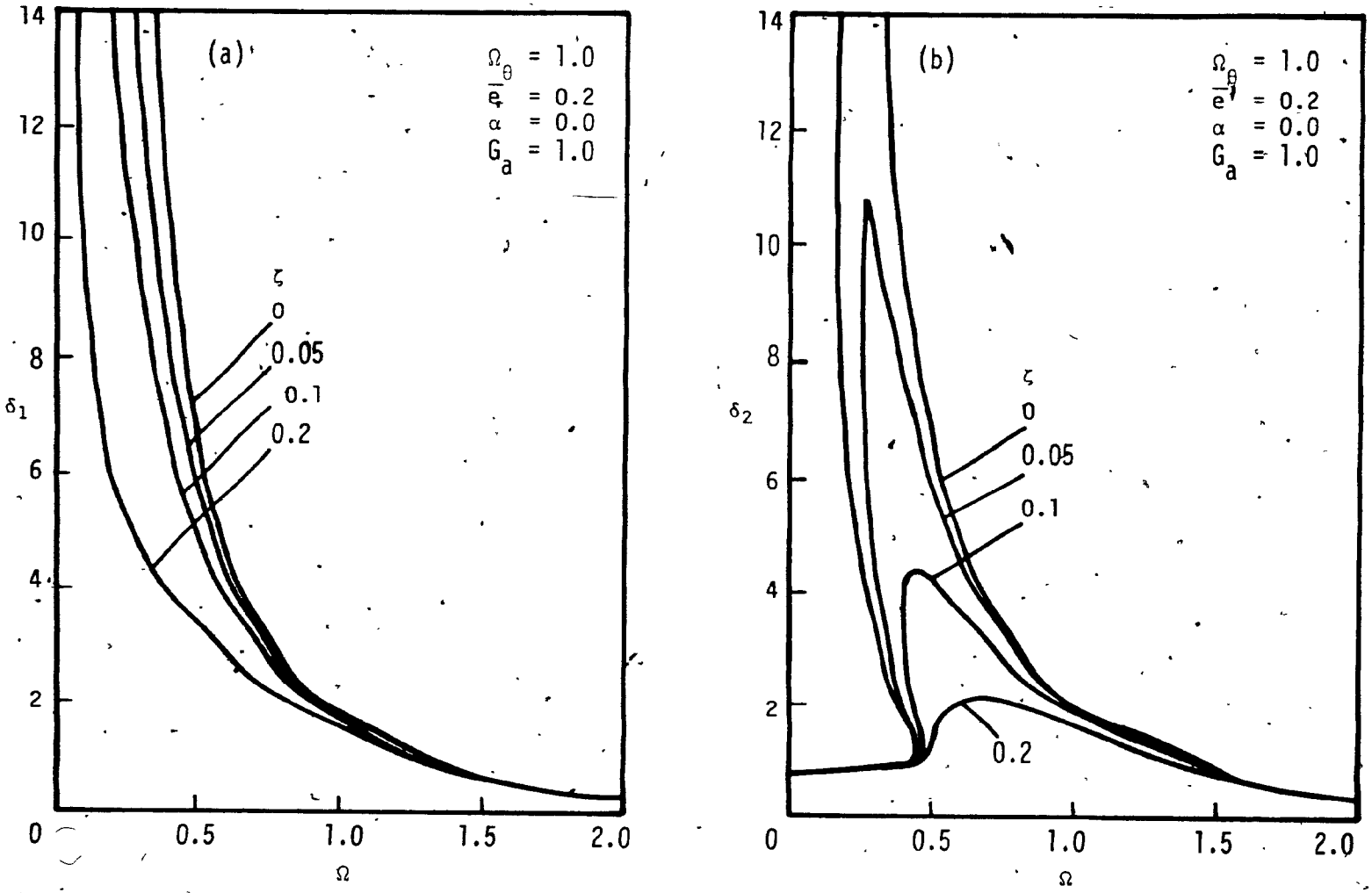

Figure 5.12 Effect of viscous damping ζ on response amplitudes of resisting elements for pinched elasto-plastic structures.

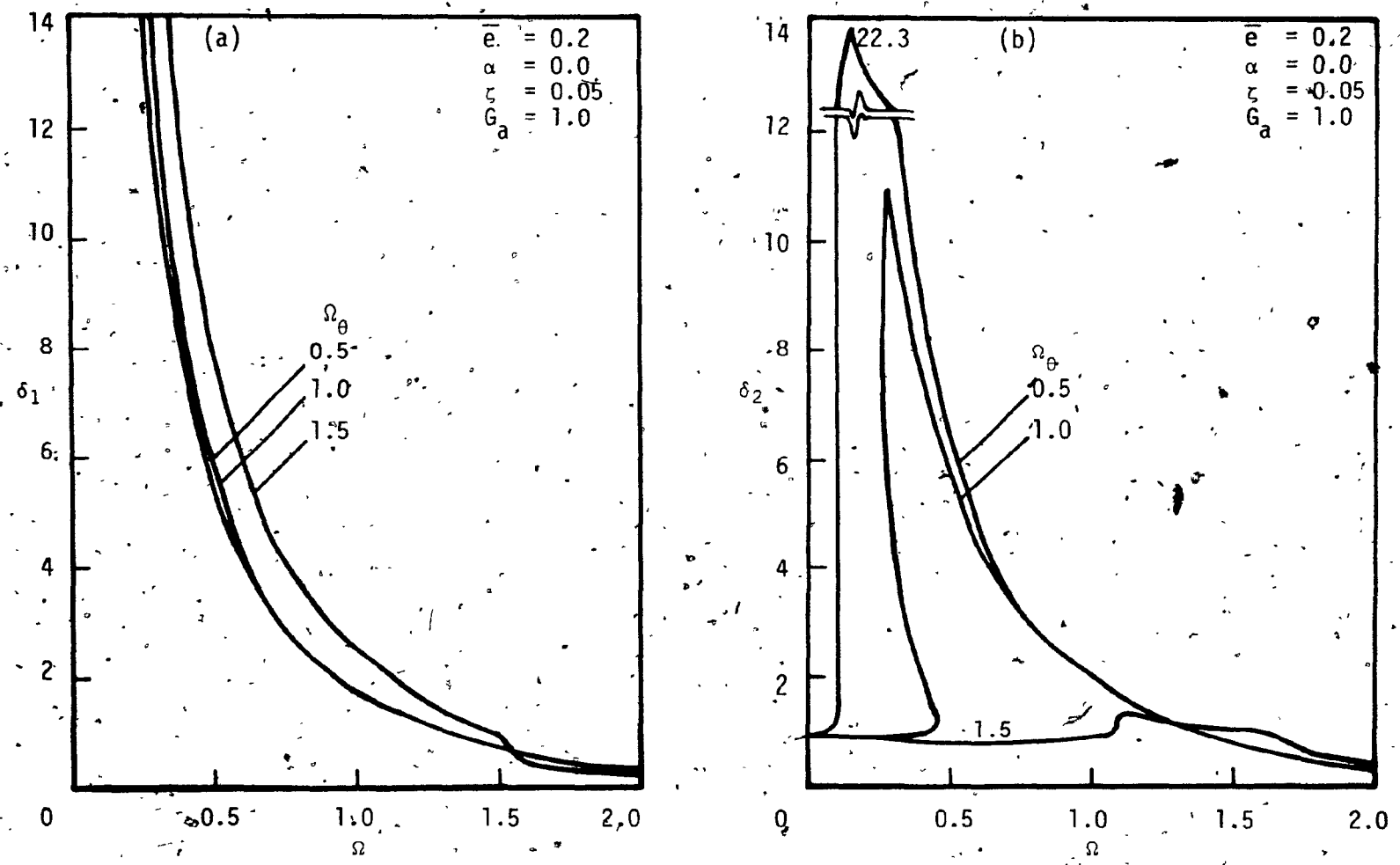

Figure 5.13 Effect of torsional to translational frequency ratio Ω_θ on element response amplitudes for pinched elasto-plastic structures.

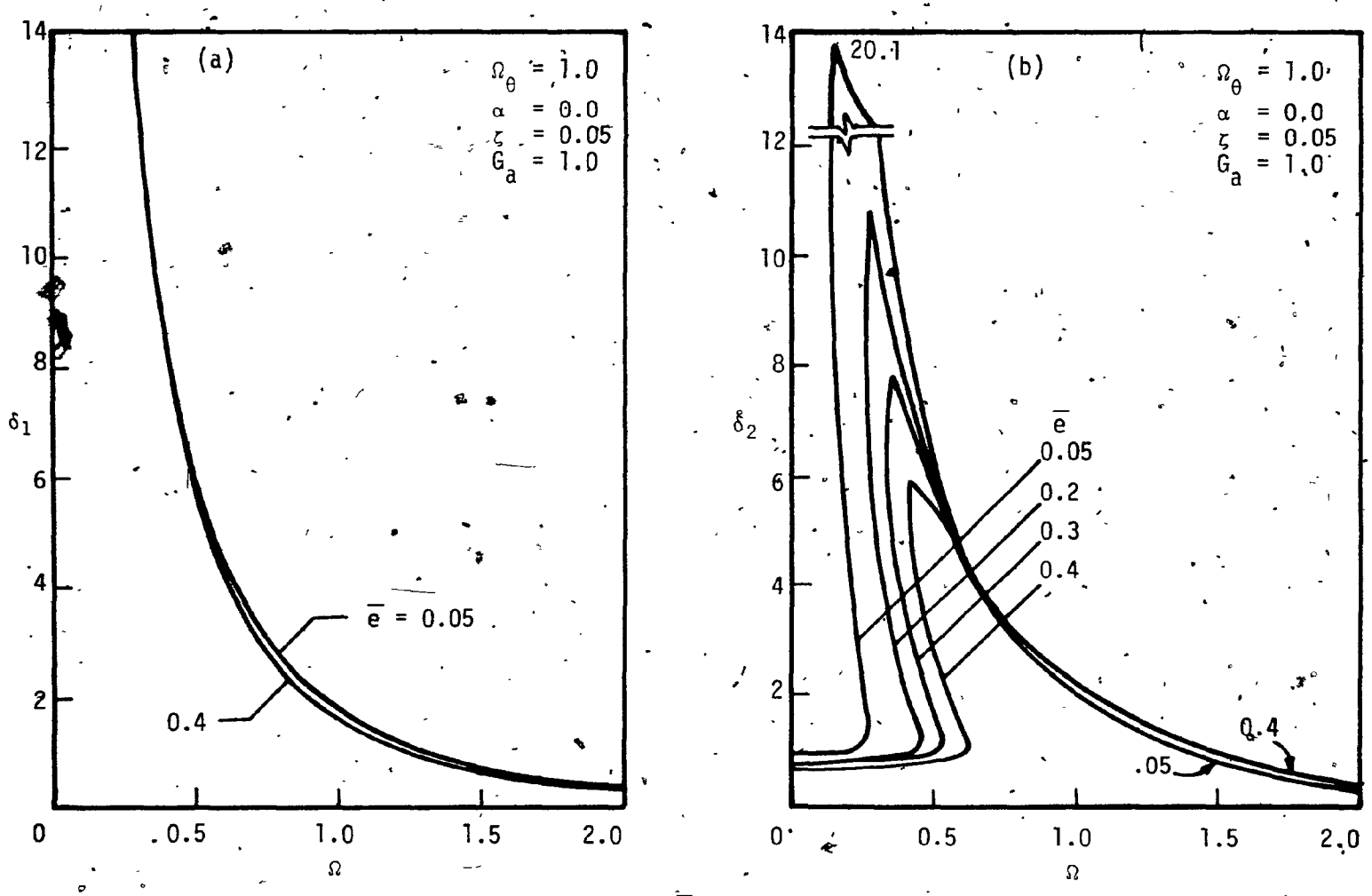

Figure 5.14 Effect of eccentricity $\bar{e}$ on element response amplitudes for pinched elasto-plastic structures.

CHAPTER VI

SUMMARY AND CONCLUSIONS

6.1. SUMMARY AND CONCLUSIONS

This study is concerned with the coupled dynamic response of both symmetric and unsymmetric structures for nonlinear elastic resisting elements and for elements governed by bilinear hysteretic characteristics.

In Chapter II work is confined to a symmetric single-story building model; as an extension to earlier studies this study examines the importance of torsional damping as well as the distribution and geometric arrangement of the lateral load resisting elements. Moreover, a relationship between two sets of stability diagrams with potentially conflicting stability interpretations derived in previous studies has been clarified. The load-displacement characteristics of the resisting elements, similar to earlier studies, are considered to be nonlinear elastic and of the softening type. Both torsional stability bounds and critical torsional damping are found to be influenced by various system parameters - namely, nonlinearity parameter λ, building plan aspect ratio r, translational damping coefficient ζ_x, stiffness distribution coefficient E, normalized system frequency Ω_θ and normalized input frequency Ω. It has been found that parametric excitation in a structure is possible only when the magnitude of torsional frequency of the system is slightly higher than the translational exciting frequency. It has also been found that, because the distribution of resisting elements can influence stability against

induced torsion, a selective rearrangement of resisting elements can eliminate torsional coupling. Furthermore, the susceptibility to nonlinear torsional coupling is presented in the form of generalized stability diagrams and critical torsional damping in $\hat{\Omega}_\theta$-$\hat{\Omega}$ and $\hat{\zeta}_{\theta,cr}$-$\hat{\Omega}_\theta$ parameter spaces respectively, which are applicable to any structure having general configurations of load-resisting elements in a symmetric structure.

In Chapter III work is further extended to both singly and doubly eccentric structures. The formulation is essentially similar to that of Chapter II but with eccentricity as an additional parameter. The importance of torsional damping on induced coupling is investigated. It is shown here that the nonlinear equations of motion of these monosymmetric and doubly eccentric structures are governed by a set of two and three damped coupled Mathieu-Hill equations, respectively. The stability diagrams are presented in the frequency parameter space and the critical torsional damping curves are presented as functions of system and input excitation parameters. It is observed that, for buildings with small eccentricity and for nominally symmetric buildings, the stability diagrams and critical torsional damping remain similar to those of a symmetric system.

Chapter IV is devoted to an understanding of the coupled inelastic response characteristics of a simple single-story monosymmetric building subjected to harmonic ground shaking. The load-displacement characteristics of resisting elements are idealized as bilinear hysteretic for which elastic and purely elasto-plastic are two special cases. It is shown that a steady state harmonic response analysis, because of its simpler mathematical manipulation, can provide

important insight into the dynamic behaviour of structures. A set of four coupled nonlinear algebraic equations consisting of basic system parameters with unknown steady state response amplitudes and phase angles are derived using the well-known method of averaging. It is found that, the system and element responses of purely bilinear hysteretic structures are stable even when viscous damping is absent. Both torsional and translational damping are found to be equally effective in reducing response amplitudes.

A nominally eccentric structure with close torsional and translational frequencies is found to have no significant torsional coupling in constrast to earlier observations for linear elastic structures. Similar behaviour in inelastic structures but with earthquake ground shaking has been reported by Tso and Sadek [14].

It is observed that, for medium to large eccentric and torsionally flexible structures, the peak ductility demand of the weaker element is influenced significantly whereas stiffer element remains relatively unaffected. Moreover, the response of the stiffer element approaches gradually the elastic range with increase in torsional stiffness of the structure. This observation is partly in disagreement with the observations of Irvine and Kountouris [12] who reported an absence of strong correlation between PDD and eccentricity derived analytically for elastic behaviour and time history response.

The peak ductility demand in resisting elements, as well as for the system as a whole, is found to be almost bilinearly related to ground acceleration amplitude, with a much larger second slope due to the considerable deterioration of elastic stiffness at higher amplitudes of ground acceleration. Similar conclusions employing earthquake ground motion have been reported by Irvine and Kountouris [12].

Chapter V examines the behaviour of several idealized hysteretic models representative of common structural systems: namely, reinforced concrete or steel moment resisting frames, shear walls, steel braced frames, etc. The idealized models are grouped into four main categories: these are purely bilinear hysteretic, elasto-plastic, pinched bilinear hysteretic and pinched elasto-plastic. A frequency sweep analysis for these models reveals the following two important characteristics: (i) the systems exhibit softening behaviour; (ii) pinched bilinear and pinched elasto-plastic systems experience instability or the so-called "jump phenomenon", whereas fully bilinear and fully elasto-plastic systems remain stable at all frequencies.

It is found that, for unstable systems, the response of only the stiffer resisting element undergoes instability. This instability can be eliminated altogether by increasing viscous damping in the structure. It is also observed that the instability is, in terms of the extent of the frequency zone of instability, most severe for a pinched elasto-plastic system representing steel cross-braced frames.

A parametric study on the pinched elasto-plastic structure reveals some important findings. A torsionally flexible structure of this type is found to be marginally stable, whereas a torsionally stiff structure is perfectly stable. A structure with nearly equal torsional and translational frequencies exhibits the jump-type instability. Also, the jump-phenomenon or instability is found to be present for nominal to large eccentricity with approximately the same frequency band-width of instability.

The instability in a torsionally coupled system is an important observation of the present study; emphasis is also placed on the

important role of viscous damping in stabilizing motion in addition to its well-known role of decreasing response amplitude.

6.2 SCOPE FOR FUTURE RESEARCH

Research on coupled lateral-torsional behaviour of inelastic structures is at present a growing field of activity. Additional research on several important aspects, to be described below, is still lacking. At the same time, the results from existing work remain to be digested before implementation in building codes as design guidelines is possible.

Thus, the future scope of research activity in this field can be visualized in the following two important areas:

1. Since the ultimate goal of research in lateral-torsional coupling under seismic loading is to improve the design of structures to better withstand seismic forces, the currently available research findings on inelastic coupled response need to be translated into a form that is comprehensible to practicing design engineers.

A closely related need in this area is to update the standard code of practice. Thus, similar to earlier work on code evaluation for torsionally coupled elastic structures [15,23,24], a promising field of research activity can be to identify inadequacies in inelastic seismic design of eccentric structures according to current practice and to prepare new guidelines as proposals for revision to existing codes.

2. Additional research in the following important areas seems necessary in order to fully understand the seismic behaviour of an inelastic eccentric structure:

(i) Research is needed in the field of random vibrations to investigate the inelastic lateral-torsional coupling of both

nondeteriorating and deteriorating structures.

(ii) Further investigation is necessary on seismic behaviour of eccentric structures consisting of resisting elements subjected to inelastic interaction effects.

(iii) A promising area of future research is the seismic lateral-torsional response of structures with various base-isolation systems, namely: sliding structures, structures supported on rubber bearings, soft-story structures, and structures supported on flexible foundations allowing partial lift-off.

(iv) Another field of interest is the inelastic response of torsionally coupled systems including the effect of foundation or soil-structure interaction.

(v) Important research can also involve the inelastic response of eccentric structures subjected to the simultaneous action of several components of ground motion, especially base translation together with base rotation.

However, as a direct extension to the work of this thesis, the following additional studies could be performed:

(a) Work on nonlinear elastic coupling can be expanded to examine the behaviour of large eccentric structures and to determine the effects of combination and arrangement of different resisting elements.

(b) Further investigation can be performed for multi-story structures including the effect of simutaneous multi-directional ground motion on torsional coupling of both symmetric and unsymmetric nonlinear elastic structures.

(c) Further study could apply the method of averaging in exploring

the behaviour of inelastic eccentric systems with unequal strength and stiffness ratios.

(d) Experimental work dedicated to improvement of the force-deformation behaviour to eliminate the pinching effect is an important area of investigation. Joint and connection detailing appears to be the critical area of interest here.

REFERENCES

[1] Evensen, D.A., "Nonlinear Flexural Vibrations of Thin Circular Ring", Journal of Applied Mechanics, ASME Transactions, Vol. 33, 1966, pp. 553-560.

[2] Evensen, D.A., "Nonlinear Flexural Vibrations of Thin Circular Ring", Ph.D. Thesis, California Institute of Technology, Pasadena, California, 1964.

[3] El-Zaouk, B.R., and Dym, C.L., "Non-linear Vibrations of Orthotropic Doubly-Curved Shallow Shells", Journal of Sound and Vibrations, Vol. 31 (1), 1973, pp. 89-103.

[4] Bolotin, V.V., "The Dynamic Stability of Elastic Systems", Holden-Day Inc., San Franscisco, California, 1964.

[5] Tso, W.K., "Induced Torsional Oscillations in Symmetrical Structures", Journal of the Earthquake Engineering and Structural Dynamics, Vol. 3, 1975, pp. 337-346.

[6] Antonelli, R.G., Meyer, K.J., and Oppenheim, I.J., "Torsional Instability in Structures", Journal of the Earthquake Engineering and Structural Dynamics, Vol. 9, No. 3, May-June 1981, pp. 221-237.

[7] Shibata, A., Onose, J., and Shiga, T., "Torsional Response of Buildings to Strong Earthquake Motions", Proceedings of the Fourth World Conference on Earthquake Engineering; Santiago; Chile, Vol. 2-A4, 1969, pp. 123-138.

[8] Tso, W.K., and Asmis, K.G., "Torsional Vibrations of Symmetrical Structures", Proceedings of the First Canadian Conference on Earthquake Engineering, Vancouver, Canada, 1971, pp. 178-186.

[9] Kan, C.L., and Chopra, A.K., "Linear and Nonlinear Earthquake Response of Simple Torsionally Coupled Systems", Report No. UCB/EERC 79-03, Earthquake Engineering Research Center, University of California, Berkeley, California, 1979.

[10] Kan, C.L., and Chopra, A.K., "Torsional Coupling and Earthquake Response of Simple Elastic and Inelastic Systems", Journal of the Structural Division, American Society of Civil Engineers, Vol. 107, August 1981, pp. 1569-1588.

[11] Kan, C.L., and Chopra, A.K., "Simple Model for Earthquake Response Studies of Torsionally Coupled Buildings", Journal of the Engineering Mechanics Division, American Society of Civil Engineers, Vol. 107, October 1981, pp. 935-951.

[12] Irvine, H.M., and Kountouris, G.E., "Inelastic Seismic Response of a Torsionally Unbalanced Single-Story Building Model", MIT Publication No. R79-31, Massachusetts Institute of Technology, Cambridge, Massachusetts, July 1979.

[13] Irvine, H.M., and Kountouris, G.E., "Peak Ductility Demands in Simple Torsionally Unbalanced Buildings Models Subjected to Earthquake Excitation", Proceedings of the Seventh World Conference on Earthquake Engineering, Istanbul, Turkey, Vol. 4, 1980, pp. 117-120.

[14] Tso, W.K., and Sadek, A.W., "Inelastic Response of Eccentric Structues", Proceeding of the Fourth Canadian Conference on Earthquake Engineering, Vancouver, British Columbia, July 1983, pp. 261-270.

[15] Awad, A.M., "Torsional Response of a Single Storey Building Model to Ground Motion", Ph.D. Thesis, Carleton University, Ottawa, Canada, August 1982.

[16] Hoerner, J.B., "Modal Coupling and Earthquake Response of Tall Buildings", Ph.D. Thesis, Report No. EERL 71-07, Earthquake Engineering Research Laboratory, California Institute of Technology, Pasadena, California, May 1971.

[17] Kan, C.L., and Chopra, A.K., "Coupled Lateral Torsional Response of Buildings to Ground Shaking", Report No. UCB/EERC 76-13, Earthquake Engineering Research Center, University of California, Berkeley, California, May 1976.

[18] Kan, C.L., and Chopra, A.K., "Effect of Torsional Coupling on Earthquake Forces in Buildings", Journal of the Structural Division, American Society of Civil Engineers, Vol. 103, April 1977, pp. 805-819.

[19] Kan, C.L., and Chopra, A.K., "Elastic Earthquake Analysis of a Class of Torsionally Coupled Buildings", Journal of the Structural Division, American Society of Civil Engineers, Vol. 103, April 1977, pp. 821-838.

[20] Shiga, T., "Torsional Vibration of Multi-Storied Buildings", Proceedings of the Third World Conference on Earthquake Engineering, Auckland, New Zeland, Vol. 2, 1965, pp. 569-584.

[21] Dempsey, K.M., and Irvine, H.M., "Envelopes of Maximum Seismic Response for a Partially Symmetric Single Storey Building Model", Journal of the Earthquake Engineering and Structural Dynamics, Vol. 7, 1979, pp. 161-180.

[22] Pekau, O.A., and Gordon, H.A., "Coupling of Torsional-Translational Response of Buildings During Earthquakes", Canadian Journal of Civil Engineering, Vol. 7, No. 2, 1980, pp. 282-293.

[23] Tso, W.K., and Dempsey, K.M., "Seismic Torsional Provisions for Dynamic Eccentricity", Journal of the Earthquake Engineering and Structural Dynamics, Vol. 8, 1980 pp. 275-289.

[24] Tsicnias, T.G., and Hutchinson, G.L., "Evaluation of Code Requirements for the Earthquake Resistance Design of Torsionally Coupled Buildings", Proceedings of the Institution of Civil Engineers, Part 2, Vol. 71, September 1981, pp. 821-843.

[25] Rutenberg, A., and Pekau, O.A., "Dynamic Torsional Effects in Buildings - A Bibliography", Department of Civil Engineering, Concordia University, Montreal, Canada, August 1981.

[26] Newmark, N.M., "Torsion in Symmetrical Buildings". Proceedings of the Fourth World Conference on Earthquake Engineering, Santiago, Chile, 1969, pp. A3-19 to A3-32.

[27] Pekau, O.A., and Syamal, P.K., "Coupling in the Dynamic Response of Nonlinear Unsymmetric Structures", Computers and Structures, Vol. 13, No. 1-3, 1981, pp. 197-204.

[28] Syamal, P.K., and Pekau, O.A., "Dynamic Torsional Response of Symmetric Structures", Proceedings of the ASCE/EMD Speciality Conference on Dynamic Response of Structures, Atlanta, Georgia, 1981, pp. 902-916.

[29] Kryloff, N., and Bogoliuboff, N., "Introduction to Nonlinear Mechanics", Princeton University Press, New Jersey, 1947, Kraus Reprint Co., New York, 1970.

[30] Pekau, O.A., and Syamal, P.K., "Non-Linear Torsional Coupling in Symmetric Structures", Journal of Sound and Vibration, Vol. 94, No. 2, May 1984, (accepted on 28 July 1983).

[31] Brown, K.M., "A Quadratically Convergent Newton-Like Method Based upon Gaussian Elimination", SIAM Journal on Numerical Analysis, Vol. 6, No. 4, 1969, pp. 560-569.

[32] Syamal, P.K., and Pekau, O.A., "Lateral-Torsional Coupling in Dynamic Response of Structures", Proceedings of the International Conference on Numerical Methods for Coupled Problems, Swansea, Wales, U.K., September 1981.

[33] Caughey, T.K., "Sinusoidal Excitation of a System with Bilinear Hystersis", Journal of Applied Mechanics, Vol. 27, ASME Transactions, Vol. 82, Series E, No. 4, 1960, pp. 640-643.

[34] Iwan, W.D., "The Dynamic Response of the One Degree of Freedom Bilinear Hysteretic System", Proceedings of the Third World Conference on Earthquqke Engineering, Auckland, New Zealand, Vol. 2, 1965, pp. 783-796.

[35] Jennings, P.C., "Response of Simple Yielding Structures to Earthquake Excitation", Ph.D. Thesis, California Institute of Technology, Pasadena, California, 1963.

[36] Jennings, P.C., "Periodic Response of General Yielding Structures", Journal of Engineering Mechanics Division, Proceedings of the American Society of Civil Engineers, Vol. 90, No. EM2, 1964, pp. 131-166.

[37] Iwan, W.D., "The Steady-State Response of a Two-Degree-of-Freedom Bilinear Hysteretic System", Journal of Applied Mechanics, Vol. 32, Transactions of the ASME, Vol. 87, Series E, 1965, pp. 151-156.

[38] Nigam, N.C., "Inelastic Interactions in the Dynamic Response of Structures", Ph.D. Thesis, California Institute of Technology, Pasadena, California, May 1967.

[39] Nigam, N.C., and Housener, G., "Elastic and Inelastic Response of Framed Structures During Earthquakes", Proceedings of the Fourth World Conference on Earthquake Engineering, Santiago, Chile, Vol. 2, 1969, pp. A4-89 to A4-104.

[40] Foutch, D.A., "The Vibrational Characteristics of a Twelve-Storey Steel Frame Building", Journal of the Earthquake Engineering and Structural Dynamics, Vol. 6, 1978, pp. 265-294.

[41] Iwan, W.D., "Application of Nonlinear Analysis Techniques", Winter Annual Meeting of the American Society of Mechanical Engineers on Applied Mechanics in Earthquake Engineering, New York, AMD-Vol. 8, November 1974, pp. 135-161.

[42] Klotter, K., and Pinney, E., "A Comprehensive Stability Criterion for Forced Vibrations in Nonlinear Systems", Journal of Applied Mechanics, Vol. 20, Transactions of the ASME, March 1953, pp. 9-12.

[43] Stoker, J.J., "Nonlinear Vibrations in Mechanical and Electrical Systems", Inter Science Publishers, New York, 1950.

[44] Timoshenko, S., Young, D.H., and Weaver, W. Jr., "Vibration Problems in Engineering", John Wiley and Sons, New York, Fourth Edition, 1974.

[45] Thomson, W.T., "Theory of Vibration With Applications", Prentice-Hall Inc., Englewood Cliffs, New Jersey, Second Edition, 1981.

[46] Iwan, W.D., "The Steady-State Response of The Double Bilinear Hysteretic Model", Journal of Applied Mechanics, Vol. 32, Transactions of the ASME, Vol. 82, Series E, 1965, pp. 921-925.

[47] Krawinkler, H., and Popov, E.P., "Seismic Behaviour of Moment Connections and Joints", Journal of the Structural Division, Proceedings of the American Society of Civil Engineers, Vol. 108, No. ST 2, February 1982, pp. 373-391.

[48] Fenwick, R.C., "Shear Deformation in Seismic Frame Structures", Journal of the Structural Division, Proceedings of the American Society of Civil Engineers, Vol. 109, No. 4, April 1983, pp. 965-975.

[49] Popov, E.P., and Bertero, V.V., "Repaired R/C Members Under Cyclic Loading", Journal of the Earthquake Engineering and Structural Dynamics, Vol. 4, 1975, pp. 129-144.

[50] Park, R., Priestley, M.J.N., and Gill, W.D., "Ductility of Square-Confined Concrete Columns", Journal of the Structural Division, Proceedings of the American Society of Civil Engineers, Vol. 108, No. ST 4, April 1982, pp. 929-950.

[51] Takayanagi, T., and Schnobrich, W.C., "Non-Linear Analysis of Coupled Wall Systems", Journal of the Earthquake Engineering and Structural Dynamics, Vol. 7, 1979, pp. 1-22.

[52] Veletsos, A.S., "Maximum Deformations of Certain Nonlinear Systems", Proceedings of the Fourth World Conference on Earthquake Engineering, Santiago, Chile, Vol. 2, Section A4, 1969, pp. 155-170.

[53] Gates, N.C., "The Earthquake Response of Deteriorating Systems", Ph.D. Thesis, EERL77-03, California Institute of Technology, Pasadena, California, March 1977.

[54] Iwan, W.D., and Gates, N.C., "The Effective Period and Damping of a Class of Hysteretic Structures", Journal of the Earthquake Engineering and Structural Dynamics, Vol. 7, 1979, pp. 199-211.

[55] Bui, T.D., "An Algorithm in Obtaining of Dependence of Solution X (Alpha) of Equation F(X, Alpha) = 0", Private Communication, Department of Computer Science, Concordia University, Montreal, Canada, January 1983.

[56] Wellford, L.C. Jr., Dib, G.M., and Mindle, W., "Free and Steady State Vibration of Non-Linear Structures Using a Finite Element - Non-Linear Eigenvalue Technique", Journal of the Earthquake Engineering and Structural Dynamics, Vol. 8, 1980, pp. 97-115.

[57] Schricker, V., and Powell, G.H., "Inelastic Seismic Analysis of Large Panel Buildings", Report No. UCB/EERC 80-38, Earthquake Engineering Research Center, University of California, Berkeley, California, 1980.

APPENDIX A

In order to nondimensionalize the equations of motion (Equations (2.6 and (2.7)), the following changes of variables are introduced.

$$\delta_x = \frac{U}{\omega_x^2}, \qquad \tau = \omega_x t, \qquad \delta_\theta = U/(\Gamma \quad \omega_\theta^2) \tag{A1}$$

$$\Lambda_x(t) = u(t)/\delta_x \qquad \Lambda_\theta(t) = \theta(t)/\delta_\theta$$

where Γ denotes the mass radius of gyration. The following system parameters are also needed for normalization.

$$\omega_x^2 = K_x/M \qquad \omega_y^2 = K_y/M$$

$$\omega_\theta^2 = K_\theta/(M\Gamma^2) \qquad \Omega_y = \omega_y/\omega_x \tag{A2}$$

$$\Omega_\theta = \omega_\theta/\omega_x \qquad \Omega = \omega/\omega_x$$

$$\beta_0 = \frac{a}{\Gamma} = \left(\frac{3r^2}{1 + r^2}\right)^{\frac{1}{2}} \qquad \gamma_0 = \frac{b}{\Gamma} = \left(\frac{3}{1 + r^2}\right)^{\frac{1}{2}} \tag{A3}$$

$$E^2 = (\Sigma\, k_{ix} y_i^2)/(b^2\, \Sigma\, k_{ix}) \qquad F^2 = (\Sigma\, k_{iy} x_i^2)/(a^2\, \Sigma\, k_{iy}) \tag{A4}$$

Coefficients f_i and h_i for $\delta_{0,s} = U/\omega_x^2$

After substituting Equations (A1)-(A4) into Equations (2.6 and (2.7), the nondimensional form of the equations of motion expressed

by Equations (2.13) and (2.14) is obtained in which the coefficients f_i and h_i are given by the following expressions

$$
\begin{aligned}
f_1 &= 2\,\zeta_x & h_1 &= 2\,\zeta_\theta \Omega_\theta \\
f_2 &= 1.0 & h_2 &= \Omega_\theta^2 \\
f_3 &= \lambda_s & h_3 &= 3\,\lambda_s \gamma_0^2 E^2 \\
f_5 &= 3\,\lambda_s \gamma_0^2/\Omega_\theta^4 & h_4 &= \lambda_s \gamma_0^4 E^2/\Omega_\theta^4 \\
 & & h_6 &= \lambda_s \beta_0^4 \Omega_y^2 F^2/\Omega_\theta^2
\end{aligned}
\qquad \text{(A5)}
$$

in which ζ_x and ζ_θ are the translational and torsional viscous damping coefficients, respectively.

Coefficients f_i and h_i for $\delta_{o,d} = UD/\omega_x^2$

With this definition of δ_0 Equations (A1)-(A4) reduce Equations (2.6) and (2.7) to nondimensional form when the expressions for f_i and h_i are

$$
\begin{aligned}
f_1 &= 2\,\zeta_x & h_1 &= 2\,\zeta_\theta \Omega_\theta \\
f_2 &= 1.0 & h_2 &= \Omega_\theta^2 \\
f_3 &= \lambda_d/D^2 & h_3 &= 3\,\lambda_d \gamma_0^2 E^2/D^2 \\
f_5 &= 3\,\lambda_d \gamma_0^2/(\Omega_\theta^4 D^2) & h_4 &= \lambda_d \gamma_0^4 E^2/(\Omega_\theta^4 D^2) \\
 & & h_6 &= \lambda_d \beta_0^4 \Omega_y^2 F^2/(\Omega_\theta^4 D^2)
\end{aligned}
\qquad \text{(A6)}
$$

Comparing Equations (A5) and (A6), it is observed that f_1, f_2,

h_1 and h_2 remain unchanged irrespective of which normalization procedure is used. However, coefficients f_3, f_5, h_3, h_4 and h_6 are influenced by the normalization method. It should also be noted that these coefficients can be obtained from expressions (A6) by simply substituting Equation (2.12).

APPENDIX B

The method of slowly varying amplitude, i.e., the Kryloff-Bogoliuboff method [29], can be demonstrated for Equations (2.13) and (2.14) with the assumed solutions shown in Equations (2.15a) and (2.15b).

Letting $\Phi_1 = \Omega\tau + \Phi$

$$\chi_1 = \Omega\tau + \chi \tag{B1}$$

Equations (2.15a) and (2.15b) become

$$\begin{aligned} \Lambda_\chi(\tau) &= P \cos \Phi_1 \\ \Lambda_\theta(\tau) &= R \cos \chi_1 \end{aligned} \tag{B2}$$

Differentiating the above, one gets

$$\begin{aligned} \dot{\Lambda}_\chi &= -\Omega P \sin \Phi_1 + \dot{P} \cos \Phi_1 - P \dot{\Phi} \sin \Phi_1 \\ \dot{\Lambda}_\theta &= -\Omega R \sin \chi_1 + \dot{R} \cos \chi_1 - R \dot{\chi} \sin \chi_1 \end{aligned} \tag{B3}$$

In the method of averaging [29], the foregoing equations are replaced by the following set of four equations

$$\dot{\Lambda}_\chi = -\Omega P \sin \Phi_1 \tag{B4}$$

$$\dot{P} \cos \Phi_1 - P \dot{\Phi} \sin \Phi_1 = 0 \tag{B5}$$

$$\dot{\Lambda}_\theta = -\Omega R \sin \chi_1 \tag{B6}$$

$$\dot{R} \cos \chi_1 - R \dot{\chi} \sin \chi_1 = 0 \tag{B7}$$

Equation (B4) is used to compute the second derivatives of Λ_x and Λ_θ as

$$\ddot{\Lambda}_x = -\Omega^2 P \cos \Phi_1 - \dot{P} \Omega \sin \Phi_1 - P \Omega \dot{\Phi} \cos \Phi_1$$
$$\ddot{\Lambda}_\theta = -\Omega^2 R \cos \chi_1 - \dot{R} \Omega \sin \chi_1 - R \Omega \dot{\chi} \cos \chi_1 \qquad \text{(B8)}$$

These approximations for Λ_x, Λ_θ, $\dot{\Lambda}_x$, $\dot{\Lambda}_\theta$, $\ddot{\Lambda}_x$, $\ddot{\Lambda}_\theta$ are substituted into Equations (2.13) and (2.14) yielding

$$\Omega^2 P \cos \Phi_1 + \dot{P} \Omega \sin \Phi_1 + P \Omega \dot{\Phi} \cos \Phi_1 + f_1 \Omega P \sin \Phi_1$$
$$- f_2 P \cos \Phi_1 + f_3 P^3 \cos^3 \Phi_1 + f_5 P R^2 \cos \Phi_1 \cos^2 \chi_1 = \cos \Omega\tau \qquad \text{(B9)}$$

$$\Omega^2 R \cos \chi_1 + \dot{R} \Omega \sin \chi_1 + R \Omega \dot{\chi} \cos \chi_1 + h_1 \Omega R \sin \chi_1$$
$$- h_2 R \cos \chi_1 + h_3 R P^2 \cos \chi_1 \cos^2 \Phi_1 + (h_4+h_6) R^3 \cos^3 \chi_1 = 0 \qquad \text{(B10)}$$

Equations (B9) and (B10) are then subjected to the following sequence of operations:

(i) multiplying both sides of Equation (B9) by $\cos \Phi_1$ and Equation (B5) by $\Omega \sin \Phi_1$ and adding;

(ii) multiplying Equation (B9) by $\sin \Phi_1$ and Equation (B5) by $-\Omega \cos \Phi_1$ and adding;

(iii) multiplying Equation (B10) by $\cos \chi_1$ and Equation (B7) by $\Omega \sin \chi_1$ and adding;

(iv) multiplying Equation (B10) by $\sin \chi_1$ and Equation (B7) by $-\Omega \cos \chi_1$ and adding;

The above operations yield the set of four equations given below

$$(f_2-\Omega^2)\, P \cos^2 \Phi_1 - P\, \Omega\, \dot{\Phi}_1 - f_1\, \Omega\, P \sin \Phi_1 \cos \Phi_1 - f_3\, P^3 \cos^4 \Phi_1 - f_5\, P\, R^2 \cos^2 \Phi_1 \cos^2 \chi_1 = -\cos \Phi_1 \cos \Omega\tau \qquad (B11)$$

$$(f_2-\Omega^2)\, P \sin \Phi_1 \cos \Phi_1 - \dot{P}\, \Omega - f_1\, \Omega\, P \sin^2 \Phi_1 - f_3\, P^3 \sin \Phi_1 \cos^3 \Phi_1 - f_5\, P\, R^2 \sin \Phi_1 \cos \Phi_1 \cos^2 \chi_1 = -\sin \Phi_1 \cos \Omega\tau \qquad (B12)$$

$$(h_2-\Omega^2)\, R \cos^2 \chi_1 - \Omega\, R\, \dot{\chi} - h_1\, \Omega\, R \sin \chi_1 \cos \chi_1 - h_3\, R\, P^2 \cos^2 \chi_1 \cos^2 \Phi_1 - (h_4+h_6)\, R^3 \cos^4 \chi_1 = 0 \qquad (B13)$$

$$(h_2-\Omega^2)\, R \sin \chi_1 \cos \chi_1 - \Omega\, \dot{R} - h_1\, \Omega\, R \sin^2 \chi_1 - h_3\, R\, P^2 \sin \chi_1 \cos \chi_1 \cos^2 \Phi_1 - (h_4+h_6)\, R^3 \sin \chi_1 \cos^3 \chi_1 = 0 \qquad (B14)$$

Equations (B15) through (B18) are averaged by integrating both sides of each equation over one period for Φ_1 (say Φ_1=0 to 2π) in Equations (B11) and (B12) and similarly, for χ_1 in Equations (B13) and (B14). In the integration, variables $P(\tau)$, $R(\tau)$, $\Phi(\tau)$, and $\Delta_2(\tau)$ are approximated by average values $\bar{P}$, $\bar{R}$, $\bar{\Phi}$, $\bar{\chi}$, and $\bar{\Delta}_2$ ( ) since they are assumed to vary slowly.

The result of these operations is a set of four equations involving average amplitudes $\bar{P}$, $\bar{R}$ and phases $\bar{\Phi}$ and $\bar{\chi}$ as follows

$$(f_2-\Omega^2)\,\bar{P} - 2\,\Omega\,\bar{P}\,\dot{\bar{\Phi}} - \tfrac{3}{4}\,f_3\,\bar{P}^3 - \tfrac{1}{4}\,f_5\,\bar{P}\,\bar{R}^2\,(1 + 2\cos^2\bar{\Delta}_2) = -\cos\bar{\Phi} \qquad \text{(B15)}$$

$$f_1\,\Omega\,\bar{P} + 2\,\Omega\,\dot{\bar{P}} - \tfrac{1}{4}\,f_5\,\bar{P}\,\bar{R}^2 \sin 2\bar{\Delta}_2 = \sin\bar{\Phi} \qquad \text{(B16)}$$

$$(h_2-\Omega^2)\,\bar{R} - 2\,\Omega\,\bar{R}\,\dot{\bar{\chi}} - \tfrac{1}{4}\,h_3\,\bar{R}\,\bar{P}^2\,(1 + 2\cos^2\bar{\Delta}_2) - \tfrac{3}{4}\,(h_4+h_6)\,\bar{R}^3 = 0 \qquad \text{(B17)}$$

$$h_1\,\Omega\,\bar{R} + 2\,\Omega\,\dot{\bar{R}} + \tfrac{1}{4}\,h_3\,\bar{R}\,\bar{P}^2 \sin 2\bar{\Delta}_2 = 0 \qquad \text{(B18)}$$

However, for steady state vibrations $\bar{P}$, $\bar{R}$, $\bar{\Phi}$ and $\bar{\chi}$ are constant. Under this condition $\dot{\bar{P}}$, $\dot{\bar{R}}$, $\dot{\bar{\Phi}}$ and $\dot{\bar{\chi}}$, in Equations (B15) through (B18). may be taken to be zero; thus, these equations yield Equation (2.16).

APPENDIX C

With the introduction of small perturbations $\xi_x(\tau)$ and $\xi_\theta(\tau)$ in the solution for $\Lambda_x(\tau)$ and $\Lambda_\theta^\circ(\tau)$, Equations (2.19a,b) are obtained. Thus, letting

$$\overline{\Phi}_1 = \Omega\tau + \overline{\Phi}$$

$$\overline{\chi}_1 = \Omega\tau + \overline{\chi}$$

the first and second derivatives of Equation (2.19a,b) become

$$\dot{\Lambda}_x(\tau) = -\overline{P}\,\Omega \sin\overline{\Phi}_1 + \dot{\xi}_x$$

$$\dot{\Lambda}_\theta(\tau) = -\overline{R}\,\Omega \sin\overline{\chi}_1 + \dot{\xi}_\theta$$

$$\ddot{\Lambda}_x(\tau) = -\overline{P}\,\Omega^2 \cos\overline{\Phi}_1 + \ddot{\xi}_x$$

$$\ddot{\Lambda}_\theta(\tau) = -\overline{R}\,\Omega^2 \cos\overline{\chi}_1 + \ddot{\xi}_\theta$$

Retaining only the first order terms in perturbations ξ_x, ξ_θ and after some algebraic manipulations, the above derivatives together with Λ_x and Λ_θ from Equations (2.15a,b) transform Equations (2.13) and (2.14) into

$$\ddot{\xi}_x + f_1\,\dot{\xi}_x + f_2\,\xi_x - (3\,f_3\,\overline{P}^2\cos^2\overline{\Phi}_1 + f_5\,\overline{R}^2\cos^2\overline{\chi}_1)\,\xi_x - 2\,f_5\,\overline{P}\,\overline{R}\cos\overline{\Phi}_1\cos\overline{\chi}_1\,\xi_\theta = 0 \qquad (C1)$$

$$\ddot{\xi}_\theta + h_1 \dot{\xi}_\theta + h_2 \xi_\theta - \{h_3\bar{P}^2 \cos^2 \bar{\Phi}_1 + 3(h_4+h_6)\bar{R}^2 \cos^2 \bar{\chi}_1\}\xi_\theta$$

$$- 2\, h_3\, \bar{P}\, \bar{R} \cos \bar{\Phi}_1 \cos \bar{\chi}_1\, \xi_x = 0 \qquad (C2)$$

Equations (C1) and (C2) are recognized as damped coupled Mathieu-Hill equations.

Without loss of generality, phase angles Φ_1 and χ_1 can be assumed zero, yielding

$$\bar{\Phi}_1 = \bar{\chi}_1$$

Thus, in Equations (C1) and (C2), the terms $\cos^2 \bar{\Phi}_1$, $\cos^2 \bar{\chi}_1$ and $\cos \bar{\Phi}_1 \cos \bar{\chi}_1$ will all be replaced by $\cos^2 \Omega\tau$. With the relationship

$$\cos^2 \Omega\tau = \tfrac{1}{2}(1 + \cos 2\,\Omega\tau)$$

Equations (C1) and (C2) may be written as

$$\ddot{\xi}_x + f_1 \dot{\xi}_x + f_2 \xi_x - \tfrac{1}{2}(1 + \cos 2\,\Omega\tau)[(3\, f_3\bar{P}^2 + f_5\bar{R}^2)\xi_x \qquad (C3)$$

$$+ 2\, f_5\, \bar{P}\, \bar{R}\, \xi_\theta] = 0$$

$$\ddot{\xi}_\theta + h_1 \dot{\xi}_\theta + h_2 \xi_\theta - \tfrac{1}{2}(1 + \cos 2\,\Omega\tau)[\{h_3\bar{P}^2 + 3(h_4+h_6)\bar{R}^2\}\, \xi_\theta$$

$$+ 2\, h_3\, \bar{P}\, \bar{R}\, \xi_x] = 0 \qquad (C4)$$

Dividing Equation (C3) by f_2 and (C4) by h_2, and arranging these equations in condensed matrix form, the following equation is obtained

$$\underset{\sim}{C}\,\ddot{\underset{\sim}{\xi}} + 2\,\underset{\sim}{C}\,\underset{\sim}{\varepsilon}\,\dot{\underset{\sim}{\xi}} + (\underset{\sim}{E} - \tfrac{1}{2}\,\underset{\sim}{A} - \tfrac{1}{2}\,\underset{\sim}{B}\cos 2\Omega\tau)\,\underset{\sim}{\xi} = 0 \qquad (C5)$$

where

$$\underset{\sim}{C} = \begin{bmatrix} \frac{1}{f_2} & 0 \\ 0 & \frac{1}{h_2} \end{bmatrix} \quad ; \quad \underset{\sim}{\varepsilon} = \tfrac{1}{2}\begin{bmatrix} f_1 & 0 \\ 0 & h_1 \end{bmatrix}$$

$$\underset{\sim}{A} = \underset{\sim}{B} = \begin{bmatrix} \frac{A_{11}}{f_2} & \frac{A_{12}}{f_2} \\ \frac{A_{21}}{h_2} & \frac{A_{22}}{h_2} \end{bmatrix} \quad ; \quad \underset{\sim}{E} = \begin{bmatrix} 1 & 0 \\ 0 & 1 \end{bmatrix}$$

$$A_{11} = 3\,f_3\bar{P}^2 + f_5\bar{R}^2; \qquad A_{12} = 2\,f_5\,\bar{P}\,\bar{R}$$

$$A_{21} = 2\,h_3\,\bar{P}\,\bar{R} \quad ; \quad A_{22} = h_3\bar{P}^2 + 3(h_4+h_6)\,\bar{R}^2$$

APPENDIX D

Equation (C4) of Appendix C is a coupled damped Mathieu-Hill equation resulting from perturbation of torsional displacement Λ_θ by ξ_θ, rewritten here as

$$\ddot{\xi}_\theta + h_1 \dot{\xi}_\theta + [h_2 - \tfrac{1}{2}(1 + \cos 2\,\Omega\tau)\{h_3\overline{P}^2 + 3(h_4+h_6)\overline{R}^2\}]\,\xi_\theta$$

$$- \tfrac{1}{2}(1 + \cos 2\,\Omega\tau)\,(2\,h_3\,\overline{P}\,\overline{R})\,\xi_x = 0 \qquad (D1)$$

This equation describes the magnitude of the perturbed torsional motion with periodically varying torsional stiffness. The coefficient associated with ξ_θ may be interpreted as a modified torsional frequency of the system. After algebraic operations with this coefficient, one obtains the expression

$$\ddot{\xi}_\theta + 2\,\xi_\theta\Omega_\theta\dot{\xi}_\theta + \Omega_0^2\,(1 - 2\,\mu\cos 2\,\Omega\tau)\,\xi_\theta$$

$$- h_3\,\overline{P}\,\overline{R}\,(1+\cos 2\,\Omega\tau)\,\xi_x = 0 \qquad (D2)$$

in which

$$\Omega_0^2 = h_2 - \tfrac{1}{2}\,h_3\overline{P}^2 - \tfrac{3}{2}(h_4+h_6)\,\overline{R}^2 \qquad (D3)$$

$$\mu = \frac{h_3\overline{P}^2 + 3(h_4+h_6)\,\overline{R}^2}{4\Omega_0^2} \qquad (D4)$$

In the above, Ω_0 may be identified as the apparent torsional frequency

of the system. Since $h_2 = \Omega_\theta^2$, Ω_θ^2 represents modification of Ω_θ^2 proportional to the square of the amplitudes $\bar{P}$ and $\bar{R}$.

For resisting elements with softening nonlinear characteristics, λ is considered positive, and hence the magnitude of h_3, h_4, h_6 are positive. Thus, such nonlinearity has the effect of decreasing torsional frequency ratio Ω_θ^2.

In Equation (D3) it is noticed that, for certain combinations of $\bar{P}$ and $\bar{R}$ values (hereafter called the critical amplitude combinations), apparent torsional frequency Ω_0 becomes zero. This corresponds to static torsional buckling of the structure due to lateral loading. However, it has also been noted that the magnitude of $\bar{R}$ becomes zero with suitable assumptions (Equation (2.28b)). Thus, the critical value of lateral displacement amplitude $\bar{P}$ which reduces the apparent torsional frequency Ω_0 to zero is given by

$$\bar{P}_{cr} = \frac{2\Omega_\theta^2}{h_3} \tag{D5}$$

For dynamic torsional response, it is assumed that lateral amplitude $\bar{P}$ does not reach $\bar{P}_{cr}$.

For static normalization, substituting h_3 from Equation (A5) and $\bar{P}$ from Equation (2.30), one obtains the following expression for critical torsional buckling in Ω_θ-Ω parameter space

$$\Omega_\theta^2 = \frac{9\ \lambda_s\ E^2 D^2}{2(1+r^2)} \tag{D6}$$

The corresponding expression for dynamic normalization is

$$\Omega_\theta^2 = \frac{9\,\lambda_d\,E^2}{2(1+r^2)} \qquad \text{(D7)}$$

Equations (D6) and (D7) may be expressed in generalized form as follows

$$\hat{\Omega}_\theta^2 = \frac{9\,\lambda_s\,D^2}{2(1+r^2)} \quad , \quad \text{for static normalization} \qquad \text{(D8)}$$

$$\hat{\Omega}_\theta^2 = \frac{9\lambda_d}{2(1+r^2)} \quad , \quad \text{for dynamic normalization} \qquad \text{(D9)}$$

APPENDIX E

SYSTEMS WITH SINGLE ECCENTRICITY ($e_x = 0$, $e_y \neq 0$)

The expression for coefficient matrix $\underset{\sim}{A}$ of Equations (2.20) and (C5), specialized for a single-eccentric system, is given by

$$\underset{\sim}{A} = \begin{bmatrix} \dfrac{A_{11}}{f_2} & \dfrac{A_{12}+2\ f_6}{f_2} \\ \dfrac{A_{21}+2\ h_7}{h_2} & \dfrac{A_{22}}{h_2} \end{bmatrix} \qquad \text{(E1)}$$

in which

$$\begin{aligned} A_{11} &= 3\ f_3\ \overline{P}^2 + 2\ f_4\ \overline{P}\ \overline{R} + f_5\ \overline{R}^2 \\ A_{12} &= f_4\overline{P}^2 + 2\ f_5\ \overline{P}\ \overline{R} + 3\ f_7\ \overline{R}^2 \\ A_{21} &= h_g\ \overline{R}^2 + 2\ h_3\ \overline{P}\ \overline{R} + 3\ h_8\ \overline{P}^2 \\ A_{22} &= 3(h_4+h_6)\ \overline{R}^2 + 2\ h_9\ \overline{P}\ \overline{R} + h_3\ \overline{P}^2 \end{aligned} \qquad \text{(E2)}$$

The form of $\underset{\sim}{B}$ remains the same as in Appendix C but the quantity A_{ij} needed to evaluate the elements of $\underset{\sim}{B}$ are for the eccentric system given in Equation (E2).

The principal region of instability, after expanding Equation (2.21), setting the second diagonal term to zero for to approximate of Ω, and substituting this into all the elements of the determinantal equation except the second and fourth elements of the principal diagonal, becomes in expanded form

$$\begin{vmatrix} (1-\frac{1}{4}\frac{A_{11}}{f_2}-\frac{\Omega_\theta^2}{f_2}) & -(\frac{A_{12}}{4f_2}+\frac{2f_6}{f_2}) & -\frac{\Omega_\theta f_1}{f_2} & 0 \\ -(\frac{A_{21}}{4h_2}+\frac{2h_7}{h_2}) & (1-\frac{A_{22}}{4h_2}-\frac{\Omega^2}{h_2}) & 0 & \frac{\Omega_\theta h_1}{h_2} \\ \frac{\Omega_\theta f_1}{f_2} & 0 & (1-\frac{3}{4}\frac{A_{11}}{f_2}-\frac{\Omega_\theta^2}{f_2}) & -(\frac{3}{4}\frac{A_{12}}{f_2}+\frac{2f_6}{f_2}) \\ 0 & \frac{\Omega_\theta h_1}{h_2} & -(\frac{3}{4}\frac{A_{21}}{h_2}+\frac{2h_7}{h_2}) & (1-\frac{3}{4}\frac{A_{22}}{h_2}-\frac{\Omega^2}{h_2}) \end{vmatrix} = 0 \qquad \text{(E3)}$$

APPENDIX F

SYSTEMS WITH DOUBLE ECCENTRICITY (e_x, $e_y \neq 0$)

The following additional change of variables, along with those shown in Equation (A1), are needed in order to nondimensionalize the set of three equations of motions

$$\delta_y = \frac{U}{\omega_y^2} \quad ; \qquad \Lambda_y(\tau) = \frac{v(t)}{\delta_y} \tag{F1}$$

Coefficients f_i, g_i and h_i for Example L-Shaped Building Plan with $\delta_{0,s} = U/\omega_x^2$

$$f_1 = 2\,\zeta_x$$

$$f_2 = 1.0$$

$$f_3 = \lambda$$

$$f_4 = \lambda\, C_{10} \left(\frac{\gamma_0}{\Omega_\theta^2}\right)$$

$$f_5 = \lambda\, C_{11} \left(\frac{\gamma_0}{\Omega_\theta^2}\right)^2$$

$$f_6 = -\, C_{12} \left(\frac{\gamma_0}{\Omega_\theta^2}\right)$$

$$f_7 = -\,\lambda\, C_{13} \left(\frac{\gamma_0}{\Omega_\theta^2}\right)^3$$

(F2)

$$g_1 = 2\,\zeta_y\,\Omega_y$$

$$g_2 = \Omega_y^2$$

$$g_3 = \lambda/\Omega_y^2$$

$$g_4 = -\frac{\lambda}{\Omega_y^2} C_{20}\left(\frac{\beta_0\Omega_y^2}{\Omega_\theta^2}\right)$$

$$g_5 = \frac{\lambda}{\Omega_y^2} C_{21}\left(\frac{\beta_0\Omega_y^2}{\Omega_\theta^2}\right)^2$$

$$g_6 = C_{22}\,\Omega_y^2\left(\frac{\beta_0\Omega_y^2}{\Omega_\theta^2}\right)$$

$$g_7 = \frac{\lambda}{\Omega_y^2} C_{23}\left(\frac{\beta_0\Omega_y^2}{\Omega_\theta^2}\right)^3$$

(F3)

$$h_1 = 2\,\zeta_\theta\Omega_\theta$$

$$h_2 = \Omega_\theta^2$$

$$h_3 = \lambda\gamma_0\Omega_\theta^2\, C_{30}\left(\frac{\gamma_0}{\Omega_\theta^2}\right)$$

$$h_4 = \lambda\gamma_0\Omega_\theta^2\, C_{31}\left(\frac{\gamma_0}{\Omega_\theta^2}\right)^3$$

$$h_5 = \left(\frac{\lambda\beta_0\Omega_\theta^2}{\Omega_y^4}\right) C_{32}\left(\frac{\beta_0\Omega_y^2}{\Omega_\theta^2}\right)$$

$$h_6 = \left(\frac{\lambda\beta_0\Omega_\theta^2}{\Omega_y^4}\right) C_{33}\left(\frac{\beta_0\Omega_y^2}{\Omega_\theta^2}\right)^3$$

$$h_7 = -C_{12}\,\gamma_0\Omega_\theta^2$$

(F4)

$$h_8 = \lambda\gamma_0\,\Omega_\theta^2\,C_{12}$$

$$h_9 = -\,\lambda\,\gamma_0\Omega_\theta^2\,C_{34}\left(\frac{\gamma_0}{\Omega_\theta^2}\right)^2$$

$$h_{10} = C_{22}\,\beta_0\Omega_\theta^2$$

$$h_{11} = -\left(\frac{\lambda\beta_0\Omega_\theta^2}{\Omega_y^4}\right)\,C_{22}$$

$$h_{12} = \left(\frac{\lambda\beta_0\Omega_\theta^2}{\Omega_y^4}\right)\,C_{35}\left(\frac{\beta_0\Omega_y^2}{\Omega_\theta^2}\right)^2$$

$$C_{10} = 3\,C_5/C_1$$

$$C_{11} = \frac{3}{C_1^2}\{C_3^2 - 2(C_3-C_1)(C_3-C_5)\}$$

$$C_{12} = C_5/C_1$$

$$C_{13} = \frac{1}{C_1^3}\{(C_3-C_5)(3\,C_3^2 - 6C_3C_1 + 4C_1^2) - C_3^3\}$$

(F5)

$$C_{20} = 3\,C_4/C_1$$

$$C_{21} = \frac{3}{C_1^2}\{C_2^2 - 2(C_2-C_1)(C_2-C_4)$$

$$C_{22} = C_4/C_1$$

(F6)

$$C_{23} = \frac{1}{C_1^3}\{(C_2-C_4)(3\,C_2^2 - 6C_1C_2 + 4\,C_1^2) - C_2^3\}$$

$$C_{30} = 3\,C_3^2/C_1^2$$

$$C_{31} = \{\frac{C_3^2}{C_1^2}(3\,\frac{C_3^2}{C_1^2} - 6\,\frac{C_3}{C_1} + 4) - 2\,\frac{C_3C_5}{C_1^2}(\frac{C_3}{C_1^2} - 1)(\frac{C_3}{C_1} - 2)\}$$

$$C_{32} = 3\,C_2^2/C_1^2$$

$$C_{33} = \{\frac{C_2^2}{C_1^2}(3\,\frac{C_2^2}{C_1^2} - 6\,\frac{C_2}{C_1} + 4) - 2\,\frac{C_2C_4}{C_1^2}(\frac{C_2}{C_1} - 1)(\frac{C_2}{C_1} - 1)\} \qquad \text{(F7)}$$

$$C_{34} = 3\{\frac{C_3C_5}{C_1^2}(\frac{C_3}{C_1} - 2) - 2\,\frac{C_3^2}{C_1^2}(\frac{C_3}{C_1} - 1)\}$$

$$C_{35} = 3\{\frac{C_2C_4}{C_1^2}(\frac{C_2}{C_1} - 2) - 2\,\frac{C_2^2}{C_1^2}(\frac{C_2}{C_1} - 1)\}$$

$$C_1 = \beta + \gamma - \beta\gamma$$

$$C_2 = \gamma + \beta^2\,(1-\gamma)$$

$$C_3 = \beta + \gamma^2\,(1-\beta)$$

$$C_4 = \gamma(1-\beta)^2\,(1-\gamma) \qquad \text{(F8)}$$

$$C_5 = \beta\,(1-\beta)\,(1-\gamma)^2$$

$$C_6 = C_2^2 + 4\beta\, C_4$$

$$C_7 = C_3^2 + 4\gamma\, C_5$$

$$\beta_0 = a/\Gamma = \sqrt{3}\; C_1 / \sqrt{C_6 + C_7/r^2}$$

$$\gamma_0 = a/\Gamma = \sqrt{3}\; C_1 / \sqrt{C_6 r^2 + C_7}$$

$$\Omega_\theta^2 = \left(\frac{C_3}{C_1}\gamma_0\right)^2 + \left(\frac{C_2}{C_1}\beta_0\,\Omega_y\right)^2$$

$$r = a/b$$

(F9)

APPENDIX G

Kan and Chopra [17] provided the following relationship for the translational and torsional response in a three degree-of-freedom linear unsymmetric system

$$\overline{V}_x^2 + \overline{V}_y^2 + \overline{T}^2 = 1 \qquad (G1)$$

in which

$$\overline{V}_x = \frac{V_x}{V_{xo}} \; ; \; \overline{V}_y = \frac{V_y}{V_{yo}} \; ; \; \overline{T} = \frac{T}{\Gamma V_{xo}} \qquad (G2)$$

Here V_{xo} is the response of a single degree-of-freedom uncoupled system in the x-direction, where the mass and stiffness are the same as those of the coupled system; V_x, V_y and T are the translational and torsional responses of the coupled system in the x-, y- and θ-directions, respectively.

For a weakly nonlinear elastic system V_x, V_y and V_{xo} may be assumed to be nearly equal to the force from linear stiffness multiplied by the displacement, given by

$$V_x = K_x \, \delta_x; \quad V_y = K_y \, \delta_y \; ; \; V_{xo} = K_x \, \delta_{xo} \qquad (G3)$$

Also, total torque T can be expressed as

$$T = V_x \, e_y + V_y \, e_x \qquad (G4)$$

Substituting (G3) and (G4) in (G1) and using the relations $\omega_x^2 = \frac{K_x}{M}$, $\omega_y^2 = \frac{K_y}{M}$ and $\frac{K_y}{K_x} = \Omega_y^2$, the following relation is obtained

$$(\frac{\delta_x}{\delta_{x0}})^2 [1 + (\frac{e_y}{\Gamma})^2] + (\frac{\delta_y}{\delta_{x0}})^2 \Omega_y^4 [1 + (\frac{e_x}{\Gamma})^2]$$

$$+ 2 (\frac{\delta_x}{\delta_{x0}}) (\frac{\delta_y}{\delta_{x0}}) \Omega_y^2 (\frac{e_x}{\Gamma}) (\frac{e_y}{\Gamma}) = 1 \qquad (G5)$$

Since δ_x and δ_y are the displacement amplitudes of the coupled system and δ_{x0} is that of an uncoupled system, these may be replaced by $\overline{P}$, $\overline{Q}$ and D respectively, where D is expressed by Equation (2.11). After nondimensionalizing eccentricities (i.e., $E_x = \frac{e_x}{\Gamma}$; $E_y = \frac{e_y}{\Gamma}$), Equation (G5) yields

$$(\frac{\overline{P}}{D})^2 (1 + E_y^2) + (\frac{\overline{Q}}{D})^2 \Omega_y^4 (1 + E_x^2) + 2 \frac{\overline{P}\,\overline{Q}}{D^2} \Omega_y^2 E_x E_y = 1 \qquad (G6)$$

For input ground motion in the x-direction, one may assume $\overline{Q} << \overline{P}$ in a nominally symmetric building; thus, neglecting $\overline{Q}$ in the foregoing equation yields the magnitude of $\overline{P}$ as

$$\overline{P}^2 = \frac{D^2}{(1 + E_y^2)} \qquad (G7)$$

APPENDIX H

As a check on the correctness of solution, the linear elastic case was solved by introducing $\alpha = 1.0$ in Equations (4.28), (4.29), (5.1) and (5.2). This reduces these equations for both hysteretic systems to the following form

$$\left.\begin{aligned} &C_i(\bar{A}_i) = \bar{A}_i, \quad \bar{A}_i \geq 0 \quad , \quad i=3,4 \\ &S_i(\bar{A}_i) = 0 \quad , \quad \bar{A}_i \geq 0 \quad , \quad i=3,4 \\ &C_2(r\bar{A}_2) = r\bar{A}_2 \quad , \quad \bar{A}_2 \geq 0 \\ &S_2(r\bar{A}_2) = 0 \quad , \quad \bar{A}_2 \geq 0 \end{aligned}\right\} \quad (H1)$$

After substituting Equation (H1) into Equations (4.23) through (4.26) and performing algebraic operations, the following closed form solution of system amplitudes $\bar{A}_1$, $\bar{A}_2$ and corresponding phase angles $\bar{\Phi}_1$ and $\bar{\Phi}_2$ are obtained

$$\bar{A}_1^2 = \frac{G_a^2}{\left(\left[(1-\Omega^2) - \dfrac{\gamma_0^2\eta^2\left(\gamma_0^2 + \beta_0^2\Omega_y^2 - \Omega^2\right)}{(2+\eta)^2\left\{\left(\gamma_0^2 + \beta_0^2\Omega_y^2 - \Omega^2\right)^2 + \left(2\,\zeta_\theta\Omega_\theta\Omega\right)^2\right\}}\right]^2 + \left[2\zeta_x\Omega + \dfrac{2\,\zeta_\theta\Omega_\theta\Omega\gamma_0^2\eta^2}{(2+\eta)^2\left\{\left(\gamma_0^2 + \beta_0^2\Omega_y^2 - \Omega^2\right)^2 + \left(2\,\zeta_\theta\Omega_\theta\Omega\right)^2\right\}}\right]^2\right)} \quad (H2)$$

$$\bar{A}_2^2 = \left[\frac{(\gamma_0^2\ n\ \bar{A}_1)^2}{(2+n)^2\{(\gamma_0^2 + \beta_0^2\ \Omega_y^2 - \Omega^2)^2 + (2\ \zeta_\theta \Omega_\theta \Omega)^2\}}\right] \tag{H3}$$

$$\cos \bar{\Phi}_1 = \left\{\frac{(\gamma_0^2 + \beta_0^2\Omega_y^2 - \Omega^2)\ \bar{A}_2^2 - (1-\Omega^2)\ \gamma_0^2\ \bar{A}_1^2}{\gamma_0^2 G_a \bar{A}_1}\right\} \tag{H4}$$

$$\sin \bar{\Phi}_1 = \left\{\frac{2\Omega\ (\gamma_0^2\ \zeta_x\ \bar{A}_1^2 + \zeta_\theta \Omega_\theta \bar{A}_2^2)}{\gamma_0^2\ G_a \bar{A}_1}\right\} \tag{H5}$$

$$\cos (\bar{\Phi}_1 - \bar{\Phi}_2) = \left\{\frac{(2+n)(\gamma_0^2 + \beta_0^2\Omega_y^2 - \Omega^2)\ \bar{A}_2}{\gamma_0^2\ n\ \bar{A}_1}\right\} \tag{H6}$$

$$\sin (\bar{\Phi}_1 - \bar{\Phi}_2) = \left\{\frac{(2+n)(2\ \zeta_\theta \Omega_\theta \Omega \bar{A}_2)}{\gamma_0^2 n\ \bar{A}_1}\right\} \tag{H7}$$

in which

$$G_a = \frac{U}{\delta_y \omega_x^2} \tag{H8}$$

The numerical solution obtained for Equations (4.23) through (4.26), with $\alpha = 1.0$, was found to match perfectly the closed form solution of Equation (H2) through (H7) for a typical system, thus demonstrating the correctness of the solution.